DESIGNING ALGORITHMS FOR IMPROVING QUANTUM CHEMICAL CALCULATIONS

AISHA EL SHERBINY

Your file Votre référence
ISBN: 978-0-494-55387-9
Our file Notre référence
ISBN: 978-0-494-55387-9

Designing Algorithms For Improving Quantum Chemical Calculations

by

© Aisha El Sherbiny
B.Sc. (Ain Shams University), M.Sc. (University of Cairo),
M.Sc. Memorial University of Newfoundland

A thesis submitted to the
School of Graduate Studies
in partial fulfillment of the
requirements for the degree of
Ph.D.

Department of Chemistry
Memorial University of Newfoundland

February 26, 2008

ST. JOHN'S NEWFOUNDLAND

Contents

To the people who led me to where I am

mama and papa

Abstract

This work involves studying and developing new algorithms for molecular numerical integration used for density functional theory and new algorithms for Hartree-Fock method.

New insight about molecular numerical integration is presented through a detailed study of the performance of some of the well known grids in addition to our implementation of the most recently developed MultiExp grid. A comprehensive study of numerical integration was conducted by evaluating several molecular properties: number of electrons, dipole moment, potential energy, and Coulomb repulsion energy using fifteen grids including a large benchmark grid. The standard grid (SG-1) and a slightly modified version of the Treutler and Alhrichs (TA) grid performed reasonably well. The MultiExp grid, which is more efficient, was studied as well and found to be less accurate.

Studying large molecules using Hartree-Fock method is a challenge both in terms of CPU time and memory requirements. However, there is a high demand to perform quantum chemical calculations for large molecules. Projection from a smaller basis set to a larger basis set was studied in detail. It was found that projection from the STO-

3G basis set to the 6-31G basis set performed well. Projection was used to develop a new version of a divide and conquer algorithm. Our divide and conquer algorithm was used to calculate the protonation energy for a series of peptides. Algorithms to skip calculating two-electron integrals of zero or negligible values are presented in addition to an algorithm to generate a better initial guess.

Acknowledgments

There are several individuals I would like to thank for their guidance and support while this work was being completed. First, I would like to thank my supervisor Raymond. A. Poirier for his advice and assistance which was invaluable in the completion of this work. Also, I would like to thank Dr. C. Flinn and Dr. E. Merschrod for their continued support and encouragement. I would like to express my gratitude to Dr. P. Warburton for his help and support and for providing some of the test cases used in this work. I also like to thank Prof. P.M.W. Gill and Siu-Hung Chien for providing some of the MultiExp grids. Thanks to the Department of Chemistry, the School of Graduate Studies, the National Sciences and Engineering Research Council of Canada, and Memorial University of Newfoundland for financial support and giving me the opportunity to complete my Ph.D. program.

I would like to extend a special thanks to my family and friends, especially my wonderful mother. Their continued support and encouragement throughout the completion of this project will always be greatly appreciated.

List of Tables

List of Figures

Chapter 1

Introduction

1.1 Hartree-Fock Equation

The Schrödinger equation for a molecular system can be written as [1]:

$$\hat{H}\Psi = E\Psi \tag{1.1}$$

where $\hat{H}$ is the Hamiltonian operator which represents the energy terms of the system, Ψ is the wavefunction, and E is the total energy of the system.

$$|\Psi|^2 = \Psi^*\Psi \tag{1.2}$$

is the probability density distribution function. For a molecule of N electrons and M nuclei, the Hamiltonian can be written explicitly, using atomic units, as [1]:

$$\hat{H} = -\frac{1}{2}\sum_{i=1}^{N}\nabla_i^2 - \frac{1}{2}\sum_{A=1}^{M}\frac{1}{M_A}\nabla_A^2 - \sum_{i=1}^{N}\sum_{A=1}^{M}\frac{Z_A}{r_{iA}} + \sum_{i=1}^{N}\sum_{j>i}^{N}\frac{1}{r_{ij}} + \sum_{A=1}^{M}\sum_{B>A}^{M}\frac{Z_A Z_B}{R_{AB}} \tag{1.3}$$

The first term is the kinetic energy operator of the N electrons and the second term is the kinetic energy operator of the M nuclei ,

$$M_A = \frac{m_A}{m_e} \tag{1.4}$$

m_A is the mass of a nucleus A, m_e is the mass of an electron. The third term is the potential energy operator between the nuclei and the electrons where r_{iA} is the distance between electron i and nucleus A. Z_A is the charge of nucleus A. The fourth term is the repulsion energy operator between the electrons where r_{ij} is the distance between electrons i and j. The last term is the repulsion energy between the nuclei, where R_{AB} is the distance between two nuclei A and B. Since the nuclei are much heavier than the electrons, the Born-Oppenheimer approximation treats the molecule as N electrons moving in the field of M fixed positively charged points [1] [2] [3]. Therefore the nuclear kinetic energy is neglected and the repulsion energy between nuclei is a constant. Within the Born-Oppenheimer approximation the total wavefunction Ψ is a product of the nuclear wavefunction Ψ_{nuc} and the electronic wavefunction Ψ_{ele}.

$$\Psi(\mathbf{r}_1, \ldots, \mathbf{r}_N, \mathbf{R}_1, \ldots, \mathbf{R}_M) = \Psi_{ele}(\mathbf{r}_1, \ldots, \mathbf{r}_N)\Psi_{nuc}(\mathbf{R}_1, \ldots, \mathbf{R}_M) \tag{1.5}$$

where the electronic wavefunction depends explicitly on the coordinates $\{\mathbf{r}_i\}$ of the electrons and parametrically on the $\mathbf{R}_i$ coordinates of the nuclei. The nuclear wavefunction depends only explicitly on the nuclear configuration $\mathbf{R}_i$. Thus the Schrödinger equation of the electronic system is given by:

$$\left(-\frac{1}{2}\sum_{i=1}^{N}\nabla_i^2 - \sum_{i=1}^{N}\sum_{A=1}^{M}\frac{Z_A}{r_{iA}} + \sum_{i=1}^{N}\sum_{j>i}\frac{1}{r_{ij}}\right)\Psi_{ele} = E_{ele}\Psi_{ele} \tag{1.6}$$

where E_{ele} is the electronic energy. From now on the subscript will be dropped. Let us assume we have a system of N non-interacting electrons. Then the Hamiltonian is:

$$\hat{H} = -\frac{1}{2}\sum_{i=1}^{N}\nabla_i^2 - \sum_{i=1}^{N}\sum_{A=1}^{M}\frac{Z_A}{r_{iA}} \tag{1.7}$$

which is a summation of a one-electron Hamiltonian $h(i)$:

$$h(i) = -\frac{1}{2}\nabla_i^2 - \sum_{A=1}^{M}\frac{Z_A}{r_{iA}} \tag{1.8}$$

This form of the Hamiltonian implies that the wavefunction Ψ can be written as a product of N spin orbitals χ_i, where a spin orbital is obtained from a one-electron spatial function $\psi_i(\mathbf{r})$ by multiplying $\psi_i(\mathbf{r})$ by a spin function,

$$\Psi\left(x_1, x_2, \ldots, x_N\right) = \chi_i(x_1)\chi_j(x_2)\ldots\chi_k(x_N) \tag{1.9}$$

where the coordinates $\{x_i\}$ combine the spatial coordinates $\{\mathbf{r}_i\}$ and the spin coordinates. Since this form of the wavefunction, called the Hartree product, is not antisymmetric, it does not satisfy the Pauli exclusion principle. An alternative form

of the non-interacting N-electron wavefunction which is antisymmetric and therefore satisfies the Pauli principle is the Slater determinant [1]:

$$\Psi\left(x_1, x_2, \ldots, x_N\right) = \left(\frac{1}{\sqrt{N!}}\right) \begin{vmatrix} \chi_i(x_1) & \chi_j(x_1) & \ldots & \chi_k(x_1) \\ \vdots & \vdots & \vdots & \vdots \\ \chi_i(x_N) & \chi_j(x_N) & \ldots & \chi_k(x_N) \end{vmatrix} \tag{1.10}$$

Given the full Hamiltonian of N electrons, including electron-electron repulsion, what are the "best" $\{\chi_i\}$ that constitute the wavefunction of the ground state Ψ_0? By applying the variational principle the Hartree-Fock method minimizes the energy of the ground state E_0,

$$E_0 = < \Psi_0 | \hat{H} | \Psi_0 > \tag{1.11}$$

with respect to the spin orbitals under the constraint that they remain orthonormal. This optimal set of spin orbitals satisfies the Hartree-Fock equations:

$$\hat{f}(x_1)\chi_i(x_1) = \epsilon_i \chi_i(x_1) \tag{1.12}$$

where $\hat{f}$ is the Fock operator and is defined by:

$$\hat{f}(x_1) = \hat{h}(x_1) + \sum_j \left(\hat{J}_j(x_1) - \hat{K}_j(x_1)\right) \tag{1.13}$$

$\hat{h}(x_1)$ is the sum of the kinetic energy of an electron and its potential energy with all of the nuclei. $\hat{J}_j(x_1)$ is the Coulomb operator and is defined by:

$$\hat{J}_j(x_1)\chi_i(x_1) = \left[\int \chi_j^*(x_2) r_{12}^{-1} \chi_j(x_2) dx_2\right] \chi_i(x_1) \tag{1.14}$$

$\hat{K}_j(x_1)$ is the exchange operator and is given by:

$$\hat{K}_j(x_1)\chi_i(x_1) = \left[\int \chi_j^*(x_2) r_{12}^{-1} \chi_i(x_2) dx_2\right] \chi_j(x_1) \tag{1.15}$$

ϵ_i is the energy of the spin orbital χ_i. If the χ_i's are restricted spin orbitals and all the electrons are paired, i.e. for each spatial function $\psi(\mathbf{r})$ there are two spin orbitals obtained from $\psi(\mathbf{r})$ by multiplying by a spin up and spin down function, then the Hartree-Fock equations become:

$$\hat{f}(\mathbf{r_1})\psi_\mathbf{i}(\mathbf{r_1}) = \epsilon_\mathbf{i}\psi_\mathbf{i}(\mathbf{r_1}) \tag{1.16}$$

where the spin was integrated out in equation (1.16) and $\hat{f}(\mathbf{r_1})$ is given by:

$$\hat{f}(\mathbf{r_1}) = \hat{h}(\mathbf{r_1}) + \sum_i^{N/2} \left(2\hat{J}_i(\mathbf{r_1}) - \hat{K}_i(\mathbf{r_1})\right) \tag{1.17}$$

where $\hat{J}_i$ and $\hat{K}_i$ are given by expressions similar to equations (1.14) and (1.15) except that the spin orbitals $\{\chi_i\}$ are replaced by the spatial orbitals $\{\psi_a\}$.

1.2 Roothaan's Equation

The spatial orbitals $\{\psi_i(\mathbf{r})\}$ can be expanded in terms of a set of basis functions $\{\phi_\mu(\mathbf{r})\}, \mu = 1, 2, \ldots, k$ as follows:

$$\psi_i(\mathbf{r}) = \sum_{\mu=1}^{k} C_{\mu i}\phi_\mu(\mathbf{r}) \tag{1.18}$$

$C_{\mu i}$ are the expansion coefficients and are called the molecular coefficients. Substituting equation (1.18) in the Hartree-Fock equation (1.16) leads to Roothaan's equation:

$$FC = SC\epsilon \tag{1.19}$$

where F, the Fock matrix, is the matrix representation of the Fock operator in the basis functions $\{\phi_\mu(\mathbf{r})\}$.

$$F_{\mu\nu} = \int \phi_\mu^*(\mathbf{r}_1)\hat{f}(\mathbf{r}_1)\phi_\nu(\mathbf{r}_1)d\mathbf{r}_1 \tag{1.20}$$

C is the coefficient matrix where the i^{th} column of C represents the expansion coefficients of a molecular orbital ψ_i. S is the overlap matrix, where

$$S_{\mu\nu} = \int \phi_\mu^*(\mathbf{r}_1)\phi_\nu(\mathbf{r}_1)d\mathbf{r}_1 \tag{1.21}$$

measures the degree of the overlap between the two basis functions μ and ν. ϵ is the diagonal matrix of the orbital energies ϵ_i. By substituting $\hat{f}(\mathbf{r_1})$ from equation (1.17) in equation (1.20), $F_{\mu\nu}$ can be written as:

$$F_{\mu\nu} = H_{\mu\nu} + \sum_{\lambda\sigma} P_{\lambda\sigma} \left[(\mu\nu|\sigma\lambda) - \frac{1}{2}(\mu\lambda|\sigma\nu) \right] \tag{1.22}$$

P is the density matrix and is related to the molecular coefficients by the formula:

$$P_{\lambda\sigma} = 2 \sum_{a}^{N/2} C_{\lambda a} C_{\sigma a}^{*} \tag{1.23}$$

and

$$H_{\mu\nu} = \int \phi_{\mu}^{*}(\mathbf{r}_1) \hat{h}(\mathbf{r}_1) \phi_{\nu}(\mathbf{r}_1) d\mathbf{r}_1 \tag{1.24}$$

$(\mu\nu|\sigma\lambda)$ is a two-electron integral and is given by:

$$(\mu\nu|\sigma\lambda) = \int \phi_{\mu}^{*}(\mathbf{r}_1) \phi_{\nu}(\mathbf{r}_1) r_{12}^{-1} \phi_{\sigma}^{*}(\mathbf{r}_2) \phi_{\lambda}(\mathbf{r}_2) d\mathbf{r}_1 d\mathbf{r}_2 \tag{1.25}$$

1.3 Molecular Numerical Integration

Three-dimensional integrals of the form:

$$I = \int F(\mathbf{r})\, d\mathbf{r} \tag{1.26}$$

where $F(\mathbf{r})$ is a three-dimensional molecular function occur frequently in the calculation of the electronic structure of molecules [4]. Usually, the integral I has to be evaluated numerically. Although complex, numerical integration is an essential part of density functional theory, DFT, where it is used to calculate the exchange correlation energy [5] [6]:

$$E_{xc} = \int F(\rho, \nabla\rho, \ldots)\, d\mathbf{r} \tag{1.27}$$

where F is a functional of the electron density ρ, its gradient $\nabla\rho$ and possibly other parameters. A popular solution for integrals of the form given by equation (1.27) is the nuclear weight functions proposed by Becke[7]. Becke's scheme transfers the problem from a multi-center integral over the whole molecule into a sum of three-dimensional atomic integrals over the individual atoms of the molecule. The numerical solution of the integral I, as proposed by Becke, involves dividing the molecular integrand $F(\mathbf{r})$ into atomic contributions using nuclear weight functions as follows:

$$F(\mathbf{r}) = \sum_{i=1}^{N_a} F_i(\mathbf{r}) \tag{1.28}$$

$$F_i(\mathbf{r}) = W_i(\mathbf{r}) F(\mathbf{r}) \tag{1.29}$$

where N_a is the number of atoms. The atomic contributions $F_i(\mathbf{r})$ at each point $\mathbf{r}$ are defined by the normalized atomic weight functions $W_i(\mathbf{r})$. The molecular integral I can be written as:

$$I = \sum_{i=1}^{N_a} \int F_i(\mathbf{r})\, d\mathbf{r} = \sum_{i=1}^{N_a} I_i \tag{1.30}$$

Each atomic integral I_i can be written in spherical polar coordinates as:

$$I_i = \int_0^{\infty} \int_0^{\pi} \int_0^{2\pi} F_i(r, \theta, \phi)\, r^2 dr\, \sin\theta\, d\theta\, d\phi \tag{1.31}$$

This triple integral can be rearranged into a radial integral I_r over r and a spherical integral I_ω over (θ, ϕ). While all DFT codes, to the best of our knowledge, use Becke's nuclear weight functions to divide the molecular integral into a sum of atomic integrals, many algorithms have been developed to carry out the atomic integral I_i. These algorithms use Lebedev angular grids [8] [9] [10] of different orders in addition to different radial quadratures. The rest of this section will explain in some detail the Becke weight functions, the Lebedev spherical grids, and some of the better known radial quadratures and atomic grids.

1.3.1 Becke Weight Functions

The weight functions $W_i(\mathbf{r})$ are required to fulfill [12]:

- $W_i(\mathbf{r}) \geq 0$

- $\sum_{i=1}^{N_a} W_i(\mathbf{r}) = 1$ at any point $\mathbf{r}$ in the space.

- Every $W_i(\mathbf{r})$ is zero or has a negligible value close to each nucleus of the molecule, except for the nucleus i, where it should be almost unity.

Becke started by partitioning the molecular space into the conventional Voronoi polyhedra such that each nucleus is enclosed in one of these polyhedra where the Voronoi polyhedron on a nucleus i is defined by the product [7]:

$$w_i(\mathbf{r}) = \prod_{j \neq i} s(\mu_{ij}) \tag{1.32}$$

j runs over the rest of the nuclei of the molecule. $w_i(\mathbf{r})$ is called a 'cell function' and equal to unity if $\mathbf{r}$ lies inside the cell, and zero if $\mathbf{r}$ lies outside. $s(\mu_{ij})$ is a step function given by:

$$s(\mu_{ij}) = \begin{cases} 1 & -1 \leq \mu_{ij} \leq 0 \\ \\ 0 & 0 < \mu_{ij} \leq +1 \end{cases}$$

and μ_{ij} is defined as:

$$\mu_{ij} = (r_i - r_j)/R_{ij} \qquad -1 \leq \mu_{ij} \leq 1 \tag{1.33}$$

where r_i and r_j are the distances to the nuclei i and j from a point $\mathbf{r}$ and R_{ij} is the

distance between both nuclei. To 'soften' the discontinuity at $\mu_{ij} = 0$, the mid-point between atoms i and j, $s(\mu_{ij})$ is defined in terms of $g(\mu_{ij})$:

$$s(\mu_{ij}) = \frac{1}{2}[1 - g(\mu_{ij})]. \tag{1.34}$$

$g(\mu_{ij})$ is obtained from the polynomial $h(\mu_{ij})$,

$$h(\mu_{ij}) = \frac{3}{2}\mu_{ij} - \frac{1}{2}{\mu_{ij}}^3 \tag{1.35}$$

by iterating h three times as follows:

$$g(\mu_{ij}) = h\{h[h(\mu_{ij})]\} \tag{1.36}$$

The normalized weight functions $W_i(\mathbf{r})$ can be calculated from the cell functions $w_i(\mathbf{r})$ by:

$$W_i(\mathbf{r}) = \frac{w_i(\mathbf{r})}{\sum_{j=1}^{N_a} w_j(\mathbf{r})} \tag{1.37}$$

where the summation over j in the denominator includes all nuclei in the system.
In the scheme given so far, the space is divided equally between two atoms. Becke recognized that it is important to have regions of different sizes around each atom. Therefore, Becke introduced a change of variable:

$$\nu_{ij} = \mu_{ij} + a_{ij}(1 - {\mu_{ij}}^2) \tag{1.38}$$

$$a_{ij} = \frac{u_{ij}}{{u_{ij}}^2 - 1} \tag{1.39}$$

$$u_{ij} = \frac{\chi - 1}{\chi + 1} \tag{1.40}$$

$$\chi = \frac{R_i}{R_j} \tag{1.41}$$

where R_i and R_j are Bragg-Slater radii.

1.3.2 Lebedev Grids

The spherical part of the integral I_i is usually carried out using the angular grids developed by Lebedev [8] [9] [10]. Let S be a unit sphere in the three-dimensional space, $S = \{(x, y, z) : x^2 + y^2 + z^2 = 1\}$ and

$$I(f) = \int_S f(S)\, dS \tag{1.42}$$

A quadrature of order n that integrates polynomials of order $\leq n$ on the surface S is given by the Gauss-Markov quadrature formula:

$$\begin{aligned} I_n(f) &= A_1 \sum_{i=1}^{6} f({a_i}^{(1)}) + A_2 \sum_{i=1}^{12} f({a_i}^{(2)}) + A_3 \sum_{i=1}^{8} f({a_i}^{(3)}) \\ &\quad + \sum_{k=1}^{N_1} B_k \sum_{i=1}^{24} f({b_i}^{(k)}) + \sum_{k=1}^{N_2} C_k \sum_{i=1}^{24} f({c_i}^{(k)}) + \sum_{k=1}^{N_3} D_k \sum_{i=1}^{48} f({d_i}^{(k)}) \end{aligned} \tag{1.43}$$

${a_i}^{(1)}$, ${a_i}^{(2)}$, ${a_i}^{(3)}$, ${b_i}^{(k)}$, ${c_i}^{(k)}$, and ${d_i}^{(k)}$ are called the nodes and A_1, A_2, A_3, B_k, C_k and D_k are the corresponding weights. The nodes have the following coordinates:

$$a_i^{(1)} \;:\; (0,\,0,\,\pm 1),(0,\,\pm 1,\,0),(\pm 1,\,0,\,0)$$

$$a_i^{(2)} \;:\; (\pm 2^{-1/2},\,\pm 2^{-1/2},0),(\pm 2^{-1/2},\,0,\,\pm 2^{-1/2}),(0,\,\pm 2^{-1/2},\,\pm 2^{-1/2})$$

$$a_i^{(3)} \;:\; (\pm 3^{-1/2},\,\pm 3^{-1/2},\,\pm 3^{-1/2})$$

$$b_i^{(k)} \;:\; (\pm l_k, \pm l_k, \pm m_k), (\pm l_k, \pm m_k, \pm l_k), (\pm m_k, \pm l_k, \pm l_k)$$

$$c_i^{(k)} \;:\; (\pm p_k, \pm q_k, 0), (\pm p_k, 0, \pm q_k), (0, \pm p_k, \pm q_k), (\pm q_k, 0, \pm p_k)$$

$$d_i^{(k)} \;:\; (\pm r_k, \pm u_k, \pm w_k), (\pm r_k, \pm w_k, \pm u_k), (\pm u_k, \pm r_k, \pm w_k),$$
$$(\pm u_k, \pm w_k, \pm r_k), (\pm w_k, \pm u_k, \pm r_k), (\pm w_k, \pm r_k, \pm u_k)$$

where

$$2{l_k}^2 + {m_k}^2 = 1 \tag{1.44}$$

and

$${p_k}^2 + {q_k}^2 = 1. \tag{1.45}$$

Lebedev gave the nodes and the weights for Gauss-Markov quadrature up to $n = 53$ with 974 angular points. An angular grid as large as 5810 angular points with $n = 131$ was given by Lebedev and Laikov [11].

1.3.3 The Radial Quadrature

The integration of a one-dimensional function $A(x)$ can be approximated by a quadrature of the form [13]:

$$\int_a^b A(x)\,dx \approx \sum_{i=1}^{n} a_i\,A(x_i) \tag{1.46}$$

where a_i is the weight of the function A at the point x_i and n is the number of points in the interval $[a, b]$. Some of the well known quadratures are the Gauss-Chebyshev and Euler-Maclaurin formulas. To use any of these quadratures to calculate I_r, the points $\{x_i\}$ have to be mapped to the points $\{r_i\}$ [7] where,

$$0 \leq r_i < \infty \tag{1.47}$$

i.e., into the limits of the radial part of the integral I_i. The choice of the mapping is crucial. The mapping determines how the radial points are distributed in the molecular space and if the core and the chemical bonding regions are appropriately represented in the integration.

1.3.4 Atomic Grids

The combination of both the angular grid and the radial grid constitutes what we call the atomic grid. The radial grid involves the radial quadrature and the mapping. The rest of this section presents some of the atomic grids that are used in quantum chemistry codes and are implemented in MUNgauss [14]. In all of the following the

parameter R controls the extension of the atomic grid around the nucleus.

1- Standard Grid

- The standard grid (SG-1) [15] was developed by Pople and his group. It uses Lebedev grids of 6, 38, 86, and 194 angular points to evaluate the angular part I_ω of the atomic integral I_i. The number of angular points increases from 6 points in the core to 194 points as we move further from the nucleus to the valence region.

- SG-1 uses the Euler-Maclaurin scheme to calculate the radial part I_r with 50 radial points. The mapping, nodes, and weights are given as follows:

$$r_i = R\frac{x_i^2}{(1-x_i)^2} \tag{1.48}$$

$$x_i = \frac{i}{n+1} \tag{1.49}$$

$$w_i = \frac{2R^3}{(n+1)}\frac{x_i^5}{(1-x_i)^7} \tag{1.50}$$

2- Treutler and Ahlrichs Grid/Treutler and Ahlrichs(new) Grid

- The Treutler and Ahlrichs (TA) grid [12] was developed by Treutler and Ahlrichs. It divides the atomic space into three regions and uses Lebedev grids of 14 and 50 angular points for the first and the second regions, respectively, and 194, or 302 for the third region. The choice of any of these two angular grids depends on the atomic number of the atom for which the numerical integration is performed.

- TA uses Gauss-Chebyshev quadrature of the second kind for the radial part I_r with a number of radial points in the range from 20-45 radial points. We use the M3 mapping as defined by Treutler and Ahlrichs where the mapping, nodes, and weights are given by the formulae:

$$r_i = \frac{R}{\ln 2}(1+x_i)^{\alpha}\ln\frac{2}{1-x_i} \tag{1.51}$$

$$x_i = cos\left(\frac{i\pi}{n+1}\right) \tag{1.52}$$

$$w_i = \left(\frac{R}{\ln 2}\right)^3 (1+x_i)^{3\alpha}\left(\ln\frac{2}{1-x_i}\right)^3\left(\sqrt{\frac{1+x_i}{1-x_i}}\ln\frac{1-x_i}{2}+\alpha\sqrt{\frac{1-x_i}{1+x_i}}\right)\left(\frac{\pi}{n+1}\right) \tag{1.53}$$

Treutler and Ahlrichs(new) [16], TA(new), is our new implementation of the TA grid and it uses smaller grids for the angular part of the integral I_i.

3- Becke

- The Becke grid [7] uses Lebedev grids of 110 and 194 angular points.
- Becke uses Gauss-Chebyshev quadrature with 20-45 radial points. The mapping, nodes, and weights are given by:

$$r_i = R\frac{1+x_i}{1-x_i} \tag{1.54}$$

$$x_i = cos\left(\frac{i\pi}{n+1}\right) \tag{1.55}$$

$$w_i = \frac{2\pi}{n+1}\frac{(1+x_i)^{5/2}}{(1-x_i)^{7/2}}R^3 \tag{1.56}$$

4- MultiExp Grids

- The MultiExp grids use the most recent, MultiExp radial grid [17]. We developed nine different grids based on the MultiExp grid with 20, 25, or 30 radial points [16].

- For each radial grid we designed three angular grids with Lebedev grids of 6 and 86 angular points for the core and middle parts of the atomic space. The outer grid can be as large as 110, 194, or 302 angular points.

$$r_i = -R\ln x_i \tag{1.57}$$

$$w_i = \left(\frac{a_i}{x_i}\right) R^3 \tag{1.58}$$

The points x_i are given in reference [17].

5- Benchmark

- The benchmark grid is a larger version of the SG-1 grid where 100 radial points are used and a single grid of 1202 angular points is used for the whole atomic space.

1.4 The SG0 Grid

The SG0 grid [18] was developed based on the MultiExp grid of Chien and Gill. Other than our implementation of the MultiExp grid of 20 radial points and 6, 86 and 110 angular points, the SG0 is the smallest known grid. Chien and Gill did not divide the atomic space into zones, as in most of the atomic grids, but used different angular grids on different radial points. However, they followed the technique of using very small angular grids in the core, 6 angular points, and progressed to larger grids and then to smaller grids much further from the nucleus. They used different combinations of angular grids with 6, 18, 26, 38, 50, 74, 86, 110, 146, and 170 angular points. In our code we followed all the specifications of SG0 except the 18 angular points grid was replaced by a 26 angular points grid.

Chapter 2

Numerical Integration

This chapter presents the paper 'An Evaluation of The Radial Part of The Numerical Integration Commonly Used in DFT' [16] except for the introduction part which is given in more detail in Chapter 1.

2.1 Computational Method

All calculations were performed with MUNgauss [14]. In all cases, the electron density is calculated at the HF/6-31G(d)//HF/6-31G(d) level. Our numerical integration code uses the nuclear weight functions developed by Becke. Lebedev grids with 6, 14, 38, 50, 86, 110, 194 and 302 angular points for the spherical part of the integration have been implemented. For the radial part, we have implemented the Becke grid [7], the TA grid by Treutler and Alhrichs (TA) [12], the Gill et al. grid (SG-1) [15] and the MultiExp grids by Gill and Chien [17]. The charge density is integrated to obtain the total number of electrons for a variety of molecules containing first and second

row elements in different bonding environments in addition to some closed shell atoms and third row transition metal fluorides (CuF and ZnF_2). We use the integration of the charge density to evaluate the performance of some of the numerical integration grids, both in terms of accuracy and efficiency (number of grid points). The error in the total number of electrons can only be used as an estimate of errors in other properties [12] [19]. The MultiExp grid, which uses fewer radial points and a very simple mapping from the $[0, 1)$ to $[0, \infty)$ interval, is of special interest. The accuracy of the integration is calculated using the formula given by Gill and Chien:

$$\text{accuracy} = -log_{10}\left|\frac{\text{approx}}{\text{exact}} - 1\right| \tag{2.1}$$

where "approx" is the value of the integrated charge density and "exact" is the exact number of electrons. Mean absolute deviations (MAD) in the total number of electrons are also included for comparison.

2.2 Results and Discussion

In the application of the MultiExp grid, we used the well known technique of "pruning", i.e. using very small spherical grids in the core region where the charge density is more symmetric than in the region further from the nucleus [15]. After a great deal of experimenting with the MultiExp grid we found that dividing the atomic space into three regions with larger spherical grids as we move away from the nucleus, gives errors that are well within the acceptable error. The acceptable error was defined

by Gill et al. to be within 300 μH for the energy or equivalently 3×10^{-4} for the exact number of electrons. An error of 3×10^{-4} corresponds to an accuracy, as defined by equation (2.1), of 3.5 to 5.5 for 1 to 100 electrons. All the mappings depend on a scaling parameter R. For the MultiExp grid the different values of R investigated were Bragg-Slater radii, the values used by TA [12], and those given by Gill et al [15]. The best performance was for the R values given by Gill et al. after optimizing some of them. Namely, the R values were optimized for Si, P, S, Cl, Cu and Zn for the 20, 25, and 30 radial grids. In addition, values of R were optimized for Li and F for the 25 radial grid and Li for the 30 radial grid. The optimized values of R along with the corresponding accuracies are given in Table 2.1. For the set of molecules for which R values were optimized, the average accuracy of the integration, excluding CuF and ZnF_2 (R values not available), increased from 3.90 to 6.88 for the 20 radial grid, 4.13 to 7.49 for the 25 radial grid, and from 4.46 to 7.97 for the 30 radial grid. Only the 25 and 30 radial grids gave such high accuracies for CuF and ZnF_2. In general, it is possible to optimize R values for atoms to give a very high accuracy for a given molecule. For this reason, the molecules used for optimizing R values, LiCl, HF, SiH_4, PH_3, H_2S, HCl, CuF and ZnF_2 are excluded from our test set, in order to get a more realistic measure of the performance of the MultiExp grids. For each radial grid the atomic space was partitioned into three regions, (core, middle and outer). For the 20, 25 and 30 radial grids, the space was divided into, (6,6,8), (6,8,11) and (6,10,14), respectively. For each radial grid, a spherical grid of six angular points was used for the core and 86 angular points was used for the middle region. For the outer region, we used three different spherical grids of 110, 194, and

302 angular points to give a total of 9 grids. The largest grid gives a total of 5124 grid points (6x6+10x86+14x302) per atom. For each grid, we calculated the average accuracy of the number of electrons for the set of molecules. A larger spherical grid with 302 angular points for the whole atomic space was used as a benchmark grid to evaluate the error introduced by using smaller grids in the three regions, especially the core and the middle regions. Performance of the MultiExp grid is also compared with the TA, SG-1, and Becke grids for the same set of molecules. From Table 2.2, the average accuracy for the MultiExp grids ranges from 5.03 to 6.21 while the MAD ranges from 2.62×10^{-4} to 4.00×10^{-5}. Surprisingly, even the small grid (6,6,8) with the 6-86-194 angular grid performed well (5.30) compared with the much larger SG-1 grid (5.71) and even better than the Becke grid (4.83) results given in Table 2.3. The benchmark grid gives average accuracies in the integrated charge density of 5.22, 5.79, and 6.18, for the 20, 25, and 30 radial grids, respectively. The 6-86-302 angular grid, when compared with the benchmark grid, results in no significant loss of accuracy, supporting our pruning strategy for the core and middle regions. For future calculations with first and second row elements, we recommend the use of the 20 radial points grid with the 6-86-194 angular grid, which gives an average accuracy of 5.30 and a MAD of 1.65×10^{-4} . This grid is both accurate and efficient. Table 2.3 shows that, for our set of molecules, the TA grid of Treutler and Alhrichs gives an average accuracy of 4.23 for the integrated charge density. On the other hand, as given in Table 2.4 for the atoms He, Ne, Mg, Ar and Zn, we obtain a much higher average accuracy of 6.69 which is comparable to the accuracy Treutler and Alhrichs obtained for atoms H to Kr (Table III in ref. [12]). For the TA grid, Treutler and Ahlrichs

used partitioning schemes of (10, 5, 15) for H, He, (11, 6, 18) for Li-Ne, (13, 7, 20) for Na-Ar and (15, 7, 23) for K-Kr. We investigated different divisions of the radial points with different angular grids. Again, the atomic space was divided into three regions with (6, 8, $n_r - 14$), where n_r is the total number of radial points (30, 35, 40 or 45). The best performance was obtained using a 6-86-110 angular grid for the H atom and a 6-110-194 angular grid for the other atoms. With fewer number of grid points, our new implementation of the TA grid, TA(new), gives a much better average accuracy of 5.58 for the complete set of test molecules, as given in Table 2.3. With the TA, TA(new) and Becke grids, CuF and ZnF_2 give accuracies similar to the average accuracy for the corresponding grid. As seen from Table 2.4, with TA(new) we obtain the same average accuracy as the original TA grid, of 6.69, for the atoms He, Ne, Mg, Ar and Zn. This shows that it is dangerous to draw conclusions about numerical integration algorithms based solely on atomic calculations. The same table shows the average accuracy and MAD of both SG-1 and Becke grids. It should be noted that although a grid and partitioning scheme may perform well at integrating the density, other molecular properties, such as energetics and vibrational frequencies, may not necessarily perform equally as well [25].

2.3 Conclusions

We have implemented the MultiExp grid introduced by Gill and Chien to integrate the charge density. MultiExp grids of 20, 25, and 30 radial points with different angular grids were investigated. We found that dividing the atomic space into three regions with a very small grid in the core, a medium grid in the middle, and a reasonably

large grid in the outer region works well. The 20 radial points MultiExp grid with the 6-86-194 angular grid proved to be both accurate and efficient for first and second row elements. For the third row transition metals we recommend the use of the 25 radial points with the 6-86-194 angular grid. Our new implementation of the Treutler and Alhrichs algorithm improved the accuracy of the TA grid by more than one order of magnitude with fewer grid points.

Table 2.1: Optimized Values of R (First Row) and the Corresponding Accuracies (Second Row) for the MultiExp Grids.

		radial grids		
Atom	Molecule	20	25	30
Li	LiCl	3.0769[a]	2.9770	3.3540
		4.19	9.42	8.28
F	HF	0.7692[a]	0.7360	0.7692[a]
		5.11	7.31	6.15
Si	SiH_4	1.5877	1.7260	1.6420
		7.35	7.18	7.74
P	PH_3	1.4500	1.5930	1.4670
		6.37	6.79	7.73
S	H_2S	1.3600	1.4930	1.3970
		6.61	7.12	8.72
Cl	HCl	1.2730	1.3840	1.3220
		7.18	7.15	7.41
Cu	CuF	0.7070	0.9980	0.8980
		3.84	7.83	7.89
Zn	ZnF_2	0.7010	0.8050	1.0970
		4.55	7.06	7.06
Average accuracy		5.65	7.48	7.19

[a] For these atoms we used the R-values given in ref. [15]

Table 2.2: Accuracy and total number of grid points for the three MultiExp grids using three different angular grids, 6-86-110, 6-86-194, 6-86-302 for rows 1, 2 and 3 respectively for each molecule.

Radial points	20		25		30	
Molecule	Accuracy	Total grid points	Accuracy	Total grid points	Accuracy	Total grid points
BF_3	5.17	5728	4.91	7736	5.04	9744
	6.3	8416	5.28	11432	5.56	14448
	5.79	11872	5.51	16184	6.21	20496
BH_3	4.81	5728	5.4	7736	5.65	9744
	4.67	8416	6.01	11432	5.55	14448
	4.71	11872	6.19	16184	5.93	20496
BeH_2	5.44	4296	4.97	5802	5.73	7308
	5.83	6312	4.91	8574	5.45	10836
	5.72	8904	4.93	12138	5.5	15372
C_2H_2	4.76	5728	6.08	7736	5.61	9744
	4.8	8416	6.27	11432	5.93	14448
	4.81	11872	6.08	16184	6.06	20496
C_2H_4	4.51	8592	4.32	11604	4.33	14616
	5.01	12624	5.24	17148	5.37	21672
	4.84	17808	6.08	24276	6.20	30744
CCl_4	4.89	7160	5.25	9670	5.38	12180

... continued

Table 2.2 – continued

Radial points	20		25		30	
Molecule	Accuracy	Total grid points	Accuracy	Total grid points	Accuracy	Total grid points
	5.05	10520	5.71	14290	6.19	18060
	5.04	14840	5.71	20230	6.22	25620
CF_4	5.06	7160	5.45	9670	5.05	12180
	6.37	10520	5.32	14290	6.46	18060
	6.86	14840	5.29	20230	7.03	25620
$CH_2(CH_3)_2$	5.87	15752	4.97	21274	5.03	26796
	6.15	23144	5.08	31438	5.16	39732
	5.17	32648	5.51	44506	6.12	56364
$CH_2(PH_2)_2$	4.72	12888	4.85	17406	4.86	21924
	5.38	18936	6.53	25722	5.86	32508
	5.50	26712	6.75	36414	6.73	46116
$CH_2(SH)_2$	4.84	10024	5.04	13538	5.01	17052
	5.11	14728	5.58	20006	5.45	25284
	5.28	20776	6.70	28322	5.94	35868
$CH_2(SiH_3)_2$	5.79	15752	5.23	21274	5.31	26796
	6.30	23144	5.57	31438	5.67	39732
	5.49	32648	6.39	44506	6.73	56364
CH_3-F	4.84	7160	5.32	9670	5.18	12180
	5.17	10520	5.59	14290	6.03	18060
	5.14	14840	5.66	20230	6.26	25620

... continued

Table 2.2 – continued

Radial points	20		25		30	
Molecule	Accuracy	Total grid points	Accuracy	Total grid points	Accuracy	Total grid points
CH_3-NH_2	5.25	10024	5.19	13538	5.33	17052
	5.11	14728	5.35	20006	5.57	25284
	5.00	20776	5.66	28322	6.42	35868
CH_3-OH	4.88	8592	4.64	11604	4.67	14616
	5.08	12624	5.67	17148	6.45	21672
	5.05	17808	5.82	24276	6.61	30744
CH_3-PH_2	4.99	10024	5.13	13538	5.16	17052
	5.87	14728	6.27	20006	6.19	25284
	5.74	20776	7.68	28322	6.72	35868
CH_3-SH	5.5	8592	5.16	11604	5.17	14616
	5.57	12624	5.94	17148	6.07	21672
	5.40	17808	6.58	24276	6.28	30744
CH_3-SiH_3	5.31	11456	5.10	15472	5.16	19488
	5.61	16832	7.63	22864	5.99	28896
	5.57	23744	8.34	32368	6.02	40992
CH_3Cl	5.41	7160	5.19	9670	5.32	12180
	6.25	10520	5.52	14290	5.89	18060
	6.43	14840	5.51	20230	5.84	25620
CH_4	4.63	7160	4.44	9670	4.45	12180
	5.06	10520	5.49	14290	5.63	18060

... continued

Table 2.2 – continued

Radial points	20		25		30	
Molecule	Accuracy	Total grid points	Accuracy	Total grid points	Accuracy	Total grid points
	4.95	14840	6.22	20230	6.53	25620
CO	5.37	2864	5.11	3868	5.30	4872
	5.03	4208	5.56	5716	6.80	7224
	5.04	5936	5.55	8092	7.50	10248
CO_2	5.67	4296	5.03	5802	5.16	7308
	5.03	6312	5.65	8574	6.54	10836
	5.04	8904	5.61	12138	6.97	15372
Cl_2	5.2	2864	5.34	3868	5.13	4872
	5.82	4208	5.69	5716	7.00	7224
	6.16	5936	5.72	8092	6.66	10248
H_2	4.73	2864	5.34	3868	5.94	4872
	4.73	4208	5.36	5716	6.03	7224
	4.72	5936	5.36	8092	6.02	10248
H_2CO	4.86	5728	4.57	7736	4.61	9744
	4.96	8416	5.72	11432	6.45	14448
	4.96	11872	5.69	16184	6.62	20496
H_2O	5.3	4296	5.16	5802	5.28	7308
	5.08	6312	5.5	8574	5.79	10836
	5.02	8904	5.76	12138	6.64	15372
LiF	4.92	2864	4.23	3868	5.12	4872

... continued

Table 2.2 – continued

Radial points	20		25		30	
Molecule	Accuracy	Total grid points	Accuracy	Total grid points	Accuracy	Total grid points
	4.91	4208	4.21	5716	5.09	7224
	4.91	5936	4.21	8092	5.09	10248
LiH	3.96	2864	4.2	3868	4.39	4872
	3.96	4208	4.21	5716	4.41	7224
	3.96	5936	4.21	8092	4.41	10248
NH_3	4.61	5728	4.47	7736	4.5	9744
	5.23	8416	5.48	11432	5.92	14448
	5.13	11872	5.73	16184	6.61	20496
P_2	5.49	2864	5.15	3868	5.55	4872
	5.28	4208	5.03	5716	5.31	7224
	5.34	5936	5.06	8092	5.37	10248
PF_5	5.2	8592	5.57	11604	5.35	14616
	5.06	12624	5.29	17148	6.04	21672
	5.03	17808	5.28	24276	6.16	30744
SF_6	5.24	10024	5.16	13538	4.77	17052
	5.01	14728	5.14	20006	6.09	25284
	4.95	20776	5.15	28322	6.38	35868
average	5.07		5.03		5.12	
	5.32		5.54		5.87	
	5.25		5.80		6.25	

... continued

Table 2.2 – continued

Radial points	20		25		30	
Molecule	Accuracy	Total grid points	Accuracy	Total grid points	Accuracy	Total grid points
MAD	2.62×10^{-4}		2.48×10^{-4}		2.47×10^{-4}	
	1.65×10^{-4}		1.28×10^{-4}		5.84×10^{-5}	
	1.70×10^{-4}		1.14×10^{-4}		4.00×10^{-5}	

Table 2.3: Accuracy and Total Number of Grid Points Using the Original TA, TA(new), SG-1, and Becke Grids.

	TA		TA(new)		SG-1		Becke	
Molecule	Accuracy	Total grid points	Accuracy	Total grid points	Accuracy	Total grid points	Accuracy	Total grid points
BF_3	4.18	23560	4.93	19960	5.39	14920	4.82	27160
BH_3	3.88	15790	4.93	12442	5.64	14632	3.66	13390
BeH_2	3.70	12490	5.26	9958	6.33	10998	4.11	11190
C_2H_2	4.43	30160	5.94	24928	5.48	14728	5.09	31560
C_2H_4	3.44	24980	5.57	19916	5.19	21996	4.41	22380
CCl_4	4.82	32178	8.32	28830	6.02	18426	6.01	41710
CF_4	6.35	29450	5.57	24950	4.83	18650	5.15	33950
$CH_2(CH_3)_2$	4.14	44070	5.08	34842	5.03	40262	4.60	37970
$CH_2(PH_2)_2$	4.20	38834	5.13	31814	6.32	32882	3.81	37450
$CH_2(SH)_2$	4.05	32234	5.34	26846	5.68	25614	4.44	33050
$CH_2(SiH_3)_2$	4.30	45434	5.59	36782	5.32	40150	4.30	41850
CH_3-F	4.34	21680	5.35	17432	5.96	18362	4.51	20180
CH_3-NH_2	3.63	28280	5.12	22400	5.54	25630	4.21	24580
CH_3-OH	4.36	24980	5.23	19916	6.16	21996	4.38	22380
CH_3-PH_2	3.76	28962	5.75	23370	6.25	25574	4.40	26520
CH_3-SH	4.26	25662	5.69	20886	5.28	21940	4.57	24320
CH_3-SiH_3	4.08	32262	5.30	25854	6.06	29208	4.64	28720
CH_3Cl	4.15	22362	5.95	18402	5.76	18306	4.84	22120
CH_4	3.78	19090	5.50	14926	5.65	18266	4.29	15590
CO	4.95	11780	5.91	9980	6.32	7460	5.98	13580
CO_2	5.46	17670	6.31	14970	6.12	11190	7.11	20370

... continued

Table 2.3 – continued

	TA		TA(new)		SG-1		Becke	
		Total grid		Total grid		Total grid		Total grid
Molecule	Accuracy	points	Accuracy	points	Accuracy	points	Accuracy	points
Cl_2	3.91	13144	6.72	11920	4.99	7348	6.13	17460
H_2	3.68	6600	5.30	4968	5.32	7268	3.80	4400
H_2CO	3.90	18380	5.78	14948	5.63	14728	4.71	17980
H_2O	4.36	12490	5.19	9958	6.25	10998	4.85	11190
LiF	5.81	11780	4.70	9980	4.77	7460	3.79	13580
LiH	3.90	9190	4.81	7474	5.24	7364	4.20	8990
NH_3	3.96	21680	5.41	17432	5.76	14632	6.68	8730
P_2	4.17	13144	5.96	11920	6.36	7348	4.65	20180
P_4	3.75	32860	5.95	29800	8.72	14696	5.70	17460
PF_5	3.72	36022	5.91	30910	5.01	22324	6.03	42680
SF_6	3.85	41912	5.04	35900	4.21	26054	4.61	49470
Average	4.23		5.58		5.71		4.83	
MAD	2.59×10^{-3}		1.06×10^{-4}		3.12×10^{-4}		8.34×10^{-4}	
CuF	4.87	13396	5.55	11920			4.64	16490
ZnF_2	4.71	19286	5.43	16910			4.43	23280

Table 2.4: Accuracy and Total Number of Grid Points for Atoms Using the Original TA, TA(new), SG-1, and Becke Grids.

	TA		TA(new)		SG-1		Becke	
Atom	Accuracy	Grid points	Accuracy	Grid points	Accuracy	Grid points	Accuracy	Grid points
He	7.23	3300	7.23	2484	9.31	3634	6.14	6790
Ne	7.22	5890	7.22	4990	9.11	3730	6.66	6790
Mg	6.69	6572	6.69	5960	6.52	3674	6.68	8730
Ar	6.37	6572	6.37	5960	8.36	3674	7.06	8730
Zn	5.94	7506	5.94	6930			5.97	9700
Average	6.69		6.69		8.33		6.50	
MAD	1.19×10^{-5}		1.19×10^{-5}		1.34×10^{-6}		1.04×10^{-5}	

Chapter 3

Comprehensive Study of Molecular Numerical Integration

3.1 Introduction

In Chapter 2 we compared the performance of some of the well known grids used in molecular numerical integration, both in terms of accuracy and efficiency. We concluded, based on the number of electrons only [16], that the MultiExp grid performed well compared to the grids proposed by Becke [7], Gill et al [15], and Treutler and Ahlrichs [12]. In this chapter we reexamine the performance of the same set of grids in addition to the SG0 [18] grid and the benchmark grid described in Chapter 1. Since the exact value of the numerical integration is not always available, the numerical integration accuracy is evaluated by calculating the total number of electrons or the total energy using a larger grid as a reference [12] [15] [21]. Our approach

is different. We calculated the number of electrons N_{el}, potential energy V_{ne}, dipole moment μ and coulomb potential energy V_{ee} using both Hartree-Fock theory and numerical integration, where the charge density used for numerical integration is calculated from HF theory. Therefore the HF values of V_{ne}, μ, and V_{ee} serve as exact values to compare with those calculated by numerical integration. We used a set of eighty nine molecules, see Table 3.1, representing different molecular environments, ground states, and transition states. In addition, we developed our own Fortran 90 code within the framework of MUNgauss [14].

3.2 Results and Discussion

To test the performance of the different grids, seven sets of molecules are used. The first three sets represent elements from the first, second, and third rows of the periodic table. The other four sets represent transition states, ions, complexes, and peptides. For all of the grids, the set of peptides consisted of one to five glycine amino acids except for the benchmark grid where only one and two glycine peptides were used. The error in each set was measured using the mean absolute error, MAE which is calculated by the formula:

$$MAE = \sum_{i} \mid P_{NI}^{i} - P_{HF}^{i} \mid /N \tag{3.1}$$

P_{NI}^{i} is the value of the molecular property, N_{el}, V_{ne}, μ, or V_{ee} calculated using numerical integration for a molecule i and P_{HF}^{i} is the corresponding value of the same property calculated using HF. N is the number of molecules in each set. The no-

tations 20(110), 20(194), 20(302), 25(110), 25(194), 25(302), 30(110), 30(194), and 30(302) denote MultiExp grids of 20, 25, or 30 radial points with 6-86-110, 6-86-194, or 6-86-302 angular grids. The parameter R was optimized for Ge, As, Se, and Br in the molecules CH_3GeH_3, CH_3AsH_2, CH_3SeH, and CH_2Br_2, respectively. Values of R are only available for elements up to argon for SG0 and SG-1 and up to krypton for TA and TA(new).

3.2.1 Number of Electrons

The number of electrons is calculated by integrating the electron density using the equation:

$$N_{el} = \int \rho(\mathbf{r})\, d\mathbf{r} \tag{3.2}$$

Table 3.2 gives MAE of the integration of the electron density for the seven sets of molecules described above with the 14 grids mentioned previously. For molecules containing first row atoms, the accuracy of the integration of the electron density using MultiExp grid with 20 radial points improves slightly as the angular grid for the outermost region increases from 110 angular points to 194 but it does not improve by further increasing the number of angular points to 302. The accuracy slightly increases by increasing the size of the outermost grid using MultiExp grid with 25 radial points. The 30(302) grid is the most accurate while 25(302) and 30(194) are almost of the same accuracy. SG0 and Becke are of comparable accuracies to our implementation of the 20 radial points MultiExp grid. The least accurate grid is TA. Our new implementation of the TA grid, TA(new), is almost an order of magnitude

more accurate than TA. SG-1 and TA(new) give almost the same accuracy. The third column of Table 3.2, molecules with atoms from the first and second rows, shows a similar trend for the MultiExp grids. The worst accuracy is given by the TA grid. The TA(new) grid is the most accurate grid and is more accurate than TA by more than an order of magnitude. For molecules containing third row atoms, TA is again the least accurate and the best accuracy is given by TA(new) while Becke and the nine MultiExp grids give nearly the same accuracy. For the transition states, 30(194) is the most accurate and TA is the least accurate. The performance of the MultiExp grids improves slightly by increasing the number of angular points in the outermost region. For complexes, 30(194), 30(302), TA(new) and SG-1 grids give better accuracies than the rest of the grids. The TA grid is the least accurate, almost two orders of magnitude less accurate than TA(new). For ions, 25(302) and 30(302) are the most accurate and TA is the least accurate. TA(new) and SG-1 grids are of comparable accuracies. SG0 performance is similar to our implementation of the MultiExp grid. For peptides, the 30(302) grid is the most accurate while TA is the least accurate. The 20(110) and Becke grids are of similar accuracy which is relatively low. The 25(194), 25(302), 30(194), TA(new) and SG-1 are of similar MAE which is around 2.0×10^{-4}, an order of magnitude less than that of the most accurate grid 30(302). The MAE of the benchmark grid is in the range of 1.2×10^{-7} to 2.5×10^{-8} which is extremely accurate. For all of the seven sets, the best accuracies are for the 30(194), 30(302), TA(new) and SG-1 grids while the performance of the 25(194) is reasonable.

3.2.2 Dipole Moment

The dipole moment is calculated using the formula:

$$\mu = \int \rho(\mathbf{r})\, \mathbf{r}\, d\mathbf{r} \tag{3.3}$$

Table 3.3 gives MAE for the different test sets with the 14 grids. For molecules containing first-row atoms, except for the TA grid, which gave an MAE of 4.6×10^{-3} au, the MAE for the rest of the thirteen grids was in the range of 9×10^{-4} au to 1.5×10^{-4} au. However, an improvement can be noticed as the number of angular points is increased in the outermost region from 110 to 194 and almost no improvement by increasing to 302 angular points for 20, 25 or 30 radial points. The same observation can be made for molecules containing second-row atoms. Table 3.3 shows that, for molecules containing atoms from the second and third rows, the TA grid was the least accurate. TA(new) is more accurate than TA and of the same accuracy as SG-1. It also shows that the SG0 grid performed as well as the 20(110) MultiExp grid. From the fourth column of Table 3.3, molecules containing third-row atoms, the MAE for the nine MultiExp grids, Becke and TA is almost the same and in the range of 1.3×10^{-2} au to 3.7×10^{-2} au while the MAE of TA(new) is 3.5×10^{-4} au, two orders of magnitude less than all of the other grids. For transition states, the error in calculating the dipole moment using 20(194) MultiExp grid is less than using 20(110). However, the error does not decrease by using the larger grid 20(302). The same pattern is also observed with the MultiExp grids of 25 radial points. The accuracy does not improve by increasing the grid size from 25(194) to 25(302) but the error decreases by increasing the grid from 25(110) to 25(194). The same trend

can be also observed in the dipole moment calculated using the MultiExp grids of 30 radial points. For complexes, the accuracy of 20(110), Becke, TA and SG0 are of the same order of magnitude and these grids are less accurate than the rest of the grids. It also shows that TA(new) and SG-1 are almost of the same accuracy. For ions, 20(110), 25(110), and 30(110) grids give almost the same accuracy which is less than the rest of the grids. The grid 25(302) gave the best accuracy, even better than 30(302). TA(new) is as accurate as SG-1, while SG0 is almost as accurate as 20(194). For peptides, Becke and TA grids were the least accurate grids while 30(302) was the most accurate. Again, TA(new) and SG-1 have the same accuracy. The general trend amongst the MultiExp grids is also clear. An angular grid of 194 angular points gives better accuracy than 110 while 302 does not offer an improvement over the 194 grid. The MAE of the benchmark grid for all sets is around 1.0×10^{-7} au. As in the case of number of electrons, the best performance for all sets was obtained by using 30(194), 30(302), TA(new) and SG-1.

3.2.3 Potential Energy

The potential energy between electrons and nuclei is given by:

$$V_{ne} = \sum_A Z_A \int \frac{\rho(\mathbf{r})}{|\mathbf{r} - \mathbf{R}_A|} \, d\mathbf{r} \tag{3.4}$$

where R_A is the position of the atom A of atomic charge Z_A. Table 3.4 gives MAE for the potential energy. For molecules containing first-row atoms, the highest MAE is given by the MultiExp grid of 20 radial points ($7.9 \times 10^5 \mu H$) while the lowest is given by SG-1 ($1.5 \times 10^3 \mu H$). The nine MultiExp grids from 20(110) to 30(302) give

MAE around $10^5 \mu H$. TA(new) gave MAE very close to that of SG-1. For molecules containing second-row atoms, the 20(110), 20(194), and 20(302) grids gave MAE of about 10^7 μH while the MAE for the rest of the MultiExp grids was around 10^6 μH. The most accurate grid was TA(new) followed by SG-1. For molecules containing atoms from the third row, the nine MultiExp grids gave similar accuracies while TA is slightly more accurate than TA(new). For transition states, the MultiExp grid of 20 radial points is the least accurate. Increasing the size of the outermost grid for the MultiExp grid of 20 radial points did not change the accuracy significantly, which is the same for MultiExp grids of 25 and 30 radial points. The most accurate grid for transition states is SG-1 followed by TA(new). For complexes, the MultiExp grid of 20 radial points was the least accurate grid while SG-1 is the most accurate. For complexes and ions, the nine MultiExp grids performed in a similar fashion as in the case of transition states. The most accurate grid for complexes is SG-1 while TA(new) is the most accurate grid for ions. For peptides, SG-1 is the most accurate grid followed by TA(new). The error in calculating the potential energy drops significantly when the benchmark grid is used, but is still relatively high. This huge error in potential energy suggests that the grids currently used for numerical integration are not suitable for the calculation of potential energy and that numerical integration is dependent on the form of the function to be integrated. Although the errors in calculating the potential energy using all of the 14 grids are large, the grids TA(new) and SG-1 performed relatively better than the rest of the grids. To our knowledge all DFT codes calculate the potential energy using analytical integration, probably

because it is more efficient. However, with these results, there is one more reason not to use numerical integration to calculate potential energy.

3.2.4 Coulomb Repulsion Energy V_{ee}^1

A double numerical integration was performed to calculate the Coulomb energy using the formula:

$$V_{ee}^1 = \int\int \frac{\rho(\mathbf{r}_1)\rho(\mathbf{r}_2)}{r_{12}} d\mathbf{r}_1 d\mathbf{r}_2 \tag{3.5}$$

where $\rho(\mathbf{r})$ is the electron density and r_{12} is the distance between two points $\mathbf{r_1}$ and $\mathbf{r_2}$. Table 3.5 shows MAE for V_{ee}^1 for all sets using all of the 14 grids, the error is consistently higher than 10^5 μH. These results imply that double numerical integration is very inaccurate. Using the benchmark grid, the error is still extremely high and in the range of 9.1×10^4 μH to 3.1×10^5 μH.

3.2.5 Coulomb Repulsion Energy V_{ee}^2

Since the double numerical integration is time consuming and very inaccurate, we recalculated the Coulomb energy using the formula:

$$V_{ee}^2 = \int \rho(\mathbf{r}_2)\left[\sum_{\mu\nu} P_{\mu\nu} \int \frac{\phi_\mu(\mathbf{r}_1)\phi_\nu(\mathbf{r}_1)d\mathbf{r}_1}{r_{12}}\right] d\mathbf{r}_2 \tag{3.6}$$

$P_{\mu\nu}$ is a density matrix element, ρ is the charge density and ϕ_μ and ϕ_ν are basis functions. The first integral, in the brackets, was performed analytically while the second integral was performed numerically. In density functional theory, equation 3.6

is used to calculate the Coulomb repulsion energy. Table 3.6 shows that for some of the data sets, molecules containing atoms from the first and third rows, complexes, and ions, the 20(110) grid is surprisingly more accurate than 25(194). An explanation for this apparently odd behaviour could be that the MultiExp grids of 20 and 25 radial points are too small to calculate the Coulomb energy and that their accuracies are unreliable. Another possible explanation may be that the R parameter is very critical for the accuracy of the numerical integration. Since R is optimized to give the best accuracy in the integration of the electron density, then, by reoptimizing R to give the most accurate Coulomb energy, the 20 and 25 grids may perform in a more reliable fashion. From Table 3.6, for molecules containing first-row atoms, the most accurate grid is 30(302) and the second most accurate is 30(194) and both of them are more accurate than TA(new) and SG-1. Compared to the rest of the grids, SG0 is of an average accuracy. The least accurate grid is the MultiExp grid 25(110). While the error for the 14 grids was in the range of 239 μH to 8960 μH, the error for the benchmark grid was incredibly small, 0.38 μH. For molecules containing atoms from the second row, TA(new) is by far the most accurate and its MAE is almost 30 times less than that of TA. SG-1 follows TA(new) in accuracy. The least accurate grid from the nine MultiExp grids is the 25(110) grid which is less accurate than the smaller grids 20(110) and SG0. The error varied from 675 μH to 11133 μH. The 20(194), 20(302), 30(110) and Becke grids are of similar accuracy, although they vary a lot in size. The benchmark grid is extremely accurate with a MAE of 1.81 μH. For molecules containing atoms from the third row, TA(new) is the most accurate grid. The largest error is of the MultiExp grid 25(302) which is a relatively large

grid. Again, the large errors for molecules containing third-row atoms, 445333 μH for 25(302), points to a serious problem either with the optimization of the parameter R or the MultiExp grid size. However, since the parameter R for the third-row atoms was optimized using the same technique used for the first and second-row atoms, we expect that the 20, 25, or 30 radial points grids are not large enough to calculate the Coulomb repulsion energy. Both Becke and TA grids are more accurate than the nine MultiExp grids. For transition states, the MultiExp grids performance is reasonable. For the 20, 25, and 30 radial MultiExp grids, the MAE decreases as the outermost angular grid increases from 110 to 194 angular points. However, the accuracy does not increase much as the size increases from 194 to 302 angular points. The 30(194) grid is the most accurate followed by TA(new). SG0 has a MAE almost equivalent to that of the 20(110), 25(110), and 30(110) grids. The MAE of the benchmark grid is only 1.63 μH. For complexes, TA(new) continued to be the most accurate followed by the 30(194) grid, while TA is the least accurate. For ions, 30(302) is the most accurate followed by TA(new). Again TA is by far the least accurate grid. For peptides, 30(302) is the most accurate while 30(194) is the second most accurate. In general, the accuracy of SG0 was consistent with that of 20(110). The overall performance of the TA(new) and SG-1 grids for the seven sets was the best. In general the 30(194) and 30(302) gave a relatively small MAE, however their poor performance for molecules containing third-row atoms makes them unreliable.

3.3 Some Interesting Observations

Table 3.7 gives the error in V_{ee}^2 using the Becke, TA, TA(new), SG-1, SG0, and benchmark grids for a series of five peptides ranging in size from one to five glycine amino acids. It is obvious from the table that the error changes randomly as the size of the peptide increases, even with some of the larger and more accurate grids, TA(new) and SG-1. For example, SG-1 predicts the error for 3G_pep to be smaller than the error for 2G_pep and the error with TA(new) jumps from -3,960 μH for 4G_pep to 5,890 μH for 5G_pep. The error in V_{ee}^2 increases consistently with the size of the peptide only when the benchmark grid is used. Using the benchmark grid, the error increased from 0.6 μH for 1G_pep to 24.9 μH for 5G_pep which is a relatively large error given the size of the benchmark grid. Since the benchmark grid is very time consuming, one can only wonder how big the error would be for much larger peptides and just how reliable the numerical integration would be using smaller grids.

3.4 The Effect of the Parameter R on the Integration

In Chapter 2, the parameter R of the MultiExp grid was optimized to give the best accuracy in the number of electrons. The R values were reoptimized to give the best accuracy in V_{ee}^2 for molecules containing atoms from the first and second rows. Table 3.8 gives the new R values for the MultiExp grid of 20 radial points along with the accuracy calculated using equation (2.1). Table 3.9 shows the error in the Coulomb potential V_{ee}^2 calculated using the old set of R values, R_1, and the new set

of R values, R_2. The overall MAE decreased from 8,280 μH to 7,231 μH. However, from Table 3.9, we notice that the error for the set of molecules containing chlorine did not change systematically. The error did not change for pNO_2BzCl, but changed in sign for HOCl and CH_2Cl_2, changed by half an order of magnitude in Cl_2, and dramatically changed in both sign and magnitude for NaCl, CH_3Cl, CCl_4, and ClF. The same pattern can be observed for the set of molecules containing phosphorous, P_2, PF_5, PH, CH_3PH_2, and $CH_2PH_2PH_2$ as well as the set containing sulfur, SO, SO_2, CH_3SH, and CH_2SHSH. Of special interest is the comparison of the molecules SO and SO_2. The error doubled for SO but increased more than an order of magnitude for SO_2. This analysis shows that the accuracy of the numerical integration using MultiExp grid is highly sensitive to the change in the parameter R. This dependence on R could explain the odd behaviour of MultiExp grid where a larger grid, 25(110), gave an overall mean absolute error larger than that of the smaller grid 20(110) (see the third column of Table 3.6).

3.5 Numerical Integration Efficiency

3.5.1 Number of Points of The Atomic Grid

Table 3.10 gives the number of points for the atomic grids except for SG0 where the number of points of SG0 can vary from one atom to another. The number of points of SG0 from hydrogen to chlorine is in the range of 1406 to 1480 which makes it one of the smallest grids and comparable in size to the 20(110) grid. Table 3.10 shows that except for H and He, the largest grid is the Becke grid followed by the TA grid. It can

be seen that the larger grids are not necessarily the most accurate grids and that the mapping and the radial quadrature play a crucial rule in determining the accuracy of the numerical integration. Also Table 3.10 shows that, except for H and He, the TA(new) grid is larger than the SG-1 grid, that the 30(194) grid is comparable in size to the SG-1 grid, and the 25(194) grid is medium in size between the SG0 and SG-1 grids.

3.5.2 Constructing the Atomic Grid Efficiently

To build the atomic grid around a nucleus, the radial points and their weights, the cartesian coordinates of the angular points, and the angular weights are required. The smallest grid SG0 consists of 1406 points for hydrogen while the largest grid, the Becke grid, can be as large as 8730 angular points. For large molecules, storing the atomic grid for each atom requires a large allocation of memory. To minimize the memory requirements for storing the atomic grid, we developed an algorithm [22] that only constructs the atomic grid for atoms of different atomic numbers, not for each atom in the molecule. For example the molecule C_2H_6 consists of eight atoms but it only has two atoms of different atomic numbers, hydrogen and carbon. For C_2H_6 our algorithm calculates the atomic grids for hydrogen and carbon at the center of the coordinate system. A linear transformation which involves the addition of the nuclear coordinates of a specific atom to the grid built at the centre of the coordinate system translates the grid to the position of the atom under consideration. The savings in building the grid using this algorithm will increase with the size of the molecule,

since the number of atoms of different atomic numbers could be the same or increase slightly.

3.6 Conclusions

The performance of the MultiExp grid was reexamined in addition to some of the well known grids, including the most recently developed grid SG0, and a benchmark grid. We used numerical integration to calculate the number of electrons, dipole moment, potential energy and Coulomb repulsion energy. In general, the most accurate grids are our new implementation of the Trutler and Alhrichs grid TA(new) and the standard grid SG-1. Increasing the size of the outermost grid of the MultiExp grid from 110 to 194 angular points improved the accuracy but increasing it further to 302 angular points did not. All the grids were very inaccurate in calculating the potential energy. The Coulomb energy calculations showed the inconsistency of the performance of the MultiExp grid. Also the random behaviour of the numerical integration, specifically with calculating Coulomb energy, was noticed with some of the larger grids such as SG-1 and TA(new).

Table 3.1: Set of molecules used for numerical integration calculations

1^{st} row	2^{nd} row	complexes	3^{rd} row	TS[a]	ions
BF_3	CCl_4	$(CH_2O_2)_2$	AsH_3	CH_3Cl_2	$ArNH_3^+$
BH_3	CH_2ClCl	FH-CO	CH_3Br	CH_3F_2	H_3^+O
BeH_2	$CH_2(PH_2)_2$	FH-FH	Ge_2H_6	CH_3FCl	$HCOO^-$
C_2H_2	CH_2SHSH	FH-NCH	Ge_3H_8	CH_5OF	$NH_3^+CH2COO^-$
C_2H_4	$CH_2(SiH_3)_2$	FH-NH_3	Ge_4H_{10}	Ethyl-OSO_2-CH_3	
CF_4	CH_3PH_2	FH-NN	Ge_5H_{12}	$BzCl^+CN^-$	
$CH_2CHCOOH$	CH_3SH	FH-OH_2	GeH_4		
CH_2FF	CH_3SiH_3	H_2O-CO_2	H_2Se		
$CH_2(CH_3)_2$	CH_3Cl	H_2O_H_2O			
CH_3F	CS				
CH_3NH_2	Cl_2				
CH_3OH	ClF				
CH_3CONH_2	HOCl				
CH_4	Mg				
CO	NaCl				
CO_2	P_2				
EtOTs	PF_5				
F_2	PH				
H_2	PH_3				
H_2CO	SF_6				
H_2O	SO				
H2O2	SO_2				
HCOOH	SiO				
Li_2	pNO_2BzCl[b]				
LiF	peptides				
LiH	1G_pep				
NH_3	2G_pep				
benzaldehyde	3G_pep				
cytosine	4G_pep				
formamidine	5G_pep				
methoxide					
naphthalene					
uracil					

[a] Transition states

[b] Para nitrobenzyl chloride

Table 3.2: Mean absolute error MAE for the number of electrons[a], equation (3.2)

grid	1^{st} row	2^{nd} row	3^{rd} row	TS[b]	complexes	ions	peptides
20(110)	4.3E-04	9.2E-04	8.2E-03	6.0E-04	4.5E-04	6.7E-04	1.3E-03
20(194)	2.5E-04	6.3E-04	8.4E-03	2.8E-04	4.2E-04	4.3E-04	6.8E-04
20(302)	2.4E-04	6.5E-04	8.5E-03	1.9E-04	4.2E-04	3.0E-04	6.2E-04
25(110)	5.1E-04	6.2E-04	6.1E-03	6.8E-04	4.1E-04	7.8E-04	7.1E-04
25(194)	1.2E-04	3.6E-04	6.2E-03	1.2E-04	2.1E-04	1.5E-04	2.4E-04
25(302)	7.9E-05	3.2E-04	6.2E-03	1.7E-04	2.0E-04	4.6E-05	2.7E-04
30(110)	4.7E-04	5.7E-04	5.9E-03	6.5E-04	2.6E-04	7.6E-04	8.8E-04
30(194)	6.9E-05	2.2E-04	6.0E-03	8.5E-05	5.2E-05	1.4E-04	1.1E-04
30(302)	2.9E-05	1.8E-04	6.0E-03	1.1E-04	4.7E-05	3.1E-05	1.2E-05
Becke	5.6E-04	8.4E-04	4.5E-03	2.5E-03	3.5E-04	3.8E-04	2.8E-03
TA	2.2E-03	2.7E-03	1.2E-02	2.9E-03	1.7E-03	1.9E-03	4.8E-03
TA(new)	1.8E-04	8.3E-05	2.5E-04	1.2E-04	4.6E-05	1.3E-04	2.8E-04
SG-1	1.3E-04	2.9E-04	NA	2.2E-04	4.1E-05	2.2E-04	2.1E-04
SG0	3.7E-04	5.0E-04	NA	7.0E-04	2.1E-04	4.4E-04	5.2E-04
Benchmark	3.4E-08	1.2E-07	NA	1.5E-07	2.5E-08	8.4E-08	6.0E-08[c]

[a] See Table 3.1 for list of molecules

[b] Transition states

[c] Only 1G_pep and 2G_pep are calculated

Table 3.3: Mean absolute error of the dipole moment[a] au, equation (3.3)

grid	1^{st} row	2^{nd} row	3^{rd} row	TS[b]	complexes	ions	peptides
20(110)	9.0E-04	1.7E-03	2.0E-02	1.4E-03	1.2E-03	1.7E-03	9.5E-03
20(194)	6.1E-04	3.7E-04	2.2E-02	5.6E-04	8.4E-04	7.0E-04	5.6E-03
20(302)	5.3E-04	5.0E-04	2.2E-02	5.0E-04	8.8E-04	4.9E-04	4.4E-03
25(110)	8.7E-04	1.4E-03	1.5E-02	9.9E-04	9.3E-04	1.9E-03	6.7E-03
25(194)	3.5E-04	4.4E-04	1.7E-02	2.6E-04	2.9E-04	1.6E-04	1.0E-03
25(302)	2.9E-04	2.6E-04	1.7E-02	2.9E-04	2.6E-04	2.3E-05	1.9E-03
30(110)	7.3E-04	1.4E-03	1.5E-02	1.1E-03	9.9E-04	1.9E-03	7.5E-03
30(194)	2.4E-04	2.7E-04	1.6E-02	1.9E-04	2.3E-04	2.5E-04	9.0E-04
30(302)	1.5E-04	1.5E-04	1.6E-02	1.8E-04	1.7E-04	9.1E-05	1.8E-04
Becke	8.6E-04	1.9E-03	1.3E-02	3.4E-03	1.7E-03	6.0E-04	2.0E-02
TA	4.6E-03	4.9E-03	3.7E-02	7.7E-03	6.5E-03	6.2E-03	4.6E-02
TA(new)	3.9E-04	2.1E-04	3.5E-04	3.2E-04	2.0E-04	4.8E-04	2.1E-03
SG-1	2.8E-04	3.3E-04	NA	4.7E-04	1.7E-04	3.9E-04	2.1E-03
SG0	7.1E-04	1.3E-03	NA	1.3E-03	1.1E-03	8.0E-04	2.4E-03
Benchmark	4.2E-08	2.0E-07	NA	1.9E-07	1.3E-07	1.1E-07	1.9E-07[c]

[a] See Table Table 3.1 for list of molecules

[b] Transition states

[c] Only 1G_pep and 2G_pep are calculated

Table 3.4: Mean absolute error of the potential energy[a] V_{ne} (μH), equation (3.4)

grid	1^{st} row	2^{nd} row	3^{rd} row	TS[b]	complexes	ions	peptides
20(110)	7.9E+05	1.5E+07	1.5E+08	9.8E+06	5.9E+05	6.1E+05	2.0E+06
20(194)	7.9E+05	1.5E+07	1.5E+08	9.9E+06	5.9E+05	6.1E+05	2.0E+06
20(302)	7.9E+05	1.5E+07	1.5E+08	9.9E+06	5.9E+05	6.1E+05	2.0E+06
25(110)	3.8E+05	7.4E+06	1.2E+08	4.8E+06	2.8E+05	3.1E+05	1.0E+06
25(194)	3.8E+05	7.4E+06	1.2E+08	4.8E+06	2.8E+05	3.0E+05	1.0E+06
25(302)	3.8E+05	7.4E+06	1.2E+08	4.8E+06	2.8E+05	3.0E+05	1.0E+06
30(110)	1.9E+05	3.7E+06	1.3E+08	2.4E+06	1.4E+05	1.5E+05	4.8E+05
30(194)	1.9E+05	3.7E+06	1.3E+08	2.4E+06	1.4E+05	1.4E+05	4.7E+05
30(302)	1.9E+05	3.7E+06	1.3E+08	2.4E+06	1.4E+05	1.4E+05	4.8E+05
Becke	6.0E+03	2.9E+04	6.8E+05	4.8E+04	4.8E+03	3.1E+03	6.4E+04
TA	1.6E+04	3.9E+04	1.8E+05	3.0E+04	1.8E+04	3.1E+04	6.7E+04
TA(new)	2.2E+03	5.8E+03	3.0E+05	5.7E+03	1.8E+03	1.0E+03	6.2E+03
SG-1	1.5E+03	6.5E+03	NA	4.4E+03	8.0E+02	3.1E+03	3.8E+03
Benchmark	15.8	337.0	NA	195.5	10.9	10.4	21.6[c]

[a] See Table Table 3.1 for list of molecules

[b] Transition states

[c] Only 1G_pep and 2G_pep are calculated

Table 3.5: Mean absolute error of the Coulomb energy[a] V_{ee}^{1} (μH), equation (3.5)

grid	1^{st} row	2^{nd} row	3^{rd} row	TS[b]	complexes	ions	peptides
20(110)	1.7E+06	9.1E+06	4.5E+07	7.2E+06	1.8E+06	1.9E+06	6.4E+06
20(194)	1.7E+06	9.0E+06	4.5E+07	7.1E+06	1.7E+06	1.9E+06	6.3E+06
20(302)	1.6E+06	9.0E+06	4.4E+07	7.1E+06	1.7E+06	1.9E+06	6.2E+06
25(110)	1.1E+06	6.4E+06	4.2E+07	5.0E+06	1.1E+06	1.3E+06	4.3E+06
25(194)	1.1E+06	6.4E+06	4.3E+07	5.0E+06	1.1E+06	1.3E+06	4.2E+06
25(302)	1.1E+06	6.4E+06	4.2E+07	4.9E+06	1.1E+06	1.2E+06	4.1E+06
30(110)	8.2E+05	4.3E+06	4.1E+07	3.5E+06	8.9E+05	8.7E+05	3.1E+06
30(194)	8.2E+05	4.3E+06	4.1E+07	3.4E+06	8.6E+05	9.3E+05	3.1E+06
30(302)	8.0E+05	4.3E+06	4.1E+07	3.4E+06	8.6E+05	9.1E+05	3.0E+06
Becke	5.2E+05	1.6E+06	1.0E+07	1.6E+06	6.3E+05	6.3E+05	2.0E+06
TA	4.6E+05	1.4E+06	8.9E+06	1.4E+06	5.5E+05	5.4E+05	1.9E+06
TA(new)	6.3E+05	2.0E+06	1.3E+07	1.9E+06	7.6E+05	7.4E+05	2.5E+06
SG-1	2.4E+05	2.7E+05	NA	3.9E+05	1.7E+05	3.2E+05	9.9E+05
SG0	1.6E+06	6.2E+06	NA	6.2E+06	2.2E+06	1.9E+06	6.3E+06
Benchmark	9.1E+04	3.1E+05	NA	2.8E+05	1.1E+05	1.0E+05	1.9E+05[c]

[a] See Table Table 3.1 for list of molecules

[b] Transition states

[c] Only 1G_pep and 2G_pep are calculated

Table 3.6: Mean absolute error of the Coulomb energy[a] V_{ee}^2 (μH), equation (3.6)

grid	1^{st} row	2^{nd} row	3^{rd} row	TS[b]	complexes	ions	peptides
20(110)	2,685	8,280	379,000	5,191	2,676	3,292	14,594
20(194)	3,219	5,746	382,667	3,515	3,231	5,030	12,622
20(302)	3,051	6,052	384,333	3,032	3,233	3,907	11,632
25(110)	8,960	11,133	444,111	4,048	1,933	3,958	7,345
25(194)	2,170	9,504	443,667	3,109	983	1,129	3,560
25(302)	1,840	9,385	445,333	2,966	928	654	4,176
30(110)	2,344	5,728	441,444	5,117	1,132	3,696	9,354
30(194)	481	3,390	440,111	793	194	1,248	1,248
30(302)	239	3,066	442,778	1,157	225	282	286
Becke	2,912	5,083	68,116	14,725	1,753	1,235	28,768
TA	7,930	20,587	138,228	14,632	8,285	14,225	33,628
TA(new)	991	675	2,208	844	152	442	2,890
SG-1	727	2,428	NA	1,166	266	1,460	1,915
SG0	2,535	9,510	NA	4,987	2,241	2,807	5,545
Benchmark	0.38	1.81	NA	1.63	0.22	0.23	2.07[c]

[a] See Table Table 3.1 for list of molecules

[b] Transition states

[c] Only 1G_pep and 2G_pep are calculated

Table 3.7: The error in V_{ee}^2 (μH) for peptides using Becke, TA, TA(new), SG-1, SG0, Benchmark

Molecule	Becke	TA	TA(new)	SG-1	SG0	Benchmark
1G_pep	-3,570	-7,580	-382	-263	-215	0.6
2G_pep	21,100	-49,000	-1,260	-1,390	-6,460	3.6
3G_pep	6,070	-20,100	-2,960	783	-4,350	6.8
4G_pep	14,200	-86,200	-3,960	-1,440	-8,710	13.4
5G_pep	98,900	-5,260	5,890	5,700	-7,990	24.9
MAE	28,768	33,628	2,890	1,915	5,545	9.8

Table 3.8: The new R parameters[a] for atoms from the first and second rows and the corresponding accuracies

Atom	Molecule	R	Accuracy[b]
H	H_2	0.852	6.5
Li	LiH	1.700	4.3
C	CH_4	1.233	8.3
N	NH_3	1.042	7.1
O	H_2O	0.756	7.5
F	HF	0.694	7.6
Na	Na_2	2.008	7.6
Mg	Mg_2	1.851	7.6
Si	SiH_4	1.573	6.3
P	PH_3	1.445	6.3
S	H_2S	1.356	6.1
Cl	HCl	1.268	6.0

[a] Optimized to give the best accuracy in V_{ee}^2
[b] as defined by equation (2.1)

Table 3.9: The error in V_{ee}^2 (μH) for molecules containing second-row atoms using two sets of R parameters.

Molecule	error in V_{ee}^2 ($R_1{}^a$)	error in V_{ee}^2 ($R_2{}^b$)
Cl_2	-9.2E+03	-3.43E+03
ClF	-1.3E+03	5.92E+03
HOCl	-3.7E+03	2.66E+03
pNO_2BzCl	4.9E+04	5.17E+04
NaCl	-1.8E+04	1.78E+03
CH_3Cl	-2.9E+03	3.16E+02
CCl_4	-7.8E+02	1.23E+04
CH_2Cl_2	-2.8E+03	4.20E+03
Mg	5.4E+04	1.25E+03
P_2	-4.5E+03	-2.87E+02
PF_5	-1.7E+03	1.60E+04
PH	-2.2E+03	1.03E+03
$CH_2(PH_2)_2$	-1.1E+04	-3.29E+03
CH_3PH_2	-4.2E+03	-1.83E+03
CS	-1.1E+03	8.56E+02
SF_6	5.4E+03	2.62E+04
SO	-2.1E+03	3.76E+03
SO_2	-8.4E+02	1.37E+04
$CH_2(SH)_2$	-8.5E+03	-2.57E+03
CH_3SH	-1.9E+03	1.24E+03
SiO	-2.2E+02	5.73E+03
CH_3SiH_3	-2.0E+03	2.56E+03
$CH_2(SiH_3)_2$	-4.1E+03	3.71E+03
MAE	8,280	7,231

[a] Optimized to give the best accuracy in number of electrons
[a] Optimized to give the best accuracy in V_{ee}^2

Table 3.10: Number of points of the atomic grids

	Atom			
Grid	H,He	Li-Ne	Na-Ar	K-Kr
20(110)	1432	1432	1432	1432
20(194)	2104	2104	2104	2104
20(302)	2968	2968	2968	2968
25(110)	1934	1934	1934	1934
25(194)	2858	2858	2858	2858
25(302)	4046	4046	4046	4046
30(110)	2436	2436	2436	2436
30(194)	3612	3612	3612	3612
30(302)	5124	5124	5124	5124
Becke	2200	6790	7760	8730
TA[a]	3300	5890	6572	7506
TA(new)	2484	4990	5960	6930
SG-1[b]	3752	3816	3760	NA

[a] These values are taken from reference [12]
[b] These values are taken from reference [15]

Chapter 4

Projection Between Basis Sets

4.1 Introduction

In general projection means a transformation from a larger dimension to a smaller dimension which includes a loss of information as in the case of projecting a 3-dimensional vector on a plane or projecting a vector from a plane on a line. What we mean by projection in this chapter, and throughout this thesis, is exactly the opposite, namely, projecting from a smaller dimension to a larger one. Our goal is to use the Fock matrix, density matrix, etc. that are available at the end of an SCF using a small basis such as STO-3G to predict the corresponding values for a larger basis set such as 6-31G(d).

Section 4.2 presents the relationship between different basis sets of the same vector space. Section 4.3 is an overview of the projection algorithm for the molecular coefficients that already existed in MUNgauss. Section 4.4 introduces our new version

of the projection algorithm. The rest of the chapter discusses new ways to improve the projection algorithm along with its performance.

4.2 Change of Basis

If $X = \{x_1(\mathbf{r}), \ldots, x_n(\mathbf{r})\}$ and $Y = \{y_1(\mathbf{r}), \ldots, y_n(\mathbf{r})\}$ are complete basis sets of a vector space V then, any vector $A(\mathbf{r}) \in V$ can be written as a linear combination of X as follows [1]:

$$A(\mathbf{r}) = \sum_{i}^{n} a_i x_i(\mathbf{r}) \tag{4.1}$$

and of Y as:

$$A(\mathbf{r}) = \sum_{j}^{n} b_j y_j(\mathbf{r}) \tag{4.2}$$

where $\{a_i\}$ and $\{b_j\}$ are the components of the vector $A(\mathbf{r})$ in the basis sets X and Y respectively. In addition if X and Y are orthonormal basis sets then:

$$\int x_i^*(\mathbf{r}) x_j(\mathbf{r}) d\mathbf{r} = \delta_{ij} \tag{4.3}$$

$$\int y_i^*(\mathbf{r}) y_j(\mathbf{r}) d\mathbf{r} = \delta_{ij} \tag{4.4}$$

where δ_{ij} is the Kronecker delta function. Any basis vector $x_j \in X$ can be written in terms of the basis set Y as [1]:

$$x_j = \sum_{i} y_i u_{ij} \tag{4.5}$$

Similarly a basis vector $y_j \in Y$ can be written in terms of the basis set X as:

$$y_j = \sum_i x_i u_{ij}^* \tag{4.6}$$

where u_{ij} are the elements of a unitary matrix U and defined as:

$$u_{ij} = \int x_i^*(\mathbf{r}) y_j(\mathbf{r}) d\mathbf{r} \tag{4.7}$$

Thus the two complete and orthonormal basis sets $\{X\}$ and $\{Y\}$ are related by a unitary transformation U which is the overlap matrix between $\{X\}$ and $\{Y\}$. If O_x is the matrix representation of an operator $\hat{O}$ in the basis $\{X\}$ and O_y is another matrix representation in the basis $\{Y\}$ then O_x and O_y are related by the unitary transformation U as follows [1]:

$$O_x = U O_y U^\dagger \tag{4.8}$$

Equation (4.8) represents the theoretical foundation for the projection of a matrix representation of an operator from a basis set to another.

4.3 Projection of the Molecular Coefficients

If at the end of an SCF which is carried out using basis set $X = \{x_1, \ldots, x_n\}$, we have the coefficient matrix C_x, the corresponding coefficient matrix C_y defined for a basis set Y where $Y = \{y_1, \ldots, y_m\}$ and $m > n$ can be approximated by the equation [14]:

$$C_y = S_y^{-1} U C_x \tag{4.9}$$

where U is a rectangular matrix of dimension $m \times n$ and represents the overlap between the two basis sets X and Y and S_y is the overlap matrix in the basis Y. While C_x is a square matrix of dimensions $n \times n$ and its columns represent the molecular coefficients in the basis set X, C_y is a rectangular matrix of dimension $m \times n$. The n columns of C_y represent the new representation of C_x in the basis set Y. To make C_y a square matrix, $m - n$ more columns are needed. MUNgauss uses the eigenvectors of S_y in conjunction with the n columns of C_y to produce the additional $m - n$ columns.

4.4 Projection of the Fock Matrix

The theoretical basis of our approach lies in the fact that the choice of the basis of a vector space is not unique [1], where in this context the elements of the vector space are the eigenfunctions of the Fock operator $\hat{f}$. In general if F_x is the matrix representation of the Fock operator in the basis set $X = \{x_1, \ldots, x_n\}$ and F_y is another matrix representation of $\hat{f}$ in the basis set $Y = \{y_1, \ldots, y_n\}$ where both basis sets are orthonormal, then F_x and F_y are related by a unitary transformation U, equation (4.8) :

$$F_y = U F_x U^{\dagger} \tag{4.10}$$

where the elements of the matrix U are given by equation (4.7). In practice the basis sets are not orthogonal and are of different size. One way to deal with the non-

orthogonality of the basis is to orthogonalize F_x, transform to F_y and then unorthogonalize F_y. The orthogonalization can be achieved easily by using the transformation [1]:

$$F_x^o = S_x^{-1/2} F_x S_x^{-1/2} \tag{4.11}$$

where F_x^o is the orthogonalized Fock matrix and S_x is the overlap matrix in the basis set X. Since X and Y are of different sizes, the transformation matrix U is a rectangular matrix and hence is not unitary. Then a straight forward transformation of the Fock matrix F_x to F_y where F_y is of higher dimension using equation (4.10) would be:

$$F_y = S_y^{1/2} S_{yx} S_x^{-1/2} F_x S_x^{-1/2} S_{xy} S_y^{1/2} \tag{4.12}$$

where S_{yx} is the overlap between the basis sets X and Y. The purpose of the multiplication from both sides by $S_y^{1/2}$ is to obtain the unorthogonalized Fock matrix F_y in the new basis Y which is the reverse of the transformation (4.11). The unitary characteristic of the transformation matrix U, equation (4.10), is a direct consequence of the orthonormality of the basis sets. Therefore, to make the transformation matrix S_{yx} as "unitary" as possible, we multiply S_{yx} by $S_y^{-1/2}$ from the left and by $S_x^{-1/2}$ from the right. Thus equation (4.12) becomes:

$$F_y = S_y^{1/2}(S_y^{-1/2} S_{yx} S_x^{-1/2})(S_x^{-1/2} F_x S_x^{-1/2})(S_x^{-1/2} S_{xy} S_y^{-1/2}) S_y^{1/2} \tag{4.13}$$

or

$$F_y = S_{yx} S_x^{-1} F_x S_x^{-1} S_{xy} \tag{4.14}$$

An inevitable hurdle is that the basis sets X and Y are incomplete. So even if we use two basis sets of equal size like 3-21G and 6-31G the transformation (4.14) is not exact. It is only exact for a transformation from a basis set to itself.

4.5 Improving Projection I

As was stated in the introduction, our goal of studying projection is to skip calculating some of the Fock matrix elements and to use the projected values instead. Therefore, the more accurate the projection is, the closer the Fock matrix will be to the exact one. The following two subsections present some of our attempts at increasing the accuracy of projection.

4.5.1 A Better Transformation Matrix

One way to make the projection more accurate is to improve the matrix S_{yx}. Equation (4.14) can be rewritten as:

$$S_{yx} F'_x S_{xy} = F_y \tag{4.15}$$

where

$$F'_x = S_x^{-1} F_x S_x^{-1} \tag{4.16}$$

Multiplying equation (4.15) from right by S_{yx} we obtain:

$$S_{yx}F'_xS_{xy}S_{yx} = F_yS_{yx} \tag{4.17}$$

$$S_{yx}F'_xr_x = F_yS_{yx} \tag{4.18}$$

where, $r_x = S_{xy}S_{yx}$, and

$$S_{yx} = F_yS_{yx}(F'_xr_x)^{-1} \tag{4.19}$$

or

$$S^{n+1}_{yx} = F_yS^n_{yx}(F'_xr_x)^{-1} \tag{4.20}$$

We start with the overlap matrix S_{yx} and then solve equation (4.20) iteratively for S_{yx} until we reach convergence. This algorithm was implemented but did not converge.

4.5.2 Mixing Exact and Projected Values

The Fock matrix can be written as a sum of the matrices H and G as follows:

$$F_x = H_x + G_x \tag{4.21}$$

where H_x is the matrix representation of the core Hamiltonian, G_x represents the electron-electron repulsion part of the Fock operator, and both are defined over the basis set X. Multiplying both sides of equation (4.21) from the left by $S_{yx}S_x^{-1}$ and from right by $S_x^{-1}S_{xy}$, we obtain:

$$S_{yx}S_x^{-1}F_xS_x^{-1}S_{xy} = S_{yx}S_x^{-1}H_xS_x^{-1}S_{xy} + S_{yx}S_x^{-1}G_xS_x^{-1}S_{xy} \tag{4.22}$$

which can be rewritten as:

$$F_y = H_y + G_y \tag{4.23}$$

Where H_y and G_y are the projected H_x and G_x matrices to the basis Y, respectively. From now on the subscript p will be used to denote the projected results and no subscripts will be used for the exact matrices.

Since the computational cost of calculating the H matrix is low, in general, H_p could be replaced by H and equation (4.23) becomes:

$$F_p = H + G_p \tag{4.24}$$

Using H instead of H_p in equation (4.24) makes it appealing to assume that F_p will be more accurate than the projected Fock matrix calculated by equation (4.23). By substituting some of the Fock matrix elements by elements from F_p calculated using equation (4.24), the SCF either did not converge or converged to a completely wrong answer. Since H is exact then the error must be totally in G_p. This conclusion was the beginning of the quest for a more accurate projection of the G matrix.

4.6 Improving Projection II

The exact Fock matrix F can be written as:

$$F = H + G \tag{4.25}$$

while the projected Fock matrix is given by:

$$F_p = H_p + G_p \tag{4.26}$$

Defining δ as the matrix which transforms H_p to H:

$$H_p\delta = H \tag{4.27}$$

where,

$$\delta_{ij} = \frac{H_{ij}}{(H_p)_{ij}} \tag{4.28}$$

The matrix δ serves as a correction to H_p to give the exact H. Assume that δ can be used to calculate the matrix G_c as follows

$$(G_c)_{ij} = \delta_{ij}(G_p)_{ij} \tag{4.29}$$

Since δ_{ij} is not defined for $(H_p)_{ij} = 0$, we used the following formula to calculate the corresponding $(G_c)_{ij}$:

$$(G_c)_{ij} = -1.8H_{ij} \tag{4.30}$$

δ corrects H_p to H, but it will only be a correction to G_p if $\|G - G_c\| < \|G - G_p\|$ where the following definition of the norm of a matrix A is used:

$$\| A \| = \sum_{ij} a_{ij}^2 \tag{4.31}$$

After a great deal of experimenting it was found that using a slightly different formula:

$$(G_c)_{ii} = 1.25\delta_{ii}(G_p)_{ii} \tag{4.32}$$

to calculate the diagonal elements of the G_c matrix for the d-type basis functions could improve the results. To test the improvement in the projection of the G matrix the following quantities:

$$\|\Delta G_p\| = \|G - G_p\| \tag{4.33}$$

$$\|\Delta G_c\| = \|G - G_c\| \tag{4.34}$$

were calculated for a test set of 21 molecules containing atoms from the first and second rows. The projection was performed from STO-3G to the basis sets: 3-21G, 6-31G, and 6-31G(d), see Table 4.1, Table 4.2 and Table 4.3.

In all of the tables, 1G_pep, 2G_pep, 3G_pep, 4G_pep stand for one, two, three, and four glycine amino acids, respectively. From Table 4.1, G_c is more accurate than G_p except in three cases: 2G_pep, 4G_pep and CH_3CONH_2. It is also obvious from Table 4.2 that G_p can in general be improved by the algorithm given by equation (4.28) to equation (4.32) except for 3G_pep, $CH_2PH_2PH_2$, and CH_2SHSH. The inconsistency in the improvement of the projection can also be noticed in Table 4.3. We performed a similar study for the projection from 3-21G to 6-31G and 6-31G(d), and from 6-31G to 6-31G(d) and the same pattern was observed, i.e. the projection of the G matrix can be improved but will arbitrarily fail in some cases, which makes it unreliable.

4.7 The Relation Between H, G, and F

As was stated in section 4.4, the projected Fock matrix can be calculated using one of the following formulas:

$$F_p = H_p + G_p \tag{4.35}$$

$$F'_p = H + G_p \tag{4.36}$$

To study the relation between H_p, G_p, and F_p and H, G, and F, let us define x_p and x as follows:

$$(x_p)_{ii} = \frac{(G_p)_{ii}}{(H_p)_{ii}} \tag{4.37}$$

$$x_{ii} = \frac{G_{ii}}{H_{ii}} \tag{4.38}$$

Table 4.4 shows the diagonal elements of the matrices H, H_p, G, and G_p in addition to x and x_p for the molecule SiH_4 where the projection was performed from STO-3G to 6-31G(d). Table 4.5 gives the values of the diagonal elements of the matrices F, F_p, and F'_p. Table 4.5 shows that the elements $(F_p)_{ii}$ where $i = 1, \ldots, 6$ are better estimates of F_{ii} than $(F'_p)_{ii}$ for the same set of basis functions (d-type basis functions in this case). The projection using equation (4.35) is more accurate than using equation (4.36) contrary to our earlier assumption that using H instead of H_p would give better accuracy. The value of x_p is very close to that of x for each basis function i which suggests that projection maintains the ratio between the elements of

G and H. It is obvious that the error introduced by the projection of G is canceled to some extent by the error in the projection of H. We noticed a similar pattern for other molecules such as 1G_pep, 2G_pep. Figure 4.1 shows the elements of H versus the elements of H_p for 1G_pep. Some of the elements of the H_p matrix have values close to zero while their exact values are much different than zero. The same observation can be made from Figure 4.2 which represents the elements of the G matrix against those of G_p for 1G_pep. Projection poorly predicts some of the large elements of the G matrix to be much smaller than their exact values. However, projection predicts the elements of F more accurately as shown in Figure 4.3. The same pattern can be noticed for CCl_4, Ge_5H_{12} and Sn_4H_{10} as seen in Figures 4.4 - 4.12. Those four molecules were carefully chosen to represent elements of the four first rows of the periodic table.

To further investigate the error introduced in H, G, and F, the following quantities were calculated:

$$\|\Delta H_p\| = \|H - H_p\| \tag{4.39}$$

$$\|\Delta G_p\| = \|G - G_p\| \tag{4.40}$$

$$\|\Delta F_p\| = \|F - F_p\| \tag{4.41}$$

Table 4.6 gives $\|\Delta H_p\|$, $\|\Delta G_p\|$ and $\|\Delta F_p\|$ for four sets of molecules representing the first, second, third, and fourth rows of the periodic table in addition to a series of peptides. It is clear from Table 4.6 that the error in F_p compared to the exact Fock

matrix F is consistently far smaller than the errors in both matrices H_p and G_p and that,

$$\|\Delta F_p\| \approx \|\Delta G_p\| - \|\Delta H_p\| \tag{4.42}$$

which confirms that the errors in H_p and G_p almost cancel each other giving F_p of higher accuracy than both of H_p and G_p. The error cancellation decreases as we progress to the third and fourth rows of the periodic table.

We tested the projection of the Fock matrix for a set of molecules containing atoms of the first four rows of the periodic table among the following basis sets: STO-3G, 3-21G, 6-31G, STO-3G(d), 6-31G(d), and 6-311G(d). To measure the error of the projection irrespective of the Fock matrix size or the values of its elements, we calculated the relative error in F_p as follows:

$$\text{relative error } = \frac{\| F - F_p \|}{\| F \|} \tag{4.43}$$

The first column in each of Tables 4.7 - 4.10 gives the basis sets projected from and the basis sets projected to, while the second, third , fourth, and the fifth columns give the relative error in the Fock matrix for molecules containing atoms from the first, second, third, or the fourth rows. The last column in each table gives the sum of the relative errors for each row for a projection from a basis set X to a basis set Y. From Table 4.7, the smallest sum of relative errors is that of the projection from 3-21G to 6-31G where the two basis sets are of equal size. Table 4.7 also shows that the projection from 3-21G or 6-31G to any of the basis sets STO-3G(d), 6-31G(d), and 6-311G(d) is almost equal to that from STO-3G to 6-31G(d) and 6-311G(d)

and in the range of 0.7031 to 0.7974. Since the difference in the basis set size is the largest for STO-3G to 6-311G(d), projection from STO-3G to 6-311G(d) would be more efficient. If a higher accuracy is required, a projection from STO-3G to 6-31G or from STO-3G(d) to 6-31G(d) is more accurate than any of the projections mentioned above, e.g. STO-3G to 6-31G(d). From Table 4.8, it is obvious that the most accurate projection is the one from 3-21G to 6-31G. The sums of the relative errors are in general smaller than the sums of the relative errors of Table 4.7 except for the projections from STO-3G, 3-21G, 6-31G, or 6-31G(d) to 6-311G(d) which are slightly higher than that of Table 4.7. The projection from STO-3G to 6-31G is relatively small. Table 4.9 and Table 4.10 show that for every projection from a basis set X to Y, the relative errors for molecules containing elements of the third and fourth rows are less than those of the first or the second rows see Table 4.7 and Table 4.8, respectively. From both tables the sum of the relative errors is consistently less than 0.1 for each projection. The projection from STO-3G to 3-21G is almost of the same accuracy as from STO-3G to 6-31G and therefore we recommend the projection from STO-3G to 6-31G. It is obvious from Tables 4.7, 4.8, 4.9, and 4.10 that, as the difference in size between the basis set projected from and the basis set projected to increases, the relative error increases as well.

The exact electronic energy is calculated by the formula:

$$E = \frac{1}{2}\mathrm{Tr}P\left(H + F\right) \tag{4.44}$$

Therefore the projected electronic energy can be calculated by:

$$E_{proj} = \frac{1}{2}\mathrm{Tr}P_p\left(H_p + F_p\right) \tag{4.45}$$

and the percentage error in the projected electronic energy relative to the exact electronic energy is given by:

$$\Delta E\% = \left(\frac{E - E_{proj}}{E}\right) \times 100\% \tag{4.46}$$

Tables 4.11 - 4.14 give $\Delta E\%$ for four sets of molecules containing atoms from the first, second, third and fourth rows for the projection among the basis sets shown in the first column of each table. The sum of the $\Delta E\%$ for each row is given in the last column of each table. The smallest $|\Delta E\%|$ was for the projection from 6-31G to 6-31G(d) followed by the projection from STO-3G to STO-3G(d). In addition, for all of the four tables, the projection from 3-21G to any other basis set is less accurate than the projection from STO-3G to the other basis sets except in the case of the projection from STO-3G to STO-3G(d). From Table 4.11, the projection from STO-3G to STO-3G(d) is far more accurate than the projection to 3-21G or 6-31G although STO-3G(d) is larger in size than 3-21G and 6-31G. The same observation can also be made for the projection from 3-21G to STO-3G(d) and 6-31G(d) which suggests that the difference in size between basis sets is not the only factor in determining the accuracy of the projection. How closely the basis sets are built is also important.

Equation (4.45) reflects the error in P_p, H_p, and F_p. To minimize the error, the projected energy was calculated using H and equation (4.45) becomes:

$$E_{proj} = \frac{1}{2}\mathrm{Tr}P_p\left(H + F_p\right) \tag{4.47}$$

Tables 4.15, 4.16, 4.17, and 4.18 give the percentage errors in the electronic energy using equation (4.47) for the same four sets of molecules. From Table 4.15, the error of the projection from 6-31G to 6-31G(d) is far less than the projection from the same basis set to STO-3G(d) although 6-31G(d) is larger than STO-3G(d). From Table 4.16, it is interesting to note that the projection from 3-21G to 6-31G is less accurate than the projection from 3-21G to 6-31G(d). Also, the projection from 6-31G to both of 6-31G(d) and 6-311G(d) is very accurate. A peculiar behaviour of the projection can be noticed from Table 4.18 where the projection from STO-3G to 6-31G(d) is more accurate than the projection to 6-31G. From Tables 4.15, 4.16, 4.17 and 4.18 the projection from 3-21G to 6-31G has a similar accuracy to the projection to 6-31G(d) therefore , the projection from 3-21G to 6-31G(d) is more favoured. Also the projection from STO-3G to 6-31G or 6-31G(d) is reasonable although it is less accurate compared to the projection from 3-21G for the second and fourth rows. The percentage error using H is much lower, as expected, than the percentage error using H_p. The percentage error for all molecules is under 1%, and it is amazingly small for the projection from STO-3G to 6-31G(d) for molecules of the third row elements.

To study the relationship between the molecule size and the projection, the relative error in the Fock matrix was calculated using equation(4.43) for three series of molecules. The first series is 1G_pep, 2G_pep, 3G_pep, 4G_pep, and 5G_pep, the second series is SiH_4, Si_2H_6, Si_3H_8, Si_4H_{10}, Si_5H_{12}, and Si_6H_{14}, and the third series is GeH_4, Ge_2H_6, and Ge_3H_8. Tables 4.19, 4.20 and 4.21 show the relative error in the Fock matrix for the three series. Table 4.19 shows that the relative error is almost constant for each projection from a basis set X to a basis set Y as the size of the

molecule increases from 1G_pep to 5G_pep. The same observation is also true for the second and the third series, as seen in Tables 4.20 and 4.21. The projection from 3-21G to 6-31G is the most accurate, while the projection from STO-3G to 6-31G is second in accuracy. However, there is more gain in projecting from STO-3G to 6-31G so we recommend the projection from STO-3G to 6-31G when possible.

4.8 Conclusions

We developed an algorithm to project the Fock matrix from a smaller basis set to a larger basis set. This algorithm gave poor results when the exact H matrix was mixed with the projected G matrix. It was shown that there is a ratio between the elements of the H and G matrices and that projection keeps this ratio fixed. The projection among different basis sets was studied. The closer the basis sets are in size, the more accurate the projection. The projection from STO-3G basis set to 6-31G or 6-31G(d) basis sets is reasonably accurate.

Table 4.1: Error in the projection of G from STO-3G to 3-21G

Molecule	$\|\Delta G_p\|$	$\|\Delta G_c\|$
1G_pep	45.48	36.47
2G_pep	76.50	118.52
3G_pep	104.63	70.04
4G_pep	131.01	200.08
BH_3	5.82	2.09
BeH_2	3.67	1.44
C_2H_2	13.90	3.41
C_2H_4	14.49	4.77
CCl_4	48.63	7.26
$CH_2(PH_2)_2$	26.25	12.26
$CH_2(SH)_2$	27.18	5.93
CH_3F	25.13	12.34
CH_3CONH_2	35.09	73.53
CH_4	8.365	2.73
CO_2	30.13	13.39
$FHOH_2$	27.78	7.72
H_2O	14.80	4.59
HF	19.09	6.40
N_2	19.75	5.45
NH_3	11.27	3.37
SF_6	104.99	29.00
MAD	27.09	33.41
Mean	37.81	29.74
Max	131.01	200.08
Min	3.67	1.44

Table 4.2: Error in the projection of G from STO-3G to 6-31G

Molecule	$\|\Delta G_p\|$	$\|\Delta G_c\|$
1G_pep	38.22	7.49
2G_pep	68.20	18.60
3G_pep	95.63	101.98
4G_pep	121.53	104.5
BH_3	5.04	1.76
BeH_2	3.12	1.19
C_2H_2	11.34	2.50
C_2H_4	12.22	3.33
CCl_4	46.46	6.59
$CH_2(PH_2)_2$	24.91	51.05
$CH_2(SH)_2$	25.64	63.02
CH_3F	19.39	4.65
CH_3CONH_2	29.49	6.31
CH_4	7.06	2.19
CO_2	23.41	5.98
$FHOH_2$	20.94	5.57
H_2O	10.68	3.42
HF	13.9	4.33
N_2	15.38	3.46
NH_3	8.60	2.53
SF_6	89.48	10.75
MAD	24.97	23.07
Mean	32.89	19.58
Max	121.53	104.50
Min	3.12	1.19

Table 4.3: Error in the projection of G from STO-3G to 6-31G(d)

Molecule	$\|\Delta G_p\|$	$\|\Delta G_c\|$
1G_pep	123.47	141.53
2G_pep	216.05	350.14
3G_pep	298.84	134.77
4G_pep	375.86	225.87
BH_3	15.75	4.39
BeH_2	10.29	2.72
C_2H_2	41.15	7.33
C_2H_4	43.00	7.72
CCl_4	204.8	45.01
$CH_2(PH_2)_2$	97.10	126.95
$CH_2(SH)_2$	104.07	71.06
CH_3F	53.83	8.34
CH_3CONH_2	96.75	76.76
CH_4	22.34	3.61
CO_2	73.35	38.56
$FHOH_2$	51.17	8.37
H_2O	27.06	6.59
HF	30.52	7.79
N_2	46.00	9.31
NH_3	24.47	4.11
SF_6	263.74	121.04
MAD	80.82	68.00
Mean	105.70	66.76
Max	375.86	350.14
Min	10.29	2.72

Table 4.4: The diagonal elements of H, H_p, G, G_p, x and x_p for SiH_4

(i,i)	$(H)_{ii}$	$(H_p)_{ii}$	$(G)_{ii}$	$(G_p)_{ii}$	$(x)_{ii}$	$(x_p)_{ii}$
3d-type: Si						
(1,1)	-8.45	-5.14	8.36	4.74	-0.99	-0.92
(2,2)	-8.45	-5.14	8.36	4.74	-0.99	-0.92
(3,3)	-8.46	-5.25	8.35	4.86	-0.99	-0.92
(4,4)	-7.85	-0.70	8.58	0.73	-1.09	-1.04
(5,5)	-7.83	-0.35	8.59	0.37	-1.10	-1.04
(6,6)	-7.83	-0.35	8.59	0.37	-1.10	-1.04
2p-type: Si						
(7,7)	-23.70	-23.29	19.48	19.33	-0.82	-0.83
(8,8)	-23.70	-23.29	19.48	19.33	-0.82	-0.83
(9,9)	-23.70	-23.29	19.48	19.33	-0.82	-0.83
3p-type: Si						
(10,10)	-8.64	-8.71	8.11	8.23	-0.94	-0.94
(11,11)	-8.64	-8.71	8.11	8.23	-0.94	-0.94
(12,12)	-8.64	-8.71	8.11	8.23	-0.94	-0.94
4p-type: Si						
(13,13)	-5.05	-4.05	4.85	3.80	-0.96	-0.94
(14,14)	-5.05	-4.05	4.85	3.80	-0.96	-0.94
(15,15)	-5.05	-4.05	4.85	3.80	-0.96	-0.94
1S-type: H						

... continued

Table 4.4 – continued

(i,i)	$(H)_{ii}$	$(H_p)_{ii}$	$(G)_{ii}$	$(G_p)_{ii}$	$(x)_{ii}$	$(x_p)_{ii}$
(16,16)	-5.94	-5.29	5.93	5.11	-1.00	-0.97
(17,17)	-5.94	-5.29	5.93	5.11	-1.00	-0.97
(18,18)	-5.94	-5.29	5.93	5.11	-1.00	-0.97
(19,19)	-5.94	-5.29	5.93	5.11	-1.00	-0.97
2S-type: H						
(20,20)	-5.95	-5.80	5.43	5.25	-0.91	-0.91
(21,21)	-5.95	-5.80	5.43	5.25	-0.91	-0.91
(22,22)	-5.95	-5.80	5.43	5.25	-0.91	-0.91
(23,23)	-5.95	-5.80	5.43	5.25	-0.91	-0.91
1S-type: Si						
(24,24)	-99.34	-98.29	30.59	30.35	-0.31	-0.31
2S-type: Si						
(25,25)	-28.78	-28.93	18.36	18.63	-0.64	-0.64
3S-type: Si						
(26,26)	-9.55	-9.24	8.49	8.24	-0.89	-0.89
4S-type: Si						
(27,27)	-7.38	-7.40	6.41	6.41	-0.87	-0.87

Table 4.5: The diagonal elements of F, F_p, and F'_p for SiH_4

(i,i)	F	F_p	F'_p
(1,1)	-0.10	-0.40	-3.72
(2,2)	-0.10	-0.40	-3.72
(3,3)	-0.11	-0.40	-3.60
(4,4)	0.72	0.03	-7.13
(5,5)	0.76	0.01	-7.46
(6,6)	0.76	0.01	-7.46
(7,7)	-4.23	-3.96	-4.37
(8,8)	-4.23	-3.96	-4.37
(9,9)	-4.23	-3.96	-4.37
(10,10)	-0.53	-0.49	-0.41
(11,11)	-0.53	-0.49	-0.41
(12,12)	-0.53	-0.49	-0.41
(13,13)	-0.20	-0.24	-1.24
(14,14)	-0.20	-0.24	-1.24
(15,15)	-0.20	-0.24	-1.24

... continued

Table 4.5 – continued

(i,i)	F	F_p	F'_p
(16,16)	-0.01	-0.18	-0.83
(17,17)	-0.01	-0.18	-0.83
(18,18)	-0.01	-0.18	-0.83
(19,19)	-0.01	-0.18	-0.83
(20,20)	-0.53	-0.54	-0.70
(21,21)	-0.53	-0.54	-0.70
(22,22)	-0.53	-0.54	-0.70
(23,23)	-0.53	-0.54	-0.70
(24,24)	-68.75	-67.94	-68.99
(25,25)	-10.42	-10.31	-10.16
(26,26)	-1.06	-1.00	-1.31
(27,27)	-0.97	-1.00	-0.97

Table 4.6: $\|\Delta H_p\|$, $\|\Delta G_p\|$, $\|\Delta F_p\|$

Molecule	$\|\Delta H_p\|$	$\|\Delta G_p\|$	$\|\Delta F_p\|$
CH_4	7.70	11.17	3.75
NH_3	8.73	12.23	3.86
H_2O	9.78	13.53	4.18
HF	11.12	15.26	4.65
SiH_4	15.30	16.70	1.96
PH_3	17.16	18.79	2.26
H_2S	19.35	21.27	2.60
HCl	21.47	23.53	2.64
GeH_4	52.61	55.22	7.95
AsH_3	56.68	59.53	8.40
H_2Se	61.19	64.20	8.75
HBr	65.32	68.57	9.24
SnH_4	35.19	32.72	11.55
SbH_3	37.31	34.83	11.81
H_2Te	40.43	37.99	12.22
HI	44.15	41.84	12.67
1G_pep	53.78	61.74	8.68
2G_pep	97.45	108.02	11.53
3G_pep	136.77	149.42	13.79
4G_pep	173.50	187.93	15.73
5G_pep	219.08	235.34	17.65

Table 4.7: Relative error, equation (4.43), in the projection for molecules containing atoms from the first row

Basis	CH_4	NH_3	H_2O	HF	Sum
From STO-3G to					
3-21G	0.0756	0.0725	0.0740	0.0763	0.2984
6-31G	0.0617	0.0524	0.0502	0.0514	0.2157
STO-3G(d)	0.2715	0.2148	0.1809	0.1577	0.8249
6-31G(d)	0.2461	0.1994	0.1717	0.1534	0.7706
6-311G(d)	0.1873	0.1916	0.1977	0.2019	0.7785
From 3-21G to					
6-31G	0.0114	0.0149	0.0182	0.0198	0.0643
STO-3G(d)	0.2654	0.2033	0.1673	0.1484	0.7844
6-31G(d)	0.2340	0.1820	0.1514	0.1357	0.7031
6-311G(d)	0.1659	0.1743	0.1848	0.1919	0.7169
From 6-31G to					
STO-3G(d)	0.2665	0.2078	0.1725	0.1507	0.7974
6-31G(d)	0.2343	0.1847	0.1539	0.1346	0.7075
6-311G(d)	0.1688	0.1787	0.1886	0.1947	0.7308
From STO-3G(d) to					
6-31G(d)	0.0804	0.0646	0.0543	0.0514	0.2507
6-311G(d)	0.1516	0.1474	0.1563	0.1727	0.6280
From 6-31G(d) to					
6-311G(d)	0.1274	0.1311	0.1439	0.1642	0.5665

Table 4.8: Relative error, equation (4.43), in the projection for molecules containing atoms from the second row elements

Basis	SiH_4	PH_3	H_2S	HCl	Sum
From STO-3G to					
3-21G	0.0146	0.0136	0.0129	0.0085	0.0495
6-31G	0.0166	0.0164	0.0162	0.0120	0.0612
STO-3G(d)	0.0162	0.0140	0.0140	0.0136	0.0577
6-31G(d)	0.0261	0.0258	0.0257	0.0228	0.1003
6-311G(d)	0.2139	0.2086	0.2162	0.2087	0.8473
From 3-21G to					
6-31G	0.0079	0.0077	0.0076	0.0075	0.0306
STO-3G(d)	0.0182	0.0162	0.0159	0.0132	0.0636
6-31G(d)	0.0221	0.0219	0.0218	0.0212	0.0869
6-311G(d)	0.2141	0.2088	0.2165	0.2086	0.8480
From 6-31G to					
STO-3G(d)	0.0203	0.0189	0.0192	0.0162	0.0745
6-31G(d)	0.0205	0.0202	0.0199	0.0193	0.0799
6-311G(d)	0.2139	0.2087	0.2164	0.2086	0.8476
From STO-3G(d) to					
6-31G(d)	0.0171	0.0177	0.0189	0.0174	0.0711
6-311G(d)	0.2133	0.2081	0.2158	0.2083	0.8454
From 6-31G(d) to					
6-311G(d)	0.2133	0.2080	0.2157	0.2079	0.8448

Table 4.9: Relative error, equation (4.43), in the projection for molecules containing atoms from the third row elements

Basis	GeH_4	AsH_3	H_2Se	HBr	Sum
From STO-3G to[a]					
3-21G	0.0090	0.0081	0.0081	0.0076	0.0327
6-31G	0.0165	0.0162	0.0157	0.0155	0.0639
6-31G(d)	0.0171	0.0168	0.0164	0.0162	0.0665
From 3-21G to					
6-31G	0.0115	0.0126	0.0126	0.0134	0.0501
STO-3G(d)	0.007	0.006	0.006	0.005	0.0243
6-31G(d)	0.0122	0.0133	0.0136	0.0146	0.0537
From 6-31G to					
STO-3G(d)	0.010	0.010	0.010	0.009	0.0394
6-31G(d)	0.0045	0.0050	0.0055	0.0060	0.0211
From STO-3G(d) to					
6-31G(d)	0.0171	0.0168	0.0164	0.0162	0.0665

[a] For 3^{rd} row, STO-3G=STO-3G(d)

Table 4.10: Relative error, equation (4.43), in the projection for molecules containing atoms from the fourth row elements

Basis	SnH_4	SbH_3	H_2Te	HI	Sum
From STO-3G to[a]					
3-21G	0.0066	0.0064	0.0063	0.0063	0.0255
6-31G	0.0091	0.0089	0.0088	0.0087	0.0354
6-31G(d)	0.0092	0.0090	0.0089	0.0088	0.0359
From 3-21G to					
6-31G	0.0047	0.0047	0.0046	0.0046	0.0187
STO-3G(d)	0.004	0.004	0.004	0.004	0.0158
6-31G(d)	0.0048	0.0049	0.0048	0.0048	0.0193
From 6-31G to					
STO-3G(d)	0.007	0.007	0.007	0.007	0.0283
6-31G(d)	0.0008	0.0008	0.0007	0.0008	0.0030
From STO-3G(d) to					
6-31G(d)	0.0092	0.0090	0.0089	0.0088	0.0359

[a] For 4^{th} row, STO-3G=STO-3G(d)

Table 4.11: Percentage error in energy ($\Delta E\%$), equation (4.46), using H_p for the first row elements

Basis	CH_4	NH_3	H_2O	HF	Sum
From STO-3G to					
3-21G	0.6091	0.8288	1.0361	1.2300	3.7041
6-31G	0.9082	1.1880	1.4383	1.6661	5.2006
STO-3G(d)	0.0334	0.0436	0.0429	0.0311	0.1510
6-31G(d)	0.9341	1.2143	1.4503	1.6557	5.2543
6-311G(d)	0.9208	1.1358	1.3089	1.4583	4.8239
From 3-21G to					
6-31G	0.4511	0.5200	0.5857	0.6172	2.1739
STO-3G(d)	-0.5001	-0.7398	-0.9734	-1.1681	-3.3812
6-31G(d)	0.4542	0.5392	0.6119	0.6355	2.2408
6-311G(d)	0.4689	0.5545	0.6177	0.6544	2.2955
From 6-31G to					
STO-3G(d)	-1.0088	-1.4710	-1.8448	-2.1201	-6.4447
6-31G(d)	0.0271	0.0333	0.0312	0.0187	0.1102
6-311G(d)	0.0461	0.0649	0.0635	0.0566	0.2310

Table 4.12: Percentage error in energy ($\Delta E\%$), equation (4.46), using H_p for the second row elements

Basis	SiH_4	PH_3	H_2S	HCl	Sum
From STO-3G to					
3-21G	0.7731	0.7789	0.7963	0.8352	3.1835
6-31G	1.1854	1.1681	1.1682	1.1991	4.7209
STO-3G(d)	0.0217	0.0197	0.0153	0.0201	0.0768
6-31G(d)	1.1972	1.1770	1.1698	1.1898	4.7337
6-311G(d)	1.1406	1.1281	1.1231	1.1319	4.5236
From 3-21G to					
6-31G	0.5988	0.5841	0.5745	0.5670	2.3244
STO-3G(d)	-0.6654	-0.7377	-0.8616	-0.7523	-3.0169
6-31G(d)	0.6003	0.5798	0.5636	0.5493	2.2931
6-311G(d)	0.5417	0.5279	0.5190	0.5137	2.1023
From 6-31G to					
STO-3G(d)	-1.1691	-1.2443	-1.3771	-1.2969	-5.0874
6-31G(d)	0.0165	0.0145	0.0099	0.0050	0.0458
6-311G(d)	0.0252	0.0216	0.0164	0.0118	0.0749

Table 4.13: Percentage error in the energy ($\Delta E\%$), equation (4.46), using H_p for the third row elements

Basis	GeH_4	AsH_3	H_2Se	HBr	Sum
From STO-3G to					
3-21G	1.2011	1.1334	1.0519	1.0007	4.3871
6-31G	1.3442	1.3129	1.2914	1.2712	5.2197
STO-3G(d)	0.0334	0.0436	0.0429	0.0311	0.1510
6-31G(d)	1.3295	1.2978	1.2752	1.2543	5.1567
From 3-21G to					
6-31G	0.5806	0.5729	0.5558	0.5666	2.2759
STO-3G(d)	-0.0704	-0.0897	-0.1502	-0.1732	-0.4835
6-31G(d)	0.5641	0.5588	0.5431	0.5550	2.2210
From 6-31G to					
STO-3G(d)	-1.6724	-1.5713	-1.4874	-1.4392	-6.1703
6-31G(d)	0.0031	0.0032	0.0029	0.0022	0.0114

Table 4.14: Percentage error in the energy ($\Delta E\%$), equation (4.46), using H_p for the fourth row elements

Basis	SnH_4	SbH_3	H_2Te	HI	Sum
From STO-3G to					
3-21G	0.9250	0.8894	0.8641	0.8400	3.5184
6-31G	1.2419	1.2004	1.1731	1.1481	4.7635
6-31G(d)	1.1548	1.1247	1.1057	1.0897	4.4749
From 3-21G to					
6-31G	0.4241	0.4195	0.4190	0.4236	1.6861
STO-3G(d)	-0.0078	-0.0325	-0.0559	-0.0750	-0.1712
6-31G(d)	0.4236	0.4194	0.4189	0.4234	1.6853
From 6-31G to					
STO-3G(d)	-0.4352	-0.4551	-0.4792	-0.5125	-1.8820
6-31G(d)	0.0008	0.0008	0.0007	0.0005	0.0029

Table 4.15: Percentage error in energy ($\Delta E\%$) using, equation (4.46), H for molecules containing first-row elements

Basis	CH_4	NH_3	H_2O	HF	Sum
From STO-3G to					
3-21G	0.1823	0.1868	0.1525	0.1201	0.6417
6-31G	0.3300	0.2468	0.1277	0.0179	0.7224
STO-3G(d)	0.0334	0.0436	0.0429	0.0311	0.1510
6-31G(d)	0.3525	0.3224	0.2325	0.1083	1.0156
6-311G(d)	0.4825	0.6625	0.7946	0.9083	2.8479
From 3-21G to					
6-31G	0.2206	0.2540	0.2911	0.3026	1.0682
STO-3G(d)	-0.2380	-0.4539	-0.5998	-0.7075	-1.9992
6-31G(d)	0.1948	0.2697	0.3217	0.3241	1.1104
6-311G(d)	0.2492	0.3355	0.4042	0.4421	1.4310
From 6-31G to					
STO-3G(d)	-0.4242	-0.7729	-0.9472	-1.0474	-3.1917
6-31G(d)	0.0271	0.0333	0.0312	0.0187	0.1102
6-311G(d)	0.0377	0.0454	0.0450	0.0506	0.1786
From 6-31G(d) to					
6-311G(d)	0.0121	0.0100	0.0125	0.0495	0.0841

Table 4.16: Percentage error in energy ($\Delta E\%$) using, equation (4.46), H for molecules containing second-row elements

Basis	SiH_4	PH_3	H_2S	HCl	Sum
From STO-3G to					
3-21G	0.2278	0.1778	0.1087	-0.0095	0.5049
6-31G	0.4959	0.4445	0.3687	0.1996	1.5088
STO-3G(d)	0.0217	0.0197	0.0153	0.0201	0.0768
6-31G(d)	0.4715	0.4326	0.3686	0.2191	1.4918
6-311G(d)	0.5889	0.5905	0.6081	0.3529	2.1405
From 3-21G to					
6-31G	0.3075	0.2974	0.2922	0.2905	1.1876
STO-3G(d)	-0.4288	-0.4075	-0.4765	-0.2813	-1.5941
6-31G(d)	0.2762	0.2569	0.2470	0.2387	1.0188
6-311G(d)	0.2958	0.2982	0.2945	0.2274	1.1158
From 6-31G to					
STO-3G(d)	-0.6585	-0.6525	-0.7357	-0.5383	-2.5849
6-31G(d)	0.0165	0.0145	0.0099	0.0050	0.0458
6-311G(d)	0.0178	0.0201	0.0178	0.0110	0.0667
From 6-31G(d) to					
6-311G(d)	0.0010	0.0045	0.0074	0.0058	0.0187

Table 4.17: Percentage error in the energy ($\Delta E\%$) using, equation (4.46), H for molecules containing third-row elements

Basis	GeH_4	AsH_3	H_2Se	HBr	Sum
From STO-3G to					
3-21G	0.6075	0.4995	0.4530	0.3610	1.9210
6-31G	-0.0527	-0.0190	-0.0107	0.0022	-0.0802
6-31G(d)	0.0218	0.0115	0.0171	0.0265	0.0769
From 3-21G to					
6-31G	0.1786	0.2207	0.1827	0.2162	0.7981
STO-3G(d)	-0.5178	-0.3853	-0.3456	-0.2666	-1.5152
6-31G(d)	0.2068	0.2490	0.2097	0.2415	0.9070
From 6-31G to					
STO-3G(d)	-0.7495	-0.6811	-0.6084	-0.5745	-2.6135
6-31G(d)	0.0031	0.0032	0.0029	0.0022	0.0114

Table 4.18: Percentage error in the energy ($\Delta E\%$) using, equation (4.46), H for molecules containing fourth-row elements

Basis	SnH_4	SbH_3	H_2Te	HI	Sum
From STO-3G to					
3-21G	0.3565	0.3232	0.3022	0.2781	1.2599
6-31G	0.5503	0.5121	0.4806	0.4483	1.9912
6-31G(d)	0.4529	0.4224	0.3960	0.3693	1.6407
From 3-21G to					
6-31G	0.2129	0.2132	0.2084	0.2063	0.8407
STO-3G(d)	-0.1812	-0.0944	-0.0454	-0.0240	-0.3450
6-31G(d)	0.2089	0.2104	0.2059	0.2060	0.8313
From 6-31G to					
STO-3G(d)	-0.4040	-0.3334	-0.3042	-0.2841	-1.3257
6-31G(d)	0.0008	0.0008	0.0007	0.0005	0.0029

Table 4.19: Relative error, equation (4.43), for peptides

Basis	1G_pep	2G_pep	3G_pep	4G_pep	5G_pep
From STO-3G to					
3-21G	0.0677	0.0670	0.0667	0.0665	0.0671
6-31G	0.0481	0.0480	0.0480	0.0480	0.0482
STO-3G(d)	0.2081	0.2120	0.2133	0.2141	0.2185
6-31G(d)	0.1892	0.1917	0.1924	0.1928	0.1973
6-311G(d)	0.1899	0.1887	0.1881	0.1878	0.1892
From 3-21G to					
6-31G	0.0139	0.0134	0.0132	0.0131	0.0133
STO-3G(d)	0.1967	0.1999	0.2012	0.2019	0.2185
6-31G(d)	0.1719	0.1740	0.1746	0.1750	0.1797
6-311G(d)	0.1757	0.1740	0.1731	0.1726	0.1742
From 6-31G to					
STO-3G(d)	0.2010	0.2042	0.2054	0.2062	0.2105
6-31G(d)	0.1745	0.1740	0.1772	0.1775	0.1822
6-311G(d)	0.1799	0.1781	0.1772	0.1768	0.1783
From 6-31G(d) to					
6-311G(d)	0.1327	0.1310	0.1302	0.1297	0.1306

Table 4.20: Relative error, equation (4.43), for silicon hydrides

Basis	SiH_4	Si_2H_6	Si_3H_8	Si_4H_{10}	Si_5H_{12}	Si_6H_{14}
From STO-3G to						
3-21G	0.0146	0.0140	0.0139	0.0138	0.0138	0.0138
6-31G	0.0166	0.0164	0.0164	0.0164	0.0164	0.0164
STO-3G(d)	0.0162	0.0163	0.0164	0.0165	0.0165	0.0165
6-31G(d)	0.0261	0.0260	0.0259	0.0259	0.0259	0.0259
6-311G(d)	0.2139	0.2138	0.2138	0.2138	0.2138	0.2138
From 3-21G to						
6-31G	0.0079	0.0078	0.0077	0.0077	0.0077	0.0077
STO-3G(d)	0.0182	0.0183	0.0183	0.0183	0.0183	0.0183
6-31G(d)	0.0221	0.0219	0.0218	0.0218	0.0218	0.0217
6-311G(d)	0.2141	0.2141	0.2141	0.2141	0.2140	0.2140
From 6-31G to						
STO-3G(d)	0.0203	0.0204	0.0205	0.0205	0.0205	0.0205
6-31G(d)	0.0205	0.0204	0.0203	0.0203	0.0203	0.0202
6-311G(d)	0.2139	0.2139	0.2139	0.2139	0.2139	0.2139
From 6-31G(d) to						
6-311G(d)	0.2133	0.2132	0.2132	0.2132	0.2132	0.2132

Table 4.21: Relative error, equation (4.43), for germanium hydrides

Basis	GeH_4	Ge_3H_8	Ge_4H_{10}
From STO-3G to			
3-21G	0.0090	0.0090	0.0090
6-31G	0.0165	0.0165	0.0166
6-31G(d)	0.0171	0.0171	0.0172
From 3-21G to			
6-31G	0.0115	0.0115	0.0115
STO-3G(d)	0.0068	0.0069	0.0069
6-31G(d)	0.0122	0.0122	0.0121
From 6-31G to			
STO-3G(d)	0.0104	0.0105	0.0105
6-31G(d)	0.0045	0.0045	0.0045

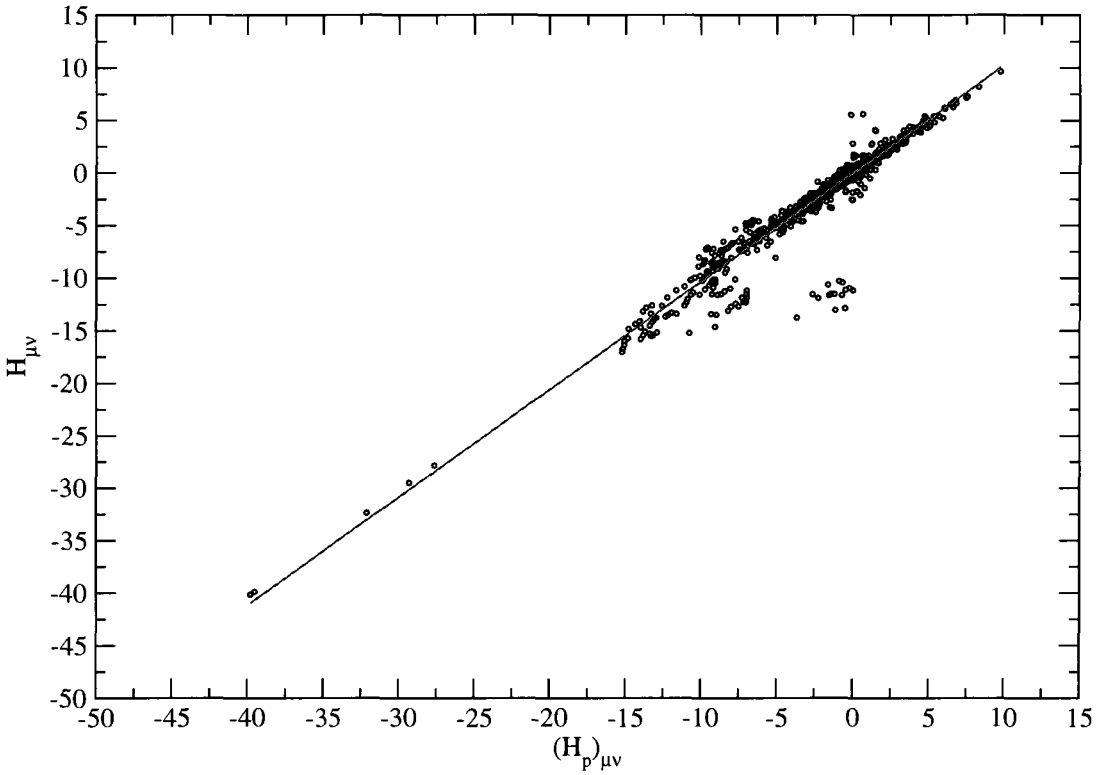

Figure 4.1: $H_{\mu\nu}$ vs $(H_p)_{\mu\nu}$ for 1G_pep

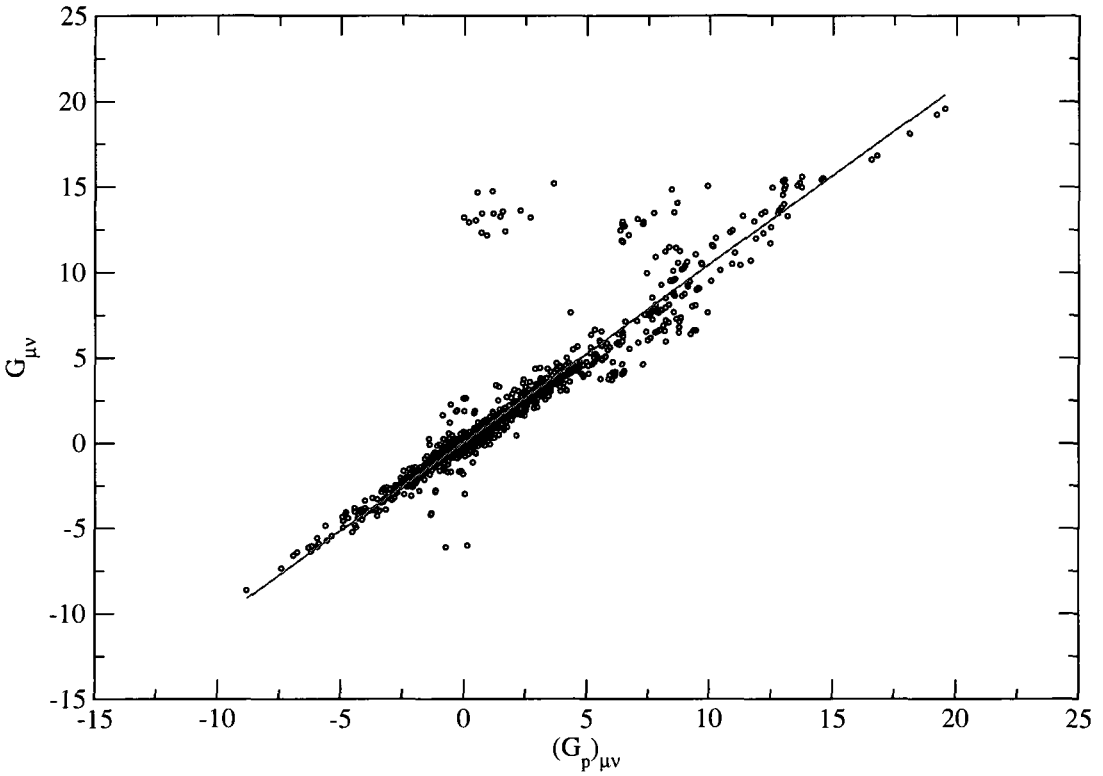

Figure 4.2: $G_{\mu\nu}$ vs $(G_p)_{\mu\nu}$ for 1G_pep

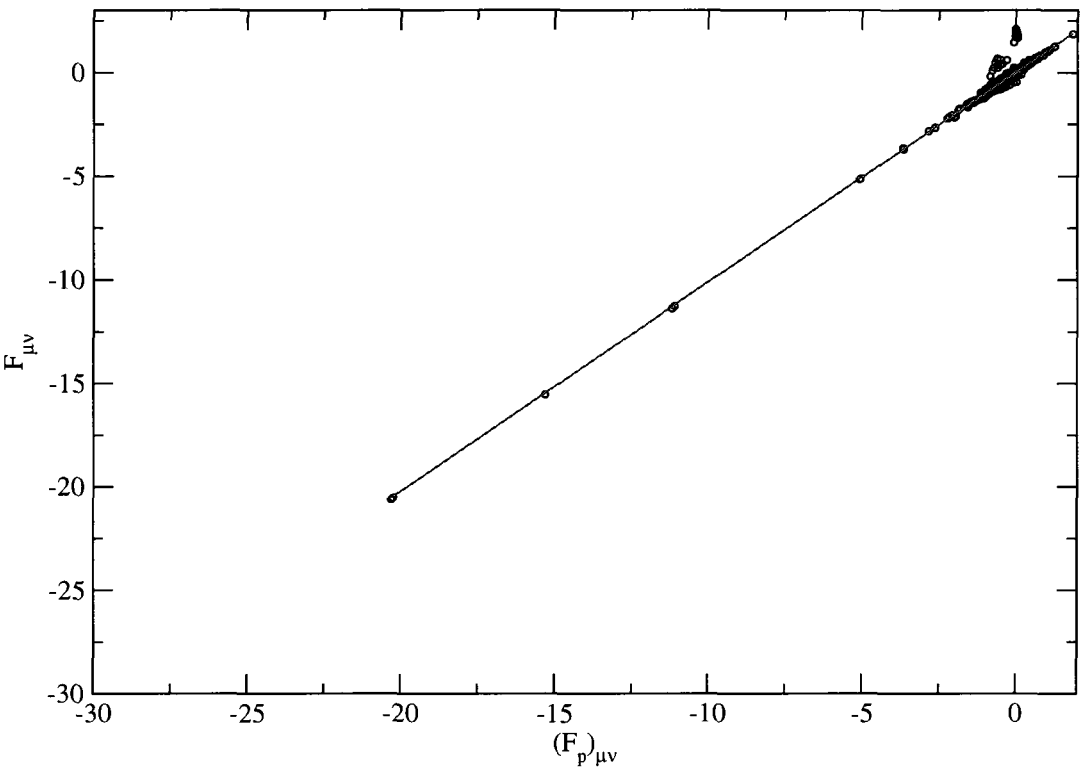

Figure 4.3: $F_{\mu\nu}$ vs $(F_p)_{\mu\nu}$ for 1G_pep

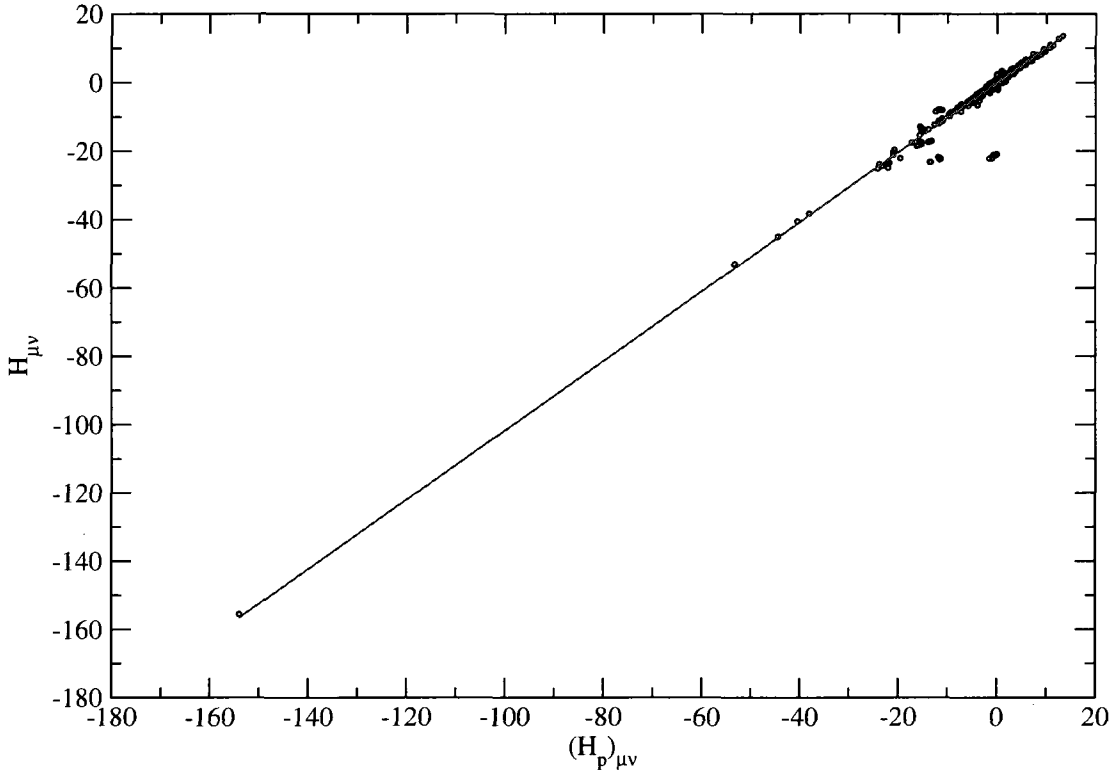

Figure 4.4: $H_{\mu\nu}$ vs $(H_p)_{\mu\nu}$ for CCl_4

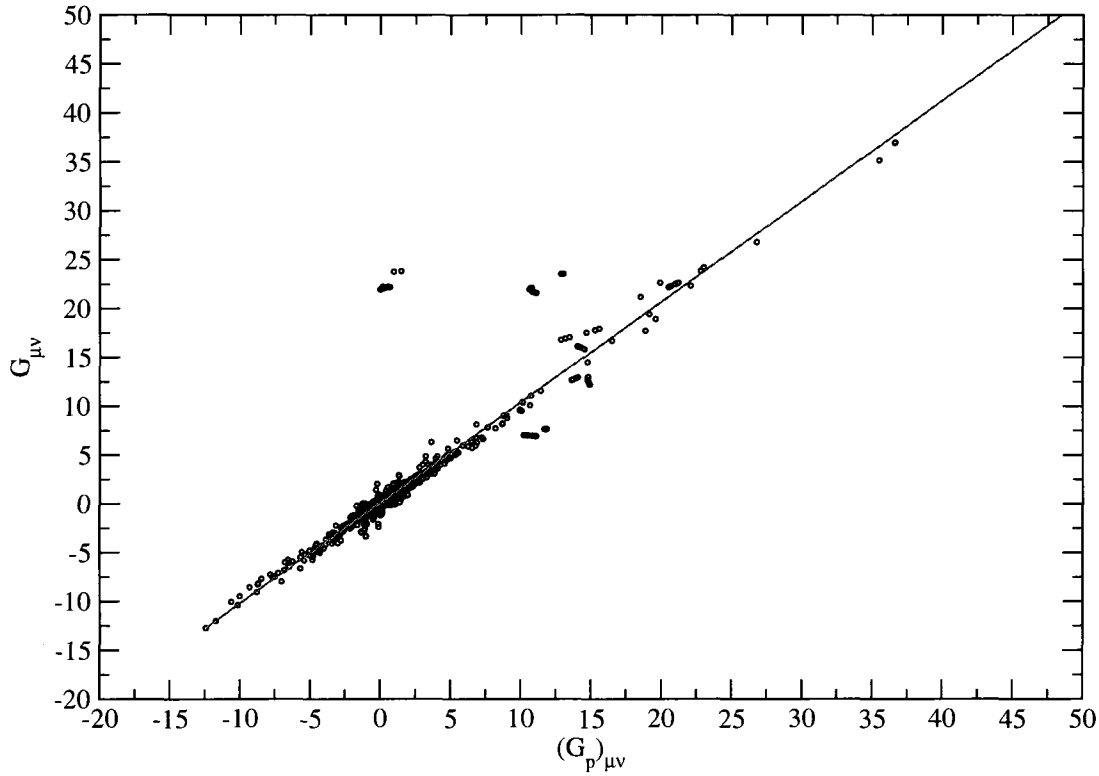

Figure 4.5: $G_{\mu\nu}$ vs $(G_p)_{\mu\nu}$ for CCl_4

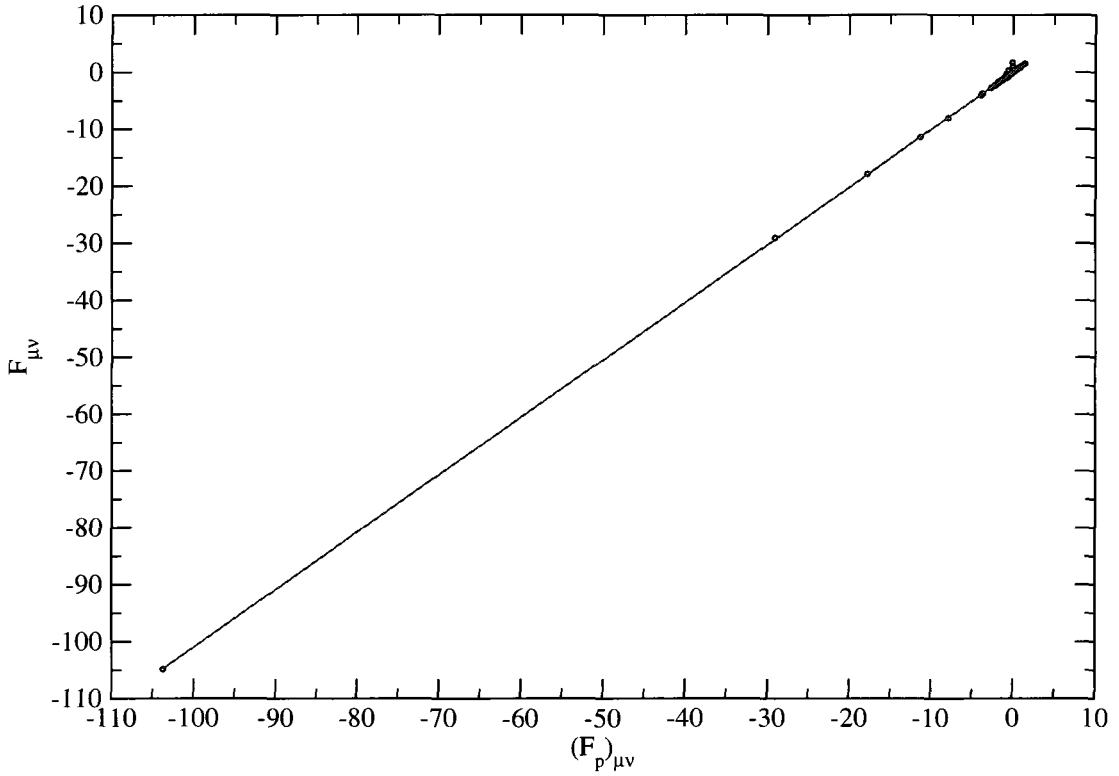

Figure 4.6: $F_{\mu\nu}$ vs $(F_p)_{\mu\nu}$ for CCl_4

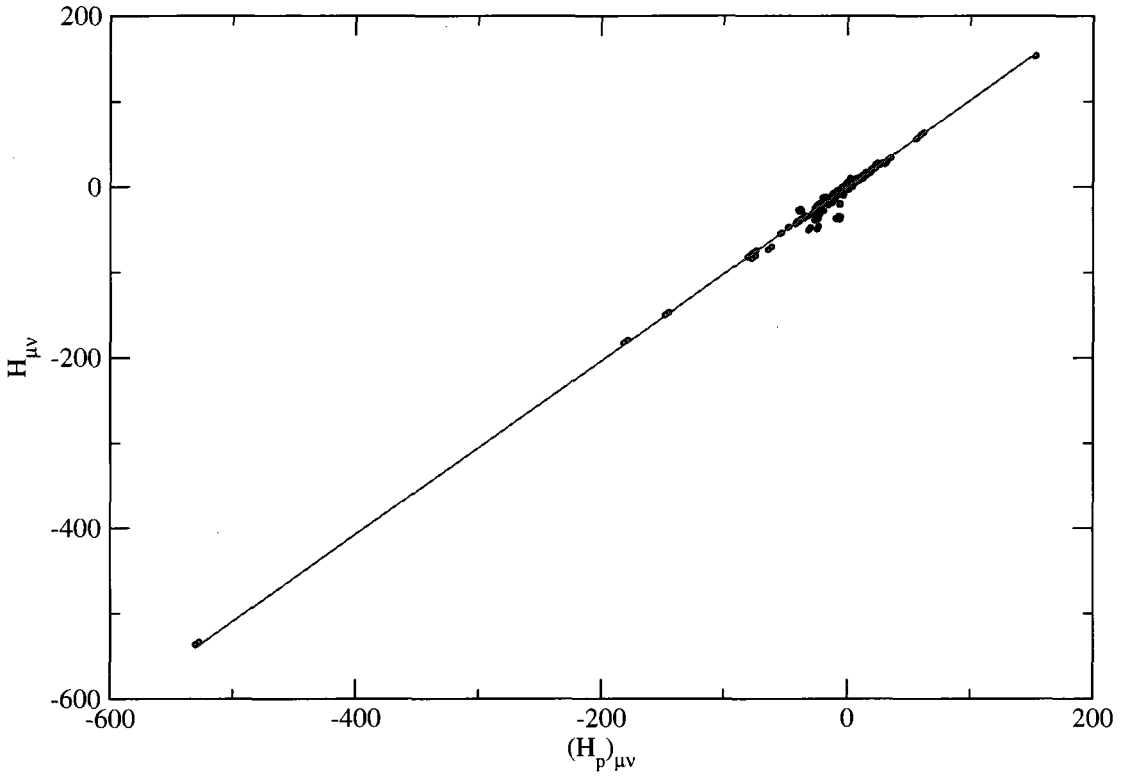

Figure 4.7: $H_{\mu\nu}$ vs $(H_p)_{\mu\nu}$ for Ge_5H_{12}

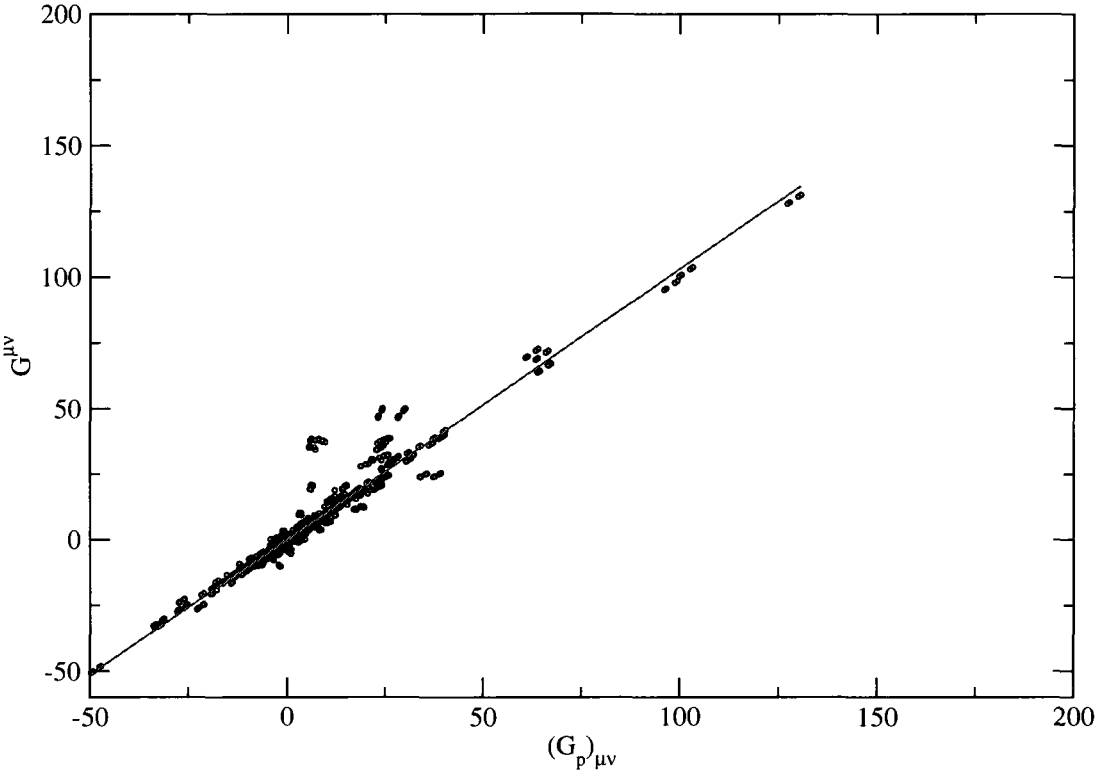

Figure 4.8: $G_{\mu\nu}$ vs $(G_p)_{\mu\nu}$ for Ge_5H_{12}

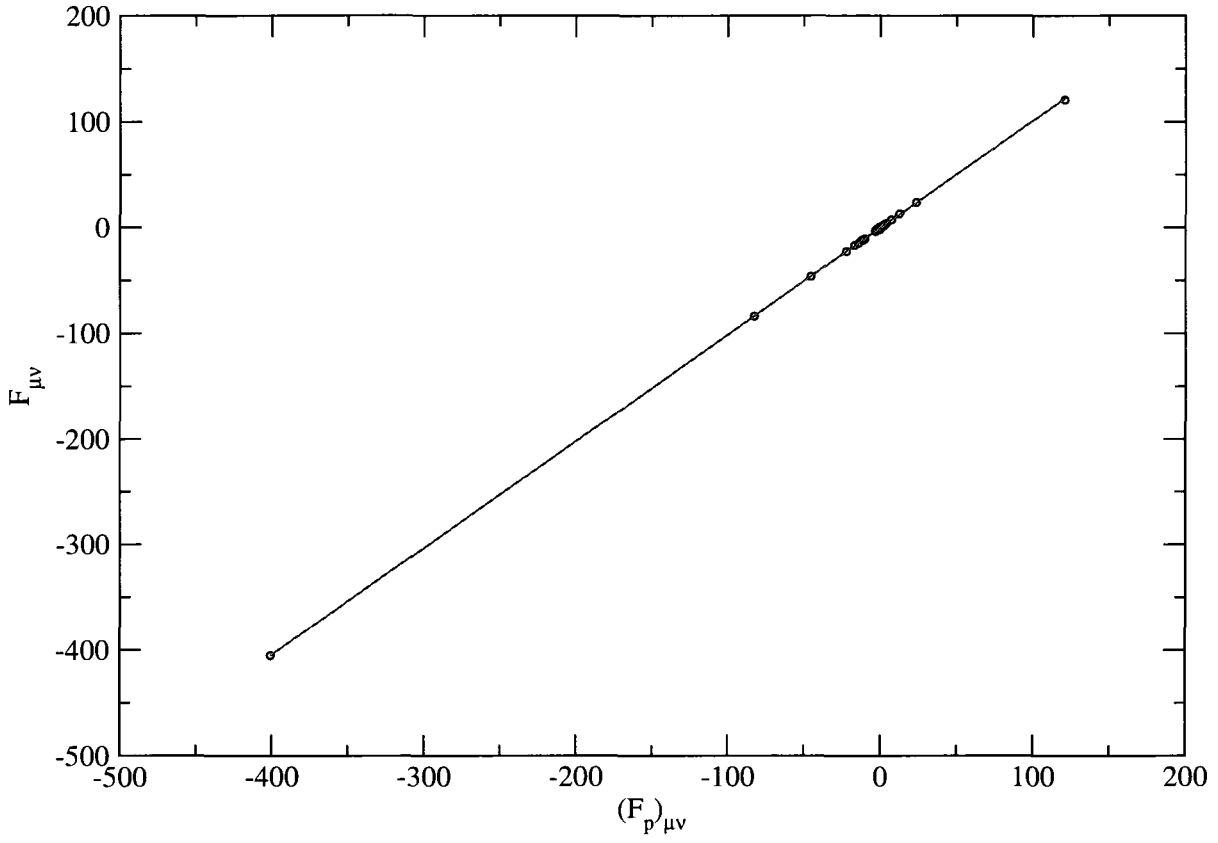

Figure 4.9: $F_{\mu\nu}$ vs $(F_p)_{\mu\nu}$ for Ge_5H_{12}

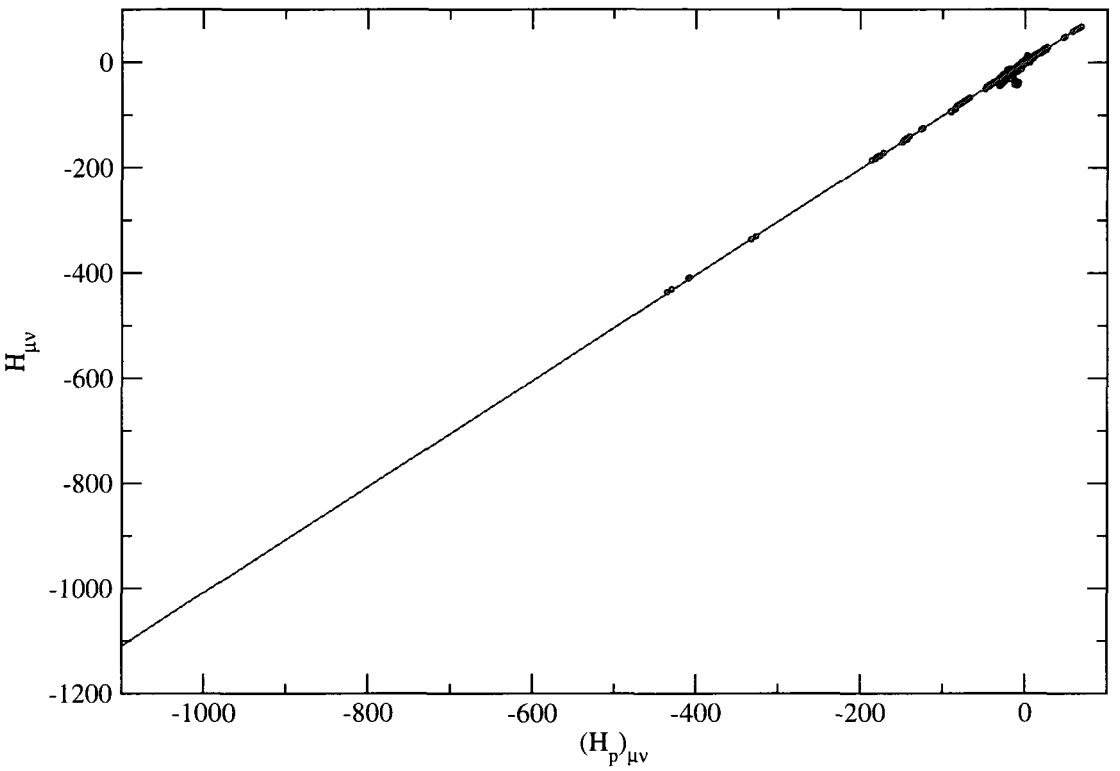

Figure 4.10: $H_{\mu\nu}$ vs $(H_p)_{\mu\nu}$ for Sn_4H_{10}

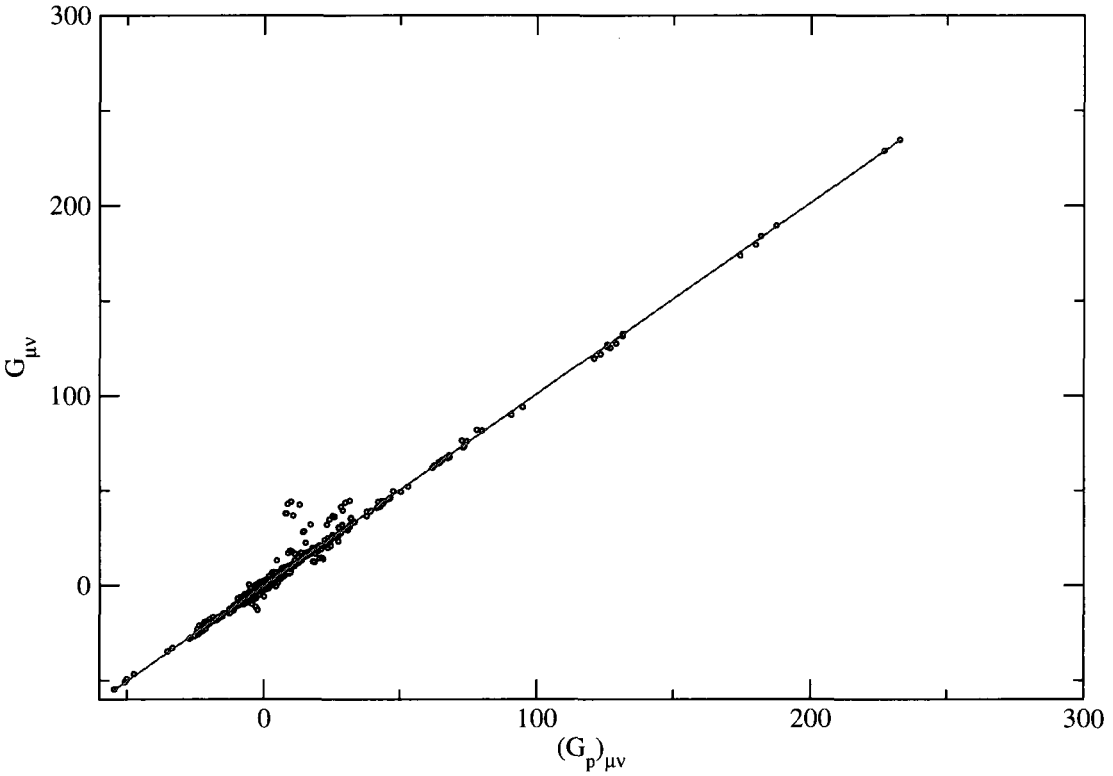

Figure 4.11: $G_{\mu\nu}$ vs $(G_p)_{\mu\nu}$ for Sn_4H_{10}

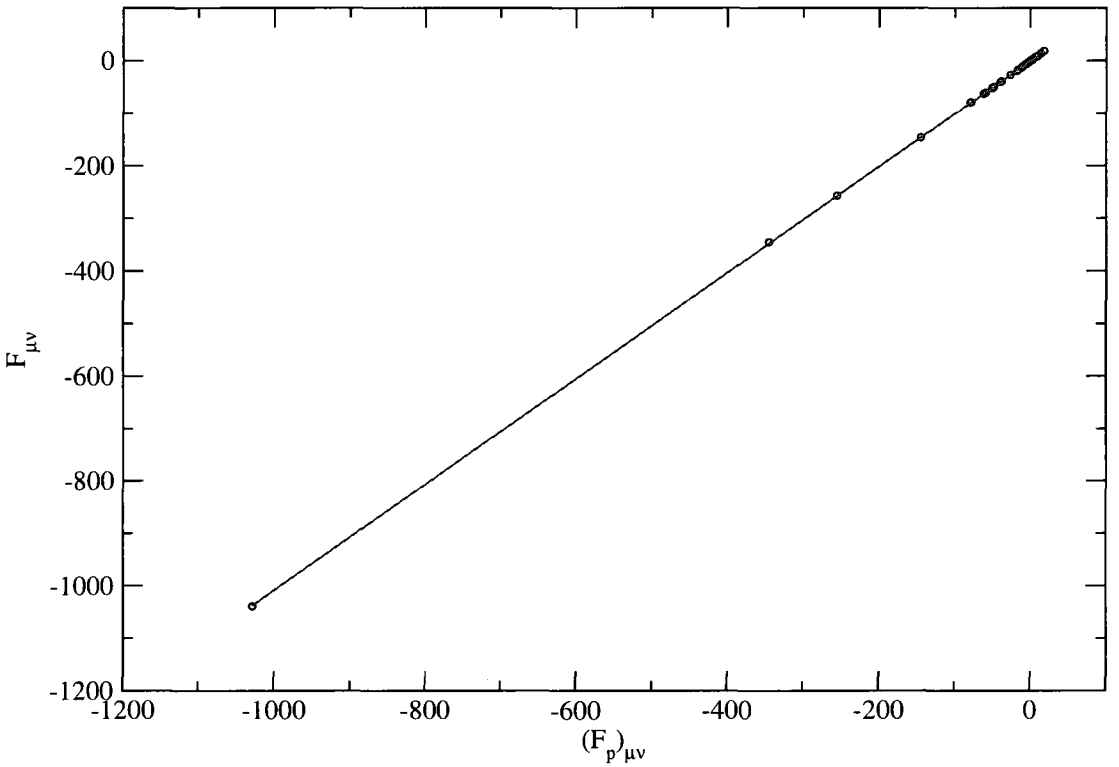

Figure 4.12: $F_{\mu\nu}$ vs $(F_p)_{\mu\nu}$ for Sn_4H_{10}

Chapter 5

Two-electron Integrals

5.1 Introduction

Calculation of the two-electron integrals is one of the bottlenecks in Hartree-Fock calculations. Formally the number of two-electron integrals scale as N^4, where N is the number of basis functions. However, many of these integrals are equal to zero or of negligible value [23]. This chapter investigates ways of predetermining two-electron integrals that can be neglected and therefore avoiding calculating them. The two-electron integral $(\mu\nu|\sigma\lambda)$ is given by:

$$(\mu\nu|\sigma\lambda) = \int\int \phi_\mu^*(\mathbf{r}_1)\phi_\nu(\mathbf{r}_1)r_{12}^{-1}\phi_\sigma^*(\mathbf{r}_2)\phi_\lambda(\mathbf{r}_2)d\mathbf{r}_1 d\mathbf{r}_2 \tag{5.1}$$

where $(\phi_\mu, \mu = 1, \ldots, k)$ are contracted basis functions. Each contracted basis function is a linear combination of primitive Gaussian functions $\{g_i\}$ [24]:

$$\phi_\mu = \sum_{i=1}^{m_\mu} d_{i\mu} g_i \tag{5.2}$$

m_μ is the number of the primitive Gaussian functions $\{g_i\}$ and $\{d_{i\mu}\}$ are the contraction coefficients. An unnormalized primitive Gaussian function g_i centered on an atom A is given by [25]:

$$g_i(\alpha, \mathbf{r} - \mathbf{R}_A) = (x - X_A)^l (y - Y_A)^m (z - Z_A)^n e^{-\alpha|\mathbf{r}-\mathbf{R}_A|^2} \tag{5.3}$$

α is the Gaussian exponent and defines its width. l ,m, and n are three nonnegative integers and the sum $l + m + n$ is the angular momentum of the Gaussian. For example $l + m + n = 0$ defines a Gaussian of spherical symmetry and is called an s-type Gaussian, $l + m + n = 1$ corresponds to a p-type Gaussian, $l + m + n = 2$ to a d-type Gaussian and so on [26]. Substituting equation (5.2) in equation (5.1), the two electron-integral can be written as:

$$(\mu\nu|\sigma\lambda) = \sum_{i=1}^{m1}\sum_{j=1}^{m2}\sum_{k=1}^{m3}\sum_{l=1}^{m4} d_{i\mu}d_{j\nu}d_{k\sigma}d_{l\lambda} \int\int g_i^*(\mathbf{r}_1) g_j(\mathbf{r}_1) r_{12}^{-1} g_k^*(\mathbf{r}_2) g_l(\mathbf{r}_2) d\mathbf{r}_1 d\mathbf{r}_2 \tag{5.4}$$

If g_i and g_j are Gaussian functions with exponents α and β centered on atoms A and B respectively then their multiplication is another Gaussian G_{ij} of exponent ϵ_1 and centered at the point p on the line connecting the two atoms A and B [24, 26]. For two $1s$ Gaussians:

$$G_{ij} = K_{AB} e^{-\epsilon_1|\mathbf{r}-\mathbf{R}_p|^2} \tag{5.5}$$

The constant K_{AB} is given by:

$$K_{AB} = exp(\frac{-\alpha\beta}{\alpha+\beta}|\mathbf{R}_A - \mathbf{R}_B|^2) \tag{5.6}$$

and

$$\epsilon_1 = \alpha + \beta \tag{5.7}$$

Similarly if g_k and g_l are centered on atoms C and D and of exponents γ and δ respectively, their multiplication is a third Gaussian G_{kl} of exponent ϵ_2 and centered at point q on the line connecting the two atoms C and D:

$$G_{kl} = K_{CD}e^{-\epsilon_2|\mathbf{r}-\mathbf{R}_q|^2} \tag{5.8}$$

where:

$$K_{CD} = exp(\frac{-\gamma\delta}{\gamma+\delta}|\mathbf{R}_C - \mathbf{R}_D|^2) \tag{5.9}$$

$$\epsilon_2 = \gamma + \delta \tag{5.10}$$

Thus a two-electron integral of the form $(\mu\nu|\sigma\lambda)$ reduces to integrals of the form $(G_{ij}|G_{kl})$:

$$(\mu\nu|\sigma\lambda) = \sum_{i=1}^{m1}\sum_{j=1}^{m2}\sum_{k=1}^{m3}\sum_{l=1}^{m4} d_{i\mu}d_{j\nu}d_{k\sigma}d_{l\lambda}(G_{ij}|G_{kl}) \tag{5.11}$$

The same discussion can be easily extended to Gaussians other than $1s$ which makes Gaussian basis functions the most efficient basis functions for calculating two-electron integrals.

A very brief overview of two-electron integral calculations in MUNgauss is presented in Section 5.2 . Section 5.3 describes a new algorithm to make the two-electron

integrals calculations more efficient. Section 3.4 presents the results of this algorithm in addition to a comparison to the present performance of MUNgauss.

5.2 Two-Electron Integral in MUNgauss

For each group of four basis functions μ, ν, σ and λ there are 24 possible permutations and consequently 24 integrals of the form $(\mu\nu|\sigma\lambda)$ need to be calculated. However, only three of the 24 integrals are unique and thus need be calculated. MUNgauss implements the concept of shells. Given four different shells a, b, c, and d, the three different combinations are $(ab|cd)$, $(ac|bd)$ and $(ad|cb)$. $(ab|cd)$, e.g., represents a set of integrals, or a block, over all of the basis functions which belong to the four shells (a, b, c, and d) taken in this order. For example if $(\mu\nu|\sigma\lambda)$ is one of these integrals, then μ represents the bases from the shell a, ν the bases from the shell b, σ the bases from the shell c, and finally λ the bases from the shell d. It often occurs that all integrals of a block are either equal to zero or so small that they can be neglected. By default, two-electron integrals of value $\leq 10^{-7}$ are considered negligible in MUNgauss. Since the value of the integral $(G_{ij}|G_{kl})$ depends on K_{AB} and K_{CD}, both K_{AB} and K_{CD}, see equations (5.5), (5.8), and (5.11), are useful parameters to predict whether to calculate $(G_{ij}|G_{kl})$ or to skip it. If all the integrals $(G_{ij}|G_{kl})$ belonging to a block $(ab|cd)$ satisfy the following condition:

$$\min\ (K_{AB} + K_{CD}) \leq \text{cutoff} \tag{5.12}$$

then these integrals will be calculated, otherwise, all such integrals are of negligible

value and thus all the two-electron integrals for this block can be avoided [14]. Given the integral $(\mu\nu|\sigma\lambda)$ where μ, ν, σ and λ are contracted basis functions as mentioned in the introduction, the inequality (5.12) can be further used to avoid calculating integrals with small values where the sum $K_{AB} + K_{CD}$ is defined over the primitive gaussians constituting the basis functions μ, ν, σ and λ.

In MUNgauss, the value of the cutoff was set to 45. However, different values of the cutoff were used in this project and it was found that, while a cutoff of 20 almost maintained the same accuracy in energy, six decimal places, it skipped calculating many integrals within the threshold of 10^{-7} as shown in Table 5.1. From now on, the term zero integrals will be used to refer to two-electron integrals with values $\leq 10^{-7}$. In Table 5.1, N_{45} is the number of negligible integrals calculated with a cutoff of 45, and N_{20} is the number of integrals calculated with a cutoff of 20 and considered to be equal to zero. The fifth column in Table 5.1 represents the percentage of the integrals that was predicted to be $\leq 10^{-7}$ and was not calculated based on the 20 cutoff.

While a cutoff of 20 did not skip calculating any integrals for small molecules, e.g. AsH_3, it saved calculating almost 90% of the zero integrals calculated with the cutoff of 45 for large molecules like N_{46} and $N_{50}H_{28}$. However, there is still a large number of integrals calculated and then discarded i.e. 1,511,100,350 for $N_{50}H_{28}$. ΔE_{20} in the sixth column in Table 5.1 represents the difference in energy in μH between the 45 cutoff and the 20 cutoff. ΔE_{20} is zero for most of the test cases and as large as 7 μH for Sn_4H_{10}, while its value is only 2 μH for the largest molecule $N_{50}H_{28}$. For the series of molecules GeH_4 to Ge_5H_{12}, SiH_4 to Si_6H_{14}, and SnH_4 to Sn_4H_{10}, $\%N_{20}$ was zero for the smallest molecules in these sets, but in general increased with the

increase in size of the molecule. This feature is desirable since it is computationally inexpensive to calculate all the two-electron integrals for small molecules while the accuracy is maintained. To confirm the adequacy of a cutoff of 20, a larger data set was used and additional molecular properties were calculated. The results, which are not shown in this thesis, indicate that a cutoff of 20 does not affect the accuracy of quantum chemical calculations. The same study was performed for cutoffs of 17, 15, and 12 and the results are given in Table 5.2. With a cutoff of 17, the error in energy was still reasonable for most members of the data set. The largest $|\Delta E_{17}|$ is 47 μH for the molecule N_{46} followed by 32 μH for $N_{50}H_{28}$. However, as Table 5.2 shows, as the cutoff decreases to 15 and then to 12, ΔE increases rapidly. The largest error is -7192 μH for the molecule N_{46} with a cutoff of 12. To evaluate the increase in the number of skipped two-electron integrals with respect to the decrease in the cutoff, $\%N_{17} - \%N_{20}$, $\%N_{15} - \%N_{17}$, $\%N_{12} - \%N_{15}$ were calculated and given in Table 5.3. This table shows that the number of two-electron integrals that could be skipped does not increase much as the cutoff decreases from 15 to 12. For instance, for the molecule $N_{32}H_{14}$, $\Delta E_{15} = 375$ and $\Delta E_{12} = 6601$ while the percentage of integrals of negligible values increased by only 0.6%. The same pattern is obvious for the series of molecules 1G_pep to 8G_pep. Although large molecules such as GaN_{25}, $N_{26}H_{16}$, and $N_{32}H_{14}$ gained dramatically from decreasing the cutoff form 45 to 20 and maintained the same accuracy in energy, the gain was almost negligible for a cutoff less than 17 with a huge loss in the accuracy of the energy. Therefore, we do not recommend using an aggressively small cutoff.

5.3 A New Algorithm for Skipping Zero Two-Electron Integrals

The H matrix can be calculated by:

$$H_{\mu\nu} = \int \phi_{\mu}^{*}(\mathbf{r}_1)\hat{h}(\mathbf{r}_1)\phi_{\nu}(\mathbf{r}_1)d\mathbf{r}_1 \tag{5.13}$$

where the one-electron integral in the above equation can be calculated easily. It was shown in Chapter 4 that there is a ratio between the elements of the H and G matrices which suggests that if the zero elements of the H matrix are known, the zero elements of the G matrix could be predicted and the calculations of the corresponding integrals could be avoided. Figure 5.1 shows the elements $H_{\mu\nu}$ and the corresponding $G_{\mu\nu}$ values for the molecule 1G_pep where:

$$-10^{-5} \leq H_{\mu\nu} \leq 10^{-5} \tag{5.14}$$

This figure shows that the elements $G_{\mu\nu}$ are well contained in the range of -6×10^{-3} to 6×10^{-3}. Figure 5.2 shows the same elements of H versus the corresponding elements of F. The relationship between the elements of H and F is almost identical to that of the elements of H and G. The same graphs for $G_{\mu\nu}$ versus $H_{\mu\nu}$ and $F_{\mu\nu}$ versus $H_{\mu\nu}$ where $H_{\mu\nu}$ is given by equation (5.14) were plotted for the molecules CCl_4, Ge_5H_{12}, and Sn_4H_{10}, see Figures 5.3, 5.4, 5.5, 5.6, 5.7, and 5.8. Elements of F and G for CCl_4 are in the interval -4×10^{-4} to 4×10^{-4}, while for Ge_5H_{12}, F and G are in the interval -4×10^{-3} to 4×10^{-3}, and for Sn_4H_{10}, F and G are in the interval -3×10^{-3} to 3×10^{-3}. Since MUNgauss implements the concept of shells and we

have to loop over shells before progressing to the basis functions belonging to these shells, it is more efficient to decide on the level of shells if a block of integrals has zero values for all of its integrals. Therefore a matrix $\mathcal{H}$ of dimensions $m \times m$, where m is the number of shells, is calculated. $\mathcal{H}_{ab}$ is defined by:

$$\mathcal{H}_{ab} = \sum_{\mu \in a, \nu \in b} |H_{\mu\nu}| \tag{5.15}$$

where μ and ν are two basis functions, a and b are two shells. In other words, the matrix H defined over k basis functions is condensed to a matrix $\mathcal{H}$ over m shells. Table 5.4 shows the number of zero integrals not calculated since they are used to calculate Fock matrix elements corresponding to elements of the $\mathcal{H}$ matrix of values $|\mathcal{H}_{ab}| \leq 10^{-5}$. The corresponding error in energy ΔE is included in Table 5.4 as well. The results in Table 5.4 were obtained in combination with a cutoff of 20 as mentioned in the previous section. While SCF did not converge for CH_4, CO_2, GeH_4, SiH_4, SnH_4, and TS_CH_3Br_2, the error in energy for Ge_2H_6 to Ge_5H_{12}, Si_2H_6 to Si_6H_{14} and Sn_2H_6 to Sn_4H_{10} was zero or at most 4 μH. It is interesting to notice that although the SCF did not converge for small molecules, for larger molecules the error was negligible and a large number of zero integrals could actually be skipped. Using the $\mathcal{H}$ matrix we could save calculating 185,530,656 unnecessary two-electron integrals for the molecule $N_{50}H_{28}$ with ΔE as small as 2 μH. For the set of molecules 1G_pep to 8G_pep the error in energy was zero. Although using the $\mathcal{H}$ matrix to bypass calculating some of the zero integrals is unreasonable for small molecules, the results in Table 5.4 show that this algorithm can be used with large molecules which is the primary goal.

The same study was repeated for $|\mathcal{H}_{ab}| \leq 10^{-4}$. In Table 5.5, column 2 presents the number of zero integrals while column 3 gives the error in energy. The SCF did not converge or converged to a completely wrong energy for the molecules CCl_4, CH_4, CO_2, GeH_4, SiH_4, SnH_4, and TS_CH_3Br_2, TS_CH_3BrI, and TS_CH_3ClBr. However, the error for the peptide series was reasonable. The largest error of any of the peptides was 67 μH for 8G_pep. For the large molecules GaN_{25}, $N_{26}H_{16}$, ScN_{25}, $N_{32}H_{14}$, N_{46}, and $N_{50}H_{28}$ the error was in the range of -48 μH to -211 μH which is smaller than the error of the diatomic molecules HI, I_2, and KI.

In this chapter two methods were presented to detect which integrals will be of zero value and therefore could be skipped. One algorithm uses the threshold introduced in the last section and the other uses the $\mathcal{H}$ matrix. To compare the performance of the two algorithms, the percentage of two-electron integrals calculated and thrown away either using a cutoff of 17 or the $\mathcal{H}$ matrix algorithm, $|\mathcal{H}_{ab}| \leq 10^{-4}$, relative to those thrown away at 20 cutoff was calculated. The second column of Table 5.6 gives the percentage of the two-electron integrals skipped using the $\mathcal{H}$ matrix and the corresponding error in energy is given in column 4. The third column gives the percentage of the two-electron integrals skipped using a threshold of 17 while the corresponding error in energy is given in the last column of Table 5.6. It is clear from Table 5.6 that the error in energy introduced by using a cutoff of 17 is less than that introduced by using the $\mathcal{H}$ matrix algorithm in addition to the advantage that there was no convergence problem using a cutoff of 17. For small molecules such as AsH_3, Br_2 and C_3H_8 the $\mathcal{H}$ matrix algorithm saved more two-electron integrals than the cutoff of 17 did. But starting from 1G_pep to the end of the Table 5.6 the

cutoff of 17 saved more two-electron integrals than the $\mathcal{H}$ matrix. Therefore using the criterion (5.12) is more efficient and accurate than the $\mathcal{H}$ matrix.

5.4 Conclusions

The cutoff used in MUNgauss to skip calculating zero integrals was studied and found to be too weak. A new value of the cutoff was suggested which skipped as many zero integrals as possible while maintaining the same accuracy of the energy, six decimal places. We developed a new algorithm based on the $\mathcal{H}$ matrix to detect the zero integrals in advance. The performance of this algorithm was studied and it was found to cause convergence problems for the SCF and huge errors for some of the test cases as a result of skipping significant integrals.

Table 5.1: The effect of changing the cutoff from 45 to 20 on the number of zero integrals calculated and the energy(μH) in addition to the % savings

Molecule	Number of basis[a]	N_{45}	N_{20}	$\%N_{20}$	ΔE_{20}
AsH_3	41	113,670	113,670	0	0
Br_2	70	816,463	288,133	64.7	0
C_2H_4	38	9,498	9,493	0.1	0
C_2H_6	42	10,327	10,305	0.2	0
C_3H_8	61	65,331	43,740	33.1	0
C_4H_{10}	80	772,709	221,397	71.4	0
C_5H_{12}	99	2,984,866	672,188	77.5	0
C_6H_{14}	118	7,784,632	1,546,541	80.1	0
CCl_4	91	2,064,989	722,665	65.0	0
CH_2Br_2	89	1,537,212	769,714	49.9	0
$(HCOOH)_2$	98	3,715,796	618,425	83.4	1
$CH_2(PH_2)_2$	65	232,316	232,316	0.0	0
$CH_2(SH)_2$	61	209,534	209,534	0.0	0
CH_3F	36	10,158	10,138	0.2	0
CH_3AsH_2	60	199,465	168,223	15.7	0
CH_3Br	56	183,900	155,890	15.2	0
CH_3CONH_2	70	140,519	86,298	38.6	0
CH_3SeH	58	190,351	161,278	15.3	0

... continued

Table 5.1 – continued

Molecule	Number of basis	N_{45}	N_{20}	$\%N_{20}$	ΔE_{20}
CH_4	23	4,698	4,698	0.0	0
CO	30	9,397	9,397	0.0	0
CO_2	45	23,820	21,646	9.1	0
EtBr	75	826,185	360,181	56.4	0
Ge_2H_6	82	1,355,250	588,950	56.5	0
Ge_3H_8	121	7,548,545	2,728,766	63.9	0
Ge_4H_{10}	160	26,391,426	7,355,882	72.1	0
Ge_5H_{12}	199	64,287,644	21,768,761	66.1	0
GeH_4	43	113,814	113,814	0.0	0
H_2	4	0	0	0.0	0
H_2O	19	4,698	4,698	0.0	0
$(H_2O)_2$	38	50,527	23,474	53.5	0
H_2Se	39	113,544	113,544	0.0	0
HF	17	4,698	4,698	0.0	0
HI	41	173,723	173,723	0.0	0
I_2	78	1,331,178	864,275	35.1	0
KI	74	776,008	391,403	49.6	0
LiF	30	9,396	9,396	0.0	0
NH_3	21	4,698	4,698	0.0	0
SbH_3	45	177,540	177,540	0.0	0
Si_2H_6	50	91,634	61,837	32.5	0

... continued

Table 5.1 – continued

Molecule	Number of basis	N_{45}	N_{20}	$\%N_{20}$	ΔE_{20}
Si_3H_8	73	792,434	358,479	54.8	0
Si_4H_{10}	96	3,409,063	1,095,550	67.9	0
Si_5H_{12}	119	9,272,778	2,595,770	72.0	0
Si_6H_{14}	142	19,068,291	4,714,937	75.3	0
SiH_4	27	11,178	11,178	0.0	0
Sn_2H_6	90	2,148,942	1,416,958	34.1	3
Sn_3H_8	133	12,815,728	6,591,339	48.6	4
Sn_4H_{10}	176	42,254,613	18,058,263	57.3	7
SnH_4	47	180,483	180,483	0.0	0
CH_3Br_2	91	2,735,407	875,462	68.0	0
CH_3BrI	95	3,421,595	1,350,152	60.5	0
CH_3ClBr	75	1,135,297	439,364	61.3	0
1G_pep	85	830,788	229,552	72.4	0
2G_pep	151	23,181,106	3,883,937	83.25	0
3G_pep	217	94,889,733	13,193,173	86.1	0
4G_pep	283	209,597,287	29,218,901	86.1	0
5G_pep	349	366,480,522	51,759,654	85.9	0
6G_pep	415	567,976,000	81,798,289	85.6	0
7G_pep	481	785,632,884	104,913,535	86.7	0
8G_pep	547	1,068,128,965	145,363,348	86.4	0
GaN_{25}	410	1,216,514,747	128,384,024	89.5	0

... continued

Table 5.1 – continued

Molecule	Number of basis	N_{45}	N_{20}	$\%N_{20}$	ΔE_{20}
$N_{26}H_{16}$	422	1,789,442,991	205,943,432	88.5	1
ScN_{25}	404	1,038,465,436	112,902,134	89.1	0
$N_{32}H_{14}$	508	2,874,861,671	301,488,732	89.5	1
N_{46}	690	9,421,886,881	800,531,450	91.5	1
$N_{50}H_{28}$	806	16,218,225,948	1,511,100,350	90.7	2

[a] 6-31G(d) basis set

Table 5.2: Percentage of skipped integrals for cutoffs of 17, 15, 12 and the corresponding $\Delta E(\mu\mathrm{H})$

Molecule	$\%N_{17}$	$\%N_{15}$	$\%N_{12}$	ΔE_{17}	ΔE_{15}	ΔE_{12}
AsH_3	0.0	0.0	0.0	0	1	10
Br_2	65.6	67.2	70.8	1	5	304
C_2H_2	0.2	0.4	0.7	0	0	-1
C_2H_4	0.2	0.5	0.9	0	0	6
C_2H_6	1.3	3.6	8.7	1	1	-4
C_3H_8	56.3	70.1	78.1	0	0	-7
C_4H_{10}	88.4	94.4	97.4	0	-1	-15
C_5H_{12}	92.0	96.9	99.1	1	-1	-18
C_6H_{14}	92.7	97.4	99.5	0	-1	-46
CCl_4	80.2	91.2	96.3	4	37	48
CH_2BrBr	60.8	71.8	79.6	2	18	155
$(HCOOH)_2$	94.5	97.6	99.0	3	25	170
$CH_2(PH_2)_2$	0.0	78.9	85.9	0	13	106
$CH_2(SH)_2$	64.9	77.7	84.6	1	11	56
CH_3F	1.4	4.2	7.5	0	1	19
CH_3AsH_2	21.3	27.7	38.4	1	10	125
CH_3Br	19.2	24.3	33.9	1	7	85
CH_3CONH_2	61.9	78.1	86.5	0	3	44
CH_3SeH	20.2	25.0	35.8	1	8	87

... continued

Table 5.2 – continued

Molecule	$\%N_{17}$	$\%N_{15}$	$\%N_{12}$	ΔE_{17}	ΔE_{15}	ΔE_{12}
CH_4	0.0	0.0	0.0	0	0	0
CO	0.0	0.0	0.0	0	0	0
CO_2	20.3	39.7	40.2	0	2	43
EtBr	68.1	78.7	83.4	1	7	47
Ge_2H_6	73.1	73.1	73.1	1	1	1
Ge_3H_8	79.0	87.4	91.3	2	0	-605
Ge_4H_{10}	83.9	90.1	94.4	3	0	-1343
Ge_5H_{12}	81.4	89.5	95.4	8	-15	-7401
GeH_4	0.0	0.0	0.0	0	1	15
H_2	0.0	0.0	0.0	0	0	0
H_2O	0.0	0.0	0.0	0	0	0
$(H_2O)_2$	78.0	79.2	81.1	1	0	31
H_2Se	0.0	0.0	0.0	0	2	8
HF	0.0	0.0	0.0	0	0	0
HI	0.0	0.0	0.0	0	0	5
I_2	56.9	65.1	66.0	-1	6	255
KI	50.7	51.2	54.4	3	5	96
LiF	0.0	0.0	0.0	0	1	14
NH_3	0.0	0.0	0.0	0	0	0
SbH_3	0.0	0.0	0.3	0	4	12
Si_2H_6	46.1	71.5	74.3	0	2	19
Si_3H_8	74.8	89.0	94.1	-1	1	-26

... continued

Table 5.2 – continued

Molecule	$\%N_{17}$	$\%N_{15}$	$\%N_{12}$	ΔE_{17}	ΔE_{15}	ΔE_{12}
Si_4H_{10}	84.6	93.1	97.2	-1	0	-85
Si_5H_{12}	87.2	94.4	98.1	-1	0	-121
Si_6H_{14}	88.9	95.1	98.5	-2	1	-182
SiH_4	0.0	0.0	0.0	0	0	6
Sn_2H_6	44.6	65.6	73.2	1	26	-3149
Sn_3H_8	61.5	76.4	86.7	-1	51	-9441
Sn_4H_{10}	69.9	81.5	90.4	-3	73	-19091
SnH_4	0.0	0.2	0.7	0	4	19
TS_CH_3Br_2	76.2	83.7	87.8	0	0	-280
TS_CH_3BrI	73.5	80.1	86.0	-2	8	127
TS_CH_3ClBr	72.6	81.2	85.7	0	-16	23
1G_pep	89.4	94.6	96.9	1	10	97
2G_pep	95.1	98.4	99.7	3	25	294
3G_pep	95.9	98.7	99.8	6	35	276
4G_pep	95.6	98.5	99.8	7	45	192
5G_pep	95.4	98.4	99.7	7	57	73
6G_pep	95.0	98.2	99.7	10	71	4
8G_pep	95.4	98.3	99.7	11	78	-736
GaN_{25}	96.9	99.0	99.8	20	180	-2965
$N_{26}H_{16}$	97.0	99.2	99.9	18	144	2320
ScN_{25}	96.4	98.9	99.9	20	194	2404
$N_{32}H_{14}$	97.2	99.3	99.9	15	193	6601

... continued

Table 5.2 – continued

Molecule	$\%N_{17}$	$\%N_{15}$	$\%N_{12}$	ΔE_{17}	ΔE_{15}	ΔE_{12}
N_{46}	98.0	99.5	99.9	47	376	-7192

Table 5.3: The percentage increase in the skipped two-electron integrals with the decrease of the cutoff

Molecule	$\%N_{17} - \%N_{20}$	$\%N_{15} - \%N_{17}$	$\%N_{12} - \%N_{15}$
AsH_3	0.0	0.0	0.0
Br_2	0.9	1.6	3.6
C_2H_2	0.3	0.1	0.3
C_2H_4	0.1	0.3	0.4
C_2H_6	1.0	2.4	5.0
C_3H_8	23.3	13.7	8.0
C_4H_{10}	17.1	6.0	2.9
C_5H_{12}	14.6	4.8	2.2
C_6H_{14}	12.6	4.7	2.1
CCl_4	15.2	11.0	5.1
CH_2Br_2	10.9	11.0	7.8
$(HCOOH)_2$	11.2	3.1	1.4
$CH_2(PH_2)_2$	0.0	78.9	7.0
$CH_2(SH)_2$	64.9	12.8	6.8
CH_3F	1.2	2.7	3.3
CH_3AsH_2	5.6	6.4	10.8
CH_3Br	4.0	5.1	9.5
CH_3CONH_2	23.4	16.2	8.3
CH_3SeH	4.9	4.8	10.9

... continued

Table 5.3 – continued

Molecule	$\%N_{17} - \%N_{20}$	$\%N_{15} - \%N_{17}$	$\%N_{12} - \%N_{15}$
CH_4	0.0	0.0	0.0
CO	0.0	0.0	0.0
CO_2	11.2	19.3	0.5
EtBr	11.7	10.6	4.6
Ge_2H_6	16.6	0.0	0.0
Ge_3H_8	15.1	8.4	3.9
Ge_4H_{10}	11.7	6.3	4.2
Ge_5H_{12}	15.2	8.2	5.8
GeH_4	0.0	0.0	0.0
H_2	0.0	0.0	0.0
H_2O	0.0	0.0	0.0
$(H_2O)_2$	24.4	1.2	1.9
H_2Se	0.0	0.0	0.0
HF	0.0	0.0	0.0
HI	0.0	0.0	0.0
I_2	21.8	8.2	0.9
KI	1.1	0.5	3.2
LiF	0.0	0.0	0.0
NH_3	0.0	0.0	0.0
SbH_3	0.0	0.0	0.3
Si_2H_6	13.6	25.5	2.7
Si_3H_8	20.0	14.2	5.1

... continued

Table 5.3 – continued

Molecule	$\%N_{17} - \%N_{20}$	$\%N_{15} - \%N_{17}$	$\%N_{12} - \%N_{15}$
Si_4H_{10}	16.7	8.6	4.1
Si_5H_{12}	15.2	7.2	3.7
Si_6H_{14}	13.6	6.2	3.4
SiH_4	0.0	0.0	0.0
Sn_2H_6	10.5	21.0	7.6
Sn_3H_8	13.0	14.9	10.2
Sn_4H_{10}	12.6	11.7	8.9
SnH_4	0.0	0.2	0.5
TS_CH_3Br_2	8.2	7.5	4.1
TS_CH_3BrI	13.0	6.6	5.9
TS_CH_3ClBr	11.3	8.5	4.5
1G_pep	17.0	5.2	2.4
2G_pep	11.9	3.3	1.2
3G_pep	9.8	2.8	1.1
4G_pep	9.6	2.9	1.2
5G_pep	9.5	3.0	1.3
6G_pep	9.4	3.2	1.5
8G_pep	9.0	2.9	1.4
GaN_{25}	7.4	2.1	0.9
$N_{26}H_{16}$	8.5	2.3	0.7
ScN_{25}	7.3	2.5	1.0
$N_{32}H_{14}$	7.6	2.1	0.6

... continued

Table 5.3 – continued

Molecule	$\%N_{17} - \%N_{20}$	$\%N_{15} - \%N_{17}$	$\%N_{12} - \%N_{15}$
N_{46}	6.5	1.5	0.5

Table 5.4: Number of zero integrals skipped and the corresponding error in energy (μH) for $|\mathcal{H}_{ab}| \leq 10^{-5}$

Molecule	zero integrals skipped	ΔE
AsH_3	2754	17
Br_2	1954	0
C_2H_2	0	0
C_2H_4	0	0
C_2H_6	0	0
C_3H_8	12256	0
C_4H_{10}	67456	-1
C_5H_{12}	253446	0
C_6H_{14}	514840	0
CCl_4	35521	27624
CH_2BrBr	5650	0
$(HCOOH)_2$	144115	1
$CH_2(PH_2)_2$	20256	0
$CH_2(SH)_2$	12912	0
CH_3-F	688	0
CH_3AsH_2	15283	17
CH_3Br	6406	62
CH_3CONH_2	21433	0
CH_3SeH	8250	35

... continued

Table 5.4 – continued

Molecule	zero integrals	ΔE
CH_4	5211	NC[a]
CO	0	0
CO_2	65179	NC[a]
EtBr	47371	0
Ge_2H_6	145680	0
Ge_3H_8	605712	1
Ge_4H_{10}	1200068	2
Ge_5H_{12}	3293523	0
GeH_4	75444	NC[a]
H_2	0	0
H_2O	0	0
$(H_2O)_2$	11868	0
H_2Se	2511	35
HF	0	0
HI	21987	-202
I_2	399813	-19
KI	16053	-158
LiF	0	0
NH_3	0	0
SbH_3	26163	-83
Si_2H_6	32280	0
Si_3H_8	201725	0

... continued

Table 5.4 – continued

Molecule	zero integrals	ΔE
Si_4H_{10}	529378	0
Si_5H_{12}	1114295	-1
Si_6H_{14}	1933084	0
SiH_4	13878	NC[a]
Sn_2H_6	178259	1
Sn_3H_8	882358	2
Sn_4H_{10}	2521562	4
SnH_4	161325	NC[a]
TS_CH_3Br_2	117483	NC[a]
TS_CH_3BrI	272553	-156
TS_CH_3ClBr	43992	0
1G_pep	77682	0
2G_pep	1170338	0
3G_pep	4015586	0
4G_pep	7683375	0
5G_pep	12822899	0
6G_pep	18876492	0
7G_pep	22425106	0
8G_pep	29370098	0
GaN_{25}	20381969	0
$N_{26}H_{16}$	31628755	1
ScN_{25}	12861056	0

... continued

Table 5.4 – continued

Molecule	zero integrals	ΔE
$N_{32}H_{14}$	40028164	0
$N_{50}H_{28}$	185530656	2

[a] Failure in convergence

Table 5.5: Number of zero integrals skipped and the corresponding error in energy (μH) for $|\mathcal{H}_{ab}| \leq 10^{-4}$

Molecule	zero integrals skipped	ΔE
AsH_3	5499	236
Br_2	66451	108
C_2H_2	637	-1
C_2H_4	0	0
C_2H_6	929	0
C_3H_8	57352	-1
C_4H_{10}	257726	-8
C_5H_{12}	705857	-1
C_6H_{14}	1635744	-7
CCl_4	702391	NC[a]
CH_2BrBr	277826	803
$(HCOOH)_2$	746114	9
$CH_2(PH_2)_2$	142282	-6
$CH_2(SH)_2$	98344	-4
CH_3-F	688	0
CH_3AsH_2	49016	229
CH_3Br	44935	748
CH_3CONH_2	82621	-11
CH_3SeH	42878	447

... continued

Table 5.5 – continued

Molecule	Skipped integrals	ΔE
CH_4	5211	NC[a]
CO	0	0
CO_2	65179	NC[a]
EtBr	253794	751
Ge_2H_6	348841	275
Ge_3H_8	1531466	141
Ge_4H_{10}	3340618	17
Ge_5H_{12}	10788551	32
GeH_4	92094	NC[a]
H_2	0	0
H_2O	0	0
$(H_2O)_2$	17537	1
H_2Se	5013	453
HF	0	0
HI	30033	10494
I_2	418388	-304
KI	87981	11164
LiF	0	0
NH_3	0	0
SbH_3	32580	9028
Si_2H_6	40715	-5
Si_3H_8	271525	-12

... continued

Table 5.5 – continued

Molecule	Skipped integrals	ΔE
Si_4H_{10}	788584	-20
Si_5H_{12}	1764628	-30
Si_6H_{14}	3063098	-40
SiH_4	13878	NC[a]
Sn_2H_6	801236	-119
Sn_3H_8	3193876	-119
Sn_4H_{10}	8262764	-134
SnH_4	216729	NC[a]
TS_CH_3Br_2	402539	NC[a]
TS_CH_3BrI	706413	NC[a]
TS_CH_3ClBr	237914	NC[a]
1G_pep	183099	-3
2G_pep	3256085	-18
3G_pep	9817960	-32
4G_pep	19617567	-36
5G_pep	31987865	-47
6G_pep	46598658	-54
7G_pep	54855668	-58
8G_pep	72761573	-67
GaN_{25}	65705393	-48
$N_{26}H_{16}$	101668193	-89
ScN_{25}	57744162	-57

... continued

Table 5.5 – continued

Molecule	Skipped integrals	ΔE
$N_{32}H_{14}$	148104509	-91
N_{46}	345934398	-211
$N_{50}H_{28}$	621063924	-179

[a] Failure in convergence

Table 5.6: Percentage of the two-electron integrals skipped using a cutoff of 17 and using the $\mathcal{H}$ matrix, see text.

Molecule	N($\mathcal{H}$)%	N(17)%	Δ E($\mathcal{H}$)	Δ E(17)
AsH_3	2.22	0	236	0
Br_2	11.75	2.43	108	1
C_2H_2	0.52	0.29	-1	0
C_2H_4	0	0.14	0	0
C_2H_6	6.96	1.04	0	1
C_3H_8	51.08	34.76	-1	0
C_4H_{10}	61.38	59.65	-8	0
C_5H_{12}	64.17	64.65	-1	1
C_6H_{14}	66.26	63.45	-7	0
CCl_4	60.56	43.44	NC	4
CH_2BrBr	29.22	21.68	803	2
$(HCOOH)_2$	66.52	67.14	9	3
$CH_2(PH_2)_2$	78.8	0	-6	0
$CH_2(SH)_2$	77.05	64.91	-4	1
CH_3F	6.79	1.23	0	0
CH_3AsH_2	20.77	6.67	229	1
CH_3Br	18.36	4.72	748	1
CH_3CONH_2	53.45	38.03	-11	0
CH_3SeH	18.44	5.78	447	1

Continued

Table 5.6 – continued

Molecule	N($\mathcal{H}$)	N(17)	Δ E($\mathcal{H}$)	Δ E(17)
CH_4	33.33	0	-79275743	0
CO	0	0	0	0
CO_2	54.6	12.33	-1311358674	0
EtBr	47.74	26.87	751	1
Ge_2H_6	46.72	38.13	275	1
Ge_3H_8	48.68	41.9	141	2
Ge_4H_{10}	40.46	42.05	17	3
Ge_5H_{12}	45.55	44.95	32	8
GeH_4	34.86	0	NC	0
H_2	0	0	0	0
H_2O	0	0	0	0
$(H_2O)_2$	49.34	52.57	1	1
H_2Se	2.2	0	453	0
HF	0	0	0	0
HI	9.34	0	10494	0
I_2	47.23	33.6	-304	-1
KI	8.97	2.18	11164	3
LiF	0	0	0	0
NH_3	0	0	0	0
SbH_3	9.18	0	9028	0
Si_2H_6	56.02	20.08	-5	0
Si_3H_8	67.4	44.2	-12	-1

Continued

Table 5.6 – continued

Molecule	N($\mathcal{H}$)	N(17)	Δ E($\mathcal{H}$)	Δ E(17)
Si_4H_{10}	63.11	51.94	-20	-1
Si_5H_{12}	60.56	54.18	-30	-1
Si_6H_{14}	58.54	54.99	-40	-2
SiH_4	40.1	0	-80598259	0
Sn_2H_6	47.21	15.99	-119	1
Sn_3H_8	44.87	25.2	-119	-1
Sn_4H_{10}	43.59	29.51	-134	-3
SnH_4	54.77	0.01	NC	0
TS_CH_3Br_2	33.03	25.52	NC	0
TS_CH_3BrI	44.55	32.9	85780057	-2
TS_CH_3ClBr	40.3	29.27	32136338	0
1G_pep	58.6	61.66	-3	1
2G_pep	62.03	70.96	-18	3
3G_pep	60.13	70.7	-32	6
4G_pep	57.01	68.74	-36	7
5G_pep	54.26	67.34	-47	7
6G_pep	51.33	65.37	-54	10
8G_pep	46.99	66.01	-67	11
GaN_{25}	46.65	70.55	-48	20
$N_{26}H_{16}$	44.75	73.66	-89	18
ScN_{25}	45.39	66.8	-57	20
$N_{32}H_{14}$	44.76	72.89	-91	15

Continued

Table 5.6 – continued

Molecule	N($\mathcal{H}$)	N(17)	Δ E($\mathcal{H}$)	Δ E(17)
N_{46}	40.46	76.82	-211	47
$N_{50}H_{28}$	39.47	74.32	-179	32

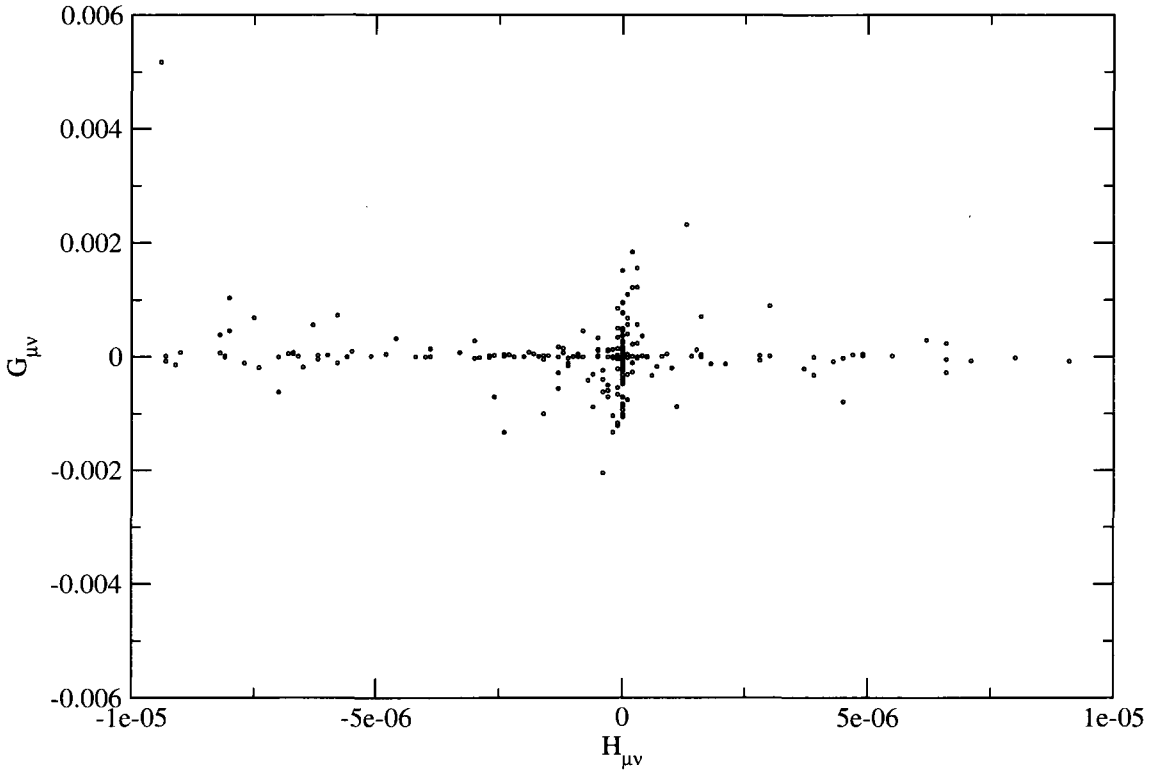

Figure 5.1: $G_{\mu\nu}$ vs $H_{\mu\nu}$ where $-10^{-5} \leq H_{\mu\nu} \leq 10^{-5}$ for 1G_pep

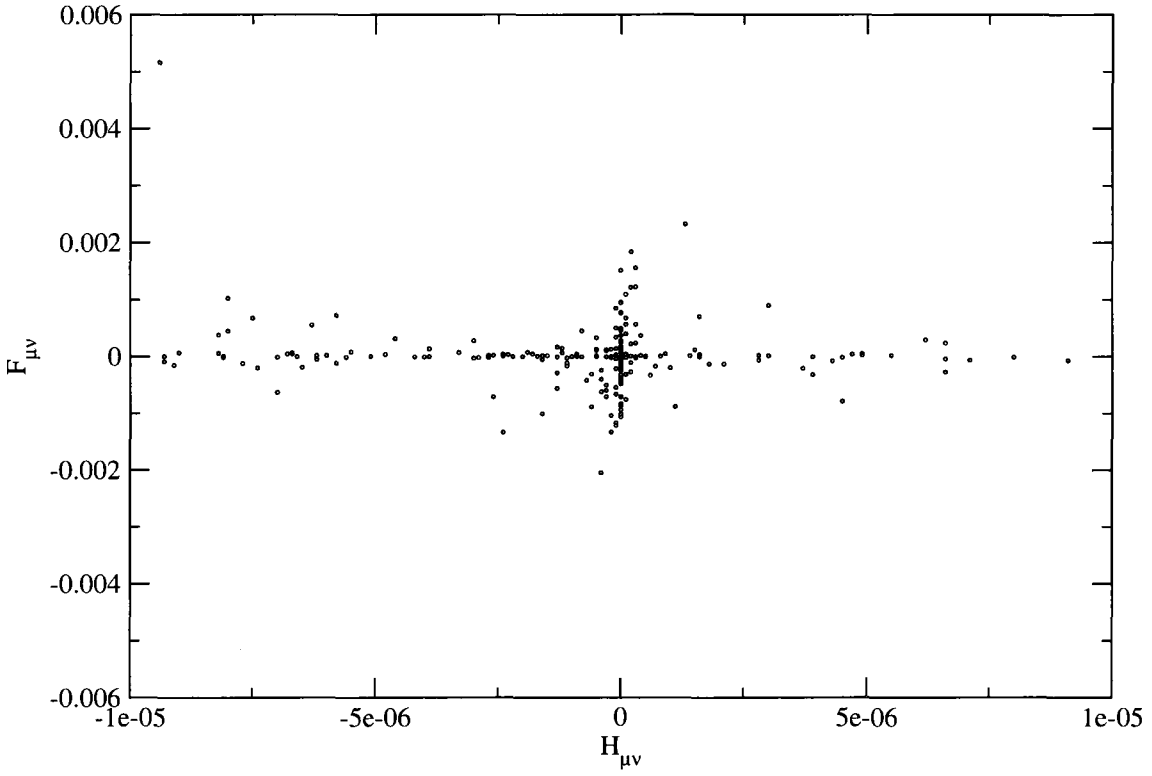

Figure 5.2: $F_{\mu\nu}$ vs $H_{\mu\nu}$ where $-10^{-5} \leq H_{\mu\nu} \leq 10^{-5}$ for 1G_pep

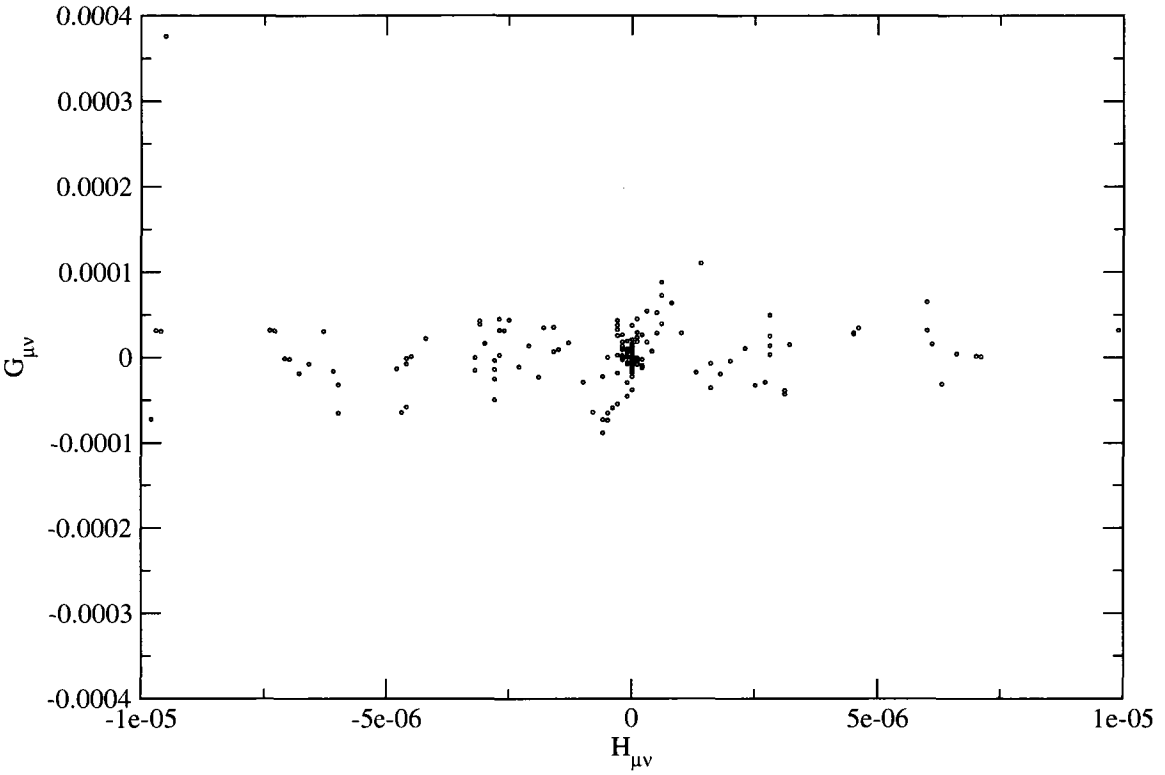

Figure 5.3: $G_{\mu\nu}$ vs $H_{\mu\nu}$ where $-10^{-5} \leq H_{\mu\nu} \leq 10^{-5}$ for CCl_4

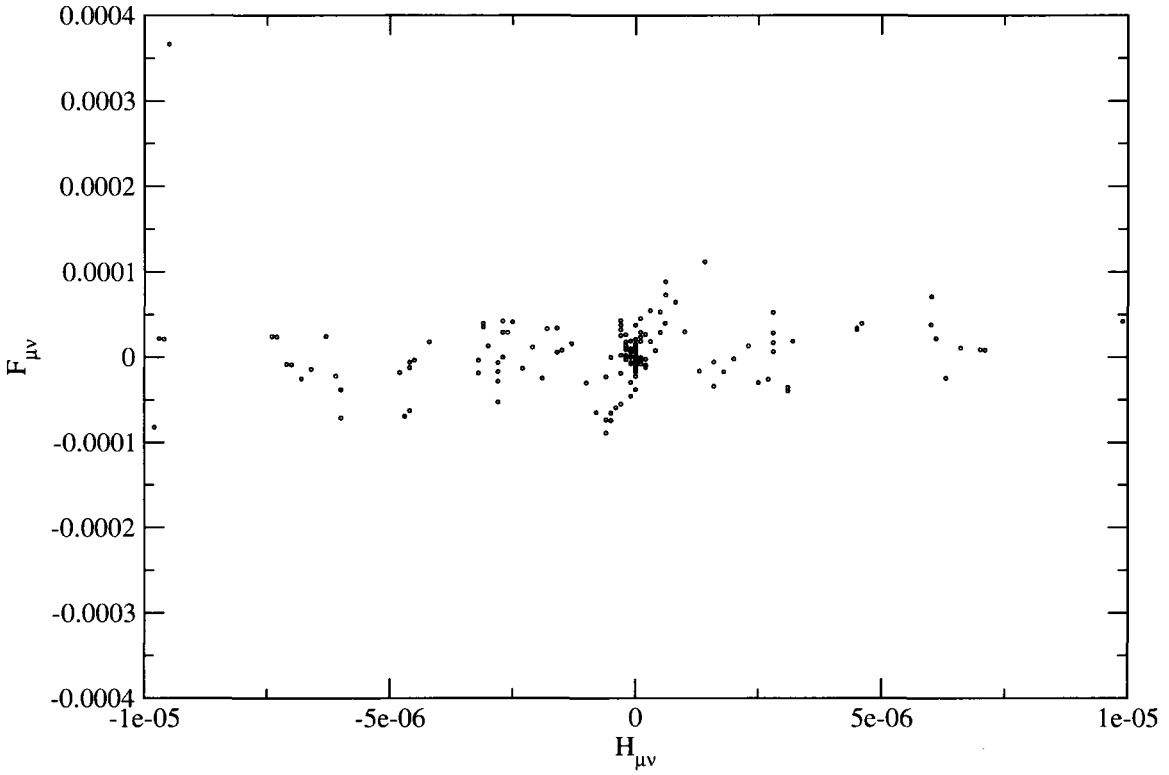

Figure 5.4: $F_{\mu\nu}$ vs $H_{\mu\nu}$ where $-10^{-5} \leq H_{\mu\nu} \leq 10^{-5}$ for CCl_4

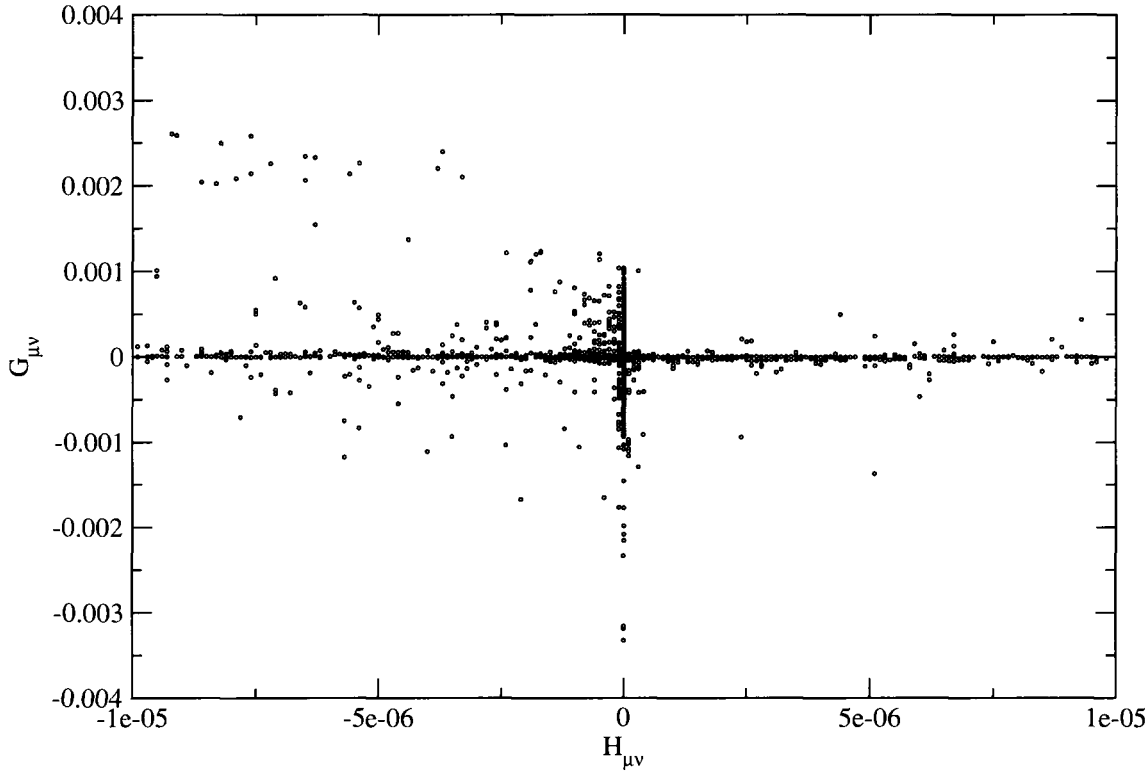

Figure 5.5: $G_{\mu\nu}$ vs $H_{\mu\nu}$ where $-10^{-5} \leq H_{\mu\nu} \leq 10^{-5}$ for Ge_5H_{12}

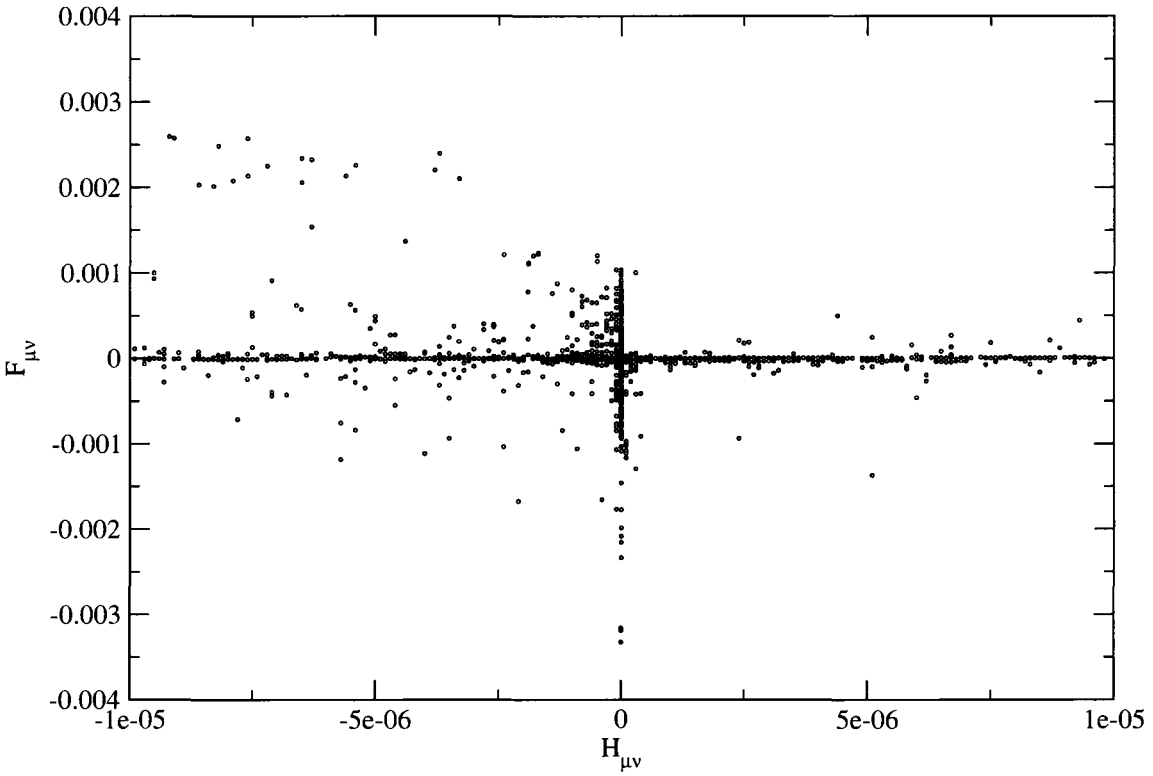

Figure 5.6: $F_{\mu\nu}$ vs $H_{\mu\nu}$ where $-10^{-5} \leq H_{\mu\nu} \leq 10^{-5}$ for Ge_5H_{12}

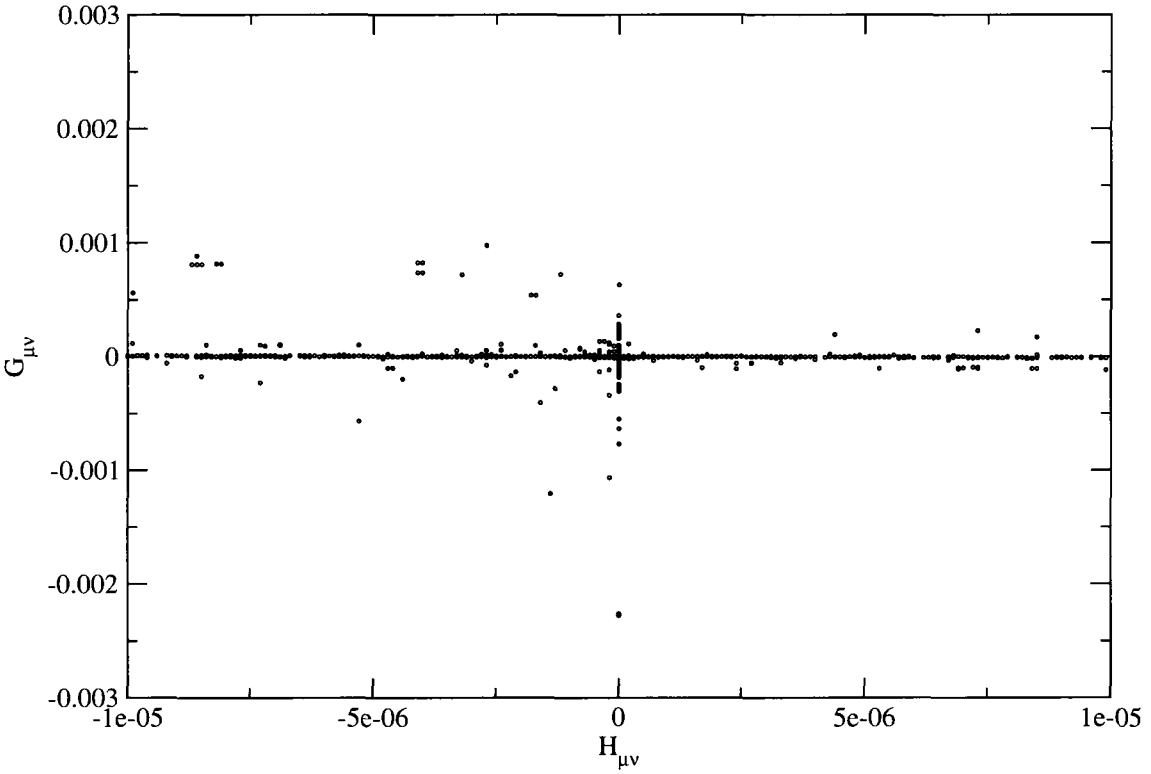

Figure 5.7: $G_{\mu\nu}$ vs $H_{\mu\nu}$ where $-10^{-5} \leq H_{\mu\nu} \leq 10^{-5}$ for Sn_4H_{10}

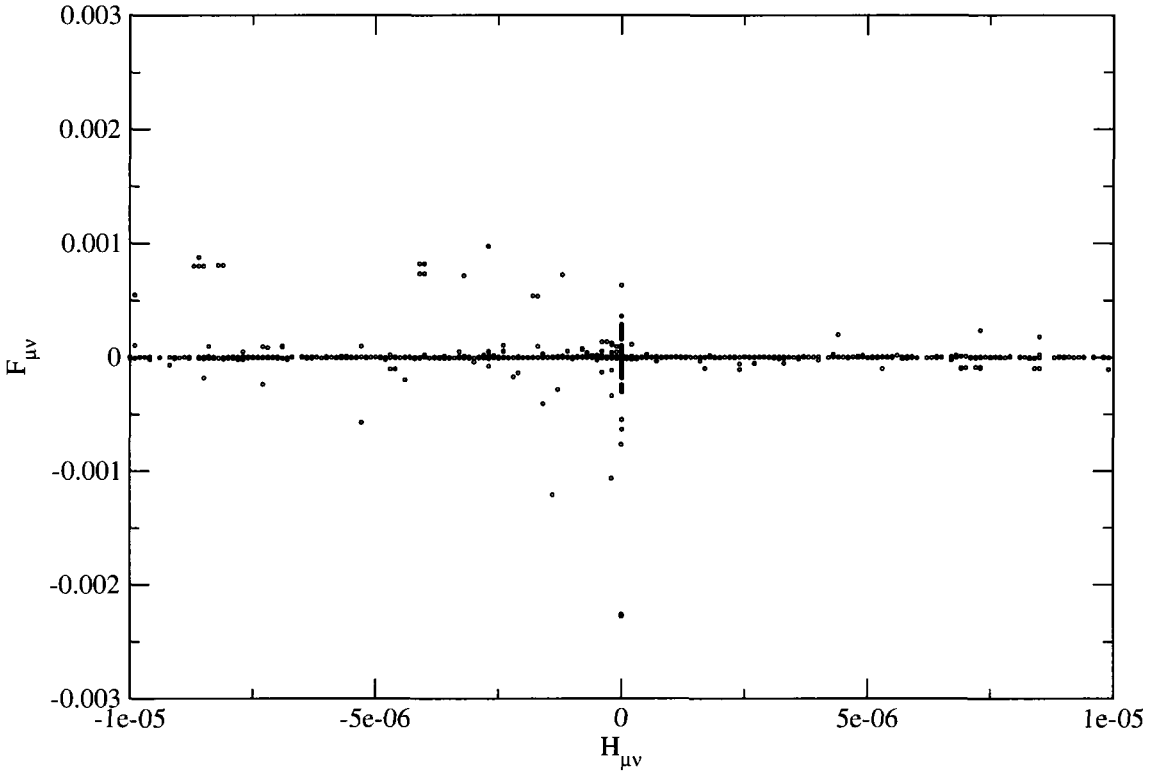

Figure 5.8: $F_{\mu\nu}$ vs $H_{\mu\nu}$ where $-10^{-5} \leq H_{\mu\nu} \leq 10^{-5}$ for Sn_4H_{10}

Chapter 6

Initial Guess for Large Basis Sets

6.1 Introduction

Roothaan's equation:

$$FC = SC\epsilon \tag{6.1}$$

has to be solved self consistently [1]. An initial guess of the density matrix P^0 should be available at the first iteration. There are different ways to produce the initial guess, e.g., by using a semiempirical method like extended Hückel [24, 26], or by projecting the Fock matrix obtained from the calculation with a smaller basis set. A brief overview of both algorithms is presented in the following two sections.

6.2 Extended Hückel

In extended Hückel (EH) theory the Fock matrix in equation (6.1) is calculated using the formula [24]:

$$F_{ij}^{EH} = \frac{1}{2}k(F_{ii} + F_{jj})S_{ij} \tag{6.2}$$

where S is the overlap matrix and k is a parameter. The diagonal element F_{ii} is the negative of the ionization potential for an electron in orbital i. The Fock matrix calculated using equation (6.2) is of the same size as for a minimal basis set (e.g., STO-3G). If the initial guess is required for a basis set larger than STO-3G, then F^{EH} is projected to the larger basis set, (see chapter 4). By substituting F^{EH} in equation (6.1) and solving for C, the density matrix P^0 can be calculated by:

$$P^0 = 2CC^\dagger \tag{6.3}$$

6.3 Initial Guess Using Projection

An alternative way to create the initial guess is:

- obtain F^x for a smaller basis set {X} than the one actually required.
- project F^x to F^y, where {Y} is a larger basis set, see chapter 4.
- diagonalize F^y to obtain the coefficient matrix and the guess density matrix.

In MUNgauss the SCF is considered converged (by default) when the norm of the difference between two density matrices calculated in consecutive iterations $\| \Delta P \|$ is given by:

$$\| \Delta P \| \leq 5 \times 10^{-6} \tag{6.4}$$

In this section we investigate the effect of using a less strict convergence criterion for the SCF performed with the smaller basis set on the quality of the initial guess. We also investigate the effect of using a smaller cutoff for the two-electron integrals on the initial guess, see Chapter 5. The quality of the initial guess is measured by the number of cycles required for the SCF, with the larger basis set, to converge to the correct density matrix. The number of SCF cycles was determined for three cases:

1. N_{app} is the number of SCF cycles where the initial guess is created from an approximate SCF converged with the criterion $\| \Delta P \| \leq 5 \times 10^{-2}$ and a cutoff of 10 is used for the two-electron integrals.

2. N_{acc} is the number of SCF cycles where the initial guess is created from a fully converged SCF, exact SCF, with a smaller basis set and the cutoff for the two-electron integrals is 45.

3. N_{EH} is the number of SCF cycles where the initial guess is created using projected extended Hückel.

These three calculations were performed for the projection from STO-3G to the following basis sets:

- 3-21G
- 6-31G
- STO-3G(d)
- 6-31G(d)

- 6-311G(d)

The SCF did not converge with a cutoff of 10 for the two-electron integrals in the case of Sn_4H_{10} while it converged with a cutoff of 12 for all cases. Table 6.1 gives the number of SCF cycles, N_{app}, N_{acc}, and N_{EH}, where the SCF was performed using 3-21G basis set. Table 6.1 shows that, for the series of molecules SnH_4, Sn_2H_6, Sn_3H_8, and Sn_4H_{10}, that the SCF converged equally well whether or not the inintial guess was created with an exact SCF or an approximate SCF ($N_{app} \sim N_{acc}$). However, the number of cycles using an initial guess created by projected EH varied a lot, from 11 cycles with SnH_4 to 20 cycles with Sn_2H_6 and Sn_4H_{10}, and SCF did not converge for Sn_3H_8. For the same series of molecules, the largest N_{app} is nine cyles while the largest N_{acc} is eight cycles. Also, from Table 6.1, $N_{app} > N_{acc}$ for GaN_{25} while $N_{acc} > N_{app}$ for 1G_pep. Calculating an initial guess by projecting with strict thresholds for SCF convergence and two-electron integrals does not necessarily lead to a smaller number of SCF cycles.

From Table 6.2, where the 6-31G basis set is used, N_{EH} is not much larger than N_{app} or N_{acc} for SnH_4 and Sn_2H_6. However, for Sn_3H_8 and Sn_4H_{10}, N_{EH} is much larger than both of N_{app} and N_{acc}. For the molecules N_{46} and GaN_{25}, N_{EH} is far larger than N_{app} and N_{acc}. Calculating the initial guess using a projected EH seems to be computationally inexpensive, but if it leads to an SCF requiring many more cycles to converge, the Hückel guess would be more expensive than other alternatives.

Table 6.3 gives the number of SCF cycles, N_{app}, N_{acc}, and N_{EH}, for the STO-3G(d) basis set. Since STO-3G and STO-3G(d) basis sets are the same for the third and fourth rows, $N_{acc} = 1$ for molecules containing atoms from the third and fourth rows.

However, the corresponding N_{app} is different than one since the SCF was not allowed to fully converge for STO-3G calculations. For STO-3G(d) calculations, a projected EH initial guess seems to do as well as an initial guess calculated from projection.

Table 6.4 gives the number of SCF cycles, N_{app}, N_{acc}, and N_{EH}, for the SCF using 6-31G(d) basis set. Using a projected EH initial guess, the SCF converged for SnH_4 in ten cyles compared to eight cycles when the projection was used to create the initial guess which implies a good parametrization is used for the EH guess. However, for Sn_2H_6, N_{EH} was almost three times larger than N_{app} and N_{acc}, and the SCF did not converge for both of Sn_3H_8 and Sn_4H_{10}. Thus a projected EH guess can produce an initial guess that leads to an SCF of similar number of cycles to that of an SCF performed with an initial guess produced by projection, an SCF with much higher number of cycles, or to an unconverged SCF. For $N_{26}H_{16}$ and $N_{50}H_{28}$, the projected EH initial guess converged in a comparable number of cycles as a projected guess which suggests that the parameters used by EH for both of hydrogen and nitrogen are reasonable. However, for N_{46} the SCF did not converge using a projected EH initial guess. Also, the SCF did not converge for GaN_{25} using a projected EH initial guess and converged when projection is used to produce the initial guess.

Table 6.5 gives N_{app}, N_{acc}, and N_{EH} where the SCF was performed using a 6-311G(d) basis set. 6-311G(d) basis set is not available for the third and fourth row atoms. The SCF did not converge using a cutoff of 10 for the two-electron integrals for $N_{50}H_{28}$ but converged with a cutoff of 12 in 13 cycles which is even less than N_{acc}. N_{app}, N_{acc}, and N_{EH} are of comparable values for all of the test cases shown in Table 6.5.

From all of the above tables, it is clear that using projection with weak criteria for SCF convergence and for two-electron integrals calculations with the STO-3G basis set to produce an initial guess for calculations with a larger basis set, the SCF converges equally well to an initial guess using projection and strict criteria.

6.4 Conclusions

Using projected extended Hückel as an initial guess can lead to a larger number of SCF cycles or to problems with SCF convergence compared to using projection from a smaller basis set to calculate the initial guess. By using very weak criteria for SCF convergence and the two-electron integrals cutoff, and using a small basis set such as STO-3G, an initial guess of high quality can be calculated which is similar in performance to the initial guess created by projection from a fully converged SCF but computationally less expensive. We recommend using the criteria $\| \Delta P \| \leq 5 \times 10^{-2}$ for SCF convergence and a cutoff of 12 for two-electron integrals with the STO-3G basis set to create an initial guess used for larger basis sets.

Table 6.1: Results for initial guess using projected extended Hückel and projection from STO-3G to 3-21G basis set

Molecule	Number of SCF Cycles		
	N_{app}	N_{acc}	N_{EH}
C_2H_2	9	9	9
C_2H_4	10	10	9
CH_4	7	8	7
CO_2	8	8	10
FH-NN	11	14	11
FH-OH_2	9	9	10
CH_3-F	9	9	10
CH_3CONH_2	14	14	15
H_2O	9	9	10
HF	8	8	9
LiH	8	6	7
N_2	7	7	7
NH_3	10	11	9
SF_6	7	7	7
CCl_4	8	9	10
$CH_2(PH_2)_2$	10	9	9
$CH_2(SH)_2$	10	11	9
$CH_2(SiH_3)_2$	8	8	11

... continued

Table 6.1 – continued

	Number of SCF Cycles		
Molecule	N_{app}	N_{acc}	N_{EH}
1G_pep	13	20	16
2G_pep	17	16	14
3G_pep	17	15	16
4G_pep	16	14	15
5G_pep	16	17	14
N_{46}	17	11	19
$N_{26}H_{16}$	13	12	17
$N_{50}H_{28}$	10	12	9
Ge_2H_6	7	7	8
Ge_3H_8	7	7	8
GeH_4	8	8	8
Br_2	7	7	8
I_2	8	8	17
Sn_2H_6	8	8	20
Sn_3H_8	9	7	NC[a]
Sn_4H_{10}	7	7	20
SnH_4	8	8	11
TS_CH_3Br_2	9	9	9
TS_CH_3ClBr	9	12	13
GaN_{25}	18	15	20

[a]SCF did not converge

Table 6.2: Results for initial guess using projected extended Hückel and projection from STO-3G to 6-31G basis set

Molecule	Number of SCF Cycles		
	N_{app}	N_{acc}	N_{EH}
BeH_2	6	6	6
C_2H_2	10	10	10
C_2H_4	9	10	9
CH_4	8	8	8
CO_2	9	9	10
FH-NN	14	11	15
FH-OH_2	11	11	12
CH_3-F	9	9	11
CH_3CONH_2	18	16	16
H_2O	10	12	11
HF	8	8	9
LiH	8	8	7
N_2	8	8	8
NH_3	10	10	11
SF_6	8	8	8
CCl_4	8	9	9
$CH_2(PH_2)_2$	11	9	9
$CH_2(SH)_2$	11	11	9

... continued

Table 6.2 – continued

	Number of SCF Cycles		
Molecule	N_{app}	N_{acc}	N_{EH}
$CH_2(SiH_3)_2$	8	9	10
1G_pep	14	18	20
2G_pep	19	14	18
3G_pep	21	18	18
4G_pep	20	18	16
5G_pep	19	17	14
N_{46}	17	14	28
$N_{26}H_{16}$	14	15	13
$N_{50}H_{28}$	11	12	11
Ge_2H_6	8	8	8
Ge_3H_8	9	9	10
GeH_4	10	10	12
Br_2	7	7	7
I_2	9	9	11
Sn_2H_6	8	8	12
Sn_3H_8	9	9	22
Sn_4H_{10}	8	8	28
SnH_4	7	7	10
TS_CH_3Br_2	12	11	12
TS_CH_3ClBr	11	11	12
GaN_{25}	19	24	30

Table 6.3: Results for initial guess using projected extended Hückel and projection from STO-3G to STO-3G(d) basis set

	Number of SCF Cycles		
Molecule	N_{app}	N_{acc}	N_{EH}
BeH_2	5	5	6
C_2H_2	6	6	6
C_2H_4	7	7	7
CH_4	7	6	7
CO_2	8	8	9
FH-NN	8	8	7
FH-OH_2	8	8	7
CH_3-F	8	9	8
CH_3CONH_2	10	9	11
H_2O	8	9	7
HF	8	8	6
LiH	9	7	7
N_2	8	7	7
NH_3	7	8	10
SF_6	7	7	8
CCl_4	9	8	14
$CH_2(PH_2)_2$	10	9	8
$CH_2(SH)_2$	9	10	10

... continued

Table 6.3 – continued

	Number of SCF Cycles		
Molecule	N_{app}	N_{acc}	N_{EH}
$CH_2(SiH_3)_2$	8	8	9
1G_pep	10	9	10
2G_pep	12	9	14
3G_pep	11	9	12
4G_pep	11	9	12
5G_pep	13	9	14
N_{46}	14	13	17
$N_{26}H_{16}$	11	10	12
$N_{50}H_{28}$	10	10	9
Ge_2H_6	5	1	7
Ge_3H_8	6	1	7
GeH_4	5	1	7
Br_2	5	1	6
I_2	4	1	6
Sn_2H_6	7	1	8
Sn_3H_8	7	1	9
Sn_4H_{10}	7	1	13
SnH_4	6	1	8
TS_CH_3Br_2	8	10	7
TS_CH_3ClBr	9	9	8
GaN_{25}	16	20	20

Table 6.4: Results for initial guess using projected extended Hückel and projection from STO-3G to 6-31G(d) basis set

Molecule	Number of SCF Cycles		
	N_{app}	N_{acc}	N_{EH}
C_2H_2	9	9	9
C_2H_4	10	10	9
CH_4	9	9	8
CO_2	8	9	8
FH-NN	12	14	11
FH-OH_2	11	11	12
CH_3-F	10	10	9
CH_3CONH_2	14	14	16
H_2O	10	11	10
HF	11	11	9
LiH	8	7	7
N_2	8	8	9
NH_3	10	11	10
SF_6	8	8	9
CCl_4	9	8	12
$CH_2(PH_2)_2$	9	9	9
$CH_2(SH)_2$	11	10	9
$CH_2(SiH_3)_2$	8	9	10

... continued

Table 6.4 – continued

	Number of SCF Cycles		
Molecule	N_{app}	N_{acc}	N_{EH}
1G_pep	19	16	12
2G_pep	15	15	15
3G_pep	16	15	16
4G_pep	15	14	15
5G_pep	18	15	15
N_{46}	17	17	NC[a]
$N_{26}H_{16}$	15	13	13
$N_{50}H_{28}$	11	11	12
Ge_2H_6	14	14	14
Ge_3H_8	12	12	12
GeH_4	14	14	14
Br_2	10	10	11
I_2	9	9	15
Sn_2H_6	8	8	23
Sn_3H_8	8	8	NC[a]
Sn_4H_{10}	8	8	NC[a]
SnH_4	8	8	10
TS_CH_3Br_2	12	15	14
TS_CH_3ClBr	12	12	12
GaN_{25}	20	25	NC[a]

[a]SCF did not converge

Table 6.5: Results for initial guess using projected extended Hückel and projection from STO-3G to 6-311G(d) basis set

Molecule	Number of SCF Cycles		
	N_{app}	N_{acc}	N_{EH}
BH_3	8	8	8
BeH_2	6	6	6
C_2H_2	9	9	9
C_2H_4	9	10	9
CH_4	7	7	8
CO_2	9	9	8
FH-NN	12	11	12
FH-OH_2	8	8	9
CH_3-F	9	9	9
CH_3CONH_2	14	10	17
H_2O	8	8	9
HF	8	8	8
LiH	7	6	7
N_2	8	8	8
NH_3	11	10	10
SF_6	8	8	13
CCl_4	12	8	13
$CH_2(PH_2)_2$	9	9	9

... continued

Table 6.5 – continued

	Number of SCF Cycles		
Molecule	N_{app}	N_{acc}	N_{EH}
$CH_2(SH)_2$	10	12	9
$CH_2(SiH_3)_2$	9	9	9
1G_pep	12	11	16
2G_pep	13	11	16
3G_pep	12	10	15
4G_pep	12	9	15
5G_pep	15	11	16
N_{46}	17	16	18
$N_{26}H_{16}$	16	15	12
$N_{50}H_{28}$	13[a]	19	14

[a] A cutoff of 12 is used for two-electron integrals

Chapter 7

Algorithms Based on Molecular Fragmentation

7.1 Introduction

Quantum mechanical calculations for macromolecules are very demanding both in terms of CPU time and memory requirements. For example, performing full Hartree-Fock calculations for proteins consisting of thousands of atoms is out of the question. However, there is more than ever a great need to perform accurate calculations on large molecules including DNA, polymers, and proteins which motivated quantum chemists to develop more efficient algorithms. The most time consuming calculations in the Hartree-Fock (HF) method are: the diagonalization of the Fock matrix to calculate the coefficient matrix and the calculation of the two-electron integrals. The diagonalization of the Fock matrix scales as N^3 where N is the number of basis

functions while the two electron integrals scale formally as N^4. With the application of a variety of algorithms designed to improve the efficiency of Hartree-Fock calculations, HF can scale as $(N^2 logN)$ which is still computationally demanding and prohibits the study of macromolecules. For almost fifteen years, there has been a great deal of research with the goal of achieving linear scaling [27] [28] [29] [30] [31] which means the computational cost increases linearly with the size of the system. The rest of this section briefly reviews some of the algorithms for macromolecules and gives an overview of the divide and conquer, D&C, algorithm. The rest of the chapter presents our new version of the D&C algorithm.

7.1.1 Efficient Algorithms Applied To the Hartree-Fock Method

One of the popular methods used to study the chemical properties of biological molecules is the QM/MM approach [32] [33] where the system is divided into two parts. One part, e.g. the active site of an enzyme, is treated quantum mechanically while the rest of the molecule is treated by molecular mechanics. The total Hamiltonian of the system is then written as:

$$\hat{H} = \hat{H}_{QM} + \hat{H}_{MM} + \hat{H}_{QM/MM} \tag{7.1}$$

$\hat{H}_{QM}$ and $\hat{H}_{MM}$ are the Hamiltonian operators of the quantum and molecular mechanics regions respectively. $\hat{H}_{QM/MM}$ represents the interaction energy between the two regions. While calculating the energy of the first two terms of equation (7.1) is straight forward, calculating the interaction energy between the two regions is problematic. There are two approaches to deal with the interface problem, the link atom

method and the local self-consistent field method LSCF [33]. In the link atom approach, hydrogen or halogen atoms are added to the covalent bonds cut in the process of dividing the molecule into two subsystems. In the LSCF approach, calculations are performed on a smaller molecule containing bonds similar to those that were cut in the biological molecules and then the corresponding molecular orbitals are transferred to the larger molecule where they are kept frozen during the SCF. Karplus et al compared the two approaches and concluded that both are of similar accuracy.

In the ONIOM approach [34], (Our own N-layer Integrated molecular Orbital+molecular Mechanics) the molecule, or the molecule and its surroundings, is divided into three regions. The active site is described quantum mechanically and the second layer surrounding the active site is described using a semi-empirical method. The rest of the system is treated with molecular mechanics. The basic difference between different implementations of the ONIOM algorithm is how the interaction between different parts is taken into account.

Other algorithms that aim at reaching linear scaling include the local self consistent field method, which is different than the one mentioned above, molecular fractionation with conjugate caps (MFCC), adjustable density matrix assembler (ADMA), density matrix minimization (DMM), and divide and conquer (D&C). The common aspect of these algorithms is that they bypass the expensive diagonalization of the Fock matrix.

In the local self consistent field method [35], Stewart replaced the Fock matrix diagonalization by the annihilation of the Fock matrix elements that connect the occupied and unoccupied localized molecular orbitals, LMOs. Since LMOs are con-

centrated over an atom or two, the Fock matrix elements between LMOs far apart on a large molecule naturally vanish and only Fock matrix elements between LMOs on neighboring atoms are annihilated.

In the density matrix assembler ADMA, see [30] [36] and references therein, approach the macromolecule is divided into fragments and the density matrix of each fragment is obtained by performing quantum chemical calculations on a smaller molecule which contains this fragment. The macromolecule is called the "target" molecule and the smaller molecules are called the "parent" molecules. The full density matrix of the target molecule is constructed by assembling the density matrices of the fragments. Properties like dipole moment, energy, and partial charges can be calculated from the full density matrix.

Da. W. Zhang and J. Z. H. Zhang developed the molecular fractionation with conjugate caps (MFCC) method [31] [37]. The MFCC is designed specifically to describe the interaction between a protein and a smaller molecule. The protein is divided into its individual amino acids. Caps are added to both sides of each amino acid. The total energy is then the sum of the interaction energies between the smaller molecule and the capped amino acids. Since the computational cost of the interaction energies is almost constant, MFCC scales linearly. Another advantage of the MFCC is the ease of parallelization.

DMM was originally proposed by Li, Nunes, and Vanderbilt [38]. It was implemented in *ab inito* calculations by different groups [39, 40, 41]. DMM replaces the diagonalization of the Fock matrix on each iteration of the SCF by minimizing the density matrix P under the following conditions:

1- $TrSP = N$ where N is the number of electrons and S is the overlap matrix.

2- P is idempotent i.e. $PSP = P$

3- At the end of the SCF P and F commute, $FP = PF$

The first two conditions satisfy the N-representability conditions. The energy functional to be minimized has the following form:

$$\Omega(P) = Tr(\widetilde{P}F + \mu(Tr(P) - N) \tag{7.2}$$

$$\widetilde{P} = 3P - 2P^3 \tag{7.3}$$

$\widetilde{P}$ is the purified density matrix using McWeeny purification transformation. This transformation converts a nearly idempotent matrix with eigenvalues in the range -0.5 to 1.5 to an idempotent matrix with eigenvalues either zero or one. The first term in the energy functional, equation (7.2), is related to the electronic energy. μ is the Lagrange multiplier which was set to the chemical potential in the original work of Li, Nunes, and Vanderbilt.

7.1.2 Divide and Conquer

Divide and conquer [27, 42, 43, 44, 45, 28, 46, 47, 48, 49, 50, 51] was first introduced by Yang in 1991 [27] where he divided a large molecular system into subsystems and calculated the total electron density in the density functional theory framework as a sum of the electron densities of the subsystems. Later Yang reformulated his scheme to divide the electron density matrix instead of the density [43]. Yang pointed out that his newer version of the divide and conquer could be implemented in Hartree-Fock

theory as well. In 1996 Merz and Dixon developed the divide and conquer algorithm in the context of molecular orbital theory [28, 47]. The following is a brief overview of the Merz and Dixon implementation. Roothaan's equation is given by:

$$FC = SC\epsilon \tag{7.4}$$

In the divide and conquer algorithm the molecule is divided into overlapping fragments and Roothan's equation for a fragment α can be written as:

$$F^{\alpha}C^{\alpha} = S^{\alpha}C^{\alpha}\epsilon^{\alpha} \tag{7.5}$$

where all matrices in equation (7.5) are of dimension $N_{\alpha} \times N_{\alpha}$ where N_{α} is the number of basis functions in the subsystem α. The overlap matrix is given by:

$$S^{\alpha}_{\mu\nu} = \int \phi^{*}_{\mu}(\mathbf{r})\phi_{\nu}(\mathbf{r})d\mathbf{r} \quad \text{where} \mu, \nu \in \alpha \tag{7.6}$$

and the Fock matrix given by F^{α}:

$$F^{\alpha}_{\mu\nu} = H^{\alpha}_{\mu\nu} + \sum_{\lambda\sigma} P_{\lambda\sigma}\left[(\mu\nu|\sigma\lambda) - \frac{1}{2}(\mu\lambda|\sigma\nu)\right] \tag{7.7}$$

where, in the equation above, the subscripts μ and ν span the basis functions in the fragment α, while λ and σ, in general, span the whole molecular system. The general definition of the density matrix for a closed shell Hartree-Fock approximation is:

$$P_{\mu\nu} = 2\sum_{i} C^{*}_{\mu i}C_{\nu i} \tag{7.8}$$

where the summation runs over the occupied molecular orbitals. This definition of the density matrix has to be modified in the case of dealing with subsystems, as it is not known exactly how many electrons occupy a molecular orbital. Yang suggested that the density matrix of a subsystem α to be given by:

$$P^{\alpha}_{\mu\nu} = \sum_{i} n^{\alpha}_{i} (C^{\alpha}_{\mu i})^{*} C^{\alpha}_{\nu i} \tag{7.9}$$

where n^{α}_{i} is the occupation number of molecular orbital i and is given by:

$$n^{\alpha}_{i} = \frac{2}{1 + \exp\left[\left(\epsilon^{\alpha}_{i} - \epsilon_{F}\right)/kT\right]} \tag{7.10}$$

ϵ_F is a common Fermi energy of the whole system, k is the Boltzmann constant, and T is the absolute temperature. Roothan's equation is solved self consistently for each fragment and at the end of the SCF the global density matrix P is calculated from the density matrices $\{P^{\alpha}\}$ by the formula:

$$P_{\mu\nu} = \sum_{\alpha=1}^{N_{sub}} D^{\alpha}_{\mu\nu} P^{\alpha}_{\mu\nu} \tag{7.11}$$

$D^{\alpha}_{\mu\nu}$ are weight functions given by:

$$D^{\alpha}_{\mu\nu} = \begin{cases} 0 & \text{if} \quad \chi_{\mu} \text{ or } \chi_{\nu} = \text{buffer functions} \\ \\ 1/n_{\mu\nu} & \text{otherwise} \end{cases}$$

where the buffer functions belong to buffer atoms defined at both ends of each fragment to reduce the truncation errors. $n_{\mu\nu}$ is the number of fragments having the basis functions μ and ν in common.

7.2 Dividing the Molecule into Fragments

There are different strategies to divide large molecules. One approach is to divide the molecule into two fragments, where one fragment includes the active site and the other fragment is the rest of the molecule. Another strategy is to divide the molecule into its building units, e.g., dividing a peptide into its individual amino acids. Our approach is to divide a molecule into two fragments A and B based on Mulliken population analysis. The number of electrons shared between two atoms i and j, N_{ij}, can be calculated using the formula:

$$N_{ij} = \sum_{\mu \in i, \nu \in j, \mu \neq \nu} P_{\mu\nu} S_{\mu\nu} \tag{7.12}$$

where P is the density matrix and S is the overlap matrix. By using equation (7.12), we can construct a square matrix of dimensions equal to the number of atoms and that represents the number of shared electrons between each pair of atoms. The minimum of this matrix corresponds to the pair of atoms, say k and l, which share the least number of electrons and we call seeds. Each seed will belong to a different fragment. The assignment of the rest of the atoms either to fragment A or to fragment B depends on how many electrons are shared between the atom in question and the atoms k and

l. For example, atom m in Figure 7.1 belongs to fragment A if $N_{km} > N_{lm}$ and will belong to fragment B if $N_{lm} > N_{km}$. This algorithm was implemented in MUNgauss and was successful in dividing a molecule into two fragments. For example C_2H_6 was divided into two methyl groups.

7.3 Partitioning The Fock Matrix

Our goal is to develop a new version of the divide and conquer approach where the global Fock matrix is constructed and diagonalized, but fewer two-electron integrals are calculated. If we divide the molecular system into two fragments A and B, the Fock matrix can be written as:

$$F = F_A + F_B + F_{AB} \tag{7.13}$$

where F_A and F_B are the Fock matrices of the fragments A and B and are calculated over basis functions that belong to A or B respectively. F_{AB} is the Fock matrix calculated over basis functions from A and B. The matrices F_A, F_B and F_{AB} are of dimensions $N \times N$ where N is the number of basis functions for the whole molecule. F_A is calculated using the formula:

$$(F_{\mu\nu})_A = (H_{\mu\nu})_A + \sum_{\lambda\sigma} P_{\lambda\sigma} \left[(\mu\nu|\sigma\lambda) - \frac{1}{2}(\mu\lambda|\sigma\nu) \right] \tag{7.14}$$

F_B is calculated by a similar formula while F_{AB} is approximated. The exact full calculations of the molecular system are performed using a smaller basis set and the converged Fock matrix is projected to the larger basis set, where the part F_{AB} is

extracted and added to F_A and F_B and the SCF continues the normal way. The quality of this D&C algorithm depends on the quality of the division of the molecule into fragments and the quality of the projection from the smaller basis set. The projection was studied in detail in Chapter 4.

7.4 Divide and Conquer II

Another approach is to divide the molecule into two fragments A and B where A presents the part of the molecule of chemical interest. As in the previous approach an SCF is performed with a smaller basis set and the Fock matrix on the larger basis set is given by:

$$F = F_A + F_{B,AB}$$

F_A is calculated exactly using the larger basis set while $F_{B,AB}$ is taken from the projected Fock matrix. $F_{B,AB}$ includes the B part and the interaction between A and B and is kept frozen during the SCF. This algorithm has the advantage that only a small fraction of the calculations on the higher level basis set needs to be done. In addition, the interaction between A and B is taken into account through projection which eliminates the boundary problems between the two fragments. We call our new version of the divide and conquer algorithm NDC. NDC was applied to cytidine where it was divided into two fragments in two ways, a and b, Figure 7.2 and Figure 7.3. The straight line in both figures defines the point of division. In Figure 7.2 the cytosine and the two water molecules were treated exactly while the sugar and the interaction between the two fragments were approximated by the projected Fock matrix from a

smaller basis set. The only difference in the second fragmentation in Figure 7.3 is that extra carbon and hydrogen atoms were added to the exact part as shown in the figure. In both figures, the approximated part of the Fock matrix was kept frozen during the SCF. For the projection from STO-3G to 3-21G, 6-31G or 6-31G(d) the SCF did not converge. However, it converged with projection from 3-21G to 6-31G and from 6-31G to 6-31G(d). Table 7.1 shows the energy barrier given by HF/3-21G, HF/6-31G and HF/6-31G(d) in addition to the NDC results with both ways of fragmentation. NDC(3-21G)/6-31G refers to NDC energy with basis set 6-31G, where the frozen part came from 3-21G results. NDC(6-31G)/6-31G(d) denotes NDC with basis set 6-31G(d) where the projection was performed from 6-31G.

To further test this algorithm, the protonation energy of the molecules 2G_pep, 3G_pep, 4G_pep and 5G_pep was calculated. Each peptide is divided into two fragments where fragments of different size were examined. Figure 7.4 shows the division of 2G_pep into two fragments, Figure 7.5 shows the division of 3G_pep into two fragments in two different ways a and b, Figure 7.6 shows the division of 4G_pep into two fragments in three different ways a, b and c, while Figure 7.7 shows the division of 5G_pep into two fragments in four different ways a, b, c and d. In each figure, the point from the straight line to the right end of the peptide is denoted exact (fragment A) while to the left end of the peptide is denoted frozen (fragment B). Table 7.2 gives the energies of the four peptides (without protonation) using the STO-3G, 6-31G and 6-31G(d) basis sets in addition to the energy of the NDC algorithm for 6-31G and 6-31G(d) basis sets where the frozen part of the Fock matrix comes from calculations performed with STO-3G. The frozen part includes the interaction between the two

fragments as well. In Table 7.2, the notations NDC(STO-3G)/6-31G and NDC(STO-3G)/6-31G(d) are used to denote NDC energies calculated with 6-31G or 6-31G(d) basis sets while the frozen part was calculated with STO-3G basis sets. Table 7.2 shows the NDC energies for the 2G_pep, 3G_pep, 4G_pep and 5G_pep with the defined divisions. In each case, the NDC energy is lower than the STO-3G energy but higher than the corresponding 6-31G or 6-31G(d) energy.

Table 7.3 shows the protonation energies for the four peptides with different fragmentations. Also, the results of exact STO-3G and 6-31G were included for comparison. The fourth column gives the protonation energy while the fifth column gives $|\Delta E|$ which is either the difference in the protonation energies between STO-3G and 6-31G or NDC and 6-31G. $|\Delta E|$ shows that NDC is more accurate than STO-3G in calculating the protonation energy for any of the peptides with any fragmentation. However, one disadvantage of NDC is that its accuracy does not improve systematically as the size of the frozen part decreases. For example $|\Delta E|$ for the 4G_pep(c), Figure 7.6(c), is 70 kJmol^{-1} and increases to 145 kJmol^{-1} for 4G_pep(b), Figure 7.6(b), and then decreases to 82 kJmol^{-1} for 4G_pep(a), Figure 7.6(a). An interesting feature of the NDC is that when the division involves the greater approximation, the error seems, in general, to decrease. The errors for 3G_pep(b), 4G_pep(c) and 5G_pep(d), where the frozen part is the largest, are 57 kJmol^{-1}, 70 kJmol^{-1} and 78 kJmol^{-1} respectively which is much less than the corresponding STO-3G values.

The same calculations with the same set of molecules were repeated for the 6-31G(d) basis set, see Table 7.4 where NDC(STO-3G)/6-31G(d) refers to the NDC energy for the 6-31G(d) basis set and the frozen part was projected from STO-3G. As

with the 6-31G basis set, the error in the protonation energy using NDC is smaller than that of STO-3G. It is also clear from Table 7.4 that the largest approximations do not give the largest error, the same characteristic which was noticed previously from Table 7.3. Since the error in projecting from STO-3G to 6-31G(d) is higher than the error in projecting from STO-3G to 6-31G, the error in the protonation energy using 6-31G(d) is in general higher than that of 6-31G which is obvious from Table 7.3 and Table 7.4.

Table 7.1: HF and NDC barriers ($kJmol^{-1}$) for the cytidine

Method/Basis	fragmentation	Energy
HF/3-21G		136
HF/6-31G		129
NDC(3-21G)/6-31G	see Figure 7.2	155
NDC(3-21G)/6-31G	see Figure 7.3	132
HF/6-31G(d)		160
NDC(6-31G)/6-31G(d)	see Figure 7.2	251
NDC(6-31G)/6-31G(d)	see Figure 7.3	233

Table 7.2: HF and NDC energies (Hartrees) for the four peptides

Peptide	Method/Basis	fragmentation	Energy
2G_pep			
	HF/STO-3G		-483.231742
	HF/6-31G		-489.405341
	NDC(STO-3G)/6-31G		-488.340146
	HF/6-31G(d)		-489.642483
	NDC(STO-3G)/6-31G(d)		-488.388743
3G_pep			
	HF/STO-3G		-687.355305
	HF/6-31G		-696.135636
	NDC(STO-3G)/6-31G	a	-695.032790
	NDC(STO-3G)/6-31G	b	-694.221828
	HF/6-31G(d)		-696.450522
	NDC(STO-3G)/6-31G(d)	a	-695.109842
	NDC(STO-3G)/6-31G(d)	b	-694.148923
4G_pep			
	HF/STO-3G		-891.483674
	HF/6-31G		-902.858087
	NDC(STO-3G)/6-31G	a	-901.733220
	NDC(STO-3G)/6-31G	b	-900.889293
	NDC(STO-3G)/6-31G	c	-900.155443
	HF/6-31G(d)		-903.266395
	NDC(STO-3G)/6-31G(d)	a	-901.898629
	NDC(STO-3G)/6-31G(d)	b	-900.899862
	NDC(STO-3G)/6-31G(d)	c	-900.049176
5G_pep			
	HF/STO-3G		-1095.612263
	HF/6-31G		-1109.580967
	NDC(STO-3G)/6-31G	a	-1108.441270
	NDC(STO-3G)/6-31G	b	-1107.580703
	NDC(STO-3G)/6-31G	c	-1106.813659
	NDC(STO-3G)/6-31G	d	-1106.098860
	HF/6-31G(d)		-1110.082602
	NDC(STO-3G)/6-31G(d)	a	-1108.697252
	NDC(STO-3G)/6-31G(d)	b	-1107.679023
	NDC(STO-3G)/6-31G(d)	c	-1106.791368
	NDC(STO-3G)/6-31G(d)	d	-1105.964010

Table 7.3: Protonation energies ($kJmol^{-1}$) using NDC and 6-31G basis

Peptide	Method/Basis	Fragmentation	Protonation Energy	$\lvert\Delta E\rvert$
2G_pep				
	HF/6-31G		998	
	HF/ STO-3G		1153	155
	NDC(STO-3G)/6-31G		1088	89
3G_pep				
	HF/6-31G		961	
	HF/STO-3G		1141	180
	NDC(STO-3G)/6-31G	a	860	101
	NDC(STO-3G)/(6-31G)	b	903	57
4G_pep				
	HF/6-31G		967	
	HF/STO-3G		1146	179
	NDC(STO-3G)/6-31G	a	885	82
	NDC(STO-3G)/6-31G	b	822	146
	NDC(STO-3G)/6-31G	c	897	71
5G_pep				
	HF/6-31G		971	
	HF/STO-3G		1149	178
	NDC(STO-3G)/6-31G	a	911	60
	NDC(STO-3G)/6-31G	b	852	119
	NDC(STO-3G)/6-31G	c	805	166
	NDC(STO-3G)/6-31G	d	893	78

Table 7.4: Protonation energies ($kJmol^{-1}$) using NDC and 6-31G(d) basis

Peptide	Method/Basis	Fragmentation	Protonation Energy	$\|\Delta E\|$
2G_pep				
	HF/6-31G(d)		961	
	HF/STO-3G		1153	192
	NDC(STO-3G)/6-31G(d)		922	39
3G_pep				
	HF/6-31G(d)		966	
	HF/STO-3G		1141	175
	NDC(STO-3G)/6-31G(d)	a	817	149
	NDC(STO-3G)/6-31G(d)	b	882	83
4G_pep				
	HF/6-31G(d)		973	
	HF/STO-3G		1146	173
	NDC(STO-3G)/6-31G(d)	a	859	114
	NDC(STO-3G)/6-31G(d)	b	782	191
	NDC(STO-3G)/6-31G(d)	c	874	98
5G_pep				
	HF/6-31G(d)		977	
	HF/STO-3G		1149	172
	NDC(STO-3G)/6-31G(d)	a	896	81
	NDC(STO-3G)/6-31G(d)	b	825	151
	NDC(STO-3G)/6-31G(d)	c	761	216
	NDC(STO-3G)/6-31G(d)	d	868	109

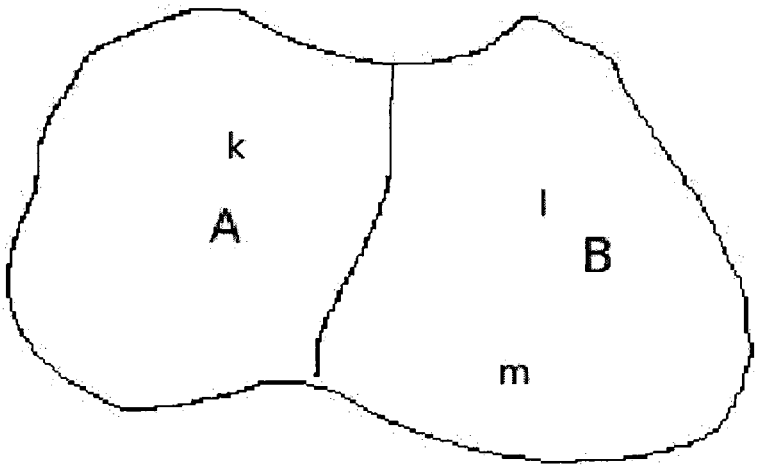

Figure 7.1: A molecule is divided into two fragments A and B

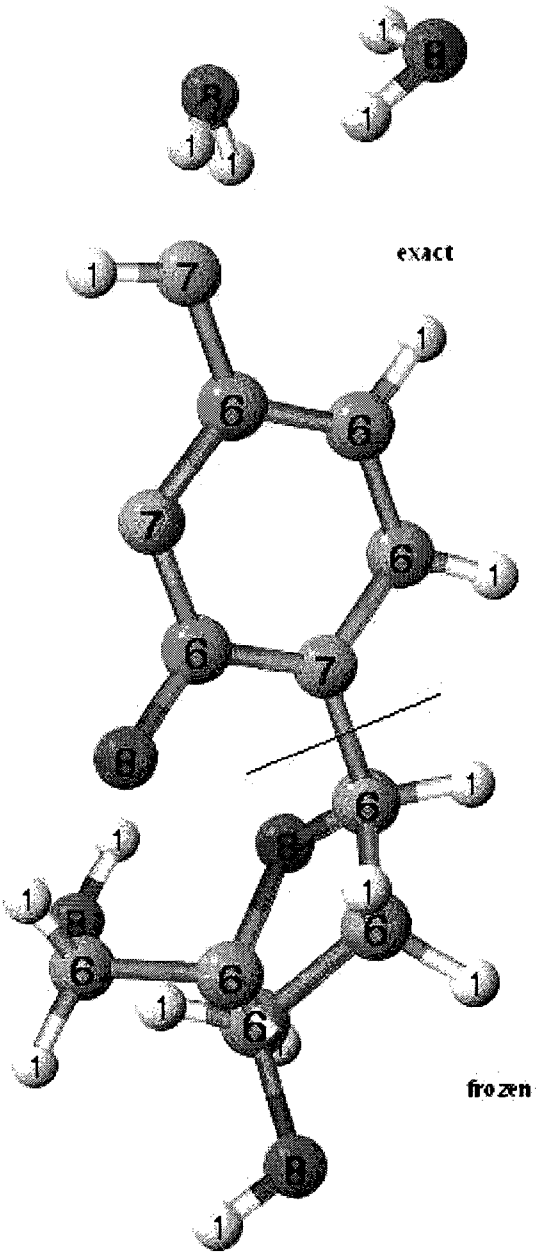

Figure 7.2: Cytidine divided into two fragments as indicated by the line, A=exact, B=frozen, fragmentation a

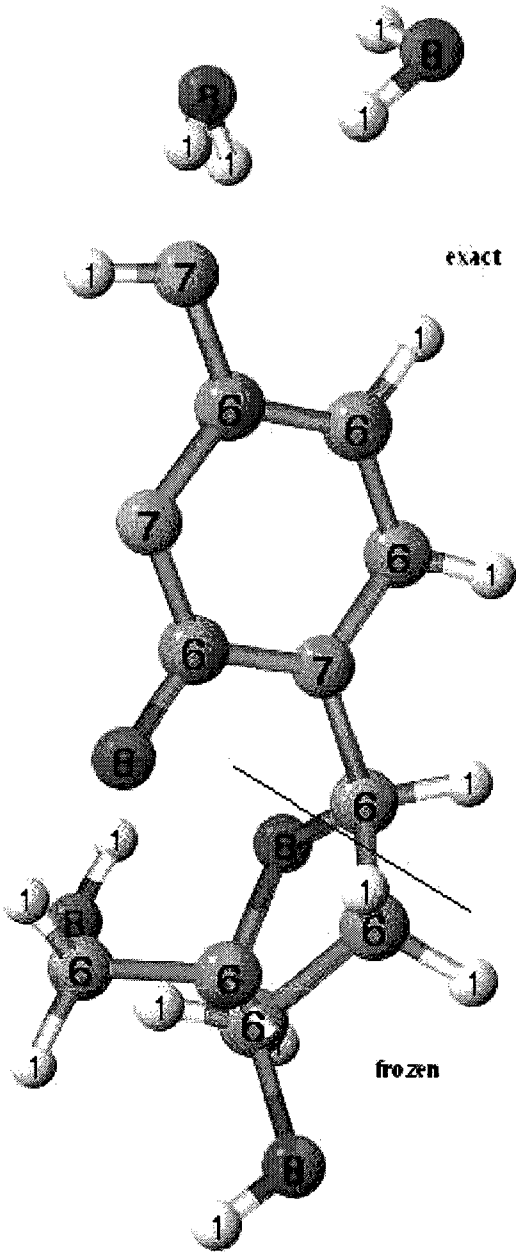

Figure 7.3: Cytidine divided into two fragments as indicated by the line, A=exact, B=frozen, fragmentation b

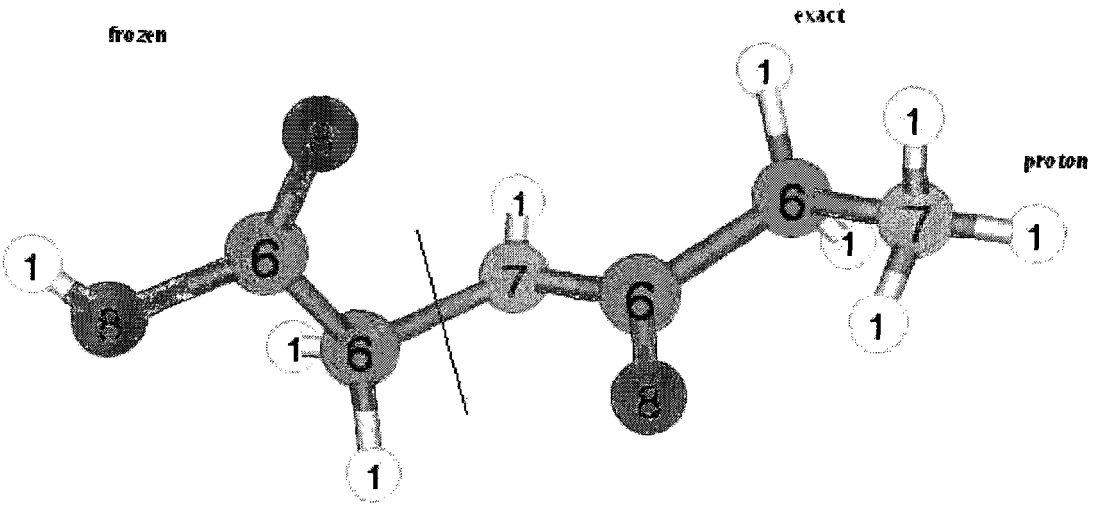

Figure 7.4: 2G_pep divided into two fragments

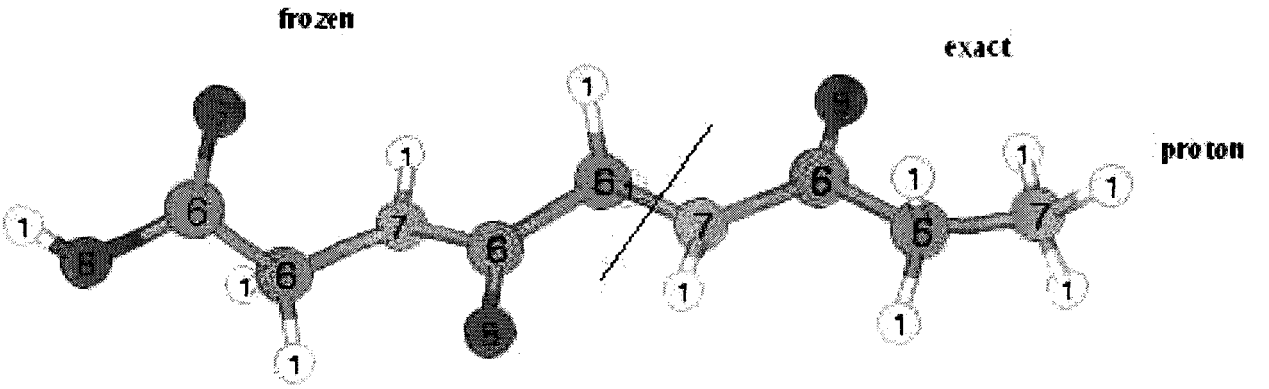

(a)

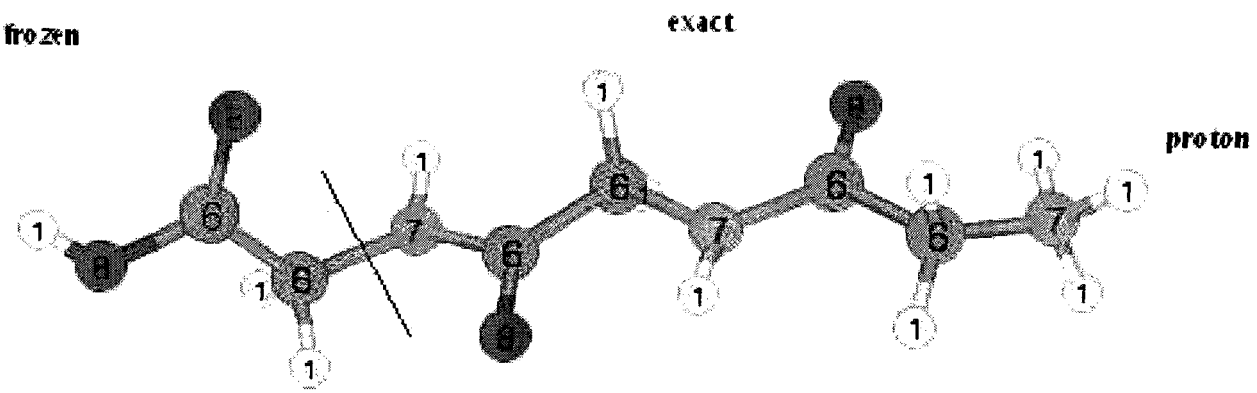

(b)

Figure 7.5: 3G_pep divided into two fragments in two different ways, a and b, in the position of the straight line

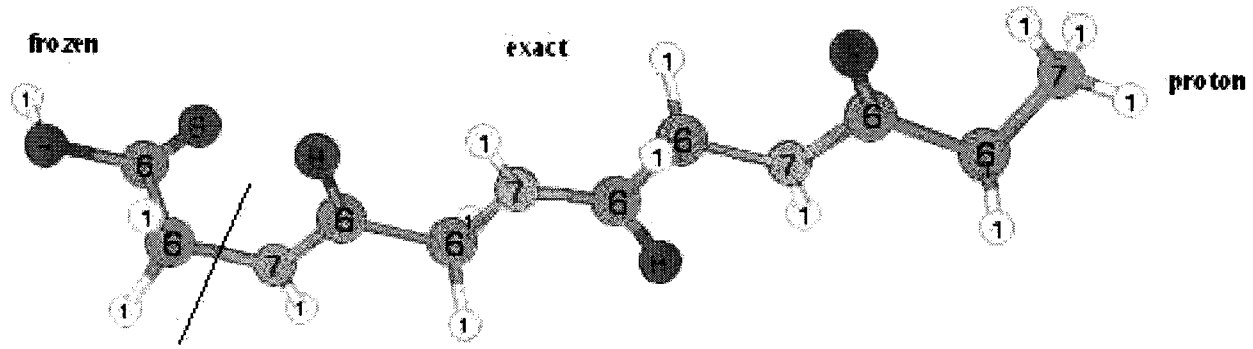

(a)

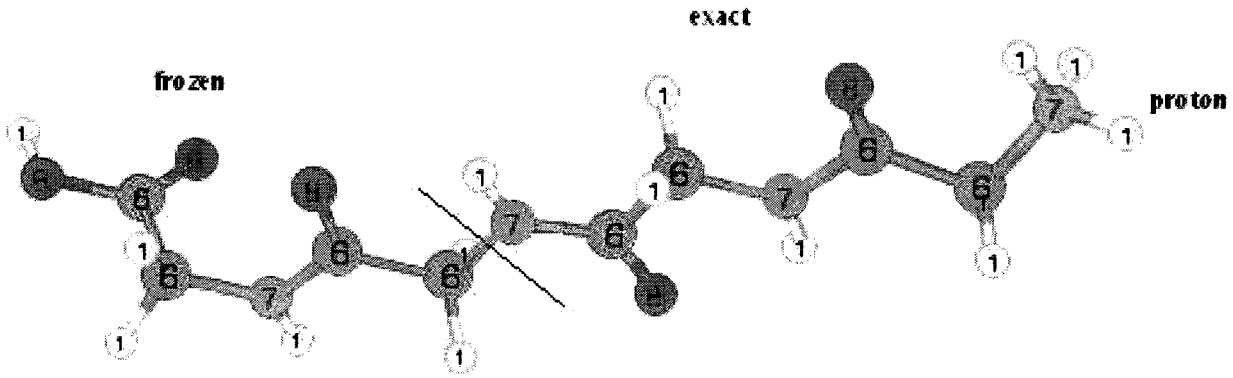

(b)

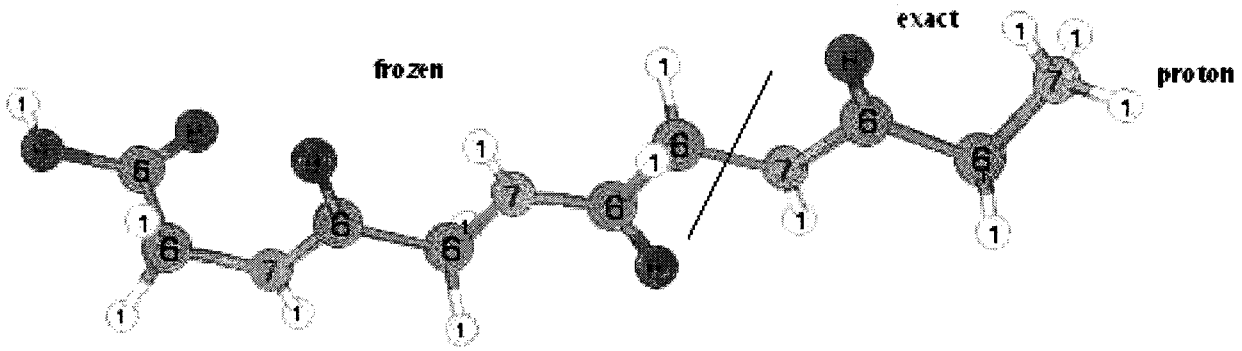

(c)

Figure 7.6: 4G_pep divided into two fragments in three different ways, a, b and c, in the position of the straight line

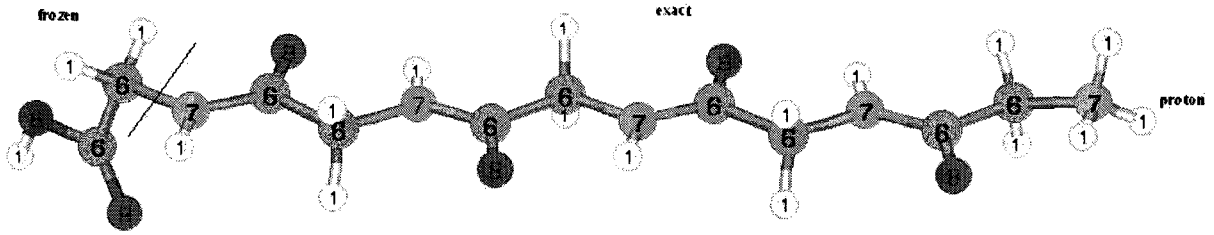

(a)

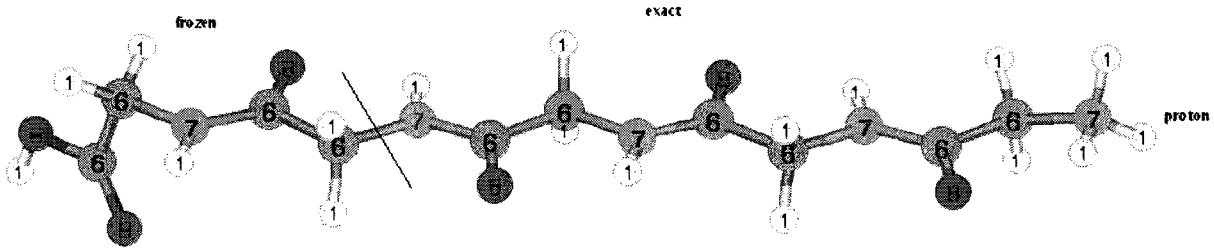

(b)

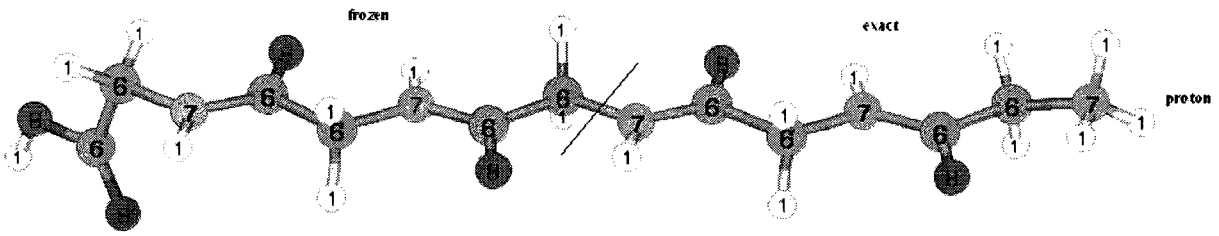

(c)

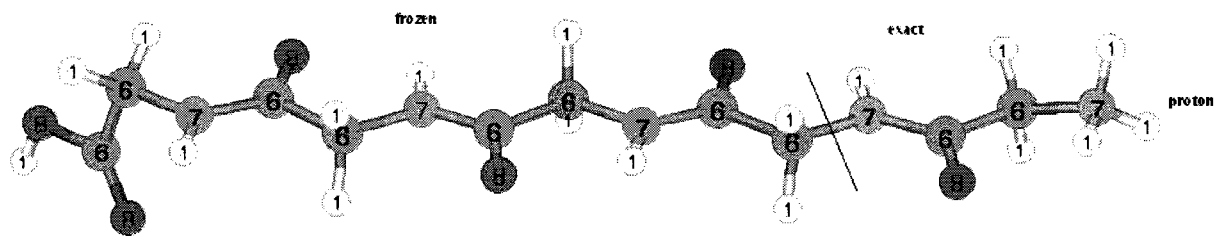

(d)

Figure 7.7: 5G_pep divided into two fragments in four different ways, a, b, c and d, in the position of the straight line

Chapter 8

Conclusions

The performance of the molecular numerical integration was studied. We recommend using the standard grid SG-1 or our new implementation of the Treutler and Alhrichs grid TA(new) for density functional theory. More efficient grids, although less accurate, are the SG0 and 25(194) grids. Both grids offer a reasonable compromise between efficiency and accuracy.

The projection from a smaller basis set to a larger basis set was studied in detail and used to develop a divide and conquer algorithm. Our divide and conquer algorithm was used to calculate the protonation energy for a series of peptides and reasonable results were obtained. Calculations of most of the zero two-electron integrals were avoided by introducing a more strict criterion to MUNgauss. An efficient algorithm to obtain the initial guess for Hartree-Fock calculations was developed.

Future work includes:

- developing a new algorithm to optimize the parameter R

- parallelizing our numerical integration code
- a more efficient way of calculating the nuclear weight functions used in numerical integration, where only the nearest neighbours are considered
- applying our new divide and conquer algorithm to larger molecules

Appendix A

Numerical Integration Results

Table A.1: *MAE* of number of electrons using MultiExp grid with 20 radial points for molecules containing 1^{st} row atoms

Molecule	20(110)	20(194)	20(302)
BF_3	-2.2E-04	-1.6E-05	5.2E-05
BH_3	1.3E-04	1.7E-04	1.6E-04
BeH_2	2.2E-05	8.8E-06	1.1E-05
C_2H_2	2.4E-04	2.2E-04	2.2E-04
C_2H_4	-5.0E-04	1.6E-04	2.3E-04
CF_4	3.6E-04	1.8E-05	5.8E-06
$CH_2CHCOOH$	-5.5E-04	3.2E-04	3.9E-04
CH_2FF	4.6E-04	3.4E-05	8.3E-05
$CH_2CH_3CH_3$	-3.5E-05	1.8E-05	1.8E-04
CH_3F	2.6E-04	1.2E-04	1.3E-04
CH_3NH_2	1.0E-04	1.4E-04	1.8E-04
CH_3OH	-2.4E-04	1.5E-04	1.6E-04
CH_3CONH_2	-1.5E-04	2.1E-04	2.3E-04
CH_4	-2.4E-04	8.6E-05	1.1E-04
CO	5.9E-05	1.3E-04	1.3E-04
CO_2	4.7E-05	2.1E-04	2.0E-04
EtOTs	1.0E-03	4.2E-04	4.3E-04
F_2	4.7E-04	1.2E-04	1.5E-04
H_2	3.8E-05	3.8E-05	3.8E-05
H_2CO	-2.2E-04	1.8E-04	1.8E-04
H_2O	5.1E-05	8.3E-05	9.6E-05
H_2O_2	2.6E-04	1.7E-04	1.5E-04
HCOOH	-4.1E-05	2.0E-04	2.1E-04
Li_2	4.1E-04	4.2E-04	4.2E-04
LiF	1.5E-04	1.5E-04	1.5E-04
NH_3	-2.5E-04	5.9E-05	7.5E-05
benzaldehyde	-2.1E-03	8.7E-04	6.8E-04
cytosine	1.0E-03	4.2E-04	5.1E-04
formamidine	6.7E-04	3.5E-04	2.7E-04
methoxide	-1.2E-04	1.3E-04	1.5E-04
naphthalene	-2.7E-03	1.6E-03	9.4E-04
uracil	-5.0E-04	5.6E-04	6.0E-04
MAE	4.3E-04	2.5E-04	2.4E-04

Table A.2: *MAE* of number of electrons using MultiExp grid with 20 radial points for molecules containing 2^{nd} row atoms

Molecule	20(110)	20(194)	20(302)
CCl_4	9.6E-04	6.6E-04	6.8E-04
CH_2ClCl	6.8E-06	3.9E-05	6.5E-05
$CH_2PH_2PH_2$	-8.0E-04	-1.8E-04	-1.3E-04
CH_2SHSH	-6.1E-04	-3.3E-04	-2.2E-04
$CH_2SiH_3SiH_3$	-6.8E-05	2.1E-05	1.4E-04
CH_3PH_2	-2.6E-04	-3.5E-05	-4.8E-05
CH_3SH	8.3E-05	-7.0E-05	-1.0E-04
CH_3SiH_3	-1.3E-04	6.4E-05	7.0E-05
CH_3Cl	-1.0E-04	-1.5E-05	-9.7E-06
CS	1.9E-04	1.9E-04	1.9E-04
Cl_2	-2.1E-04	5.2E-05	2.4E-05
ClF	9.2E-04	1.1E-03	1.0E-03
HOCl	-3.2E-05	-1.6E-04	-1.3E-04
Mg	3.6E-03	3.6E-03	3.6E-03
NaCl	-3.8E-03	-3.9E-03	-3.9E-03
P_2	2.0E-04	2.2E-04	2.0E-04
PF_5	-3.8E-04	-5.2E-04	-5.6E-04
PH	-3.6E-05	-8.7E-05	-8.4E-05
PH_3	-7.8E-06	-1.1E-04	-1.2E-04
SF_6	4.0E-04	-6.9E-04	-7.9E-04
SO	3.7E-04	2.4E-04	2.4E-04
SO_2	1.1E-03	9.3E-04	9.3E-04
SiO	8.2E-04	6.5E-04	6.5E-04
pNO_2BzCl	5.5E-03	-1.1E-04	5.8E-04
MAE	9.2E-04	6.3E-04	6.5E-04

Table A.3: *MAE* of the integration of the electron density using MultiExp grid with 20 radial points for molecules containing 3^{rd} row atoms and transition states

Molecule	20(110)	20(194)	20(302)
3rd row			
AsH_3	1.6E-03	1.2E-03	1.2E-03
CH_3Br	7.3E-03	7.4E-03	7.4E-03
Ge_2H_6	-4.1E-03	-3.1E-03	-3.3E-03
Ge_3H_8	-5.6E-03	-6.8E-03	-6.7E-03
Ge_4H_{10}	-9.9E-03	-1.0E-02	-1.0E-02
Ge_5H_{12}	-8.3E-03	-1.0E-02	-1.1E-02
GeH_4	-2.4E-03	-2.4E-03	-2.4E-03
H_2Se	6.0E-03	4.7E-03	4.8E-03
MAE	8.2E-03	8.4E-03	8.5E-03
transition states			
TS_CH_3Cl_2	-1.5E-03	-2.5E-04	-2.7E-04
TS_CH_3F_2	-1.5E-04	2.8E-04	1.6E-04
TS_CH_3FCl	-1.7E-05	8.9E-05	4.5E-05
TS_CH_5OF	4.4E-04	2.5E-04	1.8E-04
TS_Ethyl-OSO_2-CH_3	4.0E-04	2.7E-04	2.5E-04
TS_pHBzCl	-1.0E-03	5.6E-04	2.4E-04
MAE	-3.1E-04	2.0E-04	1.9E-04

Table A.4: *MAE* of the integration of the electron density using MultiExp grid with 20 radial points for complexes, ions, and peptides

Molecule	20(110)	20(194)	20(302)
complexes			
CH_2O_2-CH_2O_2	-9.2E-05	3.5E-04	3.1E-04
FH-CO	1.2E-04	1.9E-04	1.9E-04
FH-FH	6.7E-05	1.3E-04	1.3E-04
FH-NCH	2.8E-04	3.1E-04	3.1E-04
FH-NH_3	-6.2E-04	1.0E-04	9.6E-05
FH-NN	2.4E-03	2.4E-03	2.4E-03
FH-OH_2	-2.9E-05	6.2E-05	7.7E-05
H_2O-CO_2	-1.1E-04	1.2E-04	1.2E-04
H_2O-H_2O	3.1E-04	1.7E-04	1.7E-04
MAE	4.5E-04	4.2E-04	4.2E-04
ions			
$ArNH_3^+$	-2.0E-03	1.0E-03	5.2E-04
H_3O^+	-2.8E-05	4.5E-05	5.0E-05
$HCOO^-$	4.6E-05	2.3E-04	2.3E-04
$NH_3{}^+CH_2COO^-$	6.5E-04	4.1E-04	3.9E-04
MAE	-3.2E-04	4.3E-04	3.0E-04
peptides			
1G_pep	3.9E-04	3.6E-04	3.4E-04
2G_pep	1.1E-03	3.7E-04	4.7E-04
3G_pep	1.8E-03	8.3E-04	7.7E-04
4G_pep	1.7E-03	1.0E-03	1.0E-03
5G_pep	-1.4E-03	8.5E-04	4.6E-04
MAE	7.2E-04	6.8E-04	6.2E-04

Table A.5: *MAE* of number of electrons using MultiExp grid with 25 radial points for molecules containing 1^{st} row atoms

Molecule	25(110)	25(194)	25(302)
BF_3	-3.9E-04	-1.7E-04	-9.9E-05
BH_3	-3.2E-05	7.8E-06	-5.2E-06
BeH_2	-6.4E-05	-7.3E-05	-7.1E-05
C_2H_2	1.2E-05	-7.6E-06	-1.2E-05
C_2H_4	-7.7E-04	-9.2E-05	-1.3E-05
CF_4	1.5E-04	-2.0E-04	-2.2E-04
$CH_2CHCOOH$	-1.0E-03	-1.6E-04	-8.2E-05
CH_2FF	2.8E-04	-1.4E-04	-8.5E-05
$CH_2CH_3CH_3$	-2.8E-04	-2.2E-04	-8.1E-05
CH_3F	8.7E-05	-4.6E-05	-4.0E-05
CH_3NH_2	-1.2E-04	-8.0E-05	-4.0E-05
CH_3OH	-4.2E-04	-3.8E-05	-2.7E-05
CH_3CONH_2	-4.5E-04	-7.5E-05	-7.1E-05
CH_4	-3.6E-04	-3.2E-05	-6.0E-06
CO	-1.1E-04	-3.8E-05	-4.0E-05
CO_2	-2.0E-04	-5.0E-05	-5.4E-05
EtOTs	5.5E-04	-6.2E-05	-2.6E-05
F_2	3.2E-04	4.6E-06	3.1E-05
H_2	9.2E-06	8.7E-06	8.7E-06
H_2CO	-4.3E-04	-3.1E-05	-3.3E-05
H_2O	-6.9E-05	-3.1E-05	-1.7E-05
H_2O_2	7.4E-05	-1.6E-05	-2.7E-05
HCOOH	-3.0E-04	-6.0E-05	-5.0E-05
Li_2	-4.7E-05	-4.0E-05	-4.0E-05
LiF	-7.1E-04	-7.4E-04	-7.3E-04
LiH	2.5E-04	2.5E-04	2.5E-04
NH_3	-3.4E-04	-3.3E-05	-1.9E-05
benzaldehyde	-2.8E-03	7.0E-05	-6.2E-05
cytosine	3.2E-04	-2.3E-04	-1.5E-04
formamidine	3.5E-04	3.9E-05	-3.7E-05
methoxide	-3.0E-04	-4.6E-05	-3.5E-05
naphthalene	-3.7E-03	5.3E-04	2.9E-05
uracil	-1.4E-03	-2.1E-04	-1.3E-04
MAE	5.1E-04	1.2E-04	7.9E-05

Table A.6: *MAE* of the integration of the electron density using MultiExp grid with 25 radial points for molecules containing 2^{nd} row atoms

Molecule	25(110)	25(194)	25(302)
CCl_4	4.1E-04	1.4E-04	1.5E-04
CH_2ClCl	-1.3E-04	-8.8E-05	6.8E-05
$CH_2PH_2PH_2$	-6.0E-04	-1.2E-05	7.5E-06
CH_2SHSH	-3.8E-04	-1.1E-04	8.5E-06
$CH_2SiH_3SiH_3$	-2.5E-04	-1.1E-04	1.7E-05
CH_3PH_2	-1.9E-04	1.4E-05	5.4E-07
CH_3SH	1.8E-04	3.0E-05	6.9E-06
CH_3SiH_3	-2.1E-04	-6.2E-07	1.2E-07
CH_3Cl	-1.7E-04	-7.8E-05	8.0E-05
CS	1.2E-04	1.2E-04	1.2E-04
Cl_2	-1.6E-04	6.9E-05	6.5E-05
ClF	6.9E-04	7.5E-04	7.4E-04
HOCl	-2.8E-05	-1.8E-04	1.7E-04
Mg	-2.6E-03	-2.6E-03	2.6E-03
NaCl	-1.2E-03	-1.3E-03	1.3E-03
P_2	1.7E-04	2.4E-04	2.2E-04
PF_5	-1.6E-04	-3.1E-04	3.2E-04
PH	1.2E-05	-4.2E-05	3.8E-05
PH_3	1.0E-04	2.9E-06	5.8E-06
SF_6	4.9E-04	-5.0E-04	5.0E-04
SO	2.1E-04	8.6E-05	8.8E-05
SO_2	5.4E-04	2.6E-04	2.6E-04
SiO	5.3E-04	3.7E-04	3.8E-04
pNO_2BzCl	4.8E-03	-9.1E-04	1.4E-04
MAE	6.2E-04	3.6E-04	3.2E-04

Table A.7: *MAE* of the integration of the electron density using MultiExp grid with 25 radial points for molecules containing 3^{rd} row atoms and transition states

Molecule	25(110)	25(194)	25(302)
3rd row			
AsH_3	-2.8E-03	-3.2E-03	-3.2E-03
CH_3Br	-3.2E-03	-3.1E-03	-3.1E-03
Ge_2H_6	-6.3E-03	-5.2E-03	-5.3E-03
Ge_3H_8	-7.4E-03	-8.1E-03	-8.0E-03
Ge_4H_{10}	-1.1E-02	-1.1E-02	-1.1E-02
Ge_5H_{12}	-1.1E-02	-1.3E-02	-1.3E-02
GeH_4	-2.6E-03	-2.6E-03	-2.6E-03
H_2Se	-2.4E-03	-3.4E-03	-3.4E-03
MAE	6.1E-03	6.2E-03	-6.2E-03
transition states			
TS_CH_3Cl_2	-1.5E-03	-2.6E-04	-2.7E-04
TS_CH_3F_2	-3.4E-04	9.4E-05	-2.6E-05
TS_CH_3FCl	-2.3E-04	-1.4E-04	-1.6E-04
TS_CH_5OF	2.5E-04	7.5E-06	-4.9E-05
TS_Ethyl-OSO_2-CH_3	1.0E-05	-8.2E-05	-3.6E-05
TS_pHBzCl	-1.8E-03	-1.3E-04	-5.0E-04
MAE	6.8E-04	1.2E-04	1.7E-04

Table A.8: *MAE* of the integration of the electron density using MultiExp grid with 25 radial points for complexes, ions, and peptides

Molecule	25(110)	25(194)	25(302)
complexes			
CH_2O_2_CH_2O_2	-7.0E-04	-1.4E-04	-8.6E-05
FH-CO	-1.2E-04	-3.8E-05	-3.7E-05
FH-FH	-7.1E-05	-4.6E-07	3.3E-06
FH-NCH	-5.4E-05	-2.1E-05	-1.9E-05
FH-NH_3	-7.5E-04	-9.5E-06	-2.1E-05
FH-NN	1.5E-03	1.5E-03	1.5E-03
FH-OH_2	-1.3E-04	-3.8E-05	-2.2E-05
H_2O-CO_2	-2.7E-04	-6.4E-05	-6.2E-05
H_2O_H_2O	9.0E-05	-4.4E-05	-3.2E-05
MAE	4.1E-04	2.1E-04	2.0E-04
ions			
$ArNH_3^+$	-2.6E-03	4.1E-04	-5.0E-05
H_3O^+	-1.0E-04	-2.3E-05	-1.6E-05
$HCOO^-$	-2.3E-04	-6.1E-05	-5.1E-05
$NH_3^+CH_2COO^-$	1.5E-04	-8.7E-05	-6.9E-05
MAE	7.8E-04	1.5E-04	4.6E-05
peptides			
1G_pep	-3.9E-05	-7.9E-05	-8.4E-05
2G_pep	3.1E-04	-2.4E-04	-1.1E-04
3G_pep	6.0E-04	-3.1E-04	-2.8E-04
4G_pep	1.2E-04	-4.8E-04	-3.5E-04
5G_pep	-2.5E-03	-1.1E-04	-5.0E-04
MAE	7.1E-04	2.4E-04	2.7E-04

Table A.9: *MAE* of the integration of the electron density using MultiExp grid with 30 radial points for molecules containing 1^{st} row atoms

Molecule	30(110)	30(194)	30(194)
BF_3	-2.93E-04	-8.84E-05	-1.96E-05
BH_3	-1.80E-05	2.26E-05	9.39E-06
BeH_2	-1.12E-05	-2.13E-05	-1.91E-05
C_2H_2	3.45E-05	1.63E-05	1.23E-05
C_2H_4	-7.43E-04	-6.75E-05	1.01E-05
CF_4	3.76E-04	1.45E-05	3.88E-06
$CH_2CHCOOH$	-9.32E-04	-6.97E-05	6.11E-06
CH_2FF	3.48E-04	-7.81E-05	-1.40E-05
$CH_2CH_3CH_3$	-2.42E-04	-1.80E-04	-1.97E-05
CH_3F	1.18E-04	-1.69E-05	-9.92E-06
CH_3NH_2	-8.42E-05	-4.81E-05	-6.79E-06
CH_3OH	-3.85E-04	-6.43E-06	4.47E-06
CH_3CONH_2	-3.54E-04	1.32E-05	1.65E-05
CH_4	-3.51E-04	-2.35E-05	2.94E-06
CO	-6.94E-05	2.24E-06	4.45E-07
CO_2	-1.52E-04	6.39E-06	2.37E-06
EtOTs	6.25E-04	1.80E-06	4.40E-05
F_2	3.08E-04	-1.57E-05	9.96E-06
H_2	2.28E-06	1.87E-06	1.92E-06
H_2CO	-3.91E-04	5.68E-06	3.84E-06
H_2O	-5.28E-05	-1.61E-05	-2.30E-06
H_2O_2	1.07E-04	1.54E-05	2.83E-06
HCOOH	-2.48E-04	-4.65E-06	3.42E-06
Li_2	-1.98E-05	-1.03E-05	-1.08E-05
LiF	-1.05E-04	-1.36E-04	-1.34E-04
LiH	1.86E-04	1.80E-04	1.79E-04
NH_3	-3.18E-04	-1.21E-05	2.45E-06
benzaldehyde	-2.68E-03	2.28E-04	1.00E-04
cytosine	4.83E-04	-6.45E-05	8.23E-06
formamidine	4.04E-04	9.06E-05	1.51E-05
methoxide	-2.67E-04	-1.21E-05	-6.07E-07
naphthalene	-3.52E-03	7.45E-04	2.46E-04
uracil	-1.24E-03	-6.28E-05	2.84E-05
MAE	4.7E-04	6.9E-05	2.9E-05

Table A.10: *MAE* of the integration of the electron density using MultiExp grid with 30 radial points for molecules containing 2^{nd} row atoms

Molecule	30(110)	30(194)	30(194)
CCl_4	3.1E-04	4.8E-05	4.5E-05
CH_2ClCl	-1.1E-04	-5.8E-05	-4.0E-05
$CH_2PH_2PH_2$	-5.8E-04	-5.8E-05	-7.8E-06
CH_2SHSH	-4.1E-04	-1.5E-04	-4.8E-05
$CH_2SiH_3SiH_3$	-2.1E-04	-9.0E-05	7.8E-06
CH_3PH_2	-1.8E-04	1.7E-05	5.0E-06
CH_3SH	1.7E-04	2.2E-05	-1.4E-05
CH_3SiH_3	-1.8E-04	2.7E-05	2.5E-05
CH_3Cl	-1.3E-04	-3.3E-05	-3.8E-05
CS	4.9E-05	4.7E-05	4.4E-05
Cl_2	-2.5E-04	3.4E-06	-7.4E-06
ClF	4.6E-05	1.4E-04	1.3E-04
HOCl	2.4E-05	-9.0E-05	-7.4E-05
Mg	1.3E-03	1.3E-03	1.3E-03
NaCl	1.8E-03	1.7E-03	1.7E-03
P_2	1.2E-04	1.6E-04	1.4E-04
PF_5	2.7E-04	5.4E-05	4.2E-05
PH	1.2E-05	-4.8E-05	-4.2E-05
PH_3	9.9E-05	-3.4E-07	-6.2E-06
SF_6	1.2E-03	5.7E-05	2.9E-05
SO	1.1E-04	-2.2E-05	-2.1E-05
SO_2	2.7E-04	-6.5E-06	-5.1E-06
SiO	4.1E-04	2.4E-04	2.5E-04
pNO_2BzCl	5.1E-03	-6.9E-04	7.2E-05
MAE	5.71E-04	2.18E-04	1.76E-04

Table A.11: *MAE* of the integration of the electron density using MultiExp grid with 30 radial points for molecules containing 3^{rd} row atoms and transition states

Molecule	30(110)	30(194)	30(194)
3rd row			
AsH_3	-2.6E-03	-3.1E-03	-3.0E-03
CH_3Br	-2.9E-03	-2.7E-03	-2.7E-03
Ge_2H_6	-6.3E-03	-5.2E-03	-5.3E-03
Ge_3H_8	-7.3E-03	-8.1E-03	-8.0E-03
Ge_4H_{10}	-1.1E-02	-1.1E-02	-1.1E-02
Ge_5H_{12}	-1.1E-02	-1.3E-02	-1.4E-02
GeH_4	-2.6E-03	-2.6E-03	-2.6E-03
H_2Se	-2.0E-03	-3.0E-03	-3.1E-03
MAE	5.9E-03	6.0E-03	6.0E-03
transition states			
TS_CH_3Cl_2	-1.4E-03	-1.8E-04	-2.0E-04
TS_CH_3F_2	-3.2E-04	1.1E-04	-1.3E-05
TS_CH_3FCl	-1.6E-04	-3.5E-05	-6.3E-05
TS_CH_5OF	2.7E-04	5.4E-05	-6.7E-06
TS_Ethyl-OSO_2-CH_3	1.9E-04	4.4E-05	8.1E-05
TS_pHBzCl	-1.6E-03	9.3E-05	-2.7E-04
MAE	6.5E-04	8.5E-05	1.1E-04

Table A.12: *MAE* of the integration of the electron density using MultiExp grid with 30 radial points for complexes, ions, and peptides

Molecule	30(110)	30(194)	30(194)
complexes			
CH_2O_2-CH_2O_2	-5.8E-04	-2.7E-05	1.4E-05
FH-CO	-8.5E-05	-6.5E-06	-4.7E-06
FH-FH	-7.9E-05	-9.2E-06	-6.5E-06
FH-NCH	-3.5E-05	1.2E-06	2.9E-06
FH-NH_3	-7.3E-04	3.5E-06	-5.9E-06
FH-NN	-3.5E-04	-3.8E-04	-3.8E-04
FH-OH_2	-1.2E-04	-2.3E-05	-8.3E-06
H_2O-CO_2	-2.2E-04	4.5E-06	2.8E-06
H_2O-H_2O	1.2E-04	-1.3E-05	-2.0E-06
MAE	2.57E-04	5.23E-05	4.72E-05
ions			
$ArNH_3^+$	-2.5E-03	5.5E-04	9.4E-05
H_3O^+	-8.5E-05	-4.9E-06	1.3E-06
$HCOO^-$	-1.8E-04	-5.8E-06	2.2E-06
$NH_3^+CH_2COO^-$	2.5E-04	1.2E-05	2.5E-05
MAE	2.5E-04	1.2E-05	2.5E-05
peptides			
1G_pep	6.5E-05	2.1E-05	7.4E-06
2G_pep	5.5E-04	-1.0E-04	-1.3E-06
3G_pep	9.9E-04	-9.0E-06	-2.6E-05
4G_pep	6.4E-04	-5.2E-05	2.0E-05
5G_pep	-2.2E-03	3.6E-04	-7.1E-06
MAE	8.8E-04	1.1E-04	1.2E-05

Table A.13: *MAE* of the dipole moment calculated using MultiExp grid with 20 radial points for molecules containing 1^{st} row atoms

Molecule	20(110)	20(194)	20(302)
BF_3	1.6E-03	6.3E-04	5.6E-04
BH_3	5.2E-05	1.4E-04	1.4E-04
BeH_2	5.4E-05	2.2E-05	2.9E-05
C_2H_2	2.7E-04	2.5E-04	2.5E-04
C_2H_4	6.2E-04	2.0E-04	2.9E-04
CF_4	5.9E-04	2.3E-04	1.5E-04
$CH_2CHCOOH$	1.4E-03	2.4E-05	-1.5E-04
CH_2FF	-7.1E-05	-7.8E-05	-2.4E-05
$CH_2CH_3CH_3$	-6.5E-04	-2.5E-04	5.4E-05
CH_3F	1.0E-03	2.7E-04	2.7E-04
CH_3NH_2	3.2E-05	2.9E-04	2.1E-04
CH_3OH	4.3E-04	2.6E-04	1.7E-04
CH_3CONH_2	6.8E-04	3.9E-04	4.6E-04
CH_4	2.8E-04	1.4E-04	1.3E-04
CO	2.0E-04	3.5E-04	3.5E-04
CO_2	1.0E-04	4.5E-04	4.4E-04
EtOTs	-4.3E-04	5.1E-04	3.4E-04
F_2	6.0E-04	1.5E-04	1.9E-04
H_2	2.6E-05	2.6E-05	2.6E-05
H_2CO	-2.6E-04	3.4E-04	3.5E-04
H_2O	2.4E-04	9.0E-05	6.8E-05
H_2O_2	7.8E-05	1.1E-04	1.4E-04
HCOOH	-3.2E-04	2.3E-04	2.2E-04
Li_2	1.1E-03	1.1E-03	1.1E-03
LiF	-5.8E-03	-5.8E-03	-5.8E-03
LiH	1.2E-03	1.2E-03	1.2E-03
NH_3	6.1E-04	1.3E-04	7.9E-05
benzaldehyde	3.3E-03	-1.5E-03	-6.4E-04
cytosine	5.2E-04	6.8E-04	6.1E-04
formamidine	1.7E-04	-3.1E-05	4.4E-05
methoxide	7.3E-04	4.6E-04	4.2E-04
naphthalene	3.6E-03	2.1E-03	1.3E-03
uracil	2.7E-03	1.7E-03	1.5E-03
MAE	9.0E-04	6.1E-04	5.3E-04

Table A.14: *MAE* of the dipole moment calculated using MultiExp grid with 20 radial points for molecules containing 2^{nd} row atoms

Molecule	20(110)	20(194)	20(302)
CCl_4	1.1E-03	3.4E-04	3.4E-04
CH_2ClCl	1.5E-04	3.6E-04	3.9E-04
$CH_2PH_2PH_2$	1.5E-03	8.0E-04	8.0E-04
CH_2SHSH	-1.4E-03	-6.7E-04	-4.3E-04
$CH_2SiH_3SiH_3$	-1.3E-03	-9.9E-05	2.1E-04
CH_3PH_2	-1.9E-04	1.9E-04	1.3E-04
CH_3SH	5.4E-04	-4.8E-04	-5.6E-04
CH_3SiH_3	1.8E-04	5.1E-04	4.9E-04
CH_3Cl	-7.5E-05	-2.4E-04	-2.4E-04
CS	-4.7E-04	-4.0E-04	-4.0E-04
Cl_2	4.0E-04	9.7E-05	4.5E-05
ClF	-1.0E-04	1.6E-04	1.6E-04
HOCl	4.4E-04	3.0E-04	3.0E-04
Mg	1.6E-17	-7.6E-18	-2.2E-18
NaCl	2.3E-04	9.7E-05	1.0E-04
P_2	3.5E-04	3.8E-04	3.6E-04
PF_5	8.7E-04	3.4E-04	2.9E-04
PH	9.1E-04	9.4E-04	9.4E-04
SF_6	-7.4E-12	-1.4E-11	-1.5E-11
SO	-1.9E-04	-4.5E-04	-4.5E-04
SO_2	3.5E-04	1.0E-04	1.1E-04
SiO	8.8E-04	5.8E-04	5.9E-04
pNO_2BzCl	2.7E-02	1.0E-03	4.2E-03
MAE	1.7E-03	3.7E-04	5.0E-04

Table A.15: *MAE* of the Dipole moment calculated using MultiExp grid with 20 radial points for molecules containing 3^{rd} row atoms and transition states

Molecule	20(110)	20(194)	20(302)
3rd row			
AsH_3	1.9E-02	1.9E-02	1.9E-02
CH_3Br	5.0E-02	5.0E-02	5.0E-02
Ge_2H_6	9.4E-03	7.2E-03	7.4E-03
Ge_3H_8	-1.0E-03	5.1E-03	4.8E-03
Ge_4H_{10}	5.5E-02	5.7E-02	5.7E-02
Ge_5H_{12}	2.4E-02	3.8E-02	4.0E-02
GeH_4	4.5E-04	2.6E-04	2.7E-04
H_2Se	1.9E-02	2.0E-02	2.0E-02
MAE	2.0E-02	2.2E-02	2.2E-02
transition states			
TS_CH_3Cl_2	2.6E-04	5.6E-05	1.4E-04
TS_CH_3F_2	4.2E-05	2.3E-04	1.2E-04
TS_CH_3FCl	4.6E-04	1.7E-03	1.7E-03
TS_CH_5OF	-8.1E-04	6.8E-05	-3.8E-05
TS_Ethyl-OSO_2-CH_3	2.0E-03	7.6E-04	6.7E-04
TS_pHBzCl	-5.1E-03	-5.9E-04	4.0E-04
MAE	1.4E-03	5.6E-04	5.0E-04

Table A.16: *MAE* of the Dipole moment calculated using MultiExp grid with 20 radial points for complexes, ions, and peptides

Molecule	20(110)	20(194)	20(302)
complexes			
CH_2O_2-CH_2O_2	-3.5E-04	1.3E-03	1.2E-03
FH-CO	-1.7E-03	-1.6E-03	-1.8E-03
FH-FH	4.0E-04	3.6E-04	3.7E-04
FH-NCH	4.4E-04	8.7E-04	8.8E-04
FH-NH_3	-2.6E-03	1.8E-04	5.4E-04
FH-NN	-2.6E-03	-2.6E-03	-2.6E-03
FH-OH_2	5.4E-04	8.4E-05	5.5E-05
H_2O-CO_2	6.1E-04	1.2E-04	1.1E-04
H_2O-H_2O	-1.3E-03	-4.7E-04	-4.5E-04
MAE	1.2E-03	8.4E-04	8.8E-04
ions			
$ArNH_3^+$	-2.6E-03	2.1E-03	1.4E-03
H_3O^+	4.0E-04	5.7E-05	1.8E-05
$HCOO^-$	3.0E-05	2.1E-04	1.9E-04
$NH_3^+CH_2COO^-$	-3.7E-03	-5.0E-04	-3.8E-04
MAE	1.7E-03	7.0E-04	4.9E-04
peptides			
1G_pep	4.0E-04	7.4E-05	3.8E-05
2G_pep	3.5E-03	1.2E-03	1.1E-03
3G_pep	1.8E-02	8.0E-03	6.3E-03
4G_pep	1.3E-02	9.9E-03	9.3E-03
5G_pep	-1.3E-02	8.7E-03	5.3E-03
MAE	9.5E-03	5.6E-03	4.4E-03

Table A.17: *MAE* of the dipole moment calculated using MultiExp grid of 25 radial points for molecules containing 1^{st} row atoms

Molecule	25(110)	25(194)	25(302)
BF_3	1.1E-03	1.1E-04	4.3E-05
BH_3	1.8E-04	1.4E-05	1.0E-05
BeH_2	1.6E-04	1.9E-04	1.8E-04
C_2H_2	1.3E-05	8.5E-06	1.3E-05
C_2H_4	9.5E-04	1.1E-04	1.7E-05
CF_4	4.3E-04	1.6E-04	-6.2E-06
$CH_2CHCOOH$	1.6E-03	2.1E-04	6.1E-05
CH_2FF	-2.2E-04	-2.3E-04	-1.6E-04
$CH_2CH_3CH_3$	-7.7E-04	-3.0E-04	-1.0E-04
CH_3F	7.3E-04	-2.5E-05	-2.6E-05
CH_3NH_2	-1.8E-04	8.9E-05	1.0E-05
CH_3OH	2.2E-04	3.4E-05	-4.6E-05
CH_3CONH_2	2.6E-04	-1.1E-05	8.4E-05
CH_4	1.9E-04	2.8E-05	4.1E-06
CO	-1.4E-04	-1.0E-06	-9.8E-07
CO_2	4.4E-04	1.1E-04	1.2E-04
EtOTs	-8.0E-04	6.6E-05	-6.0E-05
F_2	4.1E-04	5.8E-06	3.9E-05
H_2	6.3E-06	6.0E-06	6.0E-06
H_2CO	-6.4E-04	-4.4E-05	-4.2E-05
H_2O	1.7E-04	1.7E-05	-4.3E-06
H_2O_2	-3.9E-05	-1.1E-05	1.3E-05
HCOOH	-5.1E-04	4.5E-05	2.0E-05
Li_2	1.3E-04	1.1E-04	1.1E-04
LiF	-6.8E-03	-6.9E-03	-6.9E-03
LiH	8.0E-04	7.9E-04	7.9E-04
NH_3	5.3E-04	4.9E-05	-1.8E-06
benzaldehyde	4.0E-03	-8.2E-04	-9.1E-05
cytosine	-2.4E-04	-1.0E-04	-1.6E-04
formamidine	1.2E-04	-6.9E-05	6.1E-06
methoxide	2.6E-04	-3.7E-05	-6.8E-05
naphthalene	4.9E-03	7.1E-04	3.9E-05
uracil	6.8E-04	-1.0E-04	-2.9E-04
MAE	8.7E-04	3.5E-04	2.9E-04

Table A.18: *MAE* of the dipole moment calculated using MultiExp grid with 25 radial points for molecules containing 2^{nd} row atoms

Molecule	25(110)	25(194)	25(302)
CCl_4	1.1E-03	1.1E-04	4.2E-05
CH_2ClCl	-2.2E-04	-1.9E-06	2.7E-05
$CH_2PH_2PH_2$	3.5E-04	-3.6E-04	-1.9E-04
CH_2SHSH	-8.3E-04	-2.1E-04	3.4E-05
$CH_2SiH_3SiH_3$	-1.5E-03	-2.4E-04	2.3E-05
CH_3PH_2	-4.3E-04	-1.2E-04	-1.9E-04
CH_3SH	9.0E-04	-1.5E-04	-2.3E-04
CH_3SiH_3	-2.1E-04	1.0E-04	8.3E-05
CH_3Cl	-1.8E-04	-3.3E-04	-3.5E-04
CS	-4.5E-04	-3.9E-04	-3.8E-04
Cl_2	2.9E-04	1.3E-04	1.2E-04
ClF	-1.2E-04	8.1E-05	9.5E-05
HOCl	1.0E-04	-4.8E-05	-4.1E-05
Mg	-1.8E-17	-4.7E-18	-1.9E-18
NaCl	2.3E-03	2.1E-03	2.0E-03
P_2	3.1E-04	4.1E-04	3.8E-04
PF_5	6.6E-04	1.4E-04	6.1E-05
PH	3.4E-04	3.7E-04	3.7E-04
SF_6	-2.3E-12	-7.6E-12	-8.9E-12
SO	-2.6E-04	-5.2E-04	-5.1E-04
SO_2	-4.4E-05	-2.1E-04	-1.9E-04
SiO	4.7E-04	1.8E-04	1.9E-04
pNO_2BzCl	2.2E-02	-4.0E-03	-4.1E-04
MAE	1.4E-03	4.4E-04	2.6E-04

Table A.19: *MAE* of the dipole moment calculated using MultiExp grid with 25 radial points for molecules containing 3^{rd} row atoms and transition states

Molecule	25(110)	25(194)	25(302)
3rd row			
AsH_3	-4.5E-04	-3.9E-04	-3.7E-04
CH_3Br	-1.2E-02	-1.2E-02	-1.2E-02
Ge_2H_6	1.4E-02	1.2E-02	1.2E-02
Ge_3H_8	9.2E-03	1.5E-02	1.5E-02
Ge_4H_{10}	6.3E-02	6.0E-02	6.0E-02
Ge_5H_{12}	3.6E-02	4.8E-02	5.0E-02
GeH_4	4.5E-04	2.5E-04	2.7E-04
H_2Se	-1.2E-03	-6.7E-04	-6.8E-04
MAE	1.5E-02	1.7E-02	1.7E-02
transition states			
TS_CH_3Cl_2	8.9E-05	1.5E-04	2.9E-05
TS_CH_3F_2	1.0E-04	1.2E-04	1.1E-05
TS_CH_3FCl	-1.4E-04	5.1E-04	5.8E-04
TS_CH_5OF	-6.7E-04	3.7E-04	2.2E-04
TS_Ethyl-OSO_2-CH_3	1.2E-03	-4.2E-05	-1.9E-04
TS_pHBzCl	-3.8E-03	-3.5E-04	7.1E-04
MAE	9.9E-04	2.6E-04	2.9E-04

Table A.20: *MAE* of the dipole moment calculated using MultiExp grid with 25 radial points for complexes, ions, and peptides

Molecule	25(110)	25(194)	25(302)
complexes			
CH_2O_2-CH_2O_2	-1.4E-03	-5.2E-04	-3.2E-04
FH-CO	2.0E-04	-3.5E-05	-1.1E-04
FH-FH	5.6E-05	3.8E-05	4.7E-05
FH-NCH	-4.2E-04	2.5E-06	2.5E-05
FH-NH_3	-3.1E-03	-2.2E-04	3.6E-05
FH-NN	-1.5E-03	-1.6E-03	-1.6E-03
FH-OH_2	4.9E-04	3.5E-05	8.5E-06
H_2O-CO_2	4.7E-04	6.1E-05	3.1E-05
H_2O-H_2O	-7.7E-04	6.9E-05	8.0E-05
MAE	9.3E-04	2.9E-04	2.6E-04
ions			
$ArNH_3^+$	-4.0E-03	5.8E-04	3.6E-05
H_3O^+	3.8E-04	3.6E-05	-3.1E-06
$HCOO^-$	-1.8E-04	-2.8E-06	-2.1E-05
$NH_3^+CH_2COO^-$	-3.2E-03	-1.0E-05	3.1E-05
MAE	1.9E-03	1.6E-04	2.3E-05
peptides			
1G_pep	3.0E-04	-4.0E-06	-1.9E-05
2G_pep	1.8E-03	-3.1E-04	-3.1E-04
3G_pep	8.4E-03	-1.1E-03	-2.3E-03
4G_pep	3.2E-04	-2.9E-03	-2.8E-03
5G_pep	-2.3E-02	-9.7E-04	-4.3E-03
MAE	6.7E-03	1.0E-03	1.9E-03

Table A.21: *MAE* of the dipole moment calculated using MultiExp grid with 30 radial points for molecules containing 1^{st} row atoms

Molecule	30(110)	30(194)	30(194)
BF_3	9.8E-04	7.4E-05	1.8E-07
BH_3	1.9E-04	4.4E-06	5.0E-07
BeH_2	2.8E-05	5.4E-05	4.8E-05
C_2H_2	3.9E-05	1.8E-05	1.4E-05
C_2H_4	9.3E-04	8.4E-05	1.3E-05
CF_4	4.2E-04	1.5E-04	1.9E-06
$CH_2CHCOOH$	1.5E-03	1.6E-04	4.7E-06
CH_2FF	-1.1E-04	-1.2E-04	-3.8E-05
$CH_2CH_3CH_3$	-7.8E-04	-3.0E-04	-2.5E-05
CH_3F	7.2E-04	-4.0E-05	-4.2E-05
CH_3NH_2	-1.7E-04	9.8E-05	1.8E-05
CH_3OH	2.5E-04	6.9E-05	-1.2E-05
CH_3CONH_2	1.8E-04	-7.9E-05	1.0E-05
CH_4	1.9E-04	2.8E-05	2.8E-06
CO	-1.4E-04	5.5E-06	4.9E-06
CO_2	3.3E-04	1.4E-05	5.1E-06
EtOTs	-7.4E-04	2.0E-04	3.3E-05
F_2	3.9E-04	2.0E-05	1.3E-05
H_2	1.6E-06	1.3E-06	1.3E-06
H_2CO	-6.0E-04	-9.5E-06	-6.9E-06
H_2O	1.7E-04	1.7E-05	-4.6E-06
H_2O_2	-5.7E-05	-2.9E-05	-5.1E-06
HCOOH	-5.2E-04	2.5E-05	4.2E-06
Li_2	5.3E-05	2.7E-05	2.9E-05
LiF	-3.4E-03	-3.5E-03	-3.5E-03
LiH	5.5E-04	5.4E-04	5.4E-04
NH_3	5.2E-04	4.8E-05	-3.8E-06
benzaldehyde	3.9E-03	-9.4E-04	-2.1E-04
cytosine	-1.1E-04	5.8E-05	-1.4E-05
formamidine	9.6E-05	-9.1E-05	-1.5E-05
methoxide	3.0E-04	5.2E-06	-2.6E-05
naphthalene	4.7E-03	9.9E-04	3.3E-04
uracil	1.1E-03	2.4E-04	8.1E-05
MAE	7.3E-04	2.4E-04	1.5E-04

Table A.22: *MAE* of the dipole moment calculated using MultiExp grid with 30 radial points for molecules containing 2^{nd} row atoms

Molecule	30(110)	30(194)	30(194)
CCl_4	1.1E-03	1.1E-04	1.3E-08
CH_2ClCl	-3.2E-04	-7.5E-05	-5.0E-05
$CH_2PH_2PH_2$	3.4E-04	-2.2E-04	-2.0E-04
CH_2SHSH	-9.0E-04	-3.2E-04	-7.3E-05
$CH_2SiH_3SiH_3$	-1.5E-03	-3.3E-04	-7.0E-05
CH_3PH_2	-4.5E-04	-1.8E-04	-2.4E-04
CH_3SH	9.1E-04	-1.5E-04	-2.3E-04
CH_3SiH_3	-2.3E-04	8.8E-05	5.6E-05
CH_3Cl	-6.5E-05	-2.1E-04	-2.4E-04
CS	-1.8E-04	-1.2E-04	-1.1E-04
Cl_2	4.7E-04	6.4E-06	1.4E-05
ClF	-6.1E-04	-3.9E-04	-3.8E-04
HOCl	3.3E-05	-1.0E-04	-9.9E-05
Mg	-3.5E-17	-2.2E-17	-2.6E-17
NaCl	9.9E-05	-2.0E-05	-2.0E-05
P_2	2.0E-04	2.8E-04	2.5E-04
PF_5	5.8E-04	7.8E-05	5.6E-08
PH	1.3E-04	1.6E-04	1.6E-04
PH_3	-6.6E-05	-2.1E-04	-2.4E-04
SF_6	3.1E-12	-1.9E-12	-3.3E-12
SO	-2.6E-05	-2.9E-04	-2.8E-04
SO_2	3.9E-05	-1.3E-04	-1.2E-04
SiO	3.8E-04	8.2E-05	9.1E-05
pNO_2BzCl	2.4E-02	-2.9E-03	7.1E-04
MAE	1.4E-03	2.7E-04	1.5E-04

Table A.23: *MAE* of the dipole moment calculated using MultiExp grid with 30 radial points for molecules containing 3^{rd} row atoms and transition states

Molecule	30(110)	30(194)	30(194)
3rd row			
AsH_3	1.6E-05	7.9E-05	9.4E-05
CH_3Br	-9.8E-03	-9.7E-03	-9.8E-03
Ge_2H_6	1.4E-02	1.2E-02	1.2E-02
Ge_3H_8	9.3E-03	1.5E-02	1.5E-02
Ge_4H_{10}	6.3E-02	6.0E-02	6.0E-02
Ge_5H_{12}	3.6E-02	4.9E-02	5.1E-02
GeH_4	4.5E-04	2.4E-04	2.7E-04
H_2Se	-4.1E-04	4.9E-05	3.0E-05
MAE	1.5E-02	1.6E-02	1.6E-02
transition states			
TS_CH_3Cl_2	1.2E-04	1.3E-04	2.5E-05
TS_CH_3F_2	1.0E-04	1.1E-04	4.2E-06
TS_CH_3FCl	-3.4E-04	3.1E-04	3.4E-04
TS_CH_5OF	-8.8E-04	1.2E-04	-9.5E-06
TS_Ethyl-OSO_2-CH_3	1.2E-03	9.5E-05	-7.7E-05
TS_pHBzCl	-3.9E-03	-3.8E-04	6.6E-04
MAE	1.1E-03	1.9E-04	1.8E-04

Table A.24: *MAE* of the dipole moment calculated using MultiExp grid with 30 radial points for complexes, ions, and peptides

Molecule	30(110)	30(194)	30(194)
complexes			
CH_2O_2-CH_2O_2	-1.8E-03	-1.0E-04	5.0E-05
FH-CO	3.9E-04	2.2E-04	1.3E-04
FH-FH	-7.1E-06	-2.8E-05	-2.1E-05
FH-NCH	-4.9E-04	-6.0E-05	-4.1E-05
FH-NH_3	-3.1E-03	-3.7E-04	-9.2E-05
FH-NN	1.3E-03	1.2E-03	1.2E-03
FH-OH_2	5.1E-04	4.7E-05	2.2E-05
H_2O-CO_2	4.6E-04	1.3E-05	-6.1E-06
H_2O-H_2O	-8.5E-04	-1.2E-05	1.5E-06
MAE	9.9E-04	2.3E-04	1.7E-04
ions			
$ArNH_3^+$	-3.9E-03	8.0E-04	2.7E-04
H_3O^+	3.8E-04	3.7E-05	-1.4E-06
$HCOO^-$	-1.5E-04	3.0E-05	1.1E-05
$NH_3^+CH_2COO^-$	-3.3E-03	-1.3E-04	-7.9E-05
MAE	1.9E-03	2.5E-04	9.1E-05
peptides			
1G_pep	3.1E-04	-1.1E-05	-2.5E-05
2G_pep	2.2E-03	1.8E-05	-2.1E-05
3G_pep	1.1E-02	1.1E-03	-3.1E-04
4G_pep	3.7E-03	5.5E-04	4.1E-04
5G_pep	-2.0E-02	2.8E-03	1.3E-04
MAE	7.5E-03	9.0E-04	1.8E-04

Table A.25: MAE of the potential energy, V_{ne} calculated using MultiExp grid with 20 radial points for molecules containing 1^{st} row atoms

Molecule	20(110)	20(194)	20(302)
BF_3	8.6E+05	8.5E+05	8.5E+05
BH_3	8.9E+04	9.0E+04	9.0E+04
BeH_2	6.4E+04	6.4E+04	6.4E+04
C_2H_2	2.4E+05	2.4E+05	2.4E+05
C_2H_4	2.5E+05	2.4E+05	2.4E+05
CF_4	1.1E+06	1.1E+06	1.1E+06
$CH_2CHCOOH$	7.8E+05	7.7E+05	7.7E+05
CH_2FF	6.3E+05	6.3E+05	6.3E+05
$CH_2CH_3CH_3$	3.7E+05	3.7E+05	3.7E+05
CH_3F	3.8E+05	3.8E+05	3.8E+05
CH_3NH_2	2.8E+05	2.8E+05	2.8E+05
CH_3OH	3.3E+05	3.3E+05	3.3E+05
CH_3CONH_2	6.1E+05	6.1E+05	6.1E+05
CH_4	1.2E+05	1.2E+05	1.2E+05
CO	3.3E+05	3.3E+05	3.3E+05
CO_2	5.3E+05	5.3E+05	5.3E+05
EtOTs	1.1E+07	1.1E+07	1.1E+07
F_2	5.1E+05	5.1E+05	5.1E+05
H_2	-2.8E+01	-2.6E+01	-2.6E+01
H_2CO	3.3E+05	3.3E+05	3.3E+05
H_2O	2.1E+05	2.0E+05	2.0E+05
H_2O_2	4.1E+05	4.1E+05	4.1E+05
HCOOH	5.3E+05	5.3E+05	5.3E+05
Li_2	8.9E+04	8.8E+04	8.8E+04
LiF	2.9E+05	2.9E+05	2.9E+05
LiH	4.5E+04	4.5E+04	4.5E+04
NH_3	1.6E+05	1.6E+05	1.6E+05
benzaldehyde	1.1E+06	1.1E+06	1.1E+06
cytosine	1.2E+06	1.2E+06	1.2E+06
formamidine	4.4E+05	4.4E+05	4.4E+05
methoxide	3.3E+05	3.3E+05	3.3E+05
naphthalene	1.3E+06	1.2E+06	1.2E+06
uracil	1.2E+06	1.2E+06	1.2E+06
MAE	7.9E+05	7.9E+05	7.9E+05

Table A.26: *MAE* of the potential energy calculated using MultiExp grid with 20 radial points for molecules containing 2^{nd} row atoms

Molecule	20(110)	20(194)	20(302)
CCl_4	4.5E+07	4.5E+07	4.5E+07
CH_2ClCl	2.3E+07	2.3E+07	2.3E+07
$CH_2PH_2PH_2$	1.8E+07	1.8E+07	1.8E+07
CH_2SHSH	2.0E+07	2.0E+07	2.0E+07
$CH_2SiH_3SiH_3$	1.6E+07	1.6E+07	1.6E+07
CH_3PH_2	8.9E+06	8.9E+06	8.9E+06
CH_3SH	1.0E+07	1.0E+07	1.0E+07
CH_3SiH_3	8.0E+06	8.0E+06	8.0E+06
CH_3Cl	1.1E+07	1.1E+07	1.1E+07
CS	1.0E+07	1.0E+07	1.0E+07
Cl_2	2.3E+07	2.3E+07	2.3E+07
ClF	1.2E+07	1.2E+07	1.2E+07
HOCl	1.1E+07	1.1E+07	1.1E+07
Mg	1.6E+07	1.6E+07	1.6E+07
NaCl	3.1E+07	3.1E+07	3.1E+07
P_2	1.8E+07	1.8E+07	1.8E+07
PF_5	1.0E+07	1.0E+07	1.0E+07
PH	8.7E+06	8.7E+06	8.7E+06
PH_3	8.7E+06	8.7E+06	8.7E+06
SF_6	1.2E+07	1.2E+07	1.2E+07
SO	1.0E+07	1.0E+07	1.0E+07
SO_2	2.0E+07	2.0E+07	2.0E+07
SiO	8.1E+06	8.1E+06	8.1E+06
pNO_2BzCl	1.3E+07	1.3E+07	1.3E+07
MAE	9,059,565	9,010,435	8,990,870

Table A.27: *MAE* of the potential energy calculated using MultiExp grid with 20 radial points for molecules containing 3^{rd} row atoms and transition states

Molecule	20(110)	20(194)	20(302)
3rd row			
AsH_3	6.3E+07	6.3E+07	6.3E+07
CH_3Br	7.5E+07	7.5E+07	7.5E+07
Ge_2H_6	1.0E+08	1.0E+08	1.0E+08
Ge_3H_8	1.6E+08	1.6E+08	1.6E+08
Ge_4H_{10}	2.1E+08	2.1E+08	2.1E+08
Ge_5H_{12}	2.6E+08	2.6E+08	2.6E+08
GeH_4	5.2E+07	5.2E+07	5.2E+07
H_2Se	6.8E+07	6.8E+07	6.8E+07
MAE	126,155,556	126,155,556	126,155,556
transition states			
TS_CH_3Cl_2	2.3E+07	2.3E+07	2.3E+07
TS_CH_3F_2	6.3E+05	6.3E+05	6.3E+05
TS_CH_3FCl	1.2E+07	1.2E+07	1.2E+07
TS_CH_5OF	5.8E+05	5.8E+05	5.8E+05
TS_Ethyl-OSO_2-CH_3	1.1E+07	1.1E+07	1.1E+07
TS_pHBzCl	1.2E+07	1.2E+07	1.2E+07
MAE	9,835,833	9,852,167	9,852,500

Table A.28: *MAE* of the potential energy calculated using MultiExp grid with 20 radial points for complexes, ions, and peptides

Molecule	20(110)	20(194)	20(302)
complexes			
CH_2O_2-CH_2O_2	1.1E+06	1.1E+06	1.1E+06
FH-CO	5.8E+05	5.8E+05	5.8E+05
FH-FH	5.1E+05	5.1E+05	5.1E+05
FH-NCH	5.4E+05	5.4E+05	5.4E+05
FH-NH_3	4.2E+05	4.2E+05	4.2E+05
FH-NN	5.6E+05	5.6E+05	5.6E+05
FH-OH_2	4.6E+05	4.6E+05	4.6E+05
H_2O-CO_2	7.4E+05	7.4E+05	7.4E+05
H_2O-H_2O	4.1E+05	4.1E+05	4.1E+05
MAE	586,778	585,111	585,111
ions			
$ArNH_3^+$	9.1E+05	8.8E+05	8.9E+05
H_3O^+	2.1E+05	2.0E+05	2.0E+05
$HCOO^-$	5.3E+05	5.3E+05	5.3E+05
$NH_3^+CH_2COO^-$	8.1E+05	8.1E+05	8.1E+05
MAE	613,250	605,500	607,500
peptides			
1G_pep	8.1E+05	8.1E+05	8.1E+05
2G_pep	1.4E+06	1.4E+06	1.4E+06
3G_pep	2.0E+06	2.0E+06	2.0E+06
4G_pep	2.6E+06	2.6E+06	2.6E+06
5G_pep	3.3E+06	3.2E+06	3.3E+06
MAE	2,024,000	2,024,200	2,026,200

Table A.29: *MAE* of the potential energy calculated using MultiExp grid with 25 radial points for molecules containing 1^{st} row atoms

Molecule	25(110)	25(194)	25(302)
BF_3	3.92E+05	3.90E+05	3.89E+05
BH_3	4.36E+04	4.38E+04	4.38E+04
BeH_2	3.04E+04	3.04E+04	3.04E+04
C_2H_2	1.20E+05	1.20E+05	1.20E+05
C_2H_4	1.24E+05	1.20E+05	1.20E+05
CF_4	5.17E+05	5.21E+05	5.21E+05
$CH_2CHCOOH$	3.92E+05	3.83E+05	3.83E+05
CH_2FF	2.86E+05	2.91E+05	2.90E+05
$CH_2CH_3CH_3$	1.81E+05	1.81E+05	1.80E+05
CH_3F	1.74E+05	1.75E+05	1.75E+05
CH_3NH_2	1.39E+05	1.39E+05	1.39E+05
CH_3OH	1.63E+05	1.61E+05	1.61E+05
CH_3CONH_2	3.03E+05	3.01E+05	3.00E+05
CH_4	6.14E+04	6.00E+04	5.99E+04
CO	1.62E+05	1.62E+05	1.62E+05
CO_2	2.64E+05	2.62E+05	2.62E+05
EtOTs	5.34E+06	5.35E+06	5.35E+06
F_2	2.27E+05	2.30E+05	2.30E+05
H_2	2.71E+01	2.98E+01	2.97E+01
H_2CO	1.63E+05	1.61E+05	1.61E+05
H_2O	1.02E+05	1.01E+05	1.01E+05
H_2O_2	2.02E+05	2.02E+05	2.02E+05
HCOOH	2.64E+05	2.62E+05	2.62E+05
Li_2	3.72E+04	3.72E+04	3.72E+04
LiF	1.31E+05	1.31E+05	1.31E+05
LiH	1.84E+04	1.84E+04	1.84E+04
NH_3	8.02E+04	7.92E+04	7.91E+04
benzaldehyde	5.51E+05	5.18E+05	5.22E+05
cytosine	5.77E+05	5.81E+05	5.80E+05
formamidine	2.13E+05	2.18E+05	2.18E+05
methoxide	1.62E+05	1.61E+05	1.61E+05
naphthalene	6.40E+05	5.88E+05	5.99E+05
uracil	6.14E+05	6.02E+05	6.02E+05
MAE	384,067	381,213	381,510

Table A.30: *MAE* of the potential energy calculated using MultiExp grid with 25 radial points for molecules containing 2^{nd} row atoms

Molecule	25(110)	25(194)	25(302)
CCl_4	2.16E+07	2.17E+07	2.17E+07
CH_2ClCl	1.09E+07	1.09E+07	1.09E+07
$CH_2PH_2PH_2$	8.56E+06	8.56E+06	8.55E+06
CH_2SHSH	9.81E+06	9.80E+06	9.80E+06
$CH_2SiH_3SiH_3$	7.64E+06	7.64E+06	7.64E+06
CH_3PH_2	4.31E+06	4.31E+06	4.31E+06
CH_3SH	4.93E+06	4.93E+06	4.93E+06
CH_3SiH_3	3.85E+06	3.85E+06	3.85E+06
CH_3Cl	5.46E+06	5.46E+06	5.46E+06
CS	4.93E+06	4.93E+06	4.93E+06
Cl_2	1.08E+07	1.08E+07	1.08E+07
ClF	5.52E+06	5.52E+06	5.52E+06
HOCl	5.50E+06	5.50E+06	5.50E+06
Mg	7.38E+06	7.38E+06	7.38E+06
NaCl	1.39E+07	1.39E+07	1.39E+07
P_2	8.50E+06	8.50E+06	8.50E+06
PF_5	4.81E+06	4.82E+06	4.82E+06
PH	4.25E+06	4.25E+06	4.25E+06
PH_3	4.25E+06	4.25E+06	4.25E+06
SF_6	5.55E+06	5.56E+06	5.56E+06
SO	4.97E+06	4.97E+06	4.97E+06
SO_2	9.85E+06	9.85E+06	9.85E+06
SiO	3.89E+06	3.89E+06	3.89E+06
pNO_2BzCl	6.02E+06	6.12E+06	6.10E+06
MAE	6,413,478	6,397,826	6,370,000

Table A.31: *MAE* of the potential energy calculated using MultiExp grid with 25 radial points for molecules containing 3^{rd} row atoms and transition states

Molecule	25(110)	25(194)	25(302)
3rd row			
AsH_3	5.72E+07	5.72E+07	5.72E+07
CH_3Br	6.27E+07	6.27E+07	6.27E+07
Ge_2H_6	1.07E+08	1.07E+08	1.07E+08
Ge_3H_8	1.60E+08	1.60E+08	1.60E+08
Ge_4H_{10}	2.14E+08	2.14E+08	2.14E+08
Ge_5H_{12}	2.68E+08	2.68E+08	2.68E+08
GeH_4	5.34E+07	5.34E+07	5.34E+07
H_2Se	5.99E+07	6.00E+07	6.00E+07
MAE	123,022,222	123,033,333	123,033,333
transition states			
TS_CH_3Cl_2	1.09E+07	1.09E+07	1.09E+07
TS_CH_3F_2	2.92E+05	2.89E+05	2.90E+05
TS_CH_3FCl	5.58E+06	5.57E+06	5.58E+06
TS_CH_5OF	2.74E+05	2.76E+05	2.76E+05
TS_Ethyl-OSO_2-CH_3	5.49E+06	5.49E+06	5.49E+06
TS_pHBzCl	5.99E+06	5.96E+06	5.97E+06
MAE	4,754,333	4,747,500	4,751,000

Table A.32: *MAE* of the potential energy calculated using MultiExp grid with 25 radial points for complexes, ions, and peptides

Molecule	25(110)	25(194)	25(302)
complexes			
CH_2O_2-CH_2O_2	5.31E+05	5.25E+05	5.24E+05
FH-CO	2.78E+05	2.76E+05	2.76E+05
FH-FH	2.31E+05	2.30E+05	2.30E+05
FH-NCH	2.56E+05	2.54E+05	2.54E+05
FH-NH_3	1.99E+05	1.94E+05	1.94E+05
FH-NN	2.64E+05	2.63E+05	2.63E+05
FH-OH_2	2.17E+05	2.16E+05	2.16E+05
H_2O-CO_2	3.66E+05	3.63E+05	3.63E+05
H_2O-H_2O	2.02E+05	2.02E+05	2.02E+05
MAE	282,667	280,333	280,222
ions			
$ArNH_3^+$	4.62E+05	4.31E+05	4.39E+05
H_3O^+	1.02E+05	1.01E+05	1.01E+05
$HCOO^-$	2.63E+05	2.62E+05	2.62E+05
$NH_3^+CH_2COO^-$	3.99E+05	4.01E+05	4.01E+05
MAE	306,500	298,750	300,750
peptides			
1G-pep	4.01E+05	4.02E+05	4.02E+05
2G-pep	6.96E+05	7.04E+05	7.02E+05
3G-pep	9.90E+05	1.01E+06	1.01E+06
4G-pep	1.30E+06	1.31E+06	1.31E+06
5G-pep	1.66E+06	1.60E+06	1.61E+06
MAE	1,009,400	1,005,200	1,006,800

Table A.33: *MAE* of the potential energy calculated using MultiExp grid with 30 radial points for molecules containing 1^{st} row atoms

Molecule	30(110)	30(194)	30(194)
BF_3	2.0E+05	2.0E+05	2.0E+05
BH_3	2.1E+04	2.1E+04	2.1E+04
BeH_2	1.5E+04	1.5E+04	1.5E+04
C_2H_2	5.7E+04	5.7E+04	5.7E+04
C_2H_4	6.1E+04	5.8E+04	5.7E+04
CF_4	2.6E+05	2.7E+05	2.7E+05
$CH_2CHCOOH$	1.9E+05	1.8E+05	1.8E+05
CH_2FF	1.4E+05	1.5E+05	1.5E+05
$CH_2CH_3CH_3$	8.6E+04	8.7E+04	8.6E+04
CH_3F	8.7E+04	8.8E+04	8.8E+04
CH_3NH_2	6.6E+04	6.6E+04	6.6E+04
CH_3OH	7.8E+04	7.6E+04	7.6E+04
CH_3CONH_2	1.4E+05	1.4E+05	1.4E+05
CH_4	3.0E+04	2.9E+04	2.9E+04
CO	7.8E+04	7.7E+04	7.7E+04
CO_2	1.3E+05	1.2E+05	1.2E+05
EtOTs	2.6E+06	2.6E+06	2.6E+06
F_2	1.2E+05	1.2E+05	1.2E+05
H_2	1.8E+01	2.0E+01	2.0E+01
H_2CO	7.8E+04	7.6E+04	7.6E+04
H_2O	4.9E+04	4.8E+04	4.8E+04
H_2O_2	9.5E+04	9.5E+04	9.5E+04
HCOOH	1.3E+05	1.2E+05	1.2E+05
Li_2	2.4E+04	2.4E+04	2.4E+04
LiF	6.9E+04	6.9E+04	6.9E+04
LiH	1.2E+04	1.2E+04	1.2E+04
NH_3	3.9E+04	3.8E+04	3.7E+04
benzaldehyde	2.8E+05	2.4E+05	2.5E+05
cytosine	2.7E+05	2.8E+05	2.7E+05
formamidine	9.9E+04	1.0E+05	1.0E+05
methoxide	7.7E+04	7.6E+04	7.6E+04
naphthalene	3.2E+05	2.7E+05	2.8E+05
uracil	3.0E+05	2.9E+05	2.8E+05
MAE	187,498	184,685	184,919

Table A.34: *MAE* of the potential energy calculated using MultiExp grid with 30 radial points for molecules containing 2^{nd} row atoms

Molecule	30(110)	30(194)	30(194)
CCl_4	1.1E+07	1.1E+07	1.1E+07
CH_2ClCl	5.5E+06	5.5E+06	5.5E+06
$CH_2PH_2PH_2$	4.0E+06	4.0E+06	4.0E+06
CH_2SHSH	4.8E+06	4.8E+06	4.8E+06
$CH_2SiH_3SiH_3$	3.9E+06	3.9E+06	3.9E+06
CH_3PH_2	2.0E+06	2.0E+06	2.0E+06
CH_3SH	2.4E+06	2.4E+06	2.4E+06
CH_3SiH_3	1.9E+06	1.9E+06	1.9E+06
CH_3Cl	2.8E+06	2.8E+06	2.8E+06
CS	2.4E+06	2.4E+06	2.4E+06
Cl_2	5.5E+06	5.5E+06	5.5E+06
ClF	2.8E+06	2.8E+06	2.8E+06
HOCl	2.8E+06	2.8E+06	2.8E+06
Mg	3.2E+06	3.2E+06	3.2E+06
NaCl	6.7E+06	6.7E+06	6.7E+06
P_2	4.0E+06	4.0E+06	4.0E+06
PF_5	2.3E+06	2.3E+06	2.3E+06
PH	2.0E+06	2.0E+06	2.0E+06
SF_6	2.7E+06	2.7E+06	2.7E+06
SO	2.4E+06	2.4E+06	2.4E+06
SO_2	4.8E+06	4.8E+06	4.8E+06
SiO	2.0E+06	2.0E+06	2.0E+06
pNO_2BzCl	3.0E+06	3.1E+06	3.1E+06
MAE	3,688,696	3,692,174	3,691,304

Table A.35: *MAE* of the potential energy calculated using MultiExp grid with 30 radial points for molecules containing 3^{rd} row atoms and transition states

Molecule	30(110)	30(194)	30(194)
3rd row			
AsH_3	5.7E+07	5.7E+07	5.7E+07
CH_3Br	6.3E+07	6.3E+07	6.3E+07
Ge_2H_6	1.1E+08	1.1E+08	1.1E+08
Ge_3H_8	1.6E+08	1.6E+08	1.6E+08
Ge_4H_{10}	2.1E+08	2.1E+08	2.1E+08
Ge_5H_{12}	2.7E+08	2.7E+08	2.7E+08
GeH_4	5.3E+07	5.3E+07	5.3E+07
H_2Se	6.0E+07	6.0E+07	6.0E+07
MAE	131,500,000	131,500,000	131,500,000
transition states			
TS_CH_3Cl_2	5.6E+06	5.5E+06	5.5E+06
TS_CH_3F_2	1.5E+05	1.5E+05	1.5E+05
TS_CH_3FCl	2.9E+06	2.8E+06	2.8E+06
TS_CH_5OF	1.3E+05	1.4E+05	1.4E+05
TS_Ethyl-OSO_2-CH_3	2.7E+06	2.7E+06	2.7E+06
TS_pHBzCl	3.0E+06	3.0E+06	3.0E+06
MAE	2,397,333	2,391,833	2,392,167

Table A.36: *MAE* of the potential energy calculated using MultiExp grid with 30 radial points for complexes, ions, and peptides

Molecule	30(110)	30(194)	30(194)
complexes			
CH_2O_2-CH_2O_2	2.5E+05	2.5E+05	2.5E+05
FH-CO	1.4E+05	1.4E+05	1.4E+05
FH-FH	1.2E+05	1.2E+05	1.2E+05
FH-NCH	1.3E+05	1.3E+05	1.3E+05
FH-NH_3	1.0E+05	9.7E+04	9.7E+04
FH-NN	1.4E+05	1.4E+05	1.4E+05
FH-OH_2	1.1E+05	1.1E+05	1.1E+05
H_2O-CO_2	1.8E+05	1.7E+05	1.7E+05
H_2O-H_2O	9.6E+04	9.6E+04	9.5E+04
MAE	139,856	137,589	137,467
ions			
$ArNH_3^+$	2.3E+05	2.0E+05	2.1E+05
H_3O^+	4.9E+04	4.8E+04	4.8E+04
$HCOO^-$	1.3E+05	1.2E+05	1.2E+05
$NH_3^+CH_2COO^-$	1.9E+05	1.9E+05	1.9E+05
MAE	148,025	140,400	142,375
peptides			
1G-pep	1.9E+05	1.9E+05	1.9E+05
2G-pep	3.2E+05	3.3E+05	3.3E+05
3G-pep	4.6E+05	4.8E+05	4.8E+05
4G-pep	6.0E+05	6.2E+05	6.2E+05
5G-pep	8.1E+05	7.5E+05	7.6E+05
MAE	476,400	473,400	474,800

Table A.37: *MAE* of the Coulomb potential energy V_{ee}^{1} calculated using MultiExp grid with 20 radial points

Molecule	20(110)	20(194)	20(302)
BF_3	-2.7E+06	-2.6E+06	-2.5E+06
BH_3	-3.1E+05	-3.1E+05	-3.1E+05
BeH_2	-2.4E+05	-2.4E+05	-2.4E+05
C_2H_2	-7.1E+05	-7.1E+05	-7.0E+05
C_2H_4	-7.8E+05	-7.7E+05	-7.7E+05
CF_4	-3.5E+06	-3.4E+06	-3.3E+06
$CH_2CHCOOH$	-2.4E+06	-2.4E+06	-2.4E+06
CH_2FF	-2.0E+06	-1.9E+06	-1.9E+06
$CH_2CH_3CH_3$	-1.2E+06	-1.2E+06	-1.2E+06
CH_3F	-1.2E+06	-1.1E+06	-1.1E+06
CH_3NH_2	-8.9E+05	-8.9E+05	-8.8E+05
CH_3OH	-1.0E+06	-1.0E+06	-9.9E+05
CH_3CONH_2	-1.8E+06	-1.8E+06	-1.8E+06
CH_4	-4.0E+05	-3.9E+05	-3.9E+05
CO	-1.0E+06	-9.8E+05	-9.7E+05
CO_2	-1.6E+06	-1.6E+06	-1.6E+06
EtOTs	-8.6E+06	-8.6E+06	-8.5E+06
F_2	-1.5E+06	-1.5E+06	-1.5E+06
H_2	-9.2E+03	-7.8E+03	-8.2E+03
H_2CO	-1.0E+06	-1.0E+06	-9.8E+05
H_2O	-6.2E+05	-6.0E+05	-6.0E+05
H_2O_2	-1.2E+06	-1.2E+06	-1.2E+06
HCOOH	-1.6E+06	-1.6E+06	-1.6E+06
Li_2	-3.5E+05	-3.5E+05	-3.5E+05
LiF	-9.5E+05	-9.3E+05	-9.1E+05
LiH	-1.8E+05	-1.8E+05	-1.8E+05
NH_3	-5.0E+05	-4.9E+05	-4.9E+05
benzaldehyde	-3.3E+06	-3.3E+06	-3.3E+06
cytosine	-3.7E+06	-3.7E+06	-3.6E+06
formamidine	-1.4E+06	-1.4E+06	-1.4E+06
methoxide	-1.0E+06	-1.0E+06	-1.0E+06
naphthalene	-3.9E+06	-3.8E+06	-3.8E+06
uracil	-3.9E+06	-3.8E+06	-3.7E+06
MAE	1,682,068	1,658,662	1,637,432

Table A.38: MAE of the Coulomb potential energy V_{ee}^{1} calculated using MultiExp grid with 20 radial points

Molecule	20(110)	20(194)	20(302)
CCl_4	-2.5E+07	-2.5E+07	-2.5E+07
CH_2ClCl	-1.3E+07	-1.3E+07	-1.3E+07
$CH_2PH_2PH_2$	-1.1E+07	-1.0E+07	-1.0E+07
CH_2SHSH	-1.2E+07	-1.2E+07	-1.2E+07
$CH_2SiH_3SiH_3$	-9.6E+06	-9.6E+06	-9.5E+06
CH_3PH_2	-5.4E+06	-5.4E+06	-5.4E+06
CH_3SH	-6.0E+06	-6.0E+06	-5.9E+06
CH_3SiH_3	-5.0E+06	-5.0E+06	-5.0E+06
CH_3Cl	-6.5E+06	-6.5E+06	-6.5E+06
CS	-6.0E+06	-5.9E+06	-5.9E+06
Cl_2	-1.2E+07	-1.2E+07	-1.2E+07
ClF	-6.9E+06	-6.9E+06	-6.8E+06
HOCl	-6.7E+06	-6.7E+06	-6.7E+06
Mg	-5.1E+06	-5.1E+06	-5.1E+06
NaCl	-1.1E+07	-1.1E+07	-1.1E+07
P_2	-1.0E+07	-1.0E+07	-1.0E+07
PF_5	-8.9E+06	-8.8E+06	-8.7E+06
PH	-5.0E+06	-5.0E+06	-5.0E+06
PH_3	-5.0E+06	-5.0E+06	-5.0E+06
SF_6	-1.0E+07	-1.0E+07	-9.9E+06
SO	-6.2E+06	-6.2E+06	-6.2E+06
SO_2	-1.2E+07	-1.2E+07	-1.2E+07
SiO	-5.2E+06	-5.2E+06	-5.2E+06
pNO_2BzCl	-1.1E+07	-1.1E+07	-1.1E+07
MAE	8,675,862	8,635,517	8,617,931

Table A.39: *MAE* of the Coulomb potential energy V_{ee}^{1} calculated using MultiExp grid with 20 radial points for molecules containing 3^{rd} row atoms and transition states

Molecule	20(110)	20(194)	20(302)
3rd row			
AsH_3	-2.1E+07	-2.1E+07	-2.1E+07
CH_3Br	-2.4E+07	-2.4E+07	-2.4E+07
Ge_2H_6	-3.8E+07	-3.8E+07	-3.8E+07
Ge_3H_8	-5.7E+07	-5.7E+07	-5.7E+07
Ge_4H_{10}	-7.7E+07	-7.6E+07	-7.6E+07
Ge_5H_{12}	-9.6E+07	-9.6E+07	-9.5E+07
GeH_4	-1.9E+07	-1.9E+07	-1.9E+07
H_2Se	-2.2E+07	-2.2E+07	-2.2E+07
MAE	44,688,889	44,555,556	44,444,444
transition states			
TS_CH_3Cl_2	-1.3E+07	-1.3E+07	-1.3E+07
TS_CH_3F_2	-2.0E+06	-1.9E+06	-1.9E+06
TS_CH_3FCl	-7.3E+06	-7.3E+06	-7.2E+06
TS_CH_5OF	-1.8E+06	-1.8E+06	-1.7E+06
TS_Ethyl-OSO_2-CH_3	-9.6E+06	-9.5E+06	-9.4E+06
TS_pHBzCl	-9.9E+06	-9.7E+06	-9.7E+06
MAE	7,201,667	7,125,000	7,086,667

Table A.40: MAE of the Coulomb potential energy V_{ee}^{1} calculated using MultiExp grid with 20 radial points for complexes, ions, and peptides

Molecule	20(110)	20(194)	20(302)
complexes			
CH_2O_2-CH_2O_2	-3.2E+06	-3.2E+06	-3.1E+06
FH-CO	-1.8E+06	-1.7E+06	-1.7E+06
FH-FH	-1.5E+06	-1.5E+06	-1.5E+06
FH-NCH	-1.6E+06	-1.6E+06	-1.6E+06
FH-NH_3	-1.3E+06	-1.3E+06	-1.2E+06
FH-NN	-1.6E+06	-1.6E+06	-1.5E+06
FH-OH_2	-1.4E+06	-1.4E+06	-1.3E+06
H_2O-CO_2	-2.3E+06	-2.2E+06	-2.2E+06
H_2O-H_2O	-1.2E+06	-1.2E+06	-1.2E+06
MAE	1,772,222	1,732,222	1,711,111
ions			
$ArNH_3^+$	-2.8E+06	-2.8E+06	-2.8E+06
H_3O^+	-6.1E+05	-6.0E+05	-6.0E+05
$HCOO^-$	-1.7E+06	-1.6E+06	-1.6E+06
$NH_3^+CH_2COO^-$	-2.5E+06	-2.5E+06	-2.5E+06
MAE	1,905,750	1,885,500	1,858,750
peptides			
1G_pep	-2.5E+06	-2.5E+06	-2.5E+06
2G_pep	-4.5E+06	-4.4E+06	-4.3E+06
3G_pep	-6.4E+06	-6.3E+06	-6.2E+06
4G_pep	-8.3E+06	-8.2E+06	-8.1E+06
5G_pep	-1.0E+07	-1.0E+07	-9.9E+06
MAE	6,390,000	6,272,000	6,194,000

Table A.41: MAE of the Coulomb potential energy V_{ee}^{1} calculated using MultiExp grid with 25 radial points

Molecule	25(110)	25(194)	25(302)
BF_3	-1.8E+06	-1.7E+06	-1.6E+06
BH_3	-2.0E+05	-2.0E+05	-2.0E+05
BeH_2	-1.5E+05	-1.5E+05	-1.5E+05
C_2H_2	-5.1E+05	-5.0E+05	-5.0E+05
C_2H_4	-5.2E+05	-5.1E+05	-5.1E+05
CF_4	-2.3E+06	-2.3E+06	-2.2E+06
$CH_2CHCOOH$	-1.7E+06	-1.6E+06	-1.6E+06
CH_2FF	-1.3E+06	-1.3E+06	-1.2E+06
$CH_2CH_3CH_3$	-7.9E+05	-7.8E+05	-7.7E+05
CH_3F	-7.8E+05	-7.6E+05	-7.4E+05
CH_3NH_2	-6.0E+05	-5.9E+05	-5.8E+05
CH_3OH	-6.9E+05	-6.8E+05	-6.6E+05
CH_3CONH_2	-1.3E+06	-1.3E+06	-1.2E+06
CH_4	-2.7E+05	-2.6E+05	-2.6E+05
CO	-6.8E+05	-6.7E+05	-6.5E+05
CO_2	-1.1E+06	-1.1E+06	-1.1E+06
EtOTs	-6.1E+06	-6.0E+06	-6.0E+06
F_2	-1.0E+06	-9.9E+05	-9.4E+05
H_2	-6.1E+03	-6.4E+03	-5.6E+03
H_2CO	-6.8E+05	-6.7E+05	-6.6E+05
H_2O	-4.2E+05	-4.1E+05	-4.0E+05
H_2O_2	-8.4E+05	-8.2E+05	-8.0E+05
HCOOH	-1.1E+06	-1.1E+06	-1.1E+06
Li_2	-2.1E+05	-2.1E+05	-2.1E+05
LiF	-6.3E+05	-6.1E+05	-5.9E+05
LiH	-1.1E+05	-1.1E+05	-1.1E+05
NH_3	-3.4E+05	-3.3E+05	-3.3E+05
benzaldehyde	-2.3E+06	-2.2E+06	-2.2E+06
cytosine	-2.5E+06	-2.5E+06	-2.4E+06
formamidine	-9.3E+05	-9.2E+05	-9.0E+05
methoxide	-6.9E+05	-6.8E+05	-6.6E+05
naphthalene	-2.6E+06	-2.5E+06	-2.5E+06
uracil	-2.6E+06	-2.5E+06	-2.5E+06
MAE	1,140,307	1,118,072	1,095,049

Table A.42: MAE of the Coulomb potential energy V_{ee}^{1} calculated using MultiExp grid with 25 radial points

Molecule	25(110)	25(194)	25(302)
CCl_4	-1.8E+07	-1.8E+07	-1.8E+07
CH_2ClCl	-9.0E+06	-8.9E+06	-8.9E+06
$CH_2PH_2PH_2$	-7.5E+06	-7.4E+06	-7.4E+06
CH_2SHSH	-8.3E+06	-8.2E+06	-8.2E+06
$CH_2SiH_3SiH_3$	-6.8E+06	-6.8E+06	-6.8E+06
CH_3PH_2	-3.9E+06	-3.9E+06	-3.8E+06
CH_3SH	-4.2E+06	-4.2E+06	-4.2E+06
CH_3SiH_3	-3.5E+06	-3.5E+06	-3.5E+06
CH_3Cl	-4.6E+06	-4.6E+06	-4.6E+06
CS	-4.3E+06	-4.2E+06	-4.2E+06
Cl_2	-8.7E+06	-8.7E+06	-8.7E+06
ClF	-4.9E+06	-4.8E+06	-4.8E+06
HOCl	-4.8E+06	-4.8E+06	-4.7E+06
Mg	-3.8E+06	-3.8E+06	-3.8E+06
NaCl	-8.1E+06	-8.1E+06	-8.1E+06
P_2	-7.2E+06	-7.2E+06	-7.2E+06
PF_5	-6.2E+06	-6.1E+06	-6.0E+06
PH	-3.6E+06	-3.6E+06	-3.6E+06
SF_6	-7.0E+06	-7.0E+06	-6.8E+06
SO	-4.4E+06	-4.4E+06	-4.4E+06
SO_2	-8.4E+06	-8.4E+06	-8.3E+06
SiO	-3.7E+06	-3.7E+06	-3.7E+06
pNO_2BzCl	-7.3E+06	-7.3E+06	-7.3E+06
MAE	6,413,478	6,397,826	6,370,000

Table A.43: *MAE* of the Coulomb potential energy V_{ee}^{1} calculated using MultiExp grid with 25 radial points for molecules containing 3^{rd} row atoms and transition states

Molecule	25(110)	25(194)	25(302)
3rd row			
AsH_3	-2.0E+07	-2.0E+07	-2.0E+07
CH_3Br	-2.2E+07	-2.2E+07	-2.2E+07
Ge_2H_6	-3.7E+07	-3.7E+07	-3.7E+07
Ge_3H_8	-5.5E+07	-5.6E+07	-5.6E+07
Ge_4H_{10}	-7.3E+07	-7.4E+07	-7.4E+07
Ge_5H_{12}	-9.3E+07	-9.3E+07	-9.3E+07
GeH_4	-1.9E+07	-1.9E+07	-1.9E+07
H_2Se	-2.0E+07	-2.0E+07	-2.0E+07
MAE	42,333,333	42,477,778	42,444,444
transition states			
TS_CH_3Cl_2	-9.0E+06	-9.0E+06	-8.9E+06
TS_CH_3F_2	-1.3E+06	-1.3E+06	-1.2E+06
TS_CH_3FCl	-5.2E+06	-5.1E+06	-5.1E+06
TS_CH_5OF	-1.2E+06	-1.2E+06	-1.1E+06
TS_Ethyl-OSO_2-CH_3	-6.7E+06	-6.6E+06	-6.5E+06
TS_pHBzCl	-6.8E+06	-6.8E+06	-6.7E+06
MAE	5,035,000	4,985,000	4,935,000

Table A.44: MAE of the Coulomb potential energy V_{ee}^{1} calculated using MultiExp grid with 25 radial points for complexes, ions, and peptides

Molecule	25(110)	25(194)	25(302)
complexes			
CH_2O_2-CH_2O_2	-2.2E+06	-2.2E+06	-2.1E+06
FH-CO	-1.2E+06	-1.2E+06	-1.1E+06
FH-FH	-1.0E+06	-1.0E+06	-9.6E+05
FH-NCH	-1.1E+06	-1.1E+06	-1.0E+06
FH-NH_3	-8.6E+05	-8.3E+05	-8.1E+05
FH-NN	2.1E+05	-5.1E+05	-8.0E+05
FH-OH_2	-9.4E+05	-9.1E+05	-8.8E+05
H_2O-CO_2	-1.5E+06	-1.5E+06	-1.5E+06
H_2O-$H2_2O$	-8.4E+05	-8.3E+05	-8.0E+05
MAE	1,100,778	1,108,444	1,110,667
ions			
$ArNH_3^+$	-1.9E+06	-1.9E+06	-1.9E+06
H_3O^+	-4.2E+05	-4.1E+05	-4.0E+05
$HCOO^-$	-1.1E+06	-1.1E+06	-1.1E+06
$NH_3^+CH_2COO^-$	-1.7E+06	-1.7E+06	-1.7E+06
MAE	1,293,750	1,269,000	1,242,000
peptides			
1G_pep	-1.7E+06	-1.7E+06	-1.6E+06
2G_pep	-3.0E+06	-3.0E+06	-2.9E+06
3G_pep	-4.3E+06	-4.2E+06	-4.1E+06
4G_pep	-5.6E+06	-5.5E+06	-5.4E+06
5G_pep	-7.0E+06	-6.8E+06	-6.6E+06
MAE	4,318,000	4,224,000	4,126,000

Table A.45: MAE of the Coulomb potential energy V_{ee}^{1} calculated using MultiExp grid with 30 radial points

Molecule	30(110)	30(194)	30(194)
BF_3	-1.3E+06	-1.3E+06	-1.3E+06
BH_3	-1.5E+05	-1.5E+05	-1.5E+05
BeH_2	-1.1E+05	-1.1E+05	-1.1E+05
C_2H_2	-3.6E+05	-3.7E+05	-3.6E+05
C_2H_4	-3.7E+05	-3.8E+05	-3.7E+05
CF_4	-1.7E+06	-1.7E+06	-1.7E+06
$CH_2CHCOOH$	-1.2E+06	-1.2E+06	-1.2E+06
CH_2FF	-9.7E+05	-9.6E+05	-9.3E+05
$CH_2CH_3CH_3$	-5.6E+05	-5.8E+05	-5.6E+05
CH_3F	-5.8E+05	-5.8E+05	-5.6E+05
CH_3NH_2	-4.2E+05	-4.3E+05	-4.3E+05
CH_3OH	-5.0E+05	-5.0E+05	-4.9E+05
CH_3CONH_2	-9.4E+05	-9.3E+05	-9.1E+05
CH_4	-2.0E+05	-1.9E+05	-1.9E+05
CO	-4.9E+05	-4.9E+05	-4.8E+05
CO_2	-8.0E+05	-8.0E+05	-7.8E+05
EtOTs	-4.1E+06	-4.1E+06	-4.1E+06
F_2	-7.6E+05	-7.6E+05	-7.3E+05
H_2	-4.5E+03	-4.5E+03	-4.2E+03
H_2CO	-5.0E+05	-5.0E+05	-4.8E+05
H_2O	-2.0E+05	-2.2E+05	-2.7E+05
H_2O_2	-6.1E+05	-6.1E+05	-5.9E+05
HCOOH	-8.1E+05	-8.0E+05	-7.8E+05
Li_2	-1.7E+05	-1.7E+05	-1.7E+05
LiF	-4.7E+05	-4.7E+05	-4.5E+05
LiH	-8.7E+04	-8.6E+04	-8.6E+04
NH_3	-2.5E+05	-2.5E+05	-2.4E+05
benzaldehyde	-1.7E+06	-1.6E+06	-1.6E+06
cytosine	-1.8E+06	-1.8E+06	-1.8E+06
formamidine	-6.8E+05	-6.8E+05	-6.6E+05
methoxide	-5.1E+05	-5.0E+05	-4.9E+05
naphthalene	-1.9E+06	-1.9E+06	-1.9E+06
uracil	-1.9E+06	-1.9E+06	-1.8E+06
MAE	822,334	819,268	801,734

Table A.46: MAE of the Coulomb potential energy V_{ee}^{1} calculated using MultiExp grid with 30 radial points

Molecule	30(110)	30(194)	30(194)
CCl_4	-1.2E+07	-1.2E+07	-1.2E+07
CH_2ClCl	-6.0E+06	-6.0E+06	-6.0E+06
$CH_2PH_2PH_2$	-4.8E+06	-4.8E+06	-4.8E+06
CH_2SHSH	-5.4E+06	-5.4E+06	-5.4E+06
$CH_2SiH_3SiH_3$	-4.5E+06	-4.5E+06	-4.5E+06
CH_3PH_2	-2.5E+06	-2.5E+06	-2.5E+06
CH_3SH	-2.8E+06	-2.8E+06	-2.8E+06
CH_3SiH_3	-2.4E+06	-2.4E+06	-2.4E+06
CH_3Cl	-3.1E+06	-3.1E+06	-3.1E+06
CS	-2.8E+06	-2.8E+06	-2.8E+06
Cl_2	-5.8E+06	-5.8E+06	-5.8E+06
ClF	-3.3E+06	-3.3E+06	-3.2E+06
HOCl	-3.2E+06	-3.2E+06	-3.2E+06
Mg	-2.7E+06	-2.7E+06	-2.7E+06
NaCl	-5.7E+06	-5.6E+06	-5.6E+06
P_2	-4.6E+06	-4.6E+06	-4.6E+06
PF_5	-4.2E+06	-4.2E+06	-4.2E+06
PH	-2.3E+06	-2.3E+06	-2.3E+06
SF_6	-4.9E+06	-4.9E+06	-4.8E+06
SO	-2.9E+06	-2.9E+06	-2.9E+06
SO_2	-5.5E+06	-5.5E+06	-5.5E+06
SiO	-2.5E+06	-2.5E+06	-2.5E+06
pNO_2BzCl	-5.0E+06	-5.1E+06	-5.0E+06
MAE	4,285,217	4,288,696	4,262,174

Table A.47: *MAE* of the Coulomb potential energy V_{ee}^{1} calculated using MultiExp grid with 30 radial points for molecules containing 3^{rd} row atoms and transition states

Molecule	30(110)	30(194)	30(194)
3rd row			
AsH_3	-1.9E+07	-1.9E+07	-1.9E+07
CH_3Br	-2.1E+07	-2.1E+07	-2.1E+07
Ge_2H_6	-3.6E+07	-3.6E+07	-3.6E+07
Ge_3H_8	-5.4E+07	-5.4E+07	-5.4E+07
Ge_4H_{10}	-7.2E+07	-7.2E+07	-7.2E+07
Ge_5H_{12}	-9.0E+07	-9.0E+07	-9.0E+07
GeH_4	-1.8E+07	-1.8E+07	-1.8E+07
H_2Se	-2.0E+07	-2.0E+07	-2.0E+07
MAE	41,444,444	41,444,444	41,433,333
transition states			
TS_CH_3Cl_2	-6.0E+06	-6.0E+06	-6.0E+06
TS_CH_3F_2	-9.9E+05	-9.7E+05	-9.4E+05
TS_CH_3FCl	-3.5E+06	-3.5E+06	-3.5E+06
TS_CH_5OF	-8.9E+05	-8.8E+05	-8.5E+05
TS_Ethyl-OSO_2-CH_3	-4.6E+06	-4.6E+06	-4.5E+06
TS_pHBzCl	-4.7E+06	-4.7E+06	-4.6E+06
MAE	3,445,500	3,421,167	3,384,833

Table A.48: *MAE* of the Coulomb potential energy V_{ee}^{1} calculated using MultiExp grid with 30 radial points for complexes, ions, and peptides

Molecule	30(110)	30(194)	30(194)
complexes			
CH_2O_2-CH_2O_2	-1.6E+06	-1.6E+06	-1.6E+06
FH-CO	-8.8E+05	-8.7E+05	-8.5E+05
FH-FH	-7.7E+05	-7.6E+05	-7.3E+05
FH-NCH	-8.1E+05	-8.1E+05	-7.9E+05
FH-NH_3	-6.4E+05	-6.3E+05	-6.1E+05
FH-NN	-8.7E+05	-8.6E+05	-8.4E+05
FH-OH_2	-6.9E+05	-5.1E+05	-6.6E+05
H_2O-CO_2	-1.1E+06	-1.1E+06	-1.1E+06
H_2O-$H2_2O$	-6.1E+05	-5.3E+05	-5.9E+05
MAE	887,778	854,667	855,889
ions			
$ArNH_3^+$	-1.4E+06	-1.4E+06	-1.4E+06
H_3O^+	-3.1E+05	-3.0E+05	-2.9E+05
$HCOO^-$	-8.2E+05	-8.1E+05	-7.9E+05
$NH_3^+CH_2COO^-$	-9.6E+05	-1.3E+06	-1.2E+06
MAE	871,500	933,750	912,750
peptides			
1G_pep	-1.3E+06	-1.2E+06	-1.2E+06
2G_pep	-2.2E+06	-2.2E+06	-2.1E+06
3G_pep	-3.1E+06	-3.1E+06	-3.0E+06
4G_pep	-4.1E+06	-4.1E+06	-4.0E+06
5G_pep	-5.1E+06	-5.0E+06	-4.9E+06
MAE	3,144,000	3,114,000	3,032,000

Table A.49: MAE of the Coulomb energy V_{ee}^2 calculated using MultiExp grid with 20 radial points

Molecule	20(110)	20(194)	20(302)
BF_3	8.6E+02	2.2E+03	2.6E+03
BH_3	1.0E+03	1.0E+03	1.0E+03
BeH_2	8.4E+02	8.2E+02	8.3E+02
C_2H_2	2.1E+03	2.0E+03	2.0E+03
C_2H_4	-2.4E+02	1.8E+03	2.0E+03
CF_4	5.2E+03	3.1E+03	3.1E+03
$CH_2CHCOOH$	3.4E+02	4.7E+03	5.0E+03
CH_2FF	3.8E+03	1.3E+03	1.7E+03
$CH_2CH_3CH_3$	2.2E+03	1.8E+03	2.4E+03
CH_3F	2.2E+03	1.6E+03	1.7E+03
CH_3NH_2	1.9E+03	1.7E+03	1.8E+03
CH_3OH	6.0E+02	1.6E+03	1.7E+03
CH_3CONH_2	2.2E+03	3.3E+03	3.4E+03
CH_4	3.0E+01	7.1E+02	7.6E+02
CO	1.7E+03	2.0E+03	2.0E+03
CO_2	1.9E+03	2.8E+03	2.8E+03
EtOTs	9.9E+03	3.8E+03	3.9E+03
F_2	3.3E+03	1.6E+03	1.8E+03
H_2	2.4E+01	2.4E+01	2.4E+01
H_2CO	9.2E+02	2.0E+03	2.0E+03
H_2O	6.3E+02	7.9E+02	8.2E+02
H_2O_2	2.1E+03	1.7E+03	1.7E+03
HCOOH	1.6E+03	2.5E+03	2.6E+03
Li_2	1.4E+03	1.4E+03	1.4E+03
LiF	7.2E+03	7.2E+03	7.2E+03
LiH	5.9E+02	5.8E+02	5.8E+02
NH_3	-7.9E+01	6.0E+02	6.4E+02
benzaldehyde	-6.2E+03	1.2E+04	9.3E+03
cytosine	1.0E+04	7.3E+03	8.1E+03
formamidine	5.1E+03	3.0E+03	2.7E+03
methoxide	1.0E+03	1.5E+03	1.5E+03
naphthalene	-8.5E+03	1.9E+04	1.3E+04
uracil	2.8E+03	8.7E+03	8.8E+03
MAE	2,685	3,219	3,051

Table A.50: MAE of the Coulomb energy V_{ee}^2 calculated using MultiExp grid with 20 radial points

Molecule	20(110)	20(194)	20(302)
CCl_4	-7.8E+02	-3.9E+03	-3.6E+03
CH_2ClCl	-2.8E+03	-3.6E+03	-3.5E+03
$CH_2PH_2PH_2$	-1.1E+04	-5.3E+03	-5.1E+03
CH_2SHSH	-8.5E+03	-6.4E+03	-5.8E+03
$CH_2SiH_3SiH_3$	-4.1E+03	-3.6E+03	-3.0E+03
CH_3PH_2	-4.2E+03	-2.2E+03	-2.3E+03
CH_3SH	-1.9E+03	-2.5E+03	-2.5E+03
CH_3SiH_3	-2.0E+03	-1.2E+03	-1.2E+03
CH_3Cl	-2.9E+03	-1.9E+03	-1.8E+03
CS	-1.1E+03	-8.6E+02	-9.1E+02
Cl_2	-9.2E+03	-6.5E+03	-6.6E+03
ClF	-1.3E+03	6.0E+02	5.0E+02
HOCl	-3.7E+03	-3.8E+03	-3.6E+03
Mg	5.4E+04	5.4E+04	5.4E+04
NaCl	-1.8E+04	-1.8E+04	-1.8E+04
P_2	-4.5E+03	-3.7E+03	-3.9E+03
PF_5	-1.7E+03	-3.4E+03	-4.2E+03
PH	-2.2E+03	-2.3E+03	-2.3E+03
SF_6	5.4E+03	-3.4E+03	-5.2E+03
SO	-2.1E+03	-2.4E+03	-2.5E+03
SO_2	-8.4E+02	-6.5E+02	-6.9E+02
SiO	-2.2E+02	-1.1E+03	-1.1E+03
pNO_2BzCl	4.9E+04	1.4E+03	7.8E+03
MAE	8,280	5,746	6,052

Table A.51: MAE of the Coulomb energy V_{ee}^2 calculated using MultiExp grid with 20 radial points for molecules containing 3^{rd} row atoms and transition states

Molecule	20(110)	20(194)	20(302)
3rd row			
AsH_3	-1.9E+05	-1.9E+05	-2.0E+05
CH_3Br	-1.7E+05	-1.6E+05	-1.6E+05
Ge_2H_6	-3.4E+05	-3.3E+05	-3.3E+05
Ge_3H_8	-5.1E+05	-5.2E+05	-5.2E+05
Ge_4H_{10}	-7.4E+05	-7.3E+05	-7.4E+05
Ge_5H_{12}	-8.8E+05	-9.2E+05	-9.3E+05
GeH_4	-1.6E+05	-1.6E+05	-1.6E+05
H_2Se	-1.7E+05	-1.9E+05	-1.9E+05
	379,000	382,667	384,333
transition states			
TS_CH_3Cl_2	-1.4E+04	-6.1E+03	-6.1E+03
TS_CH_3F_2	5.9E+02	2.5E+03	1.9E+03
TS_CH_3FCl	-2.7E+03	-1.2E+03	-1.6E+03
TS_CH_5OF	2.9E+03	2.1E+03	1.9E+03
TS_Ethyl-OSO_2-CH_3	5.2E+03	2.5E+03	2.3E+03
TS_pHBzCl	-6.2E+03	6.7E+03	4.3E+03
MAE	5,191	3,515	3,032

Table A.52: MAE of the Coulomb energy V_{ee}^2 calculated using MultiExp grid with 20 radial points for complexes, ions, and peptides

Molecule	20(110)	20(194)	20(302)
complexes			
CH_2O_2-CH_2O_2	3.0E+03	5.6E+03	5.3E+03
FH-CO	2.0E+03	2.5E+03	2.6E+03
FH-FH	8.6E+02	1.4E+03	1.4E+03
FH-NCH	2.5E+03	2.9E+03	2.9E+03
FH-NH_3	-1.3E+03	8.2E+02	9.0E+02
FH-NN	9.9E+03	9.8E+03	9.9E+03
FH-OH_2	6.7E+02	1.1E+03	1.2E+03
H_2O-CO_2	1.8E+03	3.2E+03	3.2E+03
H_2O-$H2_2O$	2.0E+03	1.7E+03	1.8E+03
MAE	2,676	3,231	3,233
ions			
$ArNH_3^+$	-4.4E+03	1.2E+04	7.5E+03
H_3O^+	1.6E+02	6.3E+02	6.3E+02
$HCOO^-$	1.9E+03	2.5E+03	2.5E+03
$NH_3^+CH_2COO^-$	6.7E+03	5.2E+03	5.0E+03
MAE	3,292	5,030	3,907
peptides			
1G_pep	5.3E+03	4.5E+03	4.6E+03
2G_pep	1.3E+04	7.2E+03	7.8E+03
3G_pep	2.3E+04	1.4E+04	1.3E+04
4G_pep	2.6E+04	1.8E+04	1.8E+04
5G_pep	-6.6E+03	2.0E+04	1.4E+04
MAE	14,594	12,622	11,632

Table A.53: *MAE* of the Coulomb energy V_{ee}^2 calculated using MultiExp grid with 25 radial points

Molecule	25(110)	25(194)	25(302)
BF_3	-2,550	-1,240	-735
BH_3	-59	-59	-84
BeH_2	-87	-99	-96
C_2H_2	-117	-185	-200
C_2H_4	-2,460	-383	-203
CF_4	672	-1,450	-1,500
$CH_2CHCOOH$	-5,520	-1,240	-915
CH_2FF	1,380	-1,040	-647
$CH_2CH_3CH_3$	-837	-1,090	-582
CH_3F	189	-338	-286
CH_3NH_2	-288	-424	-314
CH_3OH	-1,310	-319	-276
CH_3CONH_2	-1,970	-827	-764
CH_4	-849	-149	-98
CO	-598	-228	-239
CO_2	-1,320	-444	-482
EtOTs	11,500	5,320	5,730
F_2	1,230	-260	-57
H_2	5	4	4
H_2CO	-1,290	-277	-281
H_2O	-356	-182	-141
H_2O_2	96	-288	-302
HCOOH	-1,490	-582	-518
Li_2	-139	-126	-125
LiF	1,240	1,160	1,180
LiH	6	-1	-1
NH_3	-904	-202	-160
benzaldehyde	-16,700	651	-1,270
cytosine	-165	-2,690	-1,960
formamidine	1,840	-190	-478
methoxide	-804	-342	-309
naphthalene	-22,800	4,630	-921
uracil	-8,960	-2,170	-1,840
MAE	2,719	866	688

Table A.54: *MAE* of the Coulomb energy V_{ee}^2 calculated using MultiExp grid with 25 radial points

Molecule	25(110)	25(194)	25(302)
CCl_4	20,900	18,200	18,300
CH_2ClCl	9,010	8,410	8,480
$CH_2PH_2PH_2$	7,180	12,500	12,500
CH_2SHSH	10,700	12,700	13,400
$CH_2SiH_3SiH_3$	6,190	6,900	7,400
CH_3PH_2	4,520	6,210	6,130
CH_3SH	7,160	6,620	6,580
CH_3SiH_3	2,910	3,720	3,730
CH_3Cl	2,930	4,040	4,050
CS	6,680	6,990	6,950
Cl_2	6,940	8,880	8,920
ClF	3,500	4,790	4,670
HOCl	3,580	3,520	3,470
Mg	-41,300	-41,300	-41,300
NaCl	-15,600	-15,800	-15,800
P_2	12,300	13,500	13,400
PF_5	7,100	4,980	4,520
PH	6,600	6,430	6,450
SF_6	11,400	4,080	3,420
SO	7,210	6,790	6,810
SO_2	14,000	13,000	13,000
SiO	5,260	4,370	4,440
pNO_2BzCl	43,100	-4,870	2,140
MAE	11,133	9,504	9,385

Table A.55: *MAE* of the Coulomb energy V_{ee}^2 calculated using MultiExp grid with 25 radial points for molecules containing 3^{rd} row atoms and transition states

Molecule	25(110)	25(194)	25(302)
3rd row			
AsH_3	-198,000	-202,000	-203,000
CH_3Br	-205,000	-199,000	-200,000
Ge_2H_6	-394,000	-372,000	-374,000
Ge_3H_8	-580,000	-585,000	-585,000
Ge_4H_{10}	-823,000	-804,000	-808,000
Ge_5H_{12}	-1,000,000	-1,030,000	-1,040,000
GeH_4	-174,000	-173,000	-174,000
H_2Se	-192,000	-209,000	-205,000
MAE	444,111	443,667	445,333
transition states			
TS_CH_3Cl_2	1,560	7,470	7,620
TS_CH_3F_2	-1,800	113	-400
TS_CH_3FCl	1,630	3,470	3,170
TS_CH_5OF	617	-259	-492
TS_Ethyl-OSO_2-CH_3	7,580	5,120	5,570
TS_pHBzCl	-11,100	2,220	-545
MAE	4,048	3,109	2,966

Table A.56: MAE of the Coulomb energy V_{ee}^2 calculated using MultiExp grid with 25 radial points for complexes, ions, and peptides

Molecule	25(110)	25(194)	25(302)
complexes			
CH_2O_2-CH_2O_2	-4,790	-1,410	-1,070
FH-CO	-943	-356	-343
FH-FH	-733	-200	-178
FH-NCH	-775	-381	-374
FH-NH_3	-2,570	-303	-287
FH-NN	4,800	4,930	4,960
FH-OH_2	-772	-284	-221
H_2O-CO_2	-1,880	-621	-612
H_2O-$H2_2O$	-137	-361	-305
MAE	1,933	983	928
ions			
$ArNH_3^+$	-13,600	2,890	-1,030
H_3O^+	-654	-164	-160
$HCOO^-$	-1,060	-506	-508
$NH_3^+CH_2COO^-$	519	-956	-917
MAE	3,958	1,129	654
peptides			
1G_pep	-316	-1,150	-1,020
2G_pep	1,330	-2,760	-1,940
3G_pep	4,200	-4,220	-4,020
4G_pep	-181	-6,580	-5,580
5G_pep	-30,700	-3,090	-8,320
MAE	7,345	3,560	4,176

Table A.57: MAE of the Coulomb energy V_{ee}^2 calculated using MultiExp grid with 30 radial points

Molecule	30(110)	30(194)	30(194)
BF_3	-1,560	-406	108
BH_3	55	55	30
BeH_2	20	5	9
C_2H_2	150	88	73
C_2H_4	-2,200	-99	74
CF_4	2,500	280	287
$CH_2CHCOOH$	-4,410	-123	193
CH_2FF	2,100	-343	113
$CH_2CH_3CH_3$	-354	-625	-17
CH_3F	540	-2	50
CH_3NH_2	56	-83	29
CH_3OH	-972	25	67
CH_3CONH_2	-949	131	188
CH_4	-724	-24	27
CO	-303	78	64
CO_2	-765	138	103
EtOTs	6,670	495	889
F_2	1,430	-93	102
H_2	1	1	1
H_2CO	-939	76	72
H_2O	-190	-17	23
H_2O_2	486	90	71
HCOOH	-856	56	106
Li_2	-47	-33	-32
LiF	1,540	1,460	1,470
LiH	37	27	28
NH_3	-701	-7	32
benzaldehyde	-14,800	2,680	817
cytosine	2,030	-414	225
formamidine	2,440	401	115
methoxide	-444	27	62
naphthalene	-20,200	7,480	1,960
uracil	-6,890	-25	454
MAE	2,344	481	239

Table A.58: MAE of the Coulomb energy V_{ee}^2 calculated using MultiExp grid with 30 radial points

Molecule	30(110)	30(194)	30(194)
CCl_4	199	-2,330	-2,320
CH_2ClCl	-1,110	-1,470	-1,370
$CH_2PH_2PH_2$	-2,460	2,220	2,530
CH_2SHSH	-1,960	22	661
$CH_2SiH_3SiH_3$	-1,680	-1,060	-546
CH_3PH_2	-228	1,330	1,260
CH_3SH	976	440	403
CH_3SiH_3	-1,000	-153	-166
CH_3Cl	-1,880	-724	-721
CS	184	549	502
Cl_2	-4,000	-1,570	-1,550
ClF	-2,080	-603	-645
HOCl	-1,130	-808	-701
Mg	24,800	24,800	24,800
NaCl	23,400	23,200	23,300
P_2	2,220	3,150	2,980
PF_5	5,320	2,710	2,230
PH	1,440	1,200	1,210
SF_6	10,700	2,200	1,400
SO	983	390	369
SO_2	1,080	330	371
SiO	1,120	73	126
pNO_2BzCl	41,800	-6,640	360
MAE	5,728	3,390	3,066

Table A.59: *MAE* of the Coulomb energy V_{ee}^2 calculated using MultiExp grid with 30 radial points for molecules containing 3^{rd} row atoms and transition states

Molecule	30(110)	30(194)	30(194)
3rd row			
AsH_3	-196,000	-200,000	-202,000
CH_3Br	-204,000	-199,000	-199,000
Ge_2H_6	-392,000	-370,000	-371,000
Ge_3H_8	-576,000	-579,000	-580,000
Ge_4H_{10}	-817,000	-796,000	-800,000
Ge_5H_{12}	-993,000	-1,020,000	-1,040,000
GeH_4	-173,000	-172,000	-173,000
H_2Se	-190,000	-206,000	-203,000
MAE	441,444	440,111	442,778
transition states			
TS_CH_3Cl_2	-8,880	-2,210	-2,270
TS_CH_3F_2	-1,310	566	54
TS_CH_3FCl	-2,530	-506	-752
TS_CH_5OF	1,100	324	78
TS_Ethyl-OSO_2-CH_3	3,880	866	1,290
TS_pHBzCl	-13,000	285	-2,500
MAE	5,117	793	1,157

Table A.60: MAE of the Coulomb energy V_{ee}^2 calculated using MultiExp grid with 30 radial points for complexes, ions, and peptides

Molecule	30(110)	30(194)	30(194)
complexes			
CH_2O_2-CH_2O_2	-3,270	29	282
FH-CO	-509	59	79
FH-FH	-504	23	34
FH-NCH	-340	86	88
FH-NH_3	-2,220	-5	35
FH-NN	-1,390	-1,340	-1,290
FH-OH_2	-532	-38	22
H_2O-CO_2	-1,200	160	143
H_2O-$H2_2O$	226	-3	49
MAE	1,132	194	225
ions			
$ArNH_3^+$	-12,100	4,620	742
H_3O^+	-464	27	31
$HCOO^-$	-441	113	101
$NH_3^+CH_2COO^-$	1,780	233	254
MAE	3,696	1,248	282
peptides			
1G_pep	972	102	187
2G_pep	4,490	-395	193
3G_pep	9,590	324	109
4G_pep	7,620	138	613
5G_pep	-24,100	5,280	329
MAE	9,354	1,248	286

Table A.61: *MAE* of the integration of the electron density using Becke, TA, TA(new), SG-1, SG0 for molecules containing 1^{st} row atoms

Molecule	Becke	TA	TA(new)	SG-1	SG0
BF_3	-4.8E-04	2.1E-03	-3.8E-04	1.3E-04	6.2E-04
BH_3	-1.7E-03	1.1E-03	9.3E-05	1.8E-05	3.4E-05
BeH_2	4.7E-04	1.2E-03	-3.3E-05	-2.8E-06	4.0E-05
C_2H_2	1.1E-04	-2.2E-03	-1.6E-05	4.7E-05	-3.6E-05
C_2H_4	6.2E-04	5.8E-03	4.3E-05	-1.0E-04	-9.9E-04
CF_4	-3.0E-04	-1.9E-05	1.1E-04	6.2E-04	1.4E-03
$CH_2CHCOOH$	4.0E-04	3.3E-04	-1.4E-04	-1.6E-04	-3.2E-04
CH_2FF	7.0E-04	-3.9E-03	-1.8E-04	-2.2E-04	1.2E-04
$CH_2CH_3CH_3$	6.5E-04	-1.9E-03	-2.1E-04	-2.4E-04	-6.2E-05
CH_3F	5.6E-04	-8.3E-04	-8.0E-05	-2.0E-05	2.0E-04
CH_3NH_2	1.1E-03	-4.2E-03	1.4E-04	-5.2E-05	1.11E-04
CH_3OH	7.5E-04	-7.9E-04	1.1E-04	-1.2E-05	-9.8E-05
CH_3CONH_2	-2.2E-04	-1.7E-03	5.3E-04	1.7E-05	7.8E-05
CH_4	5.2E-04	-1.7E-03	3.1E-05	-2.3E-05	-1.1E-04
CO	-1.5E-05	1.6E-04	1.7E-05	-6.7E-06	-2.8E-05
CO_2	1.7E-06	7.7E-05	1.1E-05	1.7E-05	-1.3E-04
EtOTs	-8.1E-04	-8.5E-03	-9.5E-04	-1.5E-04	1.8E-03
F_2	-4.7E-05	8.1E-04	-8.0E-06	1.4E-04	7.8E-04
H_2	-3.1E-04	-4.2E-04	-1.0E-05	9.5E-06	-6.2E-05
H_2CO	3.1E-04	2.0E-03	2.7E-05	3.7E-05	9.6E-05
H_2O	1.4E-04	4.4E-04	-6.5E-05	-5.6E-06	-3.8E-05
H_2O_2	6.5E-05	-8.3E-04	1.3E-05	2.2E-05	2.4E-04
HCOOH	4.8E-04	2.5E-04	-6.6E-05	-2.2E-05	1.3E-04
Li_2	-1.1E-05	1.8E-04	4.9E-06	2.2E-06	2.1E-04
LiF	1.9E-03	1.9E-05	2.4E-04	2.1E-04	9.3E-04
LiH	-2.5E-04	5.0E-04	6.2E-05	2.3E-05	-3.2E-04
NH_3	2.3E-04	-1.1E-03	-3.9E-05	-1.7E-05	8.2E-05
benzaldehyde	2.1E-04	1.3E-03	2.5E-04	3.4E-04	-3.4E-05
cytosine	4.9E-04	1.5E-03	2.2E-05	-2.9E-04	-5.4E-04
formamidine	6.0E-04	7.6E-03	2.1E-04	5.3E-05	3.8E-04
methoxide	-1.9E-04	-3.5E-05	-2.8E-06	-3.7E-05	-1.7E-04
naphthalene	3.5E-03	1.2E-02	1.7E-03	8.2E-04	1.8E-03
uracil	4.4E-04	6.2E-03	2.9E-04	-3.8E-04	-3.1E-04
MAE	5.6E-04	2.2E-03	1.8E-04	1.3E-04	3.7E-04

Table A.62: *MAE* of the integration of the electron density using Becke, TA, TA(new), SG-1, SG0 for molecules containing 2^{nd} row atoms

Molecule	Becke	TA	TA(new)	SG-1	SG0
CCl_4	-1.3E-04	1.1E-03	3.5E-07	-7.1E-05	-9.39E-04
CH_2ClCl	-4.5E-04	-1.3E-04	2.9E-06	-9.5E-06	-6.24E-04
$CH_2PH_2PH_2$	4.2E-03	-2.7E-03	3.1E-04	2.0E-05	-6.88E-04
CH_2SHSH	2.5E-03	-3.7E-03	1.9E-04	8.7E-05	5.10E-04
$CH_2SiH_3SiH_3$	-3.9E-03	2.1E-03	1.1E-04	-2.0E-04	-4.40E-04
CH_3PH_2	4.7E-04	-4.5E-03	-4.6E-05	1.5E-05	-2.33E-04
CH_3SH	2.6E-04	-1.4E-03	5.3E-05	1.4E-04	-3.38E-04
CH_3SiH_3	-4.1E-03	-2.2E-03	-1.3E-04	-2.3E-05	-7.54E-05
CH_3Cl	-2.1E-04	-1.9E-03	-2.9E-05	4.5E-05	-1.91E-04
CS	-5.3E-05	-2.3E-04	-4.9E-06	-2.0E-05	1.09E-04
Cl_2	7.9E-05	4.2E-03	6.4E-06	-3.5E-04	-6.67E-04
ClF	-8.1E-05	2.6E-03	2.1E-06	-1.3E-04	-2.08E-04
HOCl	1.6E-04	1.8E-04	4.2E-05	-1.6E-05	-2.02E-05
Mg	-5.2E-06	2.5E-06	2.5E-06	3.6E-06	9.51E-05
NaCl	1.2E-04	3.4E-03	-1.1E-05	-1.3E-04	-4.03E-04
P_2	-8.8E-05	8.0E-04	2.0E-05	2.9E-05	-1.17E-03
PF_5	7.9E-04	1.1E-02	7.3E-05	-5.8E-04	1.65E-04
PH	2.4E-04	-1.7E-03	1.3E-05	-2.7E-05	-5.46E-04
SF_6	-1.1E-03	9.9E-03	-6.4E-04	-4.4E-03	-2.22E-03
SO	-1.2E-04	-4.1E-04	-1.7E-06	1.0E-04	4.29E-04
SO_2	7.7E-05	-1.5E-03	-9.2E-06	7.4E-05	9.50E-04
SiO	-9.7E-05	1.0E-04	-2.4E-06	3.8E-05	4.05E-05
pNO_2BzCl	-1.3E-04	6.1E-03	-1.9E-04	-3.3E-04	-8.44E-04
MAE	8.4E-04	2.7E-03	8.3E-05	2.9E-04	4.9E-04

Table A.63: *MAE* of the integration of the electron density using Becke, TA, TA(new), SG-1, SG0 for molecules containing 3^{rd} row atoms and transition states

Molecule	Becke	TA	TA(new)	SG-1	SG0
3rd row					
AsH_3	-2.3E-03	2.4E-03	-1.0E-04	NA	NA
CH_3Br	7.4E-04	1.1E-03	-2.8E-05	NA	NA
Ge_2H_6	3.7E-03	1.5E-02	3.7E-05	NA	NA
Ge_3H_8	2.6E-03	1.8E-02	3.6E-04	NA	NA
Ge_4H_{10}	9.3E-03	3.4E-02	6.7E-04	NA	NA
Ge_5H_{12}	-1.3E-03	3.5E-02	8.3E-04	NA	NA
GeH_4	-1.4E-02	-1.1E-03	-6.0E-05	NA	NA
H_2Se	-2.5E-03	1.8E-03	1.2E-04	NA	NA
MAE	4.5E-03	1.2E-02	2.5E-04		
transition states					
TS_CH_3Cl_2	6.4E-03	-6.3E-04	2.2E-05	-2.7E-04	6.3E-04
TS_CH_3F_2	7.1E-04	-2.0E-03	2.3E-05	7.9E-05	2.4E-04
TS_CH_3FCl	4.4E-04	-3.5E-04	-1.9E-05	9.0E-05	4.6E-04
TS_CH_5OF	1.3E-03	-6.0E-03	3.1E-04	1.1E-04	6.9E-04
TS_Ethyl-OSO_2-CH_3	2.1E-04	-1.4E-03	-5.2E-05	1.9E-04	1.8E-03
TS_pHBzCl	5.8E-03	7.0E-03	3.1E-04	5.8E-04	4.1E-04
MAE	2.5E-03	2.9E-03	1.2E-04	2.2E-04	7.0E-04

NA: R parameters are not available

Table A.64: *MAE* of the integration of the electron density using Becke, TA, TA(new), SG-1, SG0 for complexes, ions, and peptides

Molecule	Becke	TA	TA(new)	SG-1	SG0
complexes					
CH_2O_2-CH_2O_2	5.6E-04	-4.5E-03	-9.5E-06	-1.1E-04	4.0E-04
FH-CO	-6.5E-05	3.6E-04	5.1E-05	-3.6E-06	1.1E-04
FH-FH	1.1E-05	1.5E-04	1.0E-04	3.1E-05	3.0E-04
FH-NCH	6.3E-05	8.1E-04	3.2E-05	4.6E-05	2.6E-04
FH-NH_3	3.2E-04	2.2E-03	-1.1E-05	-3.7E-07	-2.5E-06
FH-NN	-1.0E-03	3.7E-03	-2.1E-05	3.0E-05	1.8E-04
FH-OH_2	-8.0E-06	8.6E-04	-8.8E-05	-4.7E-07	-2.8E-06
H_2O-CO_2	6.3E-04	-7.7E-04	6.0E-05	1.4E-04	-4.5E-04
H_2O-$H2_2O$	5.0E-04	2.4E-03	-4.1E-05	-1.1E-05	1.8E-04
MAE	3.5E-04	1.7E-03	4.6E-05	4.1E-05	2.1E-04
ions					
$ArNH_3^+$	-9.8E-04	-2.5E-03	2.0E-04	6.6E-04	7.5E-04
H_3O^+	2.2E-04	-1.2E-03	3.5E-07	4.3E-06	-7.2E-05
$HCOO^-$	2.0E-05	6.1E-04	-3.8E-06	5.1E-05	1.7E-04
$NH_3^+CH_2COO^-$	-3.1E-04	3.2E-03	-3.1E-04	1.6E-04	-7.7E-04
MAE	3.8E-04	1.9E-03	1.3E-04	2.2E-04	4.4E-04
peptides					
1G_pep	-7.6E-04	-1.8E-03	-9.3E-06	-5.7E-05	-1.4E-05
2G_pep	2.9E-03	-8.0E-03	-8.9E-05	-1.9E-04	-8.3E-04
3G_pep	7.6E-04	-2.1E-03	-2.4E-04	1.1E-04	-3.9E-04
4G_pep	1.2E-03	-9.7E-03	-4.1E-04	-1.9E-04	-8.4E-04
5G_pep	8.5E-03	-2.3E-03	6.4E-04	5.1E-04	-5.0E-04
MAE	2.8E-03	4.8E-03	2.8E-04	2.1E-04	5.2E-04

Table A.65: *MAE* of the dipole moment calculated using Becke, TA, TA(new), SG-1, SG0 for molecules containing 1^{st} row atoms

Molecule	Becke	TA	TA(new)	SG-1	SG0
BF_3	1.1E-04	1.7E-03	3.2E-04	1.3E-03	1.4E-03
BH_3	3.1E-04	6.2E-03	1.6E-04	1.9E-05	7.7E-05
BeH_2	1.2E-03	3.0E-03	8.3E-05	7.1E-06	1.0E-04
C_2H_2	1.3E-04	5.8E-04	2.9E-04	5.2E-05	4.0E-05
C_2H_4	7.7E-04	7.2E-03	5.3E-05	1.3E-04	1.2E-03
CF_4	3.6E-04	3.2E-03	8.4E-04	9.1E-04	1.1E-03
$CH_2CHCOOH$	-1.7E-03	-6.8E-03	-6.1E-04	2.5E-04	8.8E-04
CH_2FF	-4.9E-04	7.5E-03	-4.4E-04	-1.0E-03	-6.0E-04
$CH_2CH_3CH_3$	-5.4E-04	-2.8E-03	-6.6E-04	-4.3E-04	-8.7E-04
CH_3F	3.7E-05	2.8E-04	-2.2E-04	-1.0E-04	3.6E-04
CH_3NH_2	2.7E-04	2.8E-03	-8.6E-06	8.4E-05	-2.2E-05
CH_3OH	3.2E-04	2.3E-03	-6.2E-05	7.4E-05	7.1E-05
CH_3CONH_2	-2.5E-05	6.8E-03	-8.3E-04	1.2E-04	1.5E-03
CH_4	1.4E-04	4.1E-03	1.2E-04	1.8E-05	8.3E-05
CO	-2.0E-05	-2.1E-04	2.6E-05	6.0E-06	-1.9E-04
CO_2	3.7E-06	1.7E-04	2.3E-05	3.6E-05	2.9E-04
EtOTs	-5.9E-03	-1.4E-02	-5.3E-04	-3.0E-04	1.7E-03
F_2	6.0E-05	1.0E-03	1.0E-05	1.7E-04	9.9E-04
H_2	2.2E-04	2.9E-04	6.9E-06	6.6E-06	4.2E-05
H_2CO	-8.3E-05	2.9E-03	2.4E-04	-8.6E-05	1.4E-04
H_2O	-1.2E-04	-2.1E-04	1.5E-04	3.8E-05	2.0E-04
H_2O_2	-7.1E-05	3.2E-04	-8.1E-05	-1.9E-04	-2.3E-04
HCOOH	-1.2E-04	9.6E-04	1.8E-04	-1.0E-04	-1.8E-04
Li_2	2.9E-05	4.8E-04	1.3E-05	5.8E-06	5.6E-04
LiF	3.8E-03	-4.5E-04	5.7E-04	5.1E-04	8.4E-04
LiH	1.6E-03	4.1E-04	-4.8E-04	9.0E-06	8.0E-04
NH_3	-1.8E-04	5.7E-04	-2.4E-05	1.7E-05	-7.8E-05
benzaldehyde	2.1E-03	-8.8E-03	-1.1E-03	-9.0E-04	-2.7E-03
cytosine	-1.2E-04	-1.3E-02	-5.2E-04	2.5E-04	2.7E-03
formamidine	-1.3E-03	-3.8E-03	-2.1E-04	-4.5E-05	-7.5E-04
methoxide	6.2E-04	8.0E-04	3.0E-04	-1.0E-04	-1.8E-05
naphthalene	4.6E-03	1.5E-02	2.2E-03	1.1E-03	2.4E-03
uracil	9.2E-04	3.2E-02	1.4E-03	-1.0E-03	3.6E-04
MAE	8.6E-04	4.6E-03	3.9E-04	2.8E-04	7.1E-04

Table A.66: *MAE* of the dipole moment calculated using Becke, TA, TA(new), SG-1, SG0 for molecules containing 2^{nd} row atoms

Molecule	Becke	TA	TA(new)	SG-1	SG0
CCl_4	3.5E-05	3.5E-03	2.1E-04	6.8E-04	1.4E-03
CH_2ClCl	-5.1E-04	7.7E-04	-5.1E-05	-3.6E-04	-1.7E-03
$CH_2PH_2PH_2$	-1.5E-02	1.4E-02	-9.5E-04	1.3E-04	2.0E-03
CH_2SHSH	6.3E-03	-9.2E-03	6.2E-04	2.0E-04	1.6E-03
$CH_2SiH_3SiH_3$	-2.9E-03	-1.3E-03	1.3E-03	-6.8E-04	-1.5E-03
CH_3PH_2	1.2E-03	-8.4E-05	2.1E-05	1.1E-04	-1.5E-03
CH_3SH	2.0E-04	3.8E-03	-1.1E-04	6.1E-04	-2.0E-03
CH_3SiH_3	-9.0E-03	-8.0E-04	-1.6E-04	-1.1E-04	-2.2E-04
CH_3Cl	1.1E-04	-1.6E-03	-5.4E-05	2.4E-04	-4.1E-04
CS	4.9E-05	-8.3E-05	1.3E-06	9.1E-05	-8.4E-04
Cl_2	1.5E-04	7.9E-03	1.2E-05	6.5E-04	1.3E-03
ClF	-1.4E-04	3.7E-03	-2.5E-05	2.3E-04	9.2E-04
HOCl	-1.6E-04	-2.1E-03	-6.8E-05	-3.2E-04	-2.4E-03
Mg	2.2E-17	-4.6E-18	-2.4E-17	-4.0E-17	-3.2E-17
NaCl	4.3E-04	1.2E-02	-1.0E-04	-3.4E-04	9.7E-06
P_2	1.5E-04	1.4E-03	3.6E-05	5.1E-05	2.1E-03
PF_5	2.1E-03	1.8E-03	7.4E-04	2.2E-03	2.0E-03
PH	-4.6E-04	2.6E-03	-4.3E-05	-5.7E-05	9.4E-04
SF_6	1.8E-11	2.1E-10	1.7E-11	4.6E-11	4.5E-11
SO	-2.6E-04	-2.1E-03	-1.2E-05	-2.7E-05	-5.5E-04
SO_2	2.6E-06	8.4E-03	2.3E-04	2.7E-04	-2.7E-03
SiO	-3.1E-04	5.9E-04	-2.1E-05	-7.4E-05	8.1E-04
pNO_2BzCl	-5.2E-03	3.4E-02	-1.5E-04	1.9E-04	2.5E-03
MAE	1.9E-03	4.9E-03	2.1E-04	3.3E-04	1.3E-03

Table A.67: *MAE* of the dipole moment calculated using Becke, TA, TA(new), SG-1, SG0 for molecules containing 3^{rd} row atoms and transition states

Molecule	Becke	TA	TA(new)	SG-1	SG0
3rd row					
AsH_3	-4.6E-05	-2.3E-02	3.2E-04	NA	NA
CH_3Br	1.3E-04	6.5E-04	-7.2E-05	NA	NA
Ge_2H_6	8.4E-03	3.5E-02	8.4E-05	NA	NA
Ge_3H_8	1.9E-02	1.1E-02	1.1E-03	NA	NA
Ge_4H_{10}	4.8E-02	1.9E-01	3.7E-04	NA	NA
Ge_5H_{12}	4.0E-02	-1.1E-02	7.5E-04	NA	NA
GeH_4	2.3E-03	8.5E-03	1.6E-04	NA	NA
H_2Se	2.0E-03	1.8E-02	-1.9E-04	NA	NA
MAE	1.3E-02	3.7E-02	3.5E-04		
transition states					
TS_CH_3Cl_2	2.6E-03	1.2E-02	3.6E-04	2.3E-04	2.4E-03
TS_CH_3F_2	9.2E-04	1.0E-04	8.2E-05	2.2E-04	1.3E-04
TS_CH_3FCl	-5.6E-03	6.2E-03	-5.9E-05	-2.2E-04	1.7E-03
TS_CH_5OF	-5.8E-03	1.7E-02	-5.2E-04	2.3E-05	-2.9E-04
TS_Ethyl-OSO_2-CH_3	-1.9E-03	-6.2E-03	3.2E-04	2.0E-04	1.7E-03
TS_pHBzCl	-3.7E-03	-4.5E-03	-5.8E-04	-1.9E-03	1.4E-03
MAE	3.4E-03	7.7E-03	3.2E-04	4.7E-04	1.3E-03

NA: R parameters are not available

Table A.68: *MAE* of the dipole moment calculated using Becke, TA, TA(new), SG-1, SG0 for complexes, ions, and peptides

Molecule	Becke	TA	TA(new)	SG-1	SG0
complexes					
CH_2O_2-CH_2O_2	2.1E-03	1.3E-02	-3.4E-05	-4.0E-04	1.5E-03
FH-CO	1.4E-03	-5.1E-03	-9.0E-04	-1.1E-04	-3.5E-03
FH-FH	1.4E-04	1.0E-04	8.5E-05	7.7E-05	6.1E-04
FH-NCH	-4.5E-04	2.2E-03	2.0E-04	2.5E-05	1.1E-03
FH-NH_3	-6.6E-04	-7.1E-03	-1.2E-04	-3.7E-04	-4.0E-04
FH-NN	6.2E-03	-1.7E-02	4.2E-05	-7.6E-05	-1.2E-03
FH-OH_2	4.2E-04	-9.8E-04	1.9E-04	3.8E-06	8.4E-05
H_2O-CO_2	-2.4E-03	4.6E-03	-3.3E-04	-4.5E-04	4.1E-04
H_2O-$H2_2O$	-1.3E-03	-9.2E-03	6.4E-06	-1.3E-05	-1.0E-03
MAE	1.7E-03	6.5E-03	2.0E-04	1.7E-04	1.1E-03
ions					
$ArNH_3^+$	1.4E-03	2.3E-02	9.4E-04	6.8E-04	6.6E-04
H_3O^+	-9.1E-05	6.7E-04	-1.4E-05	-6.2E-05	8.5E-05
$HCOO^-$	5.2E-04	-1.6E-03	-2.2E-04	6.4E-04	1.3E-03
$NH_3^+CH_2COO^-$	4.1E-04	-2.3E-04	7.7E-04	2.0E-04	1.2E-03
MAE	6.0E-04	6.2E-03	4.8E-04	3.9E-04	8.0E-04
peptides					
1G_pep	7.7E-04	-4.9E-03	-4.5E-05	-1.5E-04	9.7E-04
2G_pep	4.7E-03	-3.2E-02	1.2E-04	4.0E-04	-3.2E-03
3G_pep	-5.9E-03	5.9E-02	-2.1E-03	2.8E-03	2.6E-04
4G_pep	-1.6E-02	-6.3E-02	-6.1E-03	-1.1E-03	-5.1E-03
5G_pep	7.4E-02	7.3E-02	2.2E-03	5.8E-03	-2.2E-03
MAE	2.0E-02	4.6E-02	2.1E-03	2.1E-03	2.4E-03

Table A.69: *MAE* of the potential energy calculated using Becke, TA, TA(new), SG-1 for molecules containing 1^{st} row atoms

Molecule	Becke	TA	TA(new)	SG-1
BF_3	-9.4E+05	-8.2E+05	-1.2E+06	1.3E+05
BH_3	-1.1E+05	-7.3E+04	-1.1E+05	1.0E+05
BeH_2	-6.8E+04	-5.0E+04	-7.0E+04	1.0E+05
C_2H_2	-2.2E+05	-1.8E+05	-2.7E+05	2.3E+05
C_2H_4	-2.5E+05	-1.8E+05	-2.9E+05	1.9E+05
CF_4	-1.2E+06	-1.1E+06	-1.5E+06	1.4E+05
$CH_2CHCOOH$	-7.9E+05	-6.8E+05	-9.6E+05	3.8E+05
CH_2FF	-6.8E+05	-6.3E+05	-8.6E+05	1.1E+05
$CH_2CH_3CH_3$	-4.0E+05	-3.3E+05	-4.3E+05	2.8E+05
CH_3F	-4.2E+05	-3.6E+05	-5.0E+05	1.0E+05
CH_3NH_2	-3.1E+05	-2.8E+05	-3.5E+05	1.7E+05
CH_3OH	-3.6E+05	-3.1E+05	-4.2E+05	1.4E+05
CH_3CONH_2	-6.3E+05	-5.6E+05	-7.4E+05	3.2E+05
CH_4	-1.5E+05	-1.2E+05	-1.6E+05	9.2E+04
CO	-3.1E+05	-2.4E+05	-3.8E+05	1.6E+05
CO_2	-5.3E+05	-4.7E+05	-6.5E+05	2.1E+05
EtOTs	-2.0E+06	-1.9E+06	-2.4E+06	5.4E+05
F_2	-5.6E+05	-4.8E+05	-7.0E+05	3.4E+04
H_2	-1.1E+04	-7.6E+03	-1.0E+04	-5.2E+03
H_2CO	-3.3E+05	-2.8E+05	-4.0E+05	1.5E+05
H_2O	-2.4E+05	-2.0E+05	-2.7E+05	5.7E+04
H_2O_2	-4.3E+05	-3.9E+05	-5.2E+05	1.1E+05
HCOOH	-5.5E+05	-4.8E+05	-6.7E+05	2.0E+05
Li_2	-4.8E+04	-4.9E+04	-7.0E+04	2.0E+05
LiF	-3.3E+05	-2.8E+05	-3.9E+05	9.9E+04
LiH	-4.4E+04	-3.1E+04	-4.3E+04	9.5E+04
NH_3	-1.9E+05	-1.6E+05	-2.1E+05	7.7E+04
benzaldehyde	-1.0E+06	-9.1E+05	-1.0E+06	7.3E+05
cytosine	-1.2E+06	-1.0E+06	-1.4E+06	6.4E+05
formamidine	-4.6E+05	-3.4E+05	-5.4E+05	2.5E+05
methoxide	-3.6E+05	-3.1E+05	-4.2E+05	1.4E+05
naphthalene	-9.9E+05	-9.4E+05	-1.3E+06	9.6E+05
uracil	-1.2E+06	-1.0E+06	-1.5E+06	6.2E+05
MAE	5.2E+05	4.6E+05	6.3E+05	2.4E+05

Table A.70: *MAE* of the potential energy calculated using Becke, TA, TA(new), SG-1 for molecules containing 2^{nd} row atoms

Molecule	Becke	TA	TA(new)	SG-1
CCl_4	-4.2E+06	-3.9E+06	-5.4E+06	4.4E+05
CH_2ClCl	-2.2E+06	-2.0E+06	-2.8E+06	2.7E+05
$CH_2PH_2PH_2$	-1.7E+06	-1.6E+06	-2.2E+06	4.1E+05
CH_2SHSH	-1.9E+06	-1.8E+06	-2.5E+06	3.6E+05
$CH_2SiH_3SiH_3$	-1.7E+06	-1.4E+06	-2.0E+06	4.1E+05
CH_3PH_2	-9.5E+05	-8.9E+05	-1.2E+06	2.5E+05
CH_3SH	-1.1E+06	-9.6E+05	-1.3E+06	2.3E+05
CH_3SiH_3	-9.0E+05	-7.9E+05	-1.1E+06	2.5E+05
CH_3Cl	-1.2E+06	-1.1E+06	-1.5E+06	1.8E+05
CS	-1.0E+06	-9.2E+05	-1.3E+06	2.4E+05
Cl_2	-2.0E+06	-1.8E+06	-2.6E+06	1.7E+05
ClF	-1.3E+06	-1.2E+06	-1.7E+06	1.0E+05
HOCl	-1.3E+06	-1.1E+06	-1.6E+06	1.5E+05
Mg	-5.3E+05	-4.7E+05	-6.7E+05	9.7E+04
NaCl	-1.5E+06	-1.3E+06	-1.9E+06	1.1E+05
P_2	-1.6E+06	-1.4E+06	-2.0E+06	3.2E+05
PF_5	-2.2E+06	-1.7E+06	-2.8E+06	2.0E+05
PH	-8.0E+05	-7.5E+05	-1.0E+06	1.6E+05
SF_6	-2.6E+06	-2.1E+06	-3.3E+06	2.0E+05
SO	-1.1E+06	-1.0E+06	-1.4E+06	2.0E+05
SO_2	-2.0E+06	-1.9E+06	-2.6E+06	3.5E+05
SiO	-9.1E+05	-8.2E+05	-1.2E+06	2.1E+05
pNO_2BzCl	-2.5E+06	-2.1E+06	-3.0E+06	9.1E+05
MAE	1.6E+06	1.4E+06	2.0E+06	2.7E+05

Table A.71: *MAE* of the potential energy calculated using Becke, TA, TA(new), SG-1 for molecules containing 3^{rd} row atoms and transition states

Molecule	Becke	TA	TA(new)	SG-1
3rd row				
AsH_3	-4.7E+06	-4.2E+06	-5.8E+06	NA
CH_3Br	-5.4E+06	-4.9E+06	-6.8E+06	NA
Ge_2H_6	-8.7E+06	-7.7E+06	-1.1E+07	NA
Ge_3H_8	-1.3E+07	-1.2E+07	-1.7E+07	NA
Ge_4H_{10}	-1.7E+07	-1.5E+07	-2.2E+07	NA
Ge_5H_{12}	-2.2E+07	-1.9E+07	-2.8E+07	NA
GeH_4	-5.0E+06	-4.0E+06	-5.5E+06	NA
H_2Se	-5.0E+06	-4.4E+06	-6.2E+06	NA
MAE	1.0E+07	8.9E+06	1.3E+07	
transition states				
TS_CH_3Cl_2	-2.2E+06	-2.0E+06	-2.8E+06	2.6E+05
TS_CH_3F_2	-7.3E+05	-6.5E+05	-8.8E+05	9.6E+04
TS_CH_3FCl	-1.5E+06	-1.3E+06	-1.9E+06	1.7E+05
TS_CH_5OF	-6.6E+05	-6.0E+05	-7.8E+05	1.6E+05
TS_Ethyl-OSO_2-CH_3	-2.3E+06	-2.0E+06	-2.7E+06	7.2E+05
TS_pHBzCl	-2.1E+06	-1.8E+06	-2.6E+06	9.2E+05
MAE	1.6E+06	1.4E+06	1.9E+06	3.9E+05

NA: R parameters are not available

Table A.72: *MAE* of the potential energy calculated using Becke, TA, TA(new), SG-1 for complexes, ions, and peptides

Molecule	Becke	TA	TA(new)	SG-1
complexes				
CH_2O_2-CH_2O_2	-1.1E+06	-1.0E+06	-1.3E+06	4.0E+05
FH-CO	-6.0E+05	-5.0E+05	-7.5E+05	1.7E+05
FH-FH	-5.9E+05	-5.2E+05	-7.1E+05	2.6E+04
FH-NCH	-5.5E+05	-4.8E+05	-6.5E+05	2.0E+05
FH-NH_3	-4.8E+05	-4.1E+05	-5.7E+05	9.0E+04
FH-NN	-5.8E+05	-4.8E+05	-7.2E+05	2.3E+05
FH-OH_2	-5.4E+05	-4.6E+05	-6.3E+05	6.9E+04
H_2O-CO_2	-7.6E+05	-6.8E+05	-9.3E+05	2.6E+05
H_2O-$H2_2O$	-4.7E+05	-3.9E+05	-5.5E+05	1.1E+05
MAE	6.3E+05	5.5E+05	7.6E+05	1.7E+05
ions				
$ArNH_3^+$	-8.8E+05	-8.0E+05	-1.0E+06	6.8E+05
H_3O^+	-2.3E+05	-2.0E+05	-2.7E+05	5.9E+04
$HCOO^-$	-5.6E+05	-4.8E+05	-6.6E+05	1.8E+05
$NH_3^+CH_2COO^-$	-8.5E+05	-6.8E+05	-1.0E+06	3.6E+05
MAE	6.3E+05	5.4E+05	7.4E+05	3.2E+05
peptides				
1G_pep	-8.5E+05	-7.3E+05	-1.0E+06	3.7E+05
2G_pep	-1.4E+06	-1.4E+06	-1.8E+06	6.7E+05
3G_pep	-2.1E+06	-1.8E+06	-2.5E+06	9.9E+05
4G_pep	-2.7E+06	-2.5E+06	-3.3E+06	1.3E+06
5G_pep	-3.1E+06	-2.9E+06	-4.0E+06	1.6E+06
MAE	2.0E+06	1.9E+06	2.5E+06	9.9E+05

Table A.73: *MAE* of the Coulomb energy V_{ee}^{1} calculated using Becke, TA, TA(new), SG-1, SG0 for molecules containing 1^{st} row atoms

Molecule	Becke	TA	TA(new)	SG-1	SG0
BF_3	-9.4E+05	-8.2E+05	-1.2E+06	1.3E+05	-4.0E+06
BH_3	-1.1E+05	-7.3E+04	-1.1E+05	1.0E+05	-3.1E+05
BeH_2	-6.8E+04	-5.0E+04	-7.0E+04	1.0E+05	-2.7E+05
C_2H_2	-2.2E+05	-1.8E+05	-2.7E+05	2.3E+05	-5.9E+05
C_2H_4	-2.5E+05	-1.8E+05	-2.9E+05	1.9E+05	-5.9E+05
CF_4	-1.2E+06	-1.1E+06	-1.5E+06	1.4E+05	-5.2E+06
$CH_2CHCOOH$	-7.9E+05	-6.8E+05	-9.6E+05	3.8E+05	-2.4E+06
CH_2FF	-6.8E+05	-6.3E+05	-8.6E+05	1.1E+05	-2.8E+06
$CH_2CH_3CH_3$	-4.0E+05	-3.3E+05	-4.3E+05	2.8E+05	-9.8E+05
CH_3F	-4.2E+05	-3.6E+05	-5.0E+05	1.0E+05	-1.6E+06
CH_3NH_2	-3.1E+05	-2.8E+05	-3.5E+05	1.7E+05	-8.1E+05
CH_3OH	-3.6E+05	-3.1E+05	-4.2E+05	1.4E+05	-1.1E+06
CH_3CONH_2	-6.3E+05	-5.6E+05	-7.4E+05	3.2E+05	-1.8E+06
CH_4	-1.5E+05	-1.2E+05	-1.6E+05	9.2E+04	-3.4E+05
CO	-3.1E+05	-2.4E+05	-3.8E+05	1.6E+05	-1.0E+06
CO_2	-5.3E+05	-4.7E+05	-6.5E+05	2.1E+05	-1.4E+06
EtOTs	-2.0E+06	-1.9E+06	-2.4E+06	5.4E+05	-7.2E+06
F_2	-5.6E+05	-4.8E+05	-7.0E+05	3.4E+04	-2.4E+06
H_2	-1.1E+04	-7.6E+03	-1.0E+04	-5.2E+03	-1.0E+04
H_2CO	-3.3E+05	-2.8E+05	-4.0E+05	1.5E+05	-1.0E+06
H_2O	-2.4E+05	-2.0E+05	-2.7E+05	5.7E+04	-7.3E+05
H_2O_2	-4.3E+05	-3.9E+05	-5.2E+05	1.1E+05	-1.5E+06
HCOOH	-5.5E+05	-4.8E+05	-6.7E+05	2.0E+05	-1.8E+06
Li_2	-4.8E+04	-4.9E+04	-7.0E+04	2.0E+05	-1.8E+05
LiF	-3.3E+05	-2.8E+05	-3.9E+05	9.9E+04	-1.3E+06
LiH	-4.4E+04	-3.1E+04	-4.3E+04	9.5E+04	-9.6E+04
NH_3	-1.9E+05	-1.6E+05	-2.1E+05	7.7E+04	-4.8E+05
benzaldehyde	-1.0E+06	-9.1E+05	-1.0E+06	7.3E+05	-2.9E+06
cytosine	-1.2E+06	-1.0E+06	-1.4E+06	6.4E+05	-3.5E+06
formamidine	-4.6E+05	-3.4E+05	-5.4E+05	2.5E+05	-1.3E+06
methoxide	-3.6E+05	-3.1E+05	-4.2E+05	1.4E+05	-1.1E+06
naphthalene	-9.9E+05	-9.4E+05	-1.3E+06	9.6E+05	-3.1E+06
uracil	-1.2E+06	-1.0E+06	-1.5E+06	6.2E+05	-3.7E+06
MAE	5.2E+05	4.6E+05	6.3E+05	2.4E+05	1.3E+06

Table A.74: *MAE* of the Coulomb energy V_{ee}^{1} calculated using Becke, TA, TA(new), SG-1 for molecules containing 2^{nd} row atoms

Molecule	Becke	TA	TA(new)	SG-1
CCl_4	-4.2E+06	-3.9E+06	-5.4E+06	4.4E+05
CH_2ClCl	-2.2E+06	-2.0E+06	-2.8E+06	2.7E+05
$CH_2PH_2PH_2$	-1.7E+06	-1.6E+06	-2.2E+06	4.1E+05
CH_2SHSH	-1.9E+06	-1.8E+06	-2.5E+06	3.6E+05
$CH_2SiH_3SiH_3$	-1.7E+06	-1.4E+06	-2.0E+06	4.1E+05
CH_3PH_2	-9.5E+05	-8.9E+05	-1.2E+06	2.5E+05
CH_3SH	-1.1E+06	-9.6E+05	-1.3E+06	2.3E+05
CH_3SiH_3	-9.0E+05	-7.9E+05	-1.1E+06	2.5E+05
CH_3Cl	-1.2E+06	-1.1E+06	-1.5E+06	1.8E+05
CS	-1.0E+06	-9.2E+05	-1.3E+06	2.4E+05
Cl_2	-2.0E+06	-1.8E+06	-2.6E+06	1.7E+05
ClF	-1.3E+06	-1.2E+06	-1.7E+06	1.0E+05
HOCl	-1.3E+06	-1.1E+06	-1.6E+06	1.5E+05
Mg	-5.3E+05	-4.7E+05	-6.7E+05	9.7E+04
NaCl	-1.5E+06	-1.3E+06	-1.9E+06	1.1E+05
P_2	-1.6E+06	-1.4E+06	-2.0E+06	3.2E+05
PF_5	-2.2E+06	-1.7E+06	-2.8E+06	2.0E+05
PH	-8.0E+05	-7.5E+05	-1.0E+06	1.6E+05
SF_6	-2.6E+06	-2.1E+06	-3.3E+06	2.0E+05
SO	-1.1E+06	-1.0E+06	-1.4E+06	2.0E+05
SO_2	-2.0E+06	-1.9E+06	-2.6E+06	3.5E+05
SiO	-9.1E+05	-8.2E+05	-1.2E+06	2.1E+05
pNO_2BzCl	-2.5E+06	-2.1E+06	-3.0E+06	9.1E+05
MAE	1.5E+06	1.4E+06	1.9E+06	2.6E+05

Table A.75: *MAE* of the Coulomb energy V_{ee}^{1} calculated using Becke, TA, TA(new), SG-1, SG0 for molecules containing 3^{rd} row atoms and transition states

Molecule	Becke	TA	TA(new)	SG-1	SG0
3rd row					
AsH_3	-4.7E+06	-4.2E+06	-5.8E+06	NA	NA
CH_3Br	-5.4E+06	-4.9E+06	-6.8E+06	NA	NA
Ge_2H_6	-8.7E+06	-7.7E+06	-1.1E+07	NA	NA
Ge_3H_8	-1.3E+07	-1.2E+07	-1.7E+07	NA	NA
Ge_4H_{10}	-1.7E+07	-1.5E+07	-2.2E+07	NA	NA
Ge_5H_{12}	-2.2E+07	-1.9E+07	-2.8E+07	NA	NA
GeH_4	-5.0E+06	-4.0E+06	-5.5E+06	NA	NA
H_2Se	-5.0E+06	-4.4E+06	-6.2E+06	NA	NA
MAE	1.1E+07	8.9E+06	1.3E+07		
transition states					
TS_CH_3Cl_2	-2.2E+06	-2.0E+06	-2.8E+06	2.6E+05	-1.0E+07
TS_CH_3F_2	-7.3E+05	-6.5E+05	-8.8E+05	9.6E+04	-2.8E+06
TS_CH_3FCl	-1.5E+06	-1.3E+06	-1.9E+06	1.7E+05	-6.5E+06
TS_CH_5OF	-6.6E+05	-6.0E+05	-7.8E+05	1.6E+05	-2.3E+06
TS_Ethyl-OSO_2-CH_3	-2.3E+06	-2.0E+06	-2.7E+06	7.2E+05	-7.2E+06
TS_pHBzCl	-2.1E+06	-1.8E+06	-2.6E+06	9.2E+05	-7.9E+06
MAE	1.6E+06	1.4E+06	1.9E+06	3.9E+05	6.2E+06

NA: R parameters are not available

Table A.76: MAE of the Coulomb energy V_{ee}^{1} calculated using Becke, TA, TA(new), SG-1, SG0 for complexes, ions, and peptides

Molecule	Becke	TA	TA(new)	SG-1	SG0
complexes					
CH_2O_2-CH_2O_2	-1.1E+06	-1.0E+06	-1.3E+06	4.0E+05	-3.5E+06
FH-CO	-6.0E+05	-5.0E+05	-7.5E+05	1.7E+05	-2.2E+06
FH-FH	-5.9E+05	-5.2E+05	-7.1E+05	2.6E+04	-2.5E+06
FH-NCH	-5.5E+05	-4.8E+05	-6.5E+05	2.0E+05	-2.0E+06
FH-NH_3	-4.8E+05	-4.1E+05	-5.7E+05	9.0E+04	-1.7E+06
FH-NN	-5.8E+05	-4.8E+05	-7.2E+05	2.3E+05	-2.2E+06
FH-OH_2	-5.4E+05	-4.6E+05	-6.3E+05	6.9E+04	-2.0E+06
H_2O-CO_2	-7.6E+05	-6.8E+05	-9.3E+05	2.6E+05	-2.4E+06
H_2O-$H2_2O$	-4.7E+05	-3.9E+05	-5.5E+05	1.1E+05	-1.5E+06
MAE	6.3E+05	5.5E+05	7.6E+05	1.7E+05	2.2E+06
ions					
$ArNH_3^+$	-8.8E+05	-8.0E+05	-1.0E+06	6.8E+05	-2.3E+06
H_3O^+	-2.3E+05	-2.0E+05	-2.7E+05	5.9E+04	-7.3E+05
$HCOO^-$	-5.6E+05	-4.8E+05	-6.6E+05	1.8E+05	-1.8E+06
$NH_3^+CH_2COO^-$	-8.5E+05	-6.8E+05	-1.0E+06	3.6E+05	-2.6E+06
MAE	6.3E+05	5.4E+05	7.4E+05	3.2E+05	1.9E+06
peptides					
1G_pep	-8.5E+05	-7.3E+05	-1.0E+06	3.7E+05	-2.6E+06
2G_pep	-1.4E+06	-1.4E+06	-1.8E+06	6.7E+05	-4.4E+06
3G_pep	-2.1E+06	-1.8E+06	-2.5E+06	9.9E+05	-6.3E+06
4G_pep	-2.7E+06	-2.5E+06	-3.3E+06	1.3E+06	-8.2E+06
5G_pep	-3.1E+06	-2.9E+06	-4.0E+06	1.6E+06	-1.0E+07
MAE	2.0E+06	1.9E+06	2.5E+06	9.9E+05	6.3E+06

Table A.77: MAE of the Coulomb energy V_{ee}^2 calculated using Becke, TA, TA(new), SG-1, SG0 for molecules containing 1^{st} row atoms

Molecule	Becke	TA	TA(new)	SG-1	SG0
BF_3	-2,110	5,900	-3,230	365	8,460
BH_3	-3,340	1,750	168	37	-63
BeH_2	1,070	696	-56	28	84
C_2H_2	336	1,730	-74	124	-88
C_2H_4	2,670	14,200	68	-207	-2,190
CF_4	-2,420	-6,030	398	3,310	16,100
$CH_2CHCOOH$	2,180	1,660	-922	-568	-1,690
CH_2FF	4,110	-7,840	-994	-1,000	4,360
$CH_2CH_3CH_3$	4,270	-5,810	-929	-893	-203
CH_3F	2,670	-476	-457	-66	2,830
CH_3NH_2	3,730	-12,700	212	-148	412
CH_3OH	2,790	-1,160	157	-41	10
CH_3CONH_2	184	-10,200	1,770	194	-200
CH_4	1,770	-2,330	-36	-42	-288
CO	-101	445	114	46	-30
CO_2	-19	-10	80	179	-424
EtOTs	-9,670	-67,800	-6,340	-690	11,300
F_2	-386	6,160	-116	265	6,920
H_2	-70	-128	-6	13	-86
H_2CO	1,550	4,680	50	102	-21
H_2O	408	861	-71	64	103
H_2O_2	368	-1,880	24	122	1,250
HCOOH	1,970	277	-264	-7	286
Li_2	-24	161	19	10	77
LiF	8,390	1,240	2,410	-139	3,200
LiH	-1,070	78	60	27	-114
NH_3	611	-1,740	-152	-53	266
benzaldehyde	3,820	-10,000	1,160	3,330	1,480
cytosine	3,510	-4,770	378	-1,540	-3,330
formamidine	2,510	26,100	511	251	1,120
methoxide	326	-782	-13	-43	-231
naphthalene	24,800	34,100	11,000	8,160	15,200
uracil	2,830	28,000	459	-1,920	-1,230
MAE	2,912	7,930	991	727	2,535

Table A.78: *MAE* of the Coulomb energy V_{ee}^2 calculated using Becke, TA, TA(new), SG-1, SG0 for molecules containing 2^{nd} row atoms

Molecule	Becke	TA	TA(new)	SG-1	SG0
CCl_4	-2,400	10,700	532	-1,820	-25,200
CH_2ClCl	-4,150	2,550	221	-590	-11,900
$CH_2PH_2PH_2$	24,200	-15,300	2,180	-72	-31,300
CH_2SHSH	12,000	-17,800	1,170	296	-4,360
$CH_2SiH_3SiH_3$	-24,000	6,000	711	-1,600	-9,600
CH_3PH_2	3,050	-17,900	-154	11	-14,500
CH_3SH	624	-6,220	140	571	-3,850
CH_3SiH_3	-16,400	-10,400	-366	-423	-4,180
CH_3Cl	-1,580	-5,750	-24	-76	-5,110
CS	-546	-2,320	-46	-144	-3,680
Cl_2	589	27,800	365	-2,640	-11,800
ClF	-646	15,200	384	-1,570	-4,570
HOCl	764	5,020	339	-595	-5,570
Mg	-103	10	10	72	4,530
NaCl	1,260	24,900	-305	-2,250	-8,830
P_2	-1,380	6,590	366	3	-32,700
PF_5	8,120	137,000	1,840	-3,430	-810
PH	691	-3,980	67	-198	-13,600
SF_6	-7,830	105,000	-4,130	-35,100	-5,170
SO	-1,110	3,140	-44	276	-480
SO_2	17	-142	-35	714	-3,140
SiO	-819	4,990	32	76	-2,360
pNO_2BzCl	-4,640	44,800	-2,070	-3,320	-11,500
MAE	4,462	17,863	615	1,984	9,510

Table A.79: MAE of the Coulomb energy V_{ee}^2 calculated using Becke, TA, TA(new), SG-1, SG0 for molecules containing 3^{rd} row atoms and transition states

Molecule	Becke	TA	TA(new)	SG-1	SG0
3rd row					
AsH_3	-50,900	6,860	1,010	NA	NA
CH_3Br	-1,540	4,590	-1,390	NA	NA
Ge_2H_6	24,000	108,000	-3,790	NA	NA
Ge_3H_8	28,300	138,000	-2,420	NA	NA
Ge_4H_{10}	107,000	373,000	-203	NA	NA
Ge_5H_{12}	-25,400	543,000	5,570	NA	NA
GeH_4	-280,000	-14,700	-2,240	NA	NA
H_2Se	-53,000	25,800	1,050	NA	NA
MAE	68,116	138,228	2,208		
transition states					
TS_CH_3Cl_2	36,100	2,040	336	-868	-4.2E+03
TS_CH_3F_2	857	-9,010	319	367	4.8E+03
TS_CH_3FCl	-472	-2,420	304	187	-3.0E+03
TS_CH_5OF	5,160	-19,800	750	435	4.9E+03
TS_Ethyl-OSO_2-CH_3	-2,260	-4,120	-846	1,580	1.1E+04
TS_pHBzCl	43,500	50,400	2,510	3,560	-1.7E+03
MAE	14,725	14,632	844	1,166	5.0E+03

NA: R parameters are not available

Table A.80: MAE of the Coulomb energy V_{ee}^2 calculated using Becke, TA, TA(new), SG-1, SG0 for complexes, ions, and peptides

Molecule	Becke	TA	TA(new)	pople	SG0
complexes					
CH_2O_2-CH_2O_2	3,790	-32,300	-65	-610	2.3E+03
FH-CO	-245	1,300	231	70	1.8E+03
FH-FH	78	832	346	226	4.9E+03
FH-NCH	108	3,290	95	270	2.6E+03
FH-NH_3	899	2,720	-50	-79	1.4E+03
FH-NN	-5,310	22,000	-74	134	2.1E+03
FH-OH_2	18	1,890	-251	113	2.3E+03
H_2O-CO_2	3,450	-3,030	240	750	-1.8E+03
H_2O-H_2O	1,880	7,200	-21	140	9.4E+02
MAE	1,753	8,285	152	266	2.2E+03
ions					
$ArNH_3^+$	-3,070	-30,200	851	5,070	6.5E+03
H_3O^+	647	-2,090	26	42	-3.1E+00
$HCOO^-$	650	1,210	28	138	7.8E+02
$NH_3^+CH_2COO^-$	572	23,400	-864	590	-4.0E+03
MAE	1,235	14,225	442	1,460	2.8E+03
peptides					
1G_pep	-3,570	-7,580	-382	-263	-2.2E+02
2G_pep	21,100	-49,000	-1,260	-1,390	-6.5E+03
3G_pep	6,070	-20,100	-2,960	783	-4.4E+03
4G_pep	14,200	-86,200	-3,960	-1,440	-8.7E+03
5G_pep	98,900	-5,260	5,890	5,700	-8.0E+03
MAE	28,768	33,628	2,890	1,915	5,545

Bibliography

[1] A. Szabo and N.S. Ostlund. *Modern Quantum Chemistry: Introduction to Advanced Electronic Structure Theory*, McGraw-Hill, (1989).

[2] W. J. Hehre, L. Radom, P. V. R. Schleyer and J. A. Pople. *AB INITIO Molecular Orbital Theory*, John Wiley & Sons (1986).

[3] I. N. Levine. *Quantum Chemistry*, Prentice Hall (2000).

[4] J. M. Pérez-Jordá, and A. D. Becke, *J. Chem. Phys.*, 100(9), 6520 (1994).

[5] P. Hohenberg and W. Kohn, *Phys. Rev. B*, 136, 864 (1964).

[6] W. Kohn and L. J. Sham, *Phys. Rev. A*, 140, 1133 (1965).

[7] A. D. Becke. *J. Chem. Phys.*, 88, 2547 (1988).

[8] V. I. Lebedev. *Zh. Vychisl. Mat Mat. Fiz.*, 15(1),48 1975.

[9] V. I. Lebedev. *Zh. Vychisl. Mat. mat. Fiz.*, 16(2),293 1976.

[10] V. I. Lebedev and A. L. Skorokhodov. *Russ. Acad. Sci. Dokl. Math.*, 45(3) 587 (1992).

[11] V. I. Lebedev and D. N. Laikov *Dokl Akad Nauk*, 366, 741 (1999).

[12] O. Treutler and R. Ahlrichs. *J. Chem. Phys.*, 102(1),346 (1995).

[13] A. H. Stroud. *Approximate Calculation of Multiple Integrals*, Prentice Hall, (1971).

[14] R.A. Poirier, *MUNgauss* (Fortran 90 version), Chemistry Department, Memorial University of Newfoundland, St. John's, NL, A1B 3X7. With contributions from S.D. Bungay, A. El-Sherbiny, T. Gosse, J. Hollett, D. Keefe, A. Kelly, C.C. Pye, D. Reid, M.Shaw, Y. Wang and J. Xidos.

[15] P. M. W. Gill, B. G. Johnson, J. A. Pople. *Chem. Phys. Let.*, 209(5), 506 (1993).

[16] A. El-Sherbiny and R. A. Poirier. *J. Comput. Chem.*, 25(11), 1378 (2004).

[17] P. M. W. Gill and Siu-Hung Chien. *J. Comput. Chem.*, 24(6), 732 (2003).

[18] Siu-Hung Chien and P. M. W. Gill. *J. Comput. Chem.*, 27, 730 (2006).

[19] C. W. Murray, N. C. Handy, G. J. Laming. *J. Mol. Phys.*, 78(4), 997 (1993).

[20] J. M. L. Martin, Jr, C. W. Bauschlicher, A. Ricca. *Comput. Phys. Comm.*, 133, 189 (2001).

[21] M. E. Mura and P. J. Knowles. *J. Chem. Phys.*, 104(24), 9848 (1996).

[22] A. El-Sherbiny and R. A. Poirier. *IEEE digital library www.ieee.org* (2006).

[23] P.M.W. Gill, B. G. Johnson and J. A. Pople. *Chem. Phys. Let.*, 217(1), 65 (1994).

[24] A. R. Leach. *Molecular Modelling*, Longman, (1996).

[25] M. Head-Gordon and J. A. Pople. *J. Chem. Phys.*, 89(9), 5777 (1988).

[26] C. J. Cramer. *Essentials of Computational Chemistry*, Willey, (2005)

[27] W. Yang. *Phys. Rev. Lett.*, 66, 1438 (1991).

[28] S. L. Dixon and K. M. Merz. *Chem. Phys.*, 104(17) 6643 (1996).

[29] S. Goedecker. *Rev. Mod. Phys.*, 71, 1085 (1999).

[30] T. E. Exner and P. G. Mezey. *J. Phys. Chem. A*, 106, 11791 (2002).

[31] D. W. Zhang and J. Z. H. Zhang. *J. Chem. Phys.*, 119(7), 3599 (2003).

[32] V. Gogonea, D. Suarez, A. V. D. Vaart, and K. M. Merz. *Cur. Opi. Str. Bio*, 11, 217 (2001).

[33] N. Reuter, A. Dejaegere, B. Maigret, and M. Karplus *J. Phys. Chem. A*, 104, 1720 (2000).

[34] Q. Cui, H. Guo, and M. Karplus. *J. Chem. Phys.*, 117(12), 5617 (2002).

[35] J. J. P. Stewart. *Int. J. Qua. Chem.*, 58, 133 (1996).

[36] T. E. Exner and P. G. Mezey. *J. Comput. Chem.*, 24, 1980 (2003).

[37] X. H. Chen and J. Z. H. Zhang. *J. Chem. Phys.*, 120(24), 11386 (2004).

[38] X. P. Li, R. W. Nunes, and D. Vanderbilt. *Phys. Rev. B* 47, 10891 (1991).

[39] J. M. Millam and G. E. Scuseria. *J. Chem. Phys.*, 106(13), 5569 (1997).

[40] A. D. Daniels, J. M. Millam and G. E. Scuseria. *J. Chem. Phys.*, 107(2), 425 (2001).

[41] M. Challacombe. *J. Chem. Phys.*, 110(5) 2332 (1999).

[42] W. Yang. *Phys. Rev. A*, 44, 7823 (1991)

[43] W. Yang and T. Lee. *J. Chem. Phys.*, 103(13) 5674 (1995)

[44] T. Lee, D. M. York, W. Yang. *J. Chem. Phys.*, 105(7), (1996).

[45] W. Pan, T. Lee, W. Yang. *J. Comp. Chem.*, 19(9), 1101 (1998).

[46] A. V. D. Vaart, D. Suarez, K. M. Merz. *J. Chem. Phys.*, 113(23), 10512 (2000).

[47] S. L. Dixon and K. M. Merz. *J. Chem. Phys.*, 107(3), 879 (1997).

[48] A. V. D. Vaart and K. M. Merz. *J. Phys. Chem. A*, 103, 3321 (1999).

[49] A. V. D. Vaart, V. Gogonea, S. L. Dixon, K. M. Merz. *J. Comp. Chem.*, 21(16), 1494 (2000).

[50] V. Gogonea, K. M. Merz. *J. Phys. Chem. A*, 103, 5171 (1999).

[51] M. D. Ermolaeva, A. V. D. Vaart, K. M. Merz. *J. Phys. Chem. A*, 103, 1868 (1999).